Design and Analysis of a Permanent Magnet Generator for Naval Applications

by

Jonathan E. Rucker

Masters in Business Administration
Kenan-Flagler Business School, University of North Carolina at Chapel Hill, 2001
B.S.E., Electrical Engineering
Duke University, 1994

Submitted to the Department of Ocean Engineering and the Department of Electrical
Engineering and Computer Science in Partial Fulfillment of the Requirements for the Degrees of

Naval Engineer .

and

Master of Science in Electrical Engineering and Computer Science
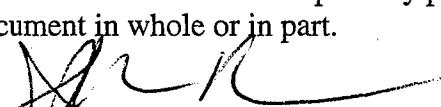
at the
Massachusetts Institute of Technology

June 2005
© 2005 Jonathan E. Rucker. All rights reserved.

The author hereby grants to MIT permission to reproduce and to distribute publicly paper and
electronic copies of this thesis document in whole or in part.
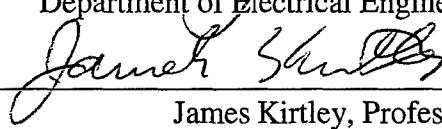
Signature of Author_____

Department of Ocean Engineering and the
Department of Electrical Engineering and Computer Science
May 11, 2005
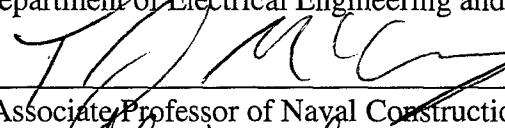
Certified by _____

James Kirtley, Professor of Electrical Engineering
Department of Electrical Engineering and Computer Science
Thesis Supervisor
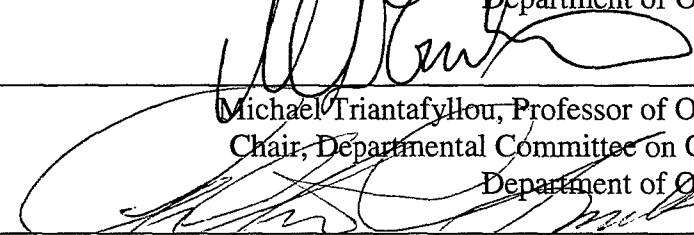
Certified by _____

Timothy J. McCoy, Associate Professor of Naval Construction and Engineering
Department of Ocean Engineering
Thesis Reader
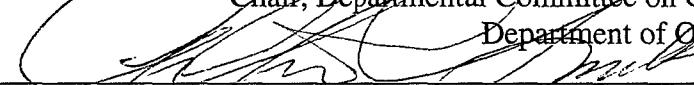
Accepted by _____

Michael Triantafyllou, Professor of Ocean Engineering
Chair, Departmental Committee on Graduate Students
Department of Ocean Engineering

Accepted by _____

Arthur C. Smith, Professor of Electrical Engineering and Computer Science
Chair, Departmental Committee on Graduate Students
Department of Electrical Engineering and Computer Science

20060516052

Page Intentionally Left Blank

Design and Analysis of a Permanent Magnet Generator for Naval Applications
by
Jonathan E. Rucker
May 11, 2005

Submitted to the Department of Ocean Engineering and the Department of Electrical Engineering and Computer Science in Partial Fulfillment of the Requirements for the Degrees of

Naval Engineer

and

Master of Science in Electrical Engineering and Computer Science

ABSTRACT

This paper discusses the electrical and magnetic design and analysis of a permanent magnet generation module for naval applications. Numerous design issues are addressed and several issues are raised about the potential improvements a PM generation system can offer. A proposed 16 MW PM generation module design is presented along with a detailed design methodology.

Eighty different machines and power conversion modules are sized, designed, and analyzed with a final design selected. Specifically, sizing and detailed machine design and analysis is performed examining the effects of numerous parameters including number of phases, number of poles, magnetic geometry, machine dimensions, and material types. Analytical models are developed to study rotor losses caused by stator winding time and space harmonics and slot space harmonics. Power electronics and conversion modules to connect the high-speed generator to a DC distribution system are designed and analyzed. In depth simulation of the eighty complete systems is performed using the software programs MATLAB (Version 12.0, Mathworks) and PSIM (Version 6.0, Powersim, Inc.).

The 16 MW permanent magnet generation module, consisting of the generator and associated power electronics, provides an excellent alternative to traditional wound rotor synchronous machines. The final design offers significant reductions in both weight and volume. Specifically, it is estimated that the PM generation module has a 7x reduction in volume and a 10x reduction in weight compared to similarly rated wound rotor systems. These reductions can provide flexibility to naval architects since power, weight, and volume are integral parts of the design and construction processes. However, further study is necessary to verify the PM generation modules thermal, structural, and mechanical performance.

Thesis Supervisor: James Kirtley
Title: Professor of Electrical Engineering

Thesis Reader: Timothy J. McCoy
Title: Associate Professor of Naval Construction and Engineering

Page Intentionally Left Blank

Table of Contents

Page Intentionally Left Blank

List of Figures

List of Tables

Page Intentionally Left Blank

Chapter 1 Introduction

1.1 Purpose

The purpose of this thesis is to design and analyze a permanent magnet generator and power module for naval applications. When deciding whether to implement an electrical technology or component onto a naval vessel, the size, weight, and cost are the major factors for successful integration. Significant performance improvements and cost reduction of power electronics, coupled with the availability and decreasing cost of high energy permanent magnet (PM) materials makes PM generators attractive for naval usage. These machines offer numerous desirable features, including light weight, small size, simple mechanical construction, easy maintenance, good reliability, and high efficiency [1].

Before analysis of a generator can begin, it must be properly designed for typical naval power requirements. This involves sizing the generator along with designing the associated power electronics for connecting the machine to the distribution system. A specific concern associated with PM generators is possible inefficiencies and excessive heating; in particular rotor losses caused by space and time harmonics during the energy conversion processes. The optimum machine design is one that delivers the required power through a matching process between the generator and the power electronic converter [2].

1.2 Problem

The Navy's commitment to develop an integrated electric power system for the next generation warships offers the expectation of using the installed generation capacity to power ship propulsion, advanced weapons components, and high power combat control systems [3]. As these electrical loads increase, it becomes increasingly important to efficiently utilize installed power as well as develop smaller, effective power generation systems. Navy ships are extremely high performance systems and therefore power and weight considerations are integral parts of the design process.

The life cycle of a navy ship is on average 2-3 times longer than a commercial ship and therefore navy ships undergo excessive modernization and upgrades throughout their service life. Many of the newer components have significantly higher power requirements than the originals

putting a burden on the power generation system. Therefore, the Navy is moving toward designing all electric ships with integrated power systems (IPS) and increased power generation that can be efficiently managed to meet future demands.

The effective integration of electrical power in future naval ships requires the development of technologies that ensure volume and mass reduction in critical mechanisms. Military ships require higher power density components, impose more stringent acoustic and EM signature requirements, and subject systems to harsher environments than commercial applications [4]. Rotating generators, coupled with prime movers, need to be lighter in weight and higher in power density. High-speed PM generators provide a substantial reduction in size and weight making them a logical choice for naval applications. Currently, the Navy has not designed or built a high power (megawatt) PM generator and therefore the need exists.

In conjunction with constructing a PM generator, a DC bus architecture is one of the preferred schemes for the future [5]. DC power distribution systems can offer a size and weight reduction compared to high-power AC systems [3]. With a DC bus distribution, the PM generator can be optimized independent of producing 60 Hz frequency as required in the past. However, conversion of the high-frequency generator AC output to DC requires power electronics. Rectification of AC to DC presents the problem of creating harmonics in the input current which are then reflected back onto the generator causing rotor losses. In addition, the generator produces space harmonics which also produce losses in the rotor. Therefore, the PM generator and power electronics module (PEM) need to de designed and optimized to deliver constant DC power while minimizing machine losses.

1.3 Background

1.3.1 History

The Navy has designed and built electric ships since the early part of the 20th century. The original advantages perceived for electric ships, superior performance, reduced manning, arrangement flexibility, and fuel efficiency, are still relevant today [6]. In the early part of the 20th century, diesel-electric submarines, small surface ships, and some battleships and carriers had electric propulsion. By the late 1940s, mechanical drive systems became popular because of improvements in metallurgy and manufacturing. However, the capability of mechanical

transmissions reached its limits in the late 20th century spawning a renewed interest in electric drive and integrated power systems for military applications.

For the last thirty years, the commercial industry has designed and operated integrated power systems (IPS). An IPS is a ship architectural paradigm in which the ship's power and propulsion are provided by a common electrical distribution system instead of having a separate mechanical drive for propulsion. For military applications, an IPS provides numerous benefits:

- Decreased life cycle costs because of increased fuel economy and efficiency (a Navy ship with IPS may consume 10-25% less fuel than a similar ship with mechanical drive [7])
- Increased ship design and arrangement flexibility since the ship is not limited to having a long mechanical shaft line
- Reduced system complexity
- Higher degree of modular design using power components
- Broad industrial base for implementing IPS design
- High levels of automation and control
- Increased power available for non-propulsion uses since a Navy ship spends a large portion of its time operating at low propulsion levels (approximately 95% of the time)
- Increased stealth, survivability, and payload

Since an IPS provides power for both the ship loads and propulsion, larger generation capability is required. As the Navy builds its new ships with IPS architectures, compact, high-power generation systems must be examined to help facilitate implementation of the new designs.

1.3.2 Power Generation & Distribution

Almost all naval core power generators to date are air-cooled 50/60 Hz machines that are military derivatives of commercial generators and are therefore size and weight excessive [8]. A typical turbine generator system is shown in Figure 1 and Table 1 contains nominal characteristics for several current commercial and naval generators.

15

Typical Turbine-Generator System

Turbine Control

Generator Control

System Inputs →

Turbine → **Generator** → Power Out

Turbine Services

Generator Services
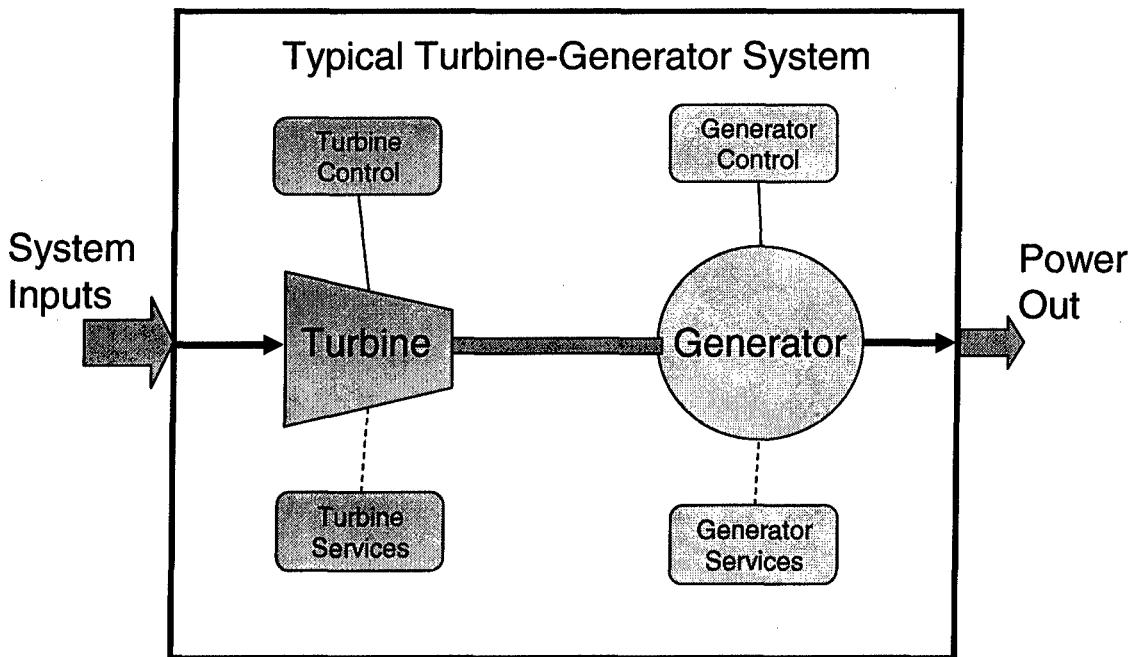
Figure 1: Typical Turbine Generator System

Table 1: Examples of Current Generator Characteristics

Machine	Phases	Power (MW)	Speed (RPM)	Length (m)	Width (m)	Height (m)	Weight (MT)
1	3	21	3600	4.7	4	3.4	50.0
2	3	36.5	3600	6.2	4.37	3.76	63.6
3	3	26	3600	6.2	3.56	4.5	68.1
4	3	25	3600	5.18	3.1	4.15	57.3

With the advent of high-power, cost-effective power electronics, it is no longer necessary to generate power at 50/60 Hz so generators can be optimized independent of frequency. High-speed, power-dense generators become the logical choice for naval purposes. Permanent magnet machines are ideal for this high-speed application due to their simple structure and high power density [9].

Since the generator can now be designed to produce higher frequencies, distribution architectures are not limited to being 60 Hz. Either a high frequency AC system or a DC system can be designed through the use of power electronics modules, with the DC distribution being preferred because of its advantages in size and weight. In this thesis, a high-power DC zonal architecture is assumed using solid state converters to generate AC where needed. Each zone is

16

electronically isolated from the other zones with automatic fault detection and reconfiguration to provide continuous power during damaged conditions. The PM generator sets and power electronic conversion modules serve as the backbone thereby providing a reliable power system for navy ships.

1.4 Scope

The scope of this thesis is limited to the PM generator and associated power electronics AC-DC conversion module. The following is accomplished:

- Determine the electrical power requirements for a Navy IPS ship in order to properly size the generator

- Compare typical wound rotor machine design to a permanent magnet design to determine applicability for IPS applications

- Conduct material analysis and selection for the generator design

- Perform initial PM generator detailed design

- Design the power electronics conversion module to perform high-power AC-DC conversion

- Conduct detailed analysis of rotor losses of the PM generator, in particular those caused by time and space harmonics

- Perform numerous iterations of machine and power electronics designs to develop optimized generation scheme

Page Intentionally Left Blank

Chapter 2 Power Requirements and Machine Selection

2.1 Machine & Module Requirements

On board Navy ships, electricity is used to provide power to virtually all components, including mission systems, support systems, combat systems, and communications systems. In addition, as ships continue to be upgraded and modernized, more power is needed for newer combat systems and weapons components. Most current naval platforms have some form of mechanical propulsion system with separate ship service electrical generators supplying the ship's power. With an IPS ship, the ship's generators provide power for propulsion and the ship's service loads, and through proper utilization, power is efficiently managed.

To properly size the PM generator, the power requirements must be identified and therefore a typical load list is developed for an IPS naval ship and is included in Appendix A. The overall power requirement for the generator is 16 MW. Since size and weight are important factors and the generator can be optimized independent of frequency, high-speed operation and maximum power-density are desired. Therefore, the highest possible speed is selected while ensuring the PM generator is compatible with both gas turbines and steam turbines.

Traditionally, gas turbines run at much higher speeds than steam turbines causing the steam turbines to be more limiting. From information collected from the Elliot Turbomachinery Company, Inc., 16,000 RPM is approximately the highest speed steam turbine that can reasonably be constructed at the megawatt power level [13]. Therefore, to provide a degree of conservatism, 13,000 RPM is selected for the nominal design speed for the PM generator.

The power electronics module (PEM) converts the AC voltage from the generator to 700 VDC. Overall, the PEM and generator must be designed so that losses suffered by the permanent magnets on the generator rotor are minimal. Table 2 lists the general requirements for the entire system.

2.2 Machine Selection

Military ships require high power density components and improved acoustic and electromagnetic signature requirements while subjecting systems to harsh environments [14]. It is therefore important to ensure the power generation system is capable and efficient.

Table 2: General Machine & Module Requirements

Parameter	Specification
Generator Power	16 MW
Generator Speed	13,000 RPM
PEM Output Voltage	700±5 VDC
PEM Output Ripple	0.7 VDC (@ 16 MW)
Generator Rotor Losses	Minimal

2.2.1 Permanent Magnet versus Wound Rotor

Reducing the size and weight of ship's turbine generator sets offers significant advantages to naval architects. Replacing older generators with lightweight ones could make it possible to decrease the size of some generator sets by as much as 50% [15]. PM generators therefore become an attractive alternative compared to wound rotor machines because of the availability and decreasing cost of high energy PM materials along with improved power electronics.

A wound rotor generator normally consists of armature windings on a stationary stator frame with field windings on an inner rotor. The rotor is turned by a prime mover, usually a gas or steam turbine, and current is supplied to the field windings through brushes or a brushless exciter. As the current-carrying field windings rotate past the stator windings, current is produced in the stator windings through Faraday's Law. An example of a wound rotor machine is shown in Figure 2 [8] and Figure 3 [16].
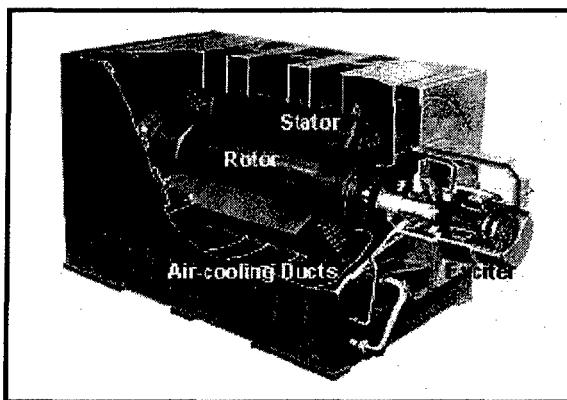
Figure 2: Example of Wound Rotor Generator
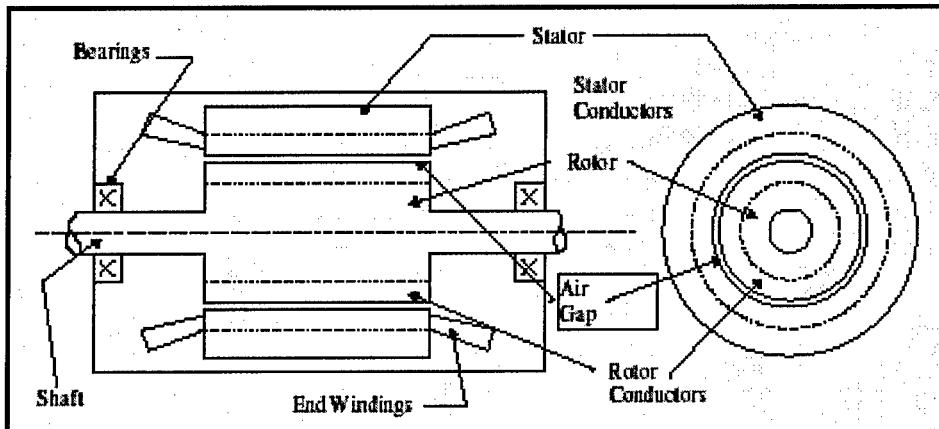
Figure 3: Cross Section of Wound Rotor Generator

Wound rotor generators have been the backbone of power generation for the U. S. Navy because they are a proven technology that is battle tested. They offer steady voltage regulation using the field windings, a large air gap for producing the rotor magnetic flux, low fault currents, and high power capabilities.

However, the machines tend to be complex, weight excessive, and they require field windings which limit design alternatives. There are several drivers which cause these problems to occur. First, to generate the necessary magnetic flux levels, wound rotor generators have large pole pitches to support the required field windings. These pole pitch windings in turn require larger end turns and thick back iron to support the magnetic flux, both of which contribute to increased size. Second, because of the winding losses in the rotor, large cooling systems can be required thus increasing the number of support components.

High speed generators offer a reduction in machine size and weight because as a machine's speed increases, its size decreases for a given output power. The PM generator is ideal for high-speed applications because of its simple structure and high power density [9]. In a PM generator, the rotor field windings are replaced by permanent magnets which do not require additional excitation. As the permanent magnets are rotated by the prime mover, current is produced in the stator windings. An example of a PM generator is shown in Figure 4 [8].
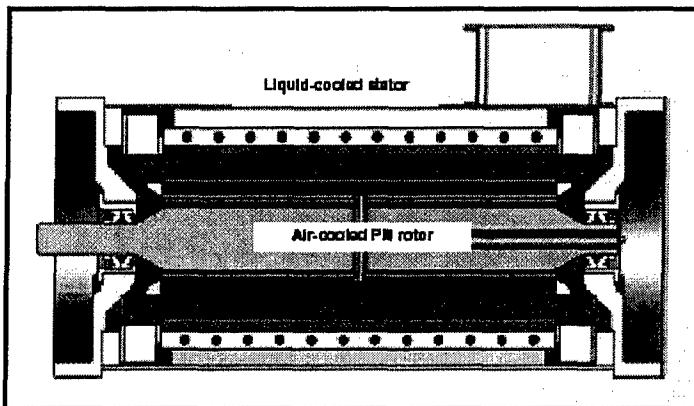
Figure 4: Example of PM Generator

PM generators offer several advantages: they have no rotor windings so they are less complicated; they have high efficiencies; the gap field flux is not dependent on large pole pitches so the machine requires less back iron and can have a greater number of smaller poles; and they usually require smaller and fewer support systems. Assuming the same flux density and circumferential arc, doubling the number of poles produces the same radial flux but requires half the stator core thickness, as shown in Figure 5.
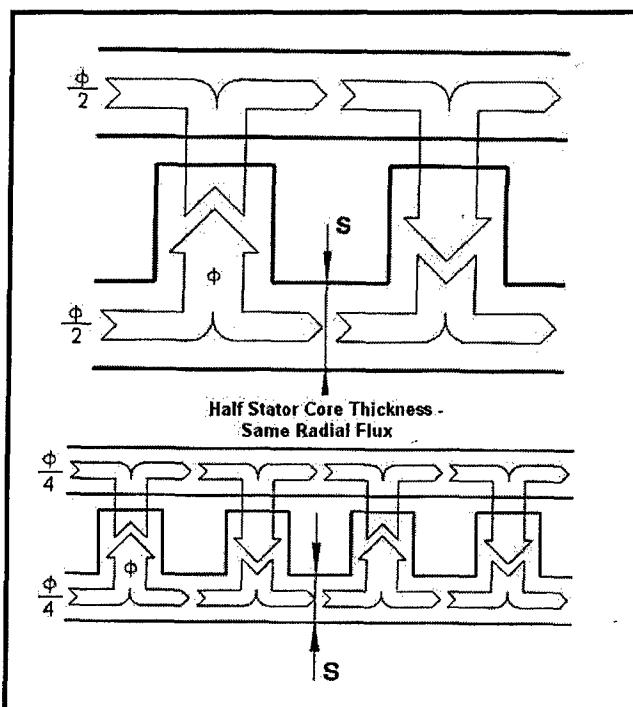
Figure 5: Flux vs. Number of Poles

22

However, PM generators also have some disadvantages. They do not possess field excitation control and therefore voltage regulation can be problematic. This can be corrected by using external voltage control such as large capacitor banks or power electronics, as well as choosing the turns on the stator winding properly to produce the anticipated required nominal voltage. Additionally, since the permanent magnet fields cannot be turned off, there exists the risk of excessive currents in the event of an internal fault. This problem can also be solved through the design of the turbine governor and controller or dynamic braking. Overall, the advantages of the PM generator over the traditional wound rotor generator make it a better alternative for high-speed navy applications. A summary comparing the different designs is given in Table 3.

Table 3: Comparison of Wound Rotor and PM Generators

Generator Type	Advantages	Disadvantages
Wound Rotor	Steady voltage regulation with field windings	Weight excessive
	High power capabilities	Large size
	Large air gap for flux	Rotor windings & associated losses
	Low fault currents	Large support systems
	Proven, robust design	
Permanent Magnet	Less complicated	Lack of inherent voltage regulation
	Reduced size and weight	Potential fault currents
	High efficiency	Magnet losses
	No excitation supply or field windings	
	High speed applicability	

2.2.2 Type of Permanent Magnet Machine

There are numerous layout possibilities for permanent magnet machines and only the most common are discussed here. These include radial flux inner rotor, radial flux outer rotor, and axial flux designs. In most PM machines, flux crosses from the rotor to the stator in the radial direction [17]. The first type, the radial flux inner rotor design, is the closest configuration to the classical AC synchronous generator. An example of this design is shown in Figure 6 [17].
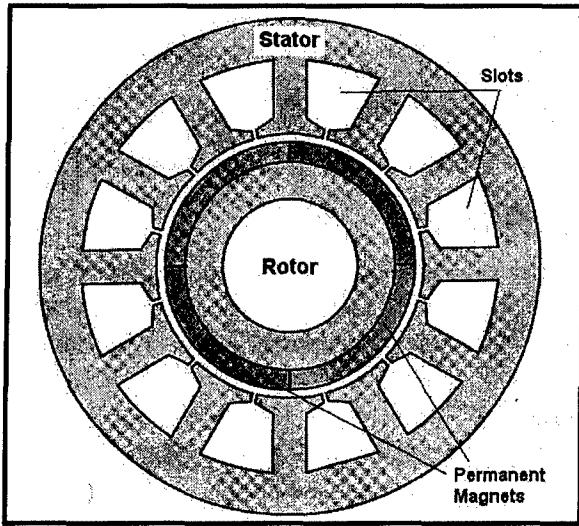
Figure 6: Example of Inner Rotor PM Machine

In this type of machine, the windings are placed on the stator, either in slots or in a slotless ring, and the magnets are surface mounted on the rotor or buried in the rotor. Buried magnet designs often result in rotors that are larger than equivalent surface-magnet machines with high-energy magnets [18]. Buried magnet machines can also have significant structural issues in high-power applications [19]. When the magnets are surface mounted and the machine is operated at high speed, the magnets are often secured with a retaining device made of either alloy steel or carbon-fiber. Overall, the inner rotor machine possesses high torque/power capability and good heat conduction and cooling properties making it ideal for high-speed, higher-power applications [18].

The radial flux outer rotor machines are commonly used in hard disk drives, small computer ventilation fans, and some blowers. This type of design is very efficient, low-cost, easy to manufacture, and applicable for low-power applications [18]. It is the opposite of the inner rotor because the stator in on the inside with the rotor and magnets on the outside. A cross section of an outer rotor machine is shown in Figure 7 [17].
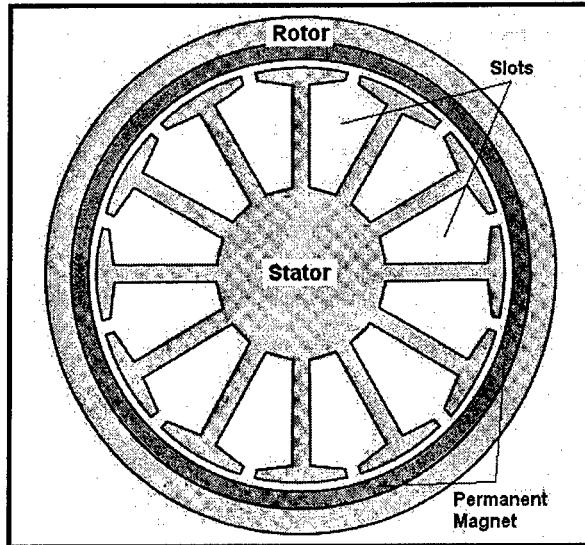
Figure 7: Example of Outer Rotor PM Machine

The axial flux machine is significantly different than the previous two because flux flows in the axial direction vice radial direction and the windings are oriented radially vice axially (see Figure 8 for an example diagram [20]).
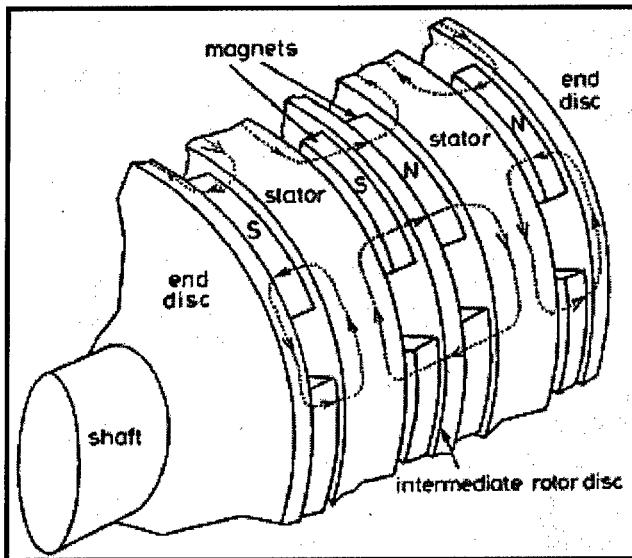
Figure 8: Example of Axial Flux PM Machine

The main advantages of this design are their low cost, flat shape, and smooth rotation. However, if axial-flux machines are operated at high speeds (above 1000 RPM), eddy-current losses and heating can become excessive [18]. Also, stator construction is difficult because it must be laminated circumferentially. An example of this design is the turntable for a record player.

Overall, because of its inherent advantages in heat removal and cooling, the abundance of manufacturing capabilities, and its high-power, high-speed applicability, the radial flux inner rotor with surface mounted magnets is selected for the 16 MW PM generator design.

Chapter 3 Material Selection and Machine Initial Design

3.1 Material Selection

One of the key considerations during the electromagnetic, structural, and thermal design of a permanent-magnet machine is the selection of the magnet, stator, and rotor materials [21]. Machine output, heat rise, weight, and cost are a few of the characteristics which are directly influenced by selection of the machine materials [22].

3.1.1 Permanent Magnets

The size and performance of high-speed PM generators depend on the permanent magnet material properties [9]. The magnets must be selected to provide the necessary air gap magnetic field and ample coercive force to compensate for possible damaging effects while minimizing the volume of material because of cost and weight considerations [23].

Ferromagnetic materials are the most common substances used in the construction of machines and their properties are normally described using B-H curves and hysteresis loops. These curves represent an average material characteristic that reflects the non-linear property of the permeability of the material but ignores the multi-valued properties [17]. An example of a B-H curve is shown in Figure 9.
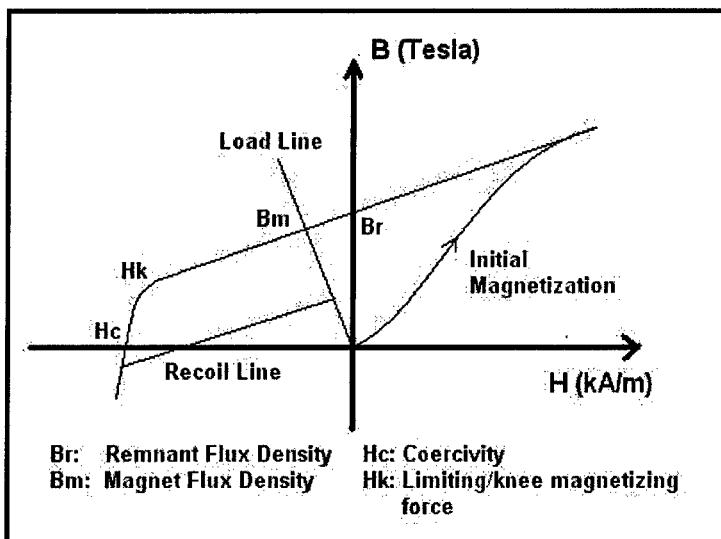
Figure 9: Example of B-H Curve

Several basic magnetic properties are of critical importance for the permanent magnets in a PM machine:

- Remnant Flux Density (B_r): It is the value of the flux density remaining after magnetization and it directly influences the air gap flux and magnet sizes.

- Coercivity (H_c): It is the value of magnetizing field needed to reduce the flux density in the magnet to zero and it gives a first order estimate of a magnet's resistance to demagnetization.

- Energy Product (BH_{max}): It is the maximum energy product of the magnet and it is inversely proportional to the total magnet volume required.

- Recoil Permeability (μ_{rec}): It is the gradient of the B-H curve and it gives the magnet's ability to return to its initial magnetization after subjected to damaging forces. If the magnet goes below H_k, then it will recoil along a lower line resulting in a lower magnet flux density.

- Load Line: It is a line drawn from the origin to the magnet operating point on the hysteresis curve (B_m). The magnitude of the slope of the load line is the permeance coefficient.

Permanent magnet materials come in many varieties and the four most common types for machine applications are Alnico, Ferrites, SmCo material, and NdFeB material. Table 4 and Figure 10 show the characteristics and typical B-H curves for these materials [18].

Table 4: Magnet Material Properties

Property	Units	Alnico	Ferrite	SmCo	NdFeB
Remanence (B_r)	T	0.6 – 1.3	0.35 – 0.43	0.7 – 1.05	1.0 – 1.3
Coercivity (H_c)	kA/m	40 – 130	180 – 400	800 – 1500	800 – 1900
Recoil Permeability (μ_{rec})		1.9 – 7	1.05 – 1.15	1.02 – 1.07	1.04 – 1.1
Energy Product (BH_{max})	kJ/m^3	20 – 100	24 – 36	140 – 220	180 – 320
Maximum Temperature	^{0}C	500 – 550	250	250 – 350	100 – 200
B_r Temperature Coefficient	%/^{0}C	-0.01 to -0.02	-0.2	-0.05	-0.08 to -0.15

The rare-earth magnets, SmCo and NdFeB, have become more popular for high performance applications because of their greater power density, high coercivity, high flux densities, and linearity of the demagnetization curves [24].

28
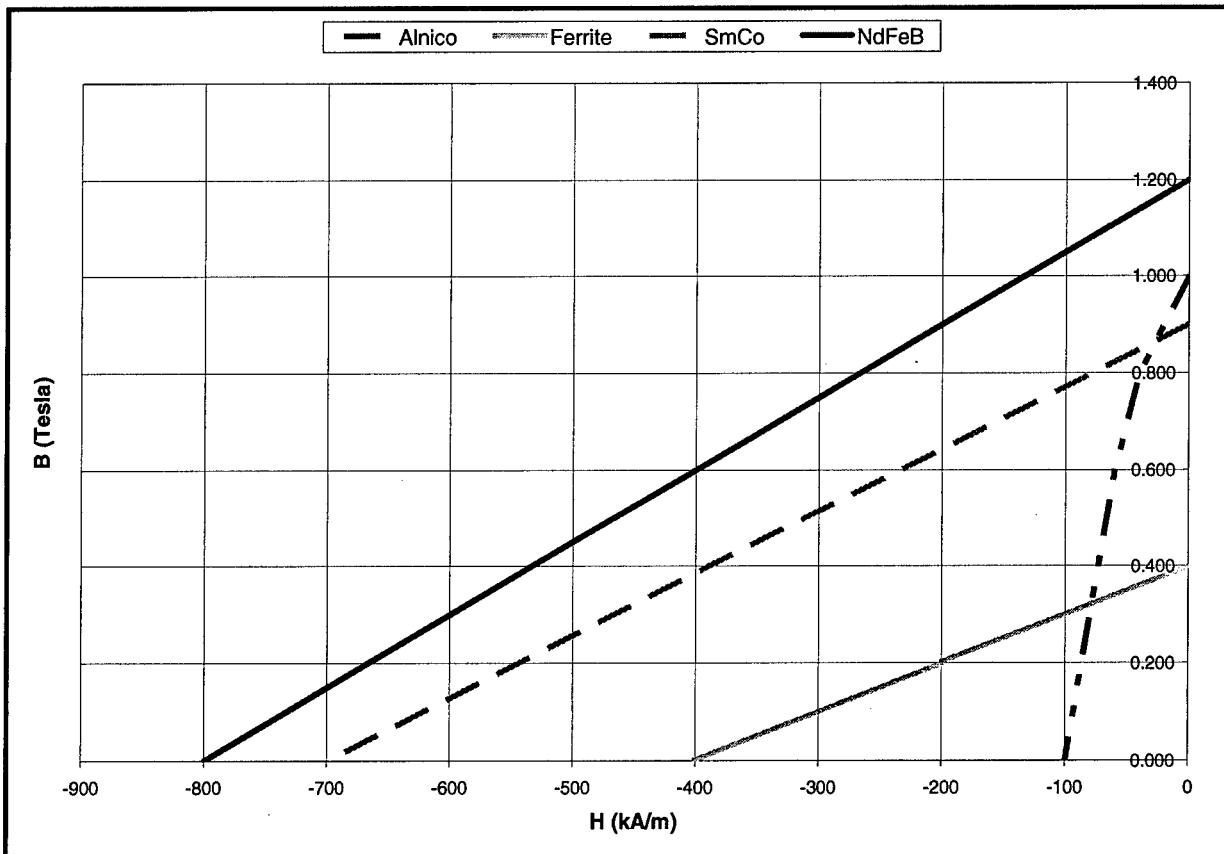
Figure 10: Typical Magnet B-H Curves

Between the two rare-earth permanent magnets, NdFeB is preferred because it is cheaper and more readily available. It does possess some adverse characteristics such as moderate corrosion and lower resistance to temperature effects, but these can be controlled using surface treatments and proper cooling [25]. Therefore, NdFeB magnets are selected for use in the PM generator with the conservatively assumed values listed in Table 5.

Table 5: Selected Magnet Properties

Property	Units	Value
Remanence (B_r)	T	1.2
Coercivity (H_c)	kA/m	900
Recoil Permeability (μ_{rec})		1.05
Energy Product (BH_{max})	kJ/m^3	260
Maximum Temperature	^{0}C	180
Resistivity	$\mu\Omega$/m	1.43

29

3.1.2 Stator and Rotor Material

The type of material chosen for the stator and rotor is important because it impacts the machine losses and efficiency. The rotor is usually built from the same material as the stator for ease of construction but is can be made of any economical steel provided it is strong enough for the given function [18]. No one material is optimum for every application and the normal criteria for selection are cost, permeability, core losses, and saturation flux. It is important that the material act as a flux guide and absorb the minimum amount of magnetomotive force (MMF) so that the flux is concentrated in the air gap. In addition, the material should minimize core losses including hysteresis and eddy current losses.

High-quality, non-oriented, electrical grade lamination steels are typically used in most machines because the laminations help minimize losses. The four main materials are low carbon steels, silicon (Si) steels, nickel (Ni) alloy steels, and cobalt (Co) alloy steels. Low carbon steels are the lowest cost and are used in high volume applications where high core losses are acceptable. Silicon steels usually have 3% silicon which increases the resistivity to reduce eddy current losses. They are selected and specified based on core loss, with each grade (M19, M27, M36, and M43) having higher core losses and lower cost [22]. The lamination thickness is a tradeoff between cost and performance and the most common sizes are 0.014 in, 0.0185 in, and 0.025 in (29 gauge, 26 gauge, and 24 gauge).

Nickel alloys are either 49% or 80% nickel and they have lower losses than the silicon steel but are much more expensive. In addition, they require careful handling and not suited for high flux density environments (above 0.8 T) because of saturation. The cobalt alloys are only used in extremely high-performance situations such as military aircraft and space applications because of the high cost. Table 6 summarizes the different stator materials and the M19, 29-gauge electrical silicon steel is selected for the PM generator because it is economical, its thin laminations minimize losses, and it has a saturation flux density of about 1.8 T [2], [18], [22].

Table 6: Laminated Steel Properties

Material Type	Core Loss	Saturation Flux Density	Permeability	Ease of Processing	Relative Cost (Si is 1.0)
Low Carbon Steel	Fair	Good	Good	Best	0.5
Si Steel	Good	Good	Fair	Good	1.0
Thin Si Steel	Better	Good	Fair	Fair	10.0
49% Ni Alloy	Good	Fair	High	Care Req'd	12.0
80% Ni Alloy	Better	Low	Best	Care Req'd	15.0
Co Alloy	Good	Best	Good	Care Req'd	45.0

3.2 Machine Design Parameters

3.2.1 Stator Mechanical Design

The stator is an important part of the machine because it serves as the main structural component, it provides the housing for the armature windings, and it completes the flux path for the magnetic circuit. The main consideration in the mechanical design of the stator is whether to make it slotted or slotless. A slotless stator has the armature windings located in the air gap of the machine as shown in Figure 11 [19].
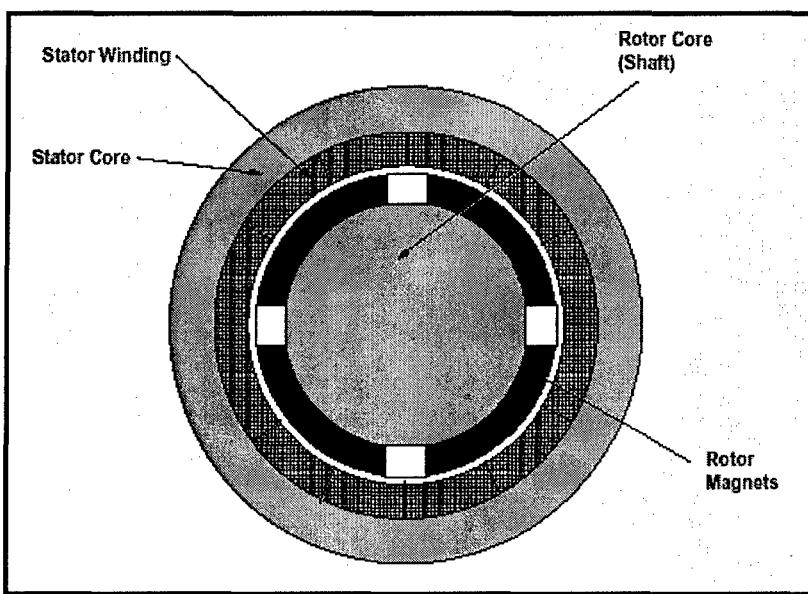
Figure 11: Slotless Stator Design

One of the advantages of the slotless construction is unique winding layouts are possible to meet specific performance goals. Another advantage is that the space available for the armature windings increases by a factor of about two since there are no stator teeth. This produces lower

conductor losses since less current flows in each winding. The flux density is reduced, however, because the effective air gap is much larger since the windings are in the air gap. Overall, there exists a higher electrical loading and a lower magnetic loading.

One disadvantage of the slotless design is there are no good conduction paths to remove the heat generated from the windings. This reduces the allowable current density in the windings and lowers the power output. Another disadvantage is that the windings are directly exposed to the rotating flux which raises the possibility of additional eddy-current loss in the conductors and further losses due to circulating currents in the windings [18]. Overall, the performance of a slotless stator is almost always lower than that of an equivalent slotted stator design and therefore slotless stators do not appear often in high-power applications [17].

Slotted stators are the traditional stator design and consist of openings around the stator for the armature windings as shown in Figure 12 [26]. The openings provide rigid housings for the conductors and associated insulation.
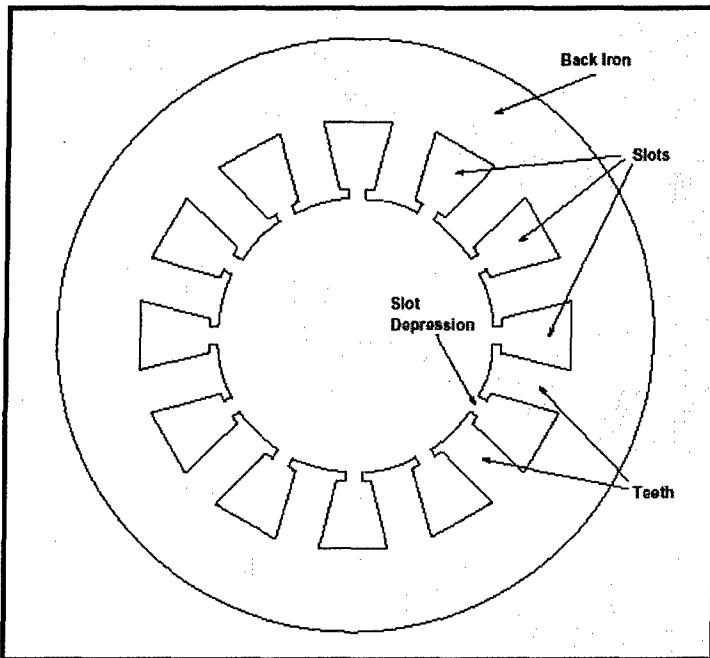
Figure 12: Slotted Stator Design

Stator slots vary in size and shape with the most common configurations being rectangular or trapezoidal. In this paper, the slots are assumed to be approximately rectangular as shown in Figure 13 and contain form-wound windings so that the depression width is the same as the slot top width.
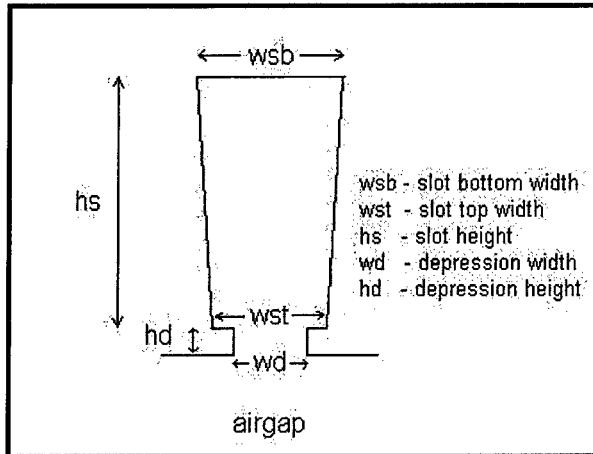
Figure 13: Stator Slot Geometry

Slotting is used because is provides a good way to achieve a narrow air gap length while keeping the winding conductors close to the magnets to maximize the flux linkage. The slots also greatly increase the surface contact area between the windings and stator steel providing a path of low thermal resistance for good heat conduction which is important for keeping the windings and magnets cool.

The resulting narrow air gap from the slots makes the permeance greater and therefore the air gap flux density greater producing a more powerful machine. In addition, the depression in the slot tops help control parasitic losses in the rotor by improving the uniformity of the air gap field. The limits of the size of the slots are twofold: the magnetic teeth must be able to carry the air-gap flux without saturating and the slots must be large enough to support the necessary current density in the windings. Typical limits for stator current density are shown in Table 7 and in this paper it is assumed that the limit on current density (J) is 3000 A/cm^2 [18].

Table 7: Stator Current Densities

Cooling Method	J (A/cm^2)
Natural Convection	450 – 550
Fan Cooled	800 – 1200
Liquid Cooled	2300 – 3200

The disadvantages of the slots are that cogging torque may be a problem and it can be costly to insert the windings if proper construction techniques are not used. Overall, however, slotted designs are preferred in high-power applications and therefore a slotted stator is selected for the 16 MW PM generator.

The number of slots in the machine is usually a function of the number of phases and windings and can vary based on the application. The initial design of the generator assumes a three-phase machine but the number of phases will be examined to determine an optimum design. In order to allow for high-power operation and the possibility of a high number of phases, 36 slots is chosen for the initial generator design.

3.2.2 Rotor Mechanical Design

For high-speed applications, the rotor aspect ratio, defined as length-to-diameter (L/D), is a critical parameter. If it is relatively low, then the rotor has high stiffness and good dynamics but a large diameter which increases the weight and makes magnet retention extremely difficult. Additionally, the centrifugal force on the surface-mounted magnets is directly proportional to the rotor diameter so the rotor radial size must not be excessive.

Permanent magnet machines offer flexibility in selecting pole sizes which allows for smaller diameters. They are therefore ideal for high-speed applications because they can have higher L/D ratios. This is because they do not have rotor field windings which have end turns necessitating big pole pitches and large diameters. A normal L/D ratio for a wound rotor machine is 0.5 – 1.0 compared to 1 – 3 for a PM machine [27]. Staying close to these ranges usually provides a first order estimate of satisfactory machine dynamic performance and acceptably low vibrations or oscillations.

The rotor radius and the rotational speed also determine the tip speed of the machine which is the surface velocity of the rotor (as defined by Eqn 3-1).

$$v_{tip} = R \cdot \omega_m$$

where ω_m = angular speed (rad/sec)
R = rotor radius (m)

Eqn 3-1

For most rotating machines, the upper limit on tip speed is between 100 – 250 m/s depending on the design. For surface magnet PM machines, retaining sleeves are sometimes used to help keep the magnets in place and allow for higher speeds. These sleeves can be constructed from alloy steel, carbon fiber, or other materials. The metal sleeves usually provide increased mechanical performance but have eddy current losses.

The carbon fiber and graphite composite sleeves have high strength-to-weight ratios which produce a thin sleeve and the sleeve's lower conductivities yield reduced eddy current losses. However, the carbon fiber and graphite composite sleeves have lower temperature ratings and lower thermal conductivities making heat removal and increased cooling for the magnets and sleeve important issues [28]. Overall, the use of a retaining sleeve is necessary for the 16 MW generator since it is operating at high-speed and this allows the maximum tip speed limit at the rotor surface to be 200 m/s. The actual material for the retaining sleeve is examined later when detailed rotor loss analysis is performed.

3.2.3   Number of Poles and Magnet Pole Design

The optimum number of poles is a complex function depending on a number of factors including the magnet material, the speed of rotation, the desired output frequency, and the mechanical assembly of the rotor. An even number of poles is always used because this provides a balanced rotational design. As the number of poles increases, the individual pole pitch goes down which reduces the amount of stator back iron needed to support the magnetic flux. In addition, for a given power/torque, as the pole number rises, the required magnet volume decreases.

Assuming a constant mechanical rotation speed, the generated electrical frequency is proportional to the number of poles as shown in Eqn 3-2.

$$N \cdot (2p) = 120 \cdot f$$

where   N = speed (RPM)
p = number of pole pairs
f = electrical frequency (Hz)

Eqn 3-2

If a PM generator is going to be the source for a DC bus through a rectifier system, a high pole number is desirable because as the electrical frequency increases, support components such as filter capacitors and inductors can be much smaller. Therefore, for a given rotational speed, one cheap and efficient solution is to have a higher number of pole pairs and frequency [27]. However, as the frequency increases, higher stator losses result because core losses are proportional to frequency squared. In addition, as the pole number gets larger, the number of slots per pole per phase decreases and can cause the voltage waveforms to become less sinusoidal so all factors must be considered.

35

The pole arc of the magnets can also be varied. Magnets seldom span the full pole pitch because the flux at the transition between north and south poles leaks between poles without linking the coils in the stator. The gaps between the poles usually contain non-magnet pieces, such as soft-iron, so that no flux crosses over the air gap between magnets. A full pole arc is θ_{me} = 180^0 E and produces a full voltage waveform but has increased harmonic content. As the pole arc is reduced (up to 20 – 30 %) and those areas are filled in with soft-iron pieces, the resulting flux waveform is more sinusoidal and has fewer harmonics and therefore lower rotor losses [29].

The magnet poles are sometimes skewed to reduce cogging torque and smooth out variations in air gap reluctance, flux, and voltage waveforms. Skewing of the magnets occurs axially along the length of the rotor to provide a constant rotational torque and prevent pole pieces from exactly lining up with stator teeth. A skew factor is used to account for this effect and is shown in Eqn 3-3.

$$k_{sn} = \frac{\sin\left(n\theta_s\right)}{\dfrac{\theta_s}{2}} \qquad \text{where} \quad \begin{aligned} &\theta_s = \text{skew angle, radE} \\ &n = \text{harmonic number} \end{aligned}$$

Eqn 3-3

As the pole number is increased, the stator conductors-per-pole decreases so that the per-unit inductance and synchronous reactance decreases with higher pole number. This can sometimes result in improved performance of the machine since the reactance is lower. Overall, the initial 16MW generator has 6 poles but this is examined later to determine an optimal design.

3.2.4 Magnetic Dimensions

The primary magnetic dimensions that affect a PM machine are the air gap and the magnet height. These two parameters play a major role in determining the air gap magnetic field, the air gap flux density, and the induced voltage in the machine. To a first order approximation, the air-gap flux density (B_g) can be represented by Eqn 3-4 [30].

The radial air gap is usually made as small as possible to maximize the air gap flux density, minimize the flux leakage, and produce a lower reluctance value since the air gap constitutes the largest part of the machine permeance/reluctance. However, the use of rare-earth permanent magnets (NdFeB or SmCo) with their higher flux density and coercive force permit some flexibility in the size of the air gap.

$$B_g = \frac{h_m}{h_m + g} \cdot B_r$$

where h_m = magnet height (mm)

         g = air gap (mm)

         B_r = magnet remnant flux density (T)

Eqn 3-4

Once the permanent magnet material is selected, the desired air gap flux density and induced voltage help determine the magnet height needed. If the magnet height is too large, the air gap flux density might be significant enough to cause the stator core material to saturate which reduces machine performance. The goal is to use the minimal amount of magnet material to achieve the desired effect because this reduces the size and weight of the machine and decreases the magnet material cost. Also, losses in the magnets can be reduced by using smaller magnets. In order to provide uniform magnetic fields, the magnet height is usually larger than the air gap by a factor of 5 – 10.

3.2.5 Number of Phases

In general, the number of phases affects a machine's power, current, and voltage ratings as shown in Eqn 3-5. If the power is fixed, then as the number of phases increases, the phase voltage and/or current decreases, assuming the total number of turns is constant.

$$|P + jQ| = q \cdot V \cdot I$$

where   P = real power (W)

         Q = reactive power (VAR)

         q = number of phases

         V = RMS phase voltage (V)

         I = RMS current (A)

Eqn 3-5

Most motors and generators are three-phase machines because it is the industry standard, it is the most common form of power, and it is the lowest number of phases that produces balanced torque with out pulsations in rotating machines. However, higher utilizations in generators can be achieved with higher phase numbers especially if the generator is connected through power electronics to a DC bus distribution. This is because the higher number of phases produces lower ripple in the DC bus voltage.

However, the AC line current harmonics are more substantial in increased phase machines because the triple-n harmonics are higher order as the phase number increases. For example, a 3-phase machine suppresses harmonics of order 3n, a 5-phase machine eliminates order 5n, and a 7-phase machine removes order 7n. Therefore, in higher phase machines, a greater number of large harmonics result in the AC line current. Also, as the number of phases increases, the phase inductances and reactances change since there are a greater number of windings influencing each other.

Most machines are usually designed with the phases balanced meaning that they have an evenly-spaced phase distribution around the stator of the machine. This produces voltage waveforms that are identical in shape from phase to phase but differ by a phase offset angle. In order to initially size the PM generator, it is assumed to have three phases but this will be optimized later in conjunction with the power electronics module. It is also assumed that the phases are always balanced.

3.2.6   Slots per Pole per Phase

The number of slots per pole per phase (m) is an extremely important design parameter when considering generator design and it is calculated using Eqn 3-6. It is used to help determine the relationship and interactions between the rotor poles and the stator windings as well as shape the generated back voltage of the machine. When m is an integer, the machine is an integral slot machine and when m has a fractional part, it is a fractional slot machine.

$$m = \frac{N_s}{2 \cdot p \cdot q}$$

where N_s = number of slots
   p = pole pairs
   q = number of phases

Eqn 3-6

In an integral slot machine, the back EMFs of all of the coils making up a phase winding are in phase with each other and add up so that the final voltage amplitude is the direct sum of the individual coil voltages. In a fractional slot machine, the back EMF of all of the coils are not in phase so the net voltage has a different shape than the individual winding voltages. Varying the number of slots/pole/phase is one method used to produce a more sinusoidal voltage waveform and reduce the harmonics generated by the machine.

3.2.7 Stator Windings

The stator windings are the location where the generator voltage is induced due to the time varying magnetic flux caused by the permanent magnets on the rotor. In a slotted machine, the winding arrangement is used to help shape the back voltage to produce a more sinusoidal waveform. The windings can be distributed by three methods: pitch, skew, or breadth/distribution.

The pitch of a winding (α) refers to the angular displacement between the sides of a coil, usually expressed in electrical degrees or radians. When the individual coil pitch differs from 180^0 E, the winding is said to be short-pitched or fractional-pitched. This causes angular segments where the back voltage is zero because the flux linkage is constant and can help produce a sinusoidal waveform when multiple coils are connected. It also has the advantage of lowering the coil resistance and making the stator end windings more manageable.

Windings in the stator can also be skewed axially along the length of the machine. This requires the stator slots to be more intricately designed which complicates the mechanical construction of large machines. Therefore, since the generator being designed is a large, high-power machine, skewing of the stator windings is not used but skewing of the rotor is employed.

The breadth of a stator winding results from the coils occupying a distribution or range of slots within a phase belt. A stator winding normally consists of several coils each separated by an electrical angle γ. The distribution of the coils causes each to link the rotor flux slightly out of phase with each other so when they are added together, they produce a more sinusoidal waveform.

Within each stator slot, there are geometric size constraints which determine how many conductors can be placed in a slot. In smaller machines, coils are composed of round insulated wires that are placed in the stator slot along with insulation material. A slot fill factor (λ_s) is used to determine how much of the slot cross-sectional area is occupied by winding material as shown in Eqn 3-7.

$$\lambda_s = \frac{WindingArea}{TotalSlotArea}$$

Eqn 3-7

In larger machines, form-wound windings are used for ease of construction and for better performance. A sketch of what a form-wound winding looks like is shown in Figure 14.

39

Typically, machines contain two coil sides per slot making the winding a double-layer design [17], [18], [19]. Overall, slot fill factors vary in value from 0.30 – 0.70, depending on the number and size of the conductors in the slots as well as the amount of labor utilized. In this paper, a slot fill factor of 0.50 is assumed.
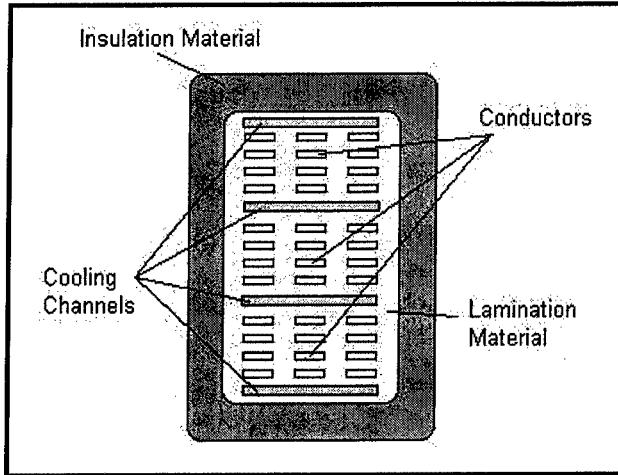
Figure 14: Example of Form-Wound Winding

In conductors that carry high-frequency currents, skin effect can become an issue and affect the operation of the machine. Skin effect is caused by eddy currents in the windings themselves due to the changing magnetic field. These eddy currents force the current flowing in the conductor to crowd to the outer edges of the conductor. This in turn causes the current to flow through a smaller cross-sectional area and increase the resistance of the conductor. However, the generator under design is expected to operate at less than 2 kHz and for frequencies below 12 kHz, $R_{AC}/R_{DC} < 1.01$ so skin effect can be neglected [32].

Within a phase, stator windings can be connected in wye or delta patterns as well as series or parallel. Almost all machines use series, wye-connected windings because they provide the safest alternative. This is because in a delta or parallel connection, the back EMFs can produce circulating currents which can result in addition losses, heating, or damage. Therefore, wye series connected windings are selected for use in the designs in this paper.

3.3 Machine Calculated Parameters

3.3.1 Basic Model

Since the machine is assumed to balanced, parameters can be determined on a per-phase basis and then applied to all of the phases. Each phase of the machine can therefore be modeled as shown in Figure 15.
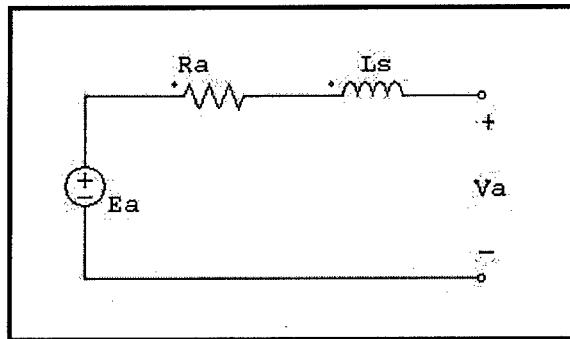
Figure 15: Per Phase Model

The armature resistance (R_a) is the resistance of the windings of the machine and it is usually relatively small. The synchronous inductance (L_s) of the machine comes from the inductance of the windings and is composed of the air gap inductance, the slot leakage inductance, and the end-turn inductance. The back voltage (E_a) is produced through the flux linkage in the windings from the rotating magnetic field in the machine. Lastly, V_a is the terminal voltage and is found using basic circuit analysis once the other parameters are known.

3.3.2 Winding Resistances

The stator coils in the machine are made of copper and therefore have some resistance to the current flow. This resistance of the copper phase windings is calculated using Eqn 3-8.

$$R_a = \frac{l}{\sigma \cdot A}$$

where   l = length of conductor
σ = winding conductivity
A = winding cross-sectional area

Eqn 3-8

The length of the conductor comes from the windings traveling twice the length of the machine and twice around the end turns of the machine. It is assumed that the end turns follow roughly a

41

circular path from one side of the machine to the other where the radius of the circle is the distance to one half the stator slot height. The cross-sectional area of the conductor is obtained from the slot area and slot fill factor as shown in Eqn 3-9, assuming form-wound windings.

$$A_{ac} = \frac{A_s \cdot \lambda_s}{2 \cdot N_c}$$

where A_s = slot area

N_c = turns per coil

Eqn 3-9

3.3.3 Winding & Magnet Factors

As discussed in section 3.2.7, windings are normally not full-pitched or concentrated but rather are short-pitched and have breadth associated with them. To account for these effects, a winding factor (k_w) is utilized which is the ratio of flux linked by an actual winding to the flux linked by a full-pitch, concentrated winding having the same number of turns. The winding factor is the product of a pitch factor (k_p) and a breadth/distribution factor (k_b) as shown in Eqn 3-10.

$$k_{wn} = k_{pn} \cdot k_{bn}$$

Eqn 3-10

The pitch factor accounts for the windings spanning α electrical degrees vice spanning a full 180^0 E as shown in Figure 16 [26].
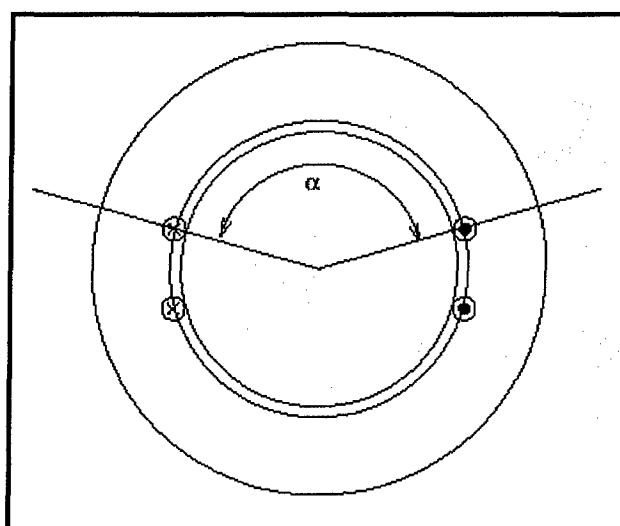
Figure 16: Short-Pitch Coil

The pitch factor is the ratio of the flux produced by a short-pitch coil to the flux produced by a full-pitch coil. Short-pitching is an important means for eliminating harmonics and improving the power quality of the machine. The pitch factor can be derived with the final result shown in Eqn 3-11.

$$k_{pn} = \sin\left(\frac{n \cdot \alpha}{2}\right) \cdot \sin\left(\frac{n \cdot \pi}{2}\right)$$

where n = harmonic number

Eqn 3-11

The breadth factor explains the effect of the windings occupying a distribution or range of slots within a phase belt. A phase winding normally consists of numerous coils connected together linking flux slightly out of phase with each other as shown in Figure 17 [26].
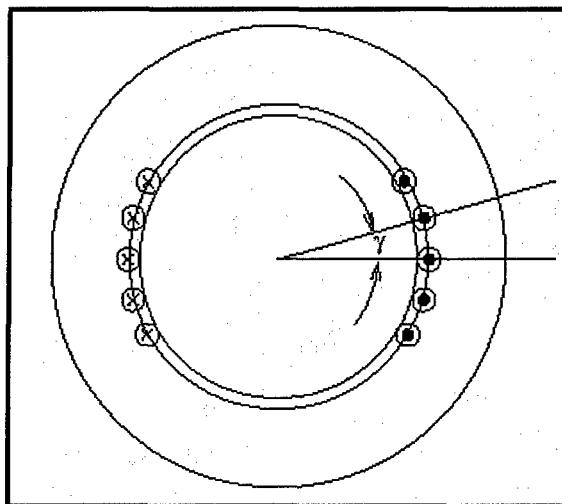
Figure 17: Winding Breadth

The breadth factor can be derived either magnetically or geometrically to obtain Eqn 3-12.

$$k_{bn} = \frac{\sin\left(\frac{n \cdot m \cdot \gamma}{2}\right)}{m \cdot \sin\left(\frac{n \cdot \gamma}{2}\right)} \qquad \text{where} \quad \begin{array}{l} n = \text{harmonic number} \\ m = \text{slots per pole per phase} \\ \gamma = \text{coil electrical angle} \end{array}$$

Eqn 3-12

In addition to estimating different winding effects, the geometry of the magnetic air gap must be represented. Field methods are utilized along with vector potential analysis to develop expressions that account for different magnetic gap geometries. Reference [19] contains detailed

derivations of the magnetic gap factor (k_{gn}) for several magnet and slot configurations. The equation for the slotted stator, surface magnet configuration is shown in Eqn 3-13.

$$k_{gn} = \frac{R_i^{np-1}}{R_s^{2np} - R_i^{2np}} \cdot \left[\left(\frac{np}{np+1} \right) \cdot \left(R_2^{np+1} - R_1^{np+1} \right) + \frac{np}{np-1} \cdot R_s^{2np} \cdot \left(R_1^{1-np} - R_2^{1-np} \right) \right]$$

where R_s = outer magnetic boundary R_2 = outer boundary of magnet
          R_i = inner magnetic boundary R_1 = inner boundary of magnet

Eqn 3-13

3.3.4 Flux and Voltage

The primary significance of the magnetic flux linkage in a machine is that it induces voltage across a winding whenever the flux varies with time as explained through Faraday's Law. The first step in the process is to determine the air gap flux density. The flux from the magnet poles crosses the air gap to the stator windings but some flux leaks along the way and this is accounted for using a leakage factor ($K_l \sim 0.95$ for surface magnets). In addition, the flux path is normally dominated by the air gap reluctance since the reluctance of the stator steel is much less than that in the air gap. However, a reluctance factor ($K_r \sim 1.05$ for surface magnets) is used to compensate for the small effects of the steel reluctance on the air gap flux.

The presence of the slots in the stator also affects the air gap flux density because of the difference in permeance caused by the slots. The flux crossing the air gap in a slot region travels farther before reaching the highly permeable stator back iron. Carter's coefficient (K_c) is used to account for this effect [17]. The air gap flux density is also affected by the magnet geometry in the air gap as previously described by Eqn 3-13. Since the magnet poles rotate north/south, the air gap flux density shape can be approximated as shown in Figure 18. This can be represented as a Fourier series using only odd components because of half-wave symmetry as shown in Eqn 3-18. Overall, the air gap flux density is calculated using Eqn 3-14 through Eqn 3-18.
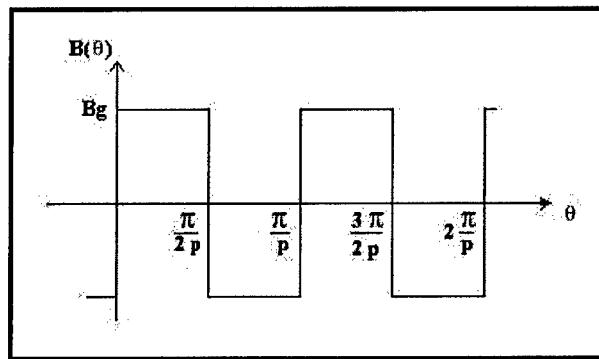
Figure 18: Air Gap Flux Density

$$K_c = \left[1 - \frac{1}{\frac{\tau_s}{w_s} \cdot \left(5 \cdot \frac{g}{w_s} + 1 \right)} \right]^{-1}$$

where w_s = average slot width
w_t = tooth width
$\tau_s = w_s + w_t$

Eqn 3-14

$$g_e = K_c \cdot g$$

where g_e = effective air gap

Eqn 3-15

$$PC = \frac{h_m}{g_e \cdot C_\phi}$$

where PC = permeance coefficient
C_ϕ = flux concentration factor (A_m / A_g)

Eqn 3-16

$$B_g = \frac{K_l \cdot C_\phi}{1 + K_r \cdot \frac{\mu_{rec}}{PC}} \cdot B_r$$

where μ_{rec} = recoil permeability
B_r = remnant flux density

Eqn 3-17

45

$$B(\theta) = \sum_{\substack{n=1 \\ n \text{ odd}}}^{\infty} B_n \cdot \sin(np\theta)$$

where $\quad B_n = \dfrac{4}{n\pi} \cdot B_g \cdot k_{gn} \cdot \sin\left(\dfrac{np\theta_m}{2}\right) \cdot \sin\left(\dfrac{n\pi}{2}\right)$

θ_m = magnet physical angle

n = harmonic number

Eqn 3-18

Once the flux density is known, the flux must be calculated. Given a machine uniform in the axial direction, the flux linked by a single, full-pitched coil which spans an angle from 0 to π/p is represented by Eqn 3-19. Assuming B_{flux} is sinusoidally distributed, the peak flux for this ideal coil is given by Eqn 3-20.

$$\Phi = \int_0^{\frac{\pi}{p}} B_{flux} \cdot R_s \cdot L_{st} \, d\theta \quad \text{where } B_{flux} = \text{radial flux through coil}$$

Eqn 3-19

$$\Phi_{pk} = \frac{2 \cdot R_s \cdot L_{st} \cdot B_{flux}}{p}$$

Eqn 3-20

Given that there are N_a coils in a stator phase winding and including all the real winding effects, the total flux linkage is shown in Eqn 3-21. Through Faraday's Law, the back EMF for the machine is given by Eqn 3-22.

$$\lambda(\theta) = \sum_{\substack{n=1 \\ n \text{ odd}}}^{\infty} \lambda_n \cdot \sin(np\theta)$$

where $\quad \lambda_n = \dfrac{2 \cdot R_s \cdot L_{st} \cdot N_a \cdot B_n \cdot k_{wn} \cdot k_{sn}}{p}$

Eqn 3-21

$$E_a = \sum_{\substack{n=1 \\ n \text{ odd}}}^{\infty} V_n \cdot \sin(np\,\theta)$$

where $V_n = \dfrac{d}{dt}\lambda_n = \omega_0 \cdot \lambda_n$

<div align="right">**Eqn 3-22**</div>

With permanent magnet excitation, the field cannot be controlled as in a wound-rotor machine so the number of turns in the stator phase windings must be chosen so that the machine EMF is close to the nominal system voltage. Another option is to use power electronics to convert the machine EMF to the system voltage thereby providing steady regulation.

Another effect that is sometimes an issue is armature reaction. It is caused by current flowing in the stator windings which creates a magnetic field that tends to distort the magnetic field established by the permanent magnets. For surface-magnet machines, because the magnet recoil permeability is approximately one and the magnet height is large compared to the air gap, the armature reaction flux density is small. As long as the stator teeth are not highly saturated due to the permanent magnets, armature reaction is negligible [17], [18].

3.3.5 Machine Inductances

In a slotted permanent magnet machine, there are three distinct components of inductance: air gap inductance, slot leakage inductance, and end-turn inductance. The most accurate means for calculating these parameters is finite element analysis but analytical methods provide almost as good results (within a couple of percent) and are used in this paper [33].

The air gap inductance is usually the largest portion of the total inductance and it is due to the interaction of the stator windings with the flux crossing the air gap. To calculate the air gap inductance, a full-pitch, concentrated winding carrying a current I is initially examined which leads to an air gap flux density shown in Eqn 3-23.

$$B_{flux} = \sum_{\substack{n=1 \\ n \text{ odd}}}^{\infty} B_n \cdot \sin(np\,\theta)$$

where $B_n = \dfrac{4}{n\pi} \cdot \dfrac{\mu_0}{(g + h_m)} \cdot \dfrac{N_a \cdot I}{2p}$

<div align="right">**Eqn 3-23**</div>

When this concept is expanded to polyphase windings with balanced operation, the air gap flux density becomes Eqn 3-24.

$$B_{flux} = \sum_{\substack{n=1 \\ n \, odd}}^{\infty} B_n \cdot \sin(np\theta) \qquad \text{where} \qquad B_n = \frac{q}{2} \cdot \frac{4}{n\pi} \cdot \frac{\mu_0}{(g + h_m)} \cdot \frac{N_a \cdot I}{2p}$$

Eqn 3-24

The flux can be found using equation Eqn 3-19 and the total flux linkage is $\lambda = N_a\Phi$. With all real winding effects included, the air gap inductance is then given by Eqn 3-25.

$$L_{ag} = \frac{\lambda}{i} = \frac{q}{2} \cdot \frac{4}{n\pi} \cdot \frac{\mu_0 \cdot R_s \cdot L_{st} \cdot N_a^2 \cdot k_{wn}^2}{n^2 \cdot p^2 \cdot (g + h_m)}$$

Eqn 3-25

In addition to the air gap, the coil currents generate a magnetic field that crosses from one side of the slot to the other producing a slot leakage inductance. For calculating the slot leakage inductance, it is assumed that the slot is rectangular with slot depressions (Figure 13) which results in a slot permeance per unit length shown in Eqn 3-26 [17], [18], [19].

$$Perm = \frac{1}{3} \cdot \frac{h_s}{w_{st}} + \frac{h_d}{w_d}$$

Eqn 3-26

Assuming m slots per pole per phase and a standard double layer winding, it can be shown that the slot leakage inductance is given by Eqn 3-27 through Eqn 3-29 [19].

$$L_{as} = 2 \cdot p \cdot L_{st} \cdot Perm \left[4 \cdot N_c^2 (m - N_{sp}) + 2 \cdot N_{sp} \cdot N_c^2 \right] \qquad \text{(self)}$$

Eqn 3-27

$$L_{am} = 2 \cdot p \cdot L_{st} \cdot Perm \cdot N_{sp} \cdot N_c^2 \qquad \text{(mutual)}$$

Eqn 3-28

48

$$L_{slot} = L_{as} - L_{am} \qquad \text{(3phase)}$$

$$L_{slot} = L_{as} - 2 \cdot L_{am} \cdot \cos\left(\frac{2\pi}{q}\right) \qquad \text{(higher odd phases)}$$

<div align="right">**Eqn 3-29**</div>

The end turn inductance is the smallest of the three components. It is created by the magnetic field that surrounds a coil after it leaves one slot and before it enters another slot. Since it is extremely difficult to accurately determine because of complex winding patterns, a rough approximation is used. It is assumed that the end turns are semi-circular with a radius equal to one-half the mean coil pitch. Using reference [17], the total end turn inductance per phase is shown in Eqn 3-30.

$$L_e = \frac{\mu_0 \cdot N_c \cdot N_a^2 \cdot \tau_s}{2} \cdot \ln\left(\frac{\tau_s \cdot \pi}{\sqrt{2 \cdot A_s}}\right)$$

<div align="right">**Eqn 3-30**</div>

The total inductance for the phase is the sum of the three inductances, ignoring other small factors..

$$L_s = L_{ag} + L_{slot} + L_e \qquad X_s = \omega_0 \cdot L_s$$

<div align="right">**Eqn 3-31**</div>

3.3.6 Basic Losses

Losses in a machine consist of core losses, conductor losses, friction and windage losses, and rotor losses. Rotor losses include magnet losses and retaining can losses, they require detailed waveform and harmonic analysis, and therefore are discussed later in Chapter 5.

3.3.6.1 Core Losses

High-speed generator stator core losses (per weight) can be greater than normal machines because of the higher frequencies. These losses are minimized by using laminated steels in the stator construction as discussed in 3.1.2 and by not generating frequencies that are too high.

Core losses consist of hysteresis and eddy current losses. Hysteresis loss results from the steel not wanting to change magnetic state. As the flux density varies, the material traverses the B-H curve and energy is lost. Eddy current loss is also caused by the variation in flux density.

Electrical currents are induced within the ferromagnetic material and circulate dissipating power because of the resistivity of the material.

Because there are usually various imperfections in materials, the best way to approximate core losses is to use empirical loss data. If the flux density is estimated for each part of a machine and the mass of the steel calculated, empirical core loss data can be used to estimate the total losses. Empirical data for M-19, 29 gauge material is obtained as shown in Figure 19.
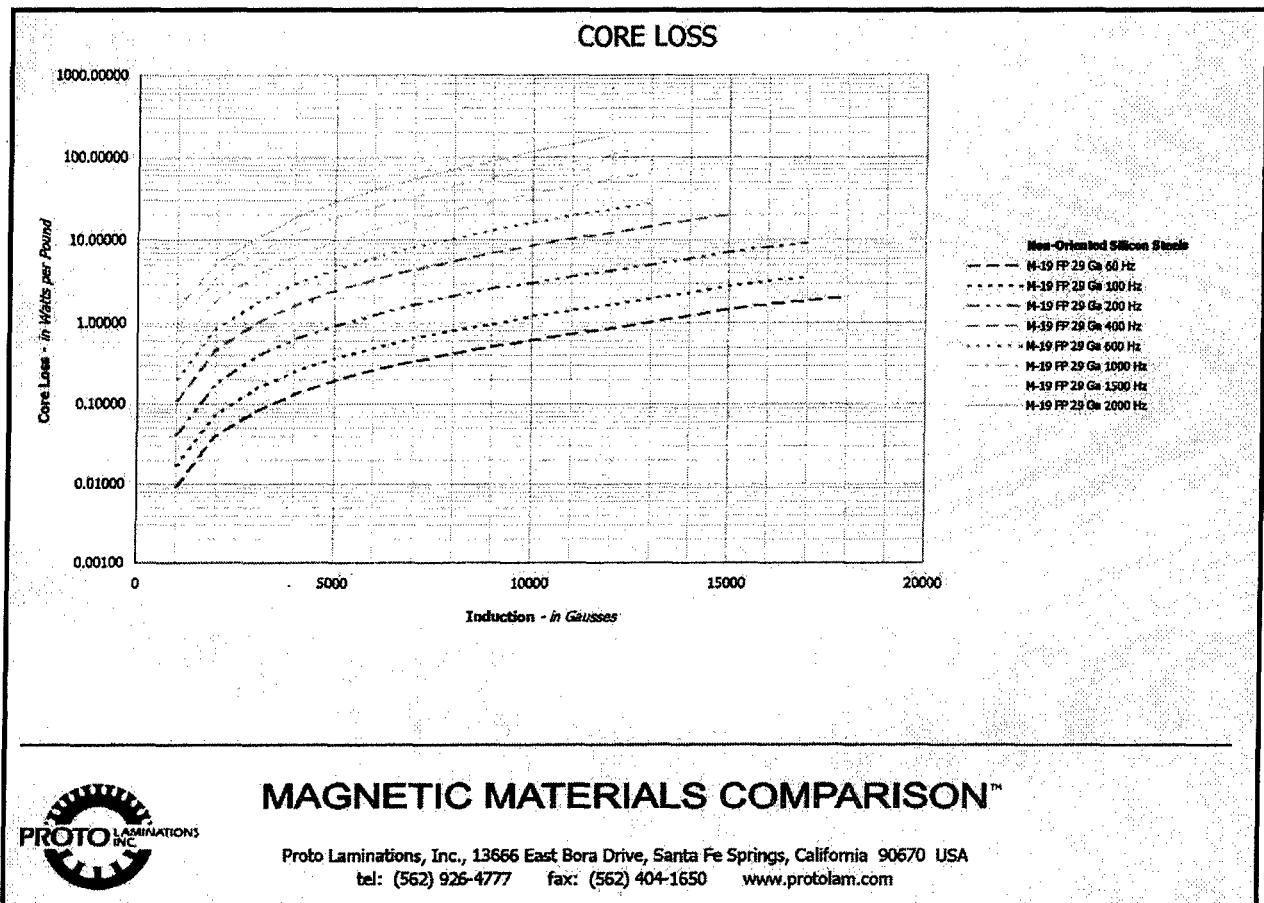
Figure 19: Core Loss Data

An exponential curve fit is then applied to the data to obtain an equation for estimating the core losses (Eqn 3-32) [9], [35], [36].

$$P_c = P_0 \cdot \left(\frac{B}{B_0}\right)^{\varepsilon_B} \cdot \left(\frac{f}{f_0}\right)^{\varepsilon_f}$$

Eqn 3-32

The values for the bases and exponents in Eqn 3-32 are listed in Table 8.

50

Table 8: Core Loss Parameters

Parameter	Value
Base Power (P_0)	36.79 W/lb
Base Flux Density (B_0)	1.0 T
Flux Density Exponent (ε_B)	2.12
Base Frequency (f_0)	1000 Hz
Frequency Exponent (ε_f)	1.68

3.3.6.2 Conductor Losses

Conductor losses arise from the current flowing in the stator windings. The resistance of the windings is calculated using Eqn 3-8 from section 3.3.2. The conductor losses are then found using the traditional power equation for a resistance (Eqn 3-33).

$$P_a = q \cdot I_a^2 \cdot R_a$$

Eqn 3-33

3.3.6.3 Friction & Windage Losses

For rotors operating at high-speed, friction and windage in air can cause losses which result in inefficiency and heat production. These losses are calculated using the power necessary to overcome the drag resistance of a rotating cylinder as given by Eqn 3-34 [32].

$$P_{wind} = C_f \cdot \pi \cdot \rho_{air} \cdot \omega^3 \cdot R^4 \cdot L_{st}$$

$$\text{where} \quad C_f = \text{friction coefficient}$$
$$\rho_{air} = \text{density of air}$$

Eqn 3-34

The friction coefficient depends on numerous factors such as surface roughness and flow region. Since the air gap is a small annulus and the rotor is spinning at high speed, it is assumed that the air in the gap is in the turbulent region. Therefore, the coefficient of friction can be approximated by Eqn 3-35 [34].

$$C_f \approx 0.0725 \cdot Rey^{-0.20}$$

$$\text{where Rey} = \text{Reynold's Number}$$

Eqn 3-35

3.4 Machine Sizing Methods

3.4.1 Basic Sizing Method

Whenever a machine is being designed, it is important to perform some back-of-the-envelope calculations to gain insight into initial sizing estimates. Most generators are constrained by two competing design parameters, air gap magnetic shear stress and rotor tip speed. Air gap magnetic shear stress (τ) is the magnetic shear force developed per unit gap area and is constrained by magnetic design and thermal management [8]. It is proportional to the product of the surface current density and magnetic flux density as shown in Eqn 3-36.

$$\tau \propto Kz \cdot B_g$$

where τ = shear stress (psi)

$\quad$ Kz = surface current density

$\quad$ B_g = air gap flux density

Eqn 3-36

Typical values for air gap shear stress for different types of generators are shown in Table 9 [8], [11], [16], [18], [31]. For the basic sizing calculations, 15 psi is assumed since the generator is a large liquid-cooled machine.

Table 9: Air Gap Shear Stress Values

Generator Type	Shear Stress (psi)
Small Air-Cooled	1 – 5 psi
Large Air-Cooled	5 – 10 psi
Large Liquid-Cooled	10 – 20 psi
High-Temperature Superconducting	30 – 50 psi

Rotor tip speed is discussed previously in section 3.2.2 and given by Eqn 3-1 with the assumed limit of 200 m/s. The fundamental machine power equation is utilized to derive the rotor radius and stack length of the machine (Eqn 3-37).

$$P = 2 \cdot \pi \cdot R \cdot L_{st} \cdot \tau \cdot v_{tip}$$

where $\quad$ R = rotor radius

$\quad\quad$ L_{st} = stack length

Eqn 3-37

In order to simplify the equation, the L/D ratio is substituted in for L_{st}. Using the air gap shear stress, the rotor tip speed limit, and the power rating of the machine (16 MW), the basic power equation is iterated to obtain a final L/D ratio, rotor radius, and stack length while matching the desired rotational speed of the machine (13,000 RPM). Using an air gap flux density of 0.8 T, a pole pair value of 3, a slot height of 15 mm, and a slot fill fraction of 0.5, the frequency and current density of the machine are found. The detailed MATLAB code is contained in Appendix B with the results shown below.

```
Basic Machine Design
Input Parameters:
Power      =     16000.0 kW        Shear Stress =      15.0 psi
L/D Ratio  =     2.85              Tip Speed    =      200.0 m/s
Pole Pairs =     3.0               Air Gap Bg   =      0.80 T
Output:
Rotor Radius =   0.147 m           Stack Length =      0.838 m
Speed      =     13000 RPM         Frequency    =      650.0 Hz
Ja         =     1757.67 A/cm2
```

3.4.2 Detailed Sizing Method One

Once basic sizing of the machine is complete, in-depth analysis is conducted to ascertain the overall performance and scale of the 16 MW generator. Two detailed sizing methods are developed using MATLAB code. To help gain an understanding for current PM machine designs, numerous articles, transactions, and proceedings are examined and a database is developed containing comprehensive specifications for over 20 different PM machines (see Appendix C). This database is used to help develop input parameters for the first method (Table 10), although many of these values are obtained after numerous iterations through the code.

Table 10: Input Parameters for Sizing Method 1

Parameter	Value	Parameter	Value
Required Power	16 MW	Number of Phases	3
Rotational Speed	13,000 RPM	Number of Slots	36
Power Factor Angle	0 deg	Slots Short-pitched	1
Rotor Radius	0.147 m	Peripheral Tooth Fraction	0.5
Magnet Height	25 mm	Slot Depth	25 mm
Stack Length	0.838 m	Slot Depression Depth	0.5 mm
Pole Pairs (p)	3	Slot Depression Width	N/A
Magnet B_r	1.2 T	Stator Back Iron Ratio	0.7
Magnet Angle	50^0 M	Turns per Coil	1
Magnet Skew Angle	10^0 M	Slot Fill Fraction	0.5

Air Gap	4 mm	Winding Conductivity	6.0×10^7 S/m
Steel Density	7700 kg/m^3	Conductor Density	8900 kg/m^3
Magnet Density	7400 kg/m^3		

Once the input parameters are entered, the first step in sizing is to generate the geometry of the machine. This includes determining the number of slots per pole per phase (Eqn 3-5), number of armature turns (Eqn 3-38), tooth width, slot dimensions, stator back iron dimensions, coil pitch, and winding end turn geometry.

$$N_a = 2 \cdot p \cdot m \cdot N_c$$

where N_c = Turns per coil

N_a assumes each slot has 2 half coils

Eqn 3-38

Next, the electrical frequency and rotor surface speed are determined using Eqn 3-1 and Eqn 3-39.

$$f = \frac{p \cdot N}{60} \qquad \omega = 2 \cdot \pi \cdot f \qquad \omega = p \cdot \omega_m$$

where ω = electrical frequency (rad/sec)

ω_m = mechanical frequency (rad/sec)

Eqn 3-39

Winding, skew, and magnetic gap factors are then estimated as discussed in sections 3.2.3 and 3.3.3. The magnitude of the air gap magnetic flux density (B_g) is determined accounting for slots, varying reluctances, and flux leakage per Eqn 3-14 through Eqn 3-17.

The magnetic flux and back voltage magnitudes can then be calculated. The fundamental component of the magnetic flux links the stator windings to create useful voltage. Therefore, only the fundamental components of Eqn 3-21 and Eqn 3-22 are used to determine the internal voltage of the generator as shown in Eqn 3-40 and Eqn 3-41.

$$B_1 = \frac{4}{\pi} \cdot B_g \cdot k_g \cdot \sin\left(\frac{p\theta_m}{2}\right)$$

Eqn 3-40

$$\lambda = \frac{2 \cdot R_s \cdot L_{st} \cdot N_a \cdot k_w \cdot k_s \cdot B_1}{p} \qquad E_a = \omega_0 \cdot \lambda$$

Utilizing equations from section 3.3.5, the machine inductances and reactances are established. The lengths, volumes, and masses of components and the overall generator are calculated using basic geometric equations and relationships. A 15% service mass fraction is added to the total mass estimate to account for the additional services associated with large liquid-cooled machines [31]. Once the mass of each of the stator parts is known, the core losses are estimated in accordance with section 3.3.6.1.

The terminal voltage and current of the machine must then be calculated accounting for conductor losses and windage losses. The vector relationship (Figure 20) between terminal voltage (V_a), internal voltage (E_a), and the synchronous reactance voltage drop is utilized to obtain Eqn 3-42. The armature resistance is usually ignored because it is much smaller than the synchronous reactance.
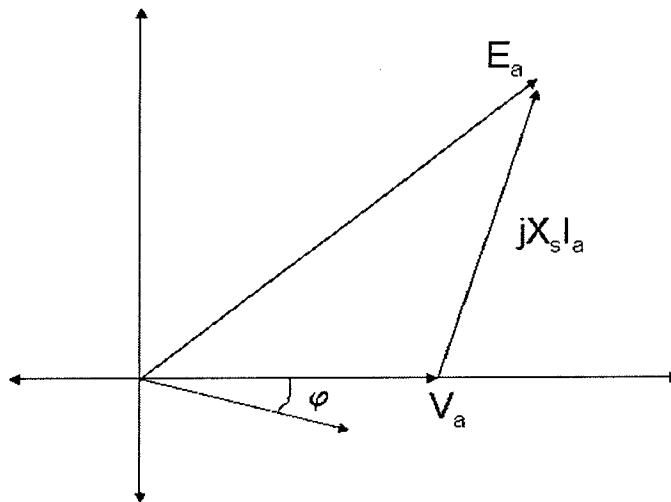
Figure 20: Voltage Vector Relationship

$$V_a = \sqrt{E_a^2 - \left(X_s \cdot I_a \cdot \cos\psi\right)^2} - X_s \cdot I_a \cdot \sin\psi$$

The machine efficiency (η) is then easily obtained. Appendix D contains the detailed MATLAB code and the results are shown below.

PM Machine Design, Version 1: Surface Magnet, Slotted Stator

Machine Size:

Machine Diameter =	0.472 m	Machine Length =	1.003 m
Rotor radius =	0.147 m	Active length =	0.838 m
Slot Avg Width =	16.493 mm	Slot Height =	25.000 mm
Back Iron Thick =	34.300 mm	Tooth Width =	15.403 mm

Machine Ratings:

Power Rating =	16000.0 kW	Speed =	13000 RPM
Va (RMS) =	2341 V	Current =	2267.5 A
Ea (RMS) =	2925 V	Arm Resistance =	0.00526 ohm
Synch Reactance =	0.768 ohm	Synch Induct =	0.188 mH
Stator Cur Den =	2199.7 A/cm2	Tip Speed =	200 m/s
Efficiency =	0.992	Power Factor =	1.000
Phases =	3	Frequency =	650.0 Hz

Stator Parameters:

Number of Slots =	36	Num Arm Turns =	12
Breadth Factor =	0.966	Pitch Factor =	0.966
Tooth Flux Den =	1.59 T	Back Iron =	1.14 T
Slots/pole/phase =	2.00		

Rotor Parameters:

Magnet Height =	25.00 mm	Magnet Angle =	50.0 degm
Air gap =	4.00 mm	Pole Pairs =	3
Magnet Remanence =	1.20 T	Aig Gap Bg =	0.80 T
Magnet Factor =	0.949	Skew Factor =	0.989

Machine Losses:

Core Loss =	11.6 kW	Armature Loss =	81.2 kW
Windage Loss =	30.7 kW	Rotor Loss =	TBD kW

Machine Weights:

Core =	396.49 kg	Shaft =	438.05 kg
Magnet =	64.74 kg	Armature =	89.58 kg
Services =	148.33 kg	Total =	1137.18 kg

3.4.3   Detailed Sizing Method Two

In order to provide a check on the methodology of the previous sizing procedure, a second MATLAB code is constructed. The second method is developed using a combination of processes from references [2], [17], [18], [19], [26], and [37].

Table 11: Input Parameters for Sizing Method 2

Parameter	Value	Parameter	Value
Required Power	16 MW	Current Density (J_a)	2200 A/cm^2
Rotational Speed	13,000 RPM	Number of Phases	3
Power Factor Angle	0 deg	Slots/Pole/Phase (m)	2
Maximum v_{tip}	200 m/s	Slots Short-pitched	1
B_{sat}	1.65 T	Avg Slot Width (w_s)	16.0 mm
Pole Pairs (p)	3	Slot Depth	25 mm
Magnet B_r	1.2 T	Slot Depression Depth	0.5 mm
Permeance Coefficient (PC)	5.74	Slot Depression Width	N/A
Magnet Skew Angle	10^0 M	Turns per Coil	1
Air Gap	4 mm	Slot Fill Fraction	0.5
Steel Density	7700 kg/m^3	Winding Conductivity	6.0 x 10^7 S/m
Magnet Density	7400 kg/m^3	Conductor Density	8900 kg/m^3

Many of the same equations used in the first method are utilized but the process differs in some of the input parameters and calculations. The second sizing method inputs are shown in Table 11 with different entries from method 1 being v_{tip}, B_{sat}, w_s, m, J_a, and PC.

First, given the maximum v_{tip} (200 m/s) and the rotational speed (13,000 RPM), the electrical frequency and rotor radius are computed. Next, the winding and skew factors are determined similar to the first sizing method. The magnet dimensions (h_m and θ_m) are then determined along with the air gap flux density. Using B_{sat}, the PC, and Eqn 3-43 through Eqn 3-46, the magnet arc width and height are iterated until the tooth width (w_t) equals the average slot width (w_s). This differs from the first method where the peripheral tooth fraction is used to set the tooth width equal to the slot top width (w_{st}).

$$C_\phi = \frac{2 \cdot \alpha_m}{1 + \alpha_m}$$

where α_m = magnet pitch coverage coefficient

Eqn 3-43

$$h_m = g_e \cdot C_\phi \cdot PC$$

Eqn 3-44

$$B_g = \frac{K_l \cdot C_\phi}{1 + K_r \cdot \dfrac{\mu_{rec}}{PC}} \cdot B_r \qquad \text{where} \quad \begin{aligned} \mu_{rec} &= \text{recoil permeability} \\ B_r &= \text{remnant flux density} \end{aligned}$$

<div align="right">**Eqn 3-45**</div>

$$w_t = \frac{\pi \cdot D_s}{N_s} \cdot \frac{B_g}{B_{sat}} \qquad \text{where } D_s = 2*(R + h_m + g)$$

<div align="right">**Eqn 3-46**</div>

The permeance coefficient (PC) normally varies between 5 – 15 with higher PCs only used for high performance space and aircraft applications [18], [37]. A PC value of 4 – 6 is typical for large PM machines where the air gap flux density is approximately 60 – 80% of the remnant flux density [17]. The PC is input as 5.74 to coincide with the PC calculated in the first sizing method.

Once the magnet dimensions are known, the geometry of the machine is generated using similar equations as the first method except for the stator core back iron depth. In the first method, the input variable "stator back iron ratio" is used whereas in the second method, the saturation flux density is applied as shown in Eqn 3-47.

$$d_c = \frac{\pi \cdot D_s \cdot \theta_m}{4 \cdot p} \cdot \frac{B_g}{B_{sat}}$$

<div align="right">**Eqn 3-47**</div>

Utilizing a power balancing procedure, the stack length, terminal voltage, and terminal current are iterated to obtain a complete design. Core losses, conductor losses, and windage losses are calculated in accordance with sections 3.3.6.1, 3.3.6.2, and 3.3.6.3. The power crossing the air gap of the machine is determined using Eqn 3-48 [2], [37].

$$P_{gap} = 4 \cdot \pi \cdot k_e \cdot k_i \cdot k_w \cdot k_g \cdot k_s \cdot \sin\left(\theta_m\right) \cdot \frac{f}{p} \cdot \left(K_z \cdot B_g\right) \cdot D_s^{\,2} \cdot L_{st}$$

<div style="padding-left: 2em;">where k_e = electrical power waveform factor
            k_i = current waveform factor</div>

<div align="right">**Eqn 3-48**</div>

<div align="center">58</div>

The electrical power waveform factor is defined in Eqn 3-49 and the current waveform factor is shown in Eqn 3-50. These factors depend on the back EMF and current waveforms generated in the machine and a detailed discussion of these factors is in reference [2].

$$k_e = \frac{1}{T} \cdot \int_0^T \frac{e(t) \cdot i(t)}{E_{pk} \cdot I_{pk}} \, dt$$

Eqn 3-49

$$k_i = \frac{I_{pk}}{I_{rms}}$$

Eqn 3-50

During the balancing procedure, the machine inductances and reactances are established per section 3.3.5. The lengths, volumes, and masses of components and the overall generator are calculated using basic geometric equations and relationships similar to the first sizing method. Once the balancing procedure is complete, the efficiency of the machine is determined. Appendix E contains the detailed MATLAB code and the results are shown below.

PM Machine Design, Version 2: Surface Magnet, Slotted Stator

Machine Size:

Machine Diameter =	0.484 m	Machine Length =	0.979 m
Rotor radius =	0.147 m	Active length =	0.813 m
Slot Avg Width =	16.000 mm	Slot Height =	25.000 mm
Back Iron Thick =	39.587 mm	Tooth Width =	15.863 mm

Machine Ratings:

Power Rating =	16000.0 kW	Speed =	13000 RPM
Va (RMS) =	2604 V	Current =	2064.1 A
Ea (RMS) =	3007 V	Arm Resistance =	0.00534 ohm
Synch Reactance =	0.723 ohm	Synch Induct =	0.177 mH
Stator Cur Den =	2064.1 A/cm2	Tip Speed =	200 m/s
Efficiency =	0.993	Power Factor =	1.000
Phases =	3	Frequency =	650.0 Hz

Stator Parameters:

Number of Slots =	36	Num Arm Turns =	12
Breadth Factor =	0.966	Pitch Factor =	0.966
Tooth Flux Den =	1.70 T	Back Iron =	1.05 T
Slots/pole/phase =	2.00		

Rotor Parameters:

Magnet Height =	26.17 mm	Magnet Angle =	47.7 degm
Air gap =	4.00 mm	Pole Pairs =	3
Magnet Remanence =	1.20 T	Aig Gap Bg =	0.85 T

Magnet Factor =	0.958	Skew Factor =	0.989
Machine Losses:			
Core Loss =	11.9 kW	Armature Loss =	77.5 kW
Windage Loss =	29.7 kW	Rotor Loss =	TBD kW
Machine Weights:			
Core =	438.62 kg	Shaft =	424.57 kg
Magnet =	62.89 kg	Armature =	85.50 kg
Services =	151.74 kg	Total =	1163.32 kg

3.4.4 Comparison of Methods

Both sizing methods produce similar sized generators with the results agreeing within 1 – 5% on most parameters. The main reasons for the differences are twofold. First, the calculations for the magnet dimensions are different. In the first method these parameters are input whereas in the second they are determined through an iterative process using material properties. Second, the procedure for determining the slot and tooth widths differs slightly.

Overall, both methods underestimate the overall dimensions (length and diameter) and weight. This is because the sizing programs do not include calculations for portions such as structure, frames, mounts, and maintenance access. These pieces are added in section 6.1 to get the total sizes and weights of the PM generators, specifically including:

- 50% weight factor added to total weight
- 0.8 m added to overall length and 0.4 m added to overall diameter

In later chapters when waveforms are examined and machine optimization occurs, the first sizing method is mostly employed with the second method used for verification.

Chapter 4 Power Electronics and Conversion

4.1 Background

In conjunction with employing a PM generator, a DC bus architecture is one of the preferred schemes for the future [5]. DC power distribution systems can offer an advantage in size and a weight over high-power AC systems [3]. Therefore, a power electronics module is required to rectify the AC generator output and then convert it to the appropriate DC distribution voltage of 700 VDC. However, conversion of the high-frequency generator AC output to DC generates harmonic voltages and currents on the AC side and ripple on the DC side. These harmonics can be reduced through proper design of the conversion module.

Since the generator is a permanent magnet machine, the field cannot be controlled like in a wound-rotor machine. The power electronics module (PEM) is needed not only to convert the machine EMF to the DC system voltage but also provide steady regulation. Also, since the frequency of the generator output is higher than the normal 60 Hz systems, the filter requirements for the PEM are less since the components can be smaller.

Many options exist for the type and model of the PEM, and a combination of a rectifier and DC-DC buck converter are chosen. This design provides a two-step conversion from the generator to the DC bus and allows for good DC bus voltage regulation while reducing harmonics reflected back to the generator. A block diagram of the system is shown in Figure 21. The calculations for the rectifier and buck converter are performed for the ideal case and ignore parasitics such as equivalent series resistance, inductance, and capacitance.
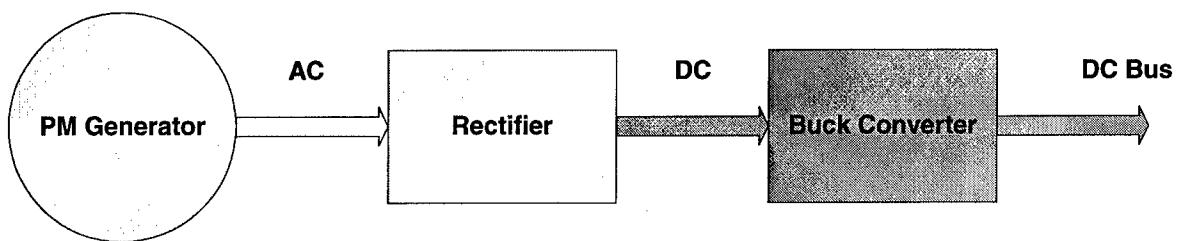
Figure 21: Basic System Layout

4.2 Rectification

The rectifier stage converts the AC voltage from the PM generator to a DC voltage. There are two main choices when designing the rectification stage: active or passive rectification and series or polyphase rectification. Active rectification uses controllable components, such as thyristors or MOSFETs, to actively rectify the AC voltage. This increases the cost and complexity of the rectifier but provides voltage regulation and control. Passive rectification consists of diode bridges to convert the AC to DC while relying on some other circuit to perform the voltage regulation. A passive rectification scheme is used in this paper because of its simplicity, potential for lower input harmonics, and lower cost.

Series rectification is when each phase is rectified independently from the others and the output DC voltage is obtained by a series connection of each single phase rectifier. Each phase conducts during the full period resulting in high power losses and higher stresses on components. Also, the output DC voltage is extremely high since each rectified phase voltage is added together. Parallel rectification is when the lines with the most positive and negative instantaneous voltages provide the forward bias to turn on two diodes. The output voltage waveform corresponds to the instantaneous difference between two line voltages. For sinusoidal voltage supplies, the equation for the output DC voltage is approximately Eqn 4-1 [38].

$$V_{DC} = \frac{2 \cdot n}{\pi} \cdot \sin\left(\frac{\pi}{n}\right) \cdot V_s$$

where V_s = peak amplitude of phase voltage

Eqn 4-1

The losses are lower with parallel rectification and its output voltage provides a better match with the buck converter. Therefore, a parallel rectification scheme is used in this paper. For the initial PM generator from section 3.4.2, the rectifier is shown in Figure 22.
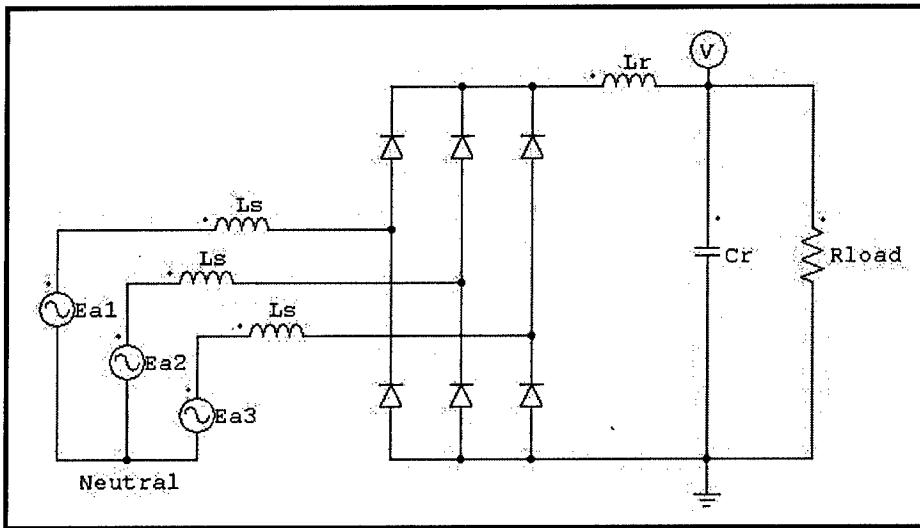
Figure 22: Basic 3-phase Rectifier

The DC-side inductor and capacitor are necessary to obtain a good DC output voltage with low ripple (large C) and an acceptable AC line current waveform (large L) [39]. The goal is to produce maximum power factor with minimal line-current harmonics. A power factor of 0.96 with low line harmonics can be achieved by selecting the inductor and capacitor values using Eqn 4-2 and Eqn 4-3 [40].

$$L_r = L_{on} \cdot \left(\frac{V_{ref}}{I_{ref} \cdot f_{ref}} \right)$$

where
$L_{on} = 0.10$
V_{ref} = nominal l-n RMS source voltage
$I_{ref} = P_{ref}/V_{ref}$ (RMS current from V_{ref})
P_{ref} = nominal output power
f_{ref} = nominal source frequency

Eqn 4-2

$$C_r = C_{on} \cdot \left(\frac{I_{ref}}{V_{ref} \cdot f_{ref}} \right)$$

where
$C_{on} = 100.0$
V_{ref} = nominal l-n RMS source voltage
$I_{ref} = P_{ref}/V_{ref}$ (RMS current from V_{ref})
P_{ref} = nominal output power
f_{ref} = nominal source frequency

Eqn 4-3

63

For the initial PM generator from section 3.4.2 where V_{ref} = 2925 V, P_{ref} = 16 MW, and f_{ref} = 650 Hz, the values for the DC-side inductor and capacitor are L_r = 82.3 μH and C_r = 287.7 mF. These values will change as the system is optimized.

4.3   DC-DC Conversion

After the rectifier converts the AC voltage to DC voltage, the DC voltage must be stepped down to the bus voltage of 700 VDC. A high-power buck converter is ideal for this application. The power circuit has a basic topology to which other circuit components are added to perform functions such as filtering and over-voltage protection [41]. The overall goal is to alter electrical energy provided by an input system to that required by an output system.

The system consists of a two-stage input filter, a converter, and a low-pass output filter as shown in Figure 23. Duty ratio control using a feedback controller could be used to provide DC bus voltage regulation during normal operation.
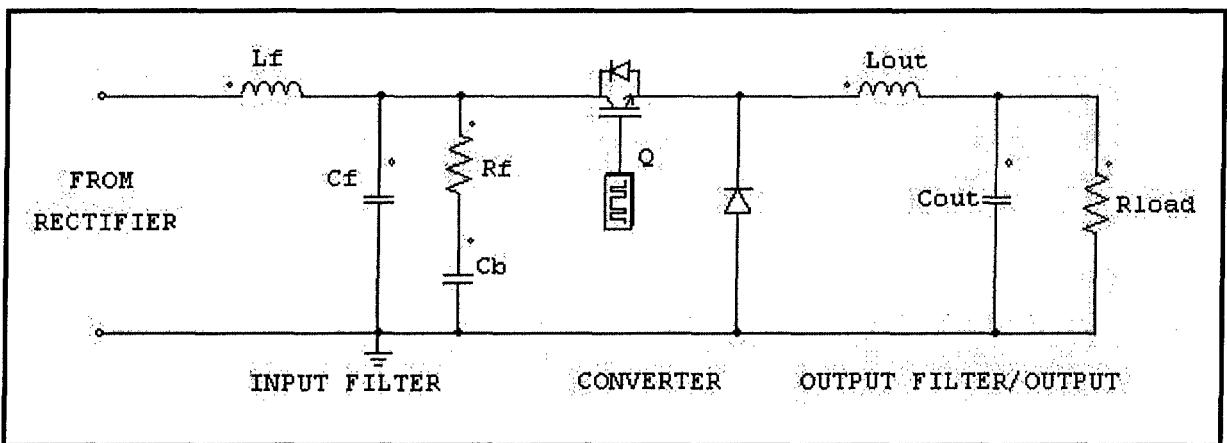
Figure 23: Basic Buck Converter

4.3.1   Buck Converter

The buck converter is considered a high-frequency DC-DC switching converter. The difference between the switching frequency and the frequency of the external waveforms allows the use of low-pass filters in the input and output to help improve performance [41]. The buck converter is designed to take a high DC voltage and reduce it to a lower DC voltage under varying loads and over a range of input voltages. The level of voltage reduction is controlled by the high frequency switching. The switch opens and closes at a specific frequency with the ratio of on-time to the period defined as D, the duty ratio.

For the buck converter, the voltage conversion ratio is dictated by Eqn 4-4.

$$\frac{V_{out}}{V_{in}} = D \qquad \frac{I_{out}}{I_{in}} = \frac{1}{D}$$

<div align="right">**Eqn 4-4**</div>

It is assumed that the required output power from the generator and PEM can be as high as the rated 16 MW and as low as 0.1 MW. Based on this, output currents and resistive load values are determined and are listed in Table 12.

Table 12: Buck Converter Load Values

Output Power	Output Voltage	Output Current	Load Resistance
0.1 MW	700 VDC	142.9 A	4.90 Ω
16 MW	700 VDC	22,857.1 A	0.031 Ω

The switching frequency for the converter is selected to be 50 kHz (T = 20 μsec). This is sufficiently fast to ensure passive components are not excessively large but also not too high speed so that there are not excessive switching losses. Additionally, current switching ratings for advanced, high-power IGBT devices are limited to the hundred kilohertz range. By selecting 50 kHz, this provides a margin below this maximum switching frequency and ensures devices are presently available or will be in the near future.

4.3.2 Output Filter

A low-pass output filter is required to help reduce the output voltage ripple to within the required specification listed in Table 2. The output voltage from the converter normally fluctuates between 0 and V_{OUT}, so the filter, consisting of an inductor and capacitor, is used to minimize this problem. It is important that the corner frequency of the filter be much lower that the switching frequency ($f_C \ll f_{SW}$) so that the switching frequency ripple is eliminated in the output voltage [42]. Normally, a factor of at least 100x is used [43], so to ensure an adequate margin for parasitics and fulfill the strict DC bus voltage ripple requirement, a factor of 400 is selected so that $f_C \sim 125$ Hz. For an LC-filter, Eqn 4-5 holds.

$$f_C = \frac{1}{2 \cdot \pi \cdot \sqrt{L \cdot C}}$$

<div align="right">**Eqn 4-5**</div>

Therefore, given the value selected for f_C:

$$L \cdot C = 1.62 \cdot 10^{-6}$$

<div align="right">**Eqn 4-6**</div>

With this equation the output filter inductor and capacitor are sized using a buck converter sizing program [44]. It is assumed that an inductor current ripple of 0.1% at maximum power (16 MW) is satisfactory for sizing the inductor and Eqn 4-7 is used where $V_F = 1.9$ V, the forward-bias diode voltage [44].

$$L = \left(\frac{1}{f}\right) \cdot \left(V_{in\_max} - V_{out}\right) \cdot \left(\frac{V_{out} + V_F}{V_{in\_max} + V_F}\right) \cdot \left(\frac{1}{\Delta I_L}\right)$$

<div align="right">**Eqn 4-7**</div>

For the initial generator of section 3.4.2, this produces an inductor size of 551 μH. Using this inductance along with Eqn 4-6, a capacitor value of 2.94 mF is calculated.

In order to validate the filter's performance, a rough estimate for the voltage ripple is calculated. It is assumed that the ripple component of inductor current flows through the capacitor and the average component of the output current flows through the load resistor [42]. Therefore, the peak-to-peak voltage ripple can be written as shown in Eqn 4-8.

$$\Delta V_o = \frac{\Delta Q}{C} = \frac{1}{C} \cdot \frac{1}{2} \cdot \frac{\Delta I_L}{2} \cdot \frac{T_s}{2}$$

<div align="right">**Eqn 4-8**</div>

The output voltage ripple is estimated to be 0.019 V which is within the specification listed in Table 2. This overall process is used later to design the converter output filter as the PM generator system is optimized.

4.3.3 Input Filter

The input filter is needed to prevent the converter switching fluctuations from affecting the voltage and current from the rectifier. The filter selected is a two-stage filter with an L-C filter and an R-C damping leg. From the switching frequency, the angular frequency is $\omega = 3.142 \times 10^5$ rad/sec. In order to examine worst case, the 16 MW, 22,857 A-output is used, and with the corresponding duty ratio of 0.1023 for the generator of section 3.4.2, an average current

of 2,338.3 A is calculated. Since the fundamental of the ripple is attenuated much less than the higher harmonics, the goal is to suppress the fundamental of the ripple along with some margin. The fundamental of the average current is calculated in Eqn 4-9.

$$i_{conv1} = \frac{4}{\pi} \cdot <i_{conv}> = \frac{4}{\pi} \cdot (2338.3) = 2977.2 Amps$$

<div align="right">**Eqn 4-9**</div>

It is assumed that the buck converter input current ripple must be kept very small (< 10 A at maximum power) to ensure no detrimental effects on the rectifier. Therefore, at the 50 kHz switching frequency, the maximum gain of filter is G as calculated in Eqn 4-10.

$$G = \frac{<i_{source}^{ripple}>}{i_{conv1}} = \frac{\dfrac{10.0 Amps}{2}}{2977.2} = 0.00168$$

<div align="right">**Eqn 4-10**</div>

In order to account for the contribution of higher harmonics and non-idealities associated with actual components, a 50% margin is used for G resulting in $G = 2.52 \times 10^{-3}$.
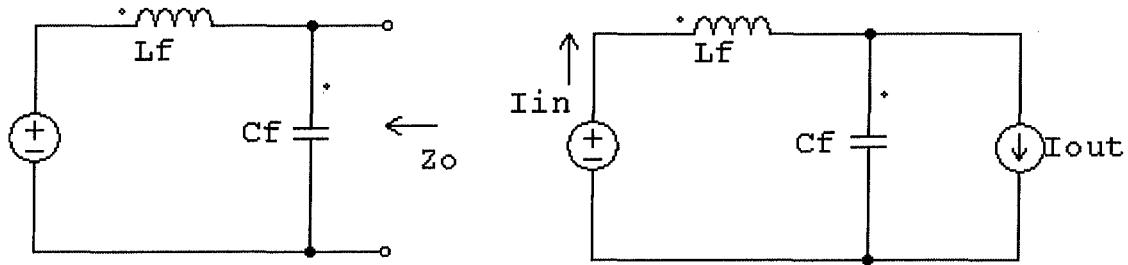
The output impedance of the input filter is also a concern because it must be sufficiently small so that it does not adversely affect the converter's performance. It is assumed that the output voltage ripple of the filter must be less than 10 V at maximum power. From this, a value of Z_O at 50 kHz is calculated (Eqn 4-11).

$$Z_o = \frac{\dfrac{10.0 \, V}{2}}{2977.2} = 0.00168$$

<div align="right">**Eqn 4-11**</div>

Using the same margin of 50% for the same reasons, the output impedance is 1.12×10^{-3}.

Initially, the L-C low pass filter portion is examined to calculate values for L_f and C_f. Then, a well-designed filter has $C_b \sim 10*C_f$, and R_f is determined using reference [39]. The calculations are listed below.

$$Z_o = \frac{Z_L \cdot Z_C}{Z_L + Z_C}$$

$$i_{in} = \frac{Z_C}{Z_C + Z_L} \cdot i_{out}$$

$$Z_o = \frac{s \cdot L}{1 + s^2 \cdot L \cdot C}$$

$$G = \frac{i_{in}}{i_{out}} = \frac{Z_C}{Z_C + Z_L}$$

$$1.12 \, 10^{-3} = \frac{s \cdot L}{1 + s^2 \cdot L \cdot C}$$

$$2.52 \, 10^{-3} = \frac{1}{1 + s^2 \cdot L \cdot C}$$

$$1.12 \, 10^{-3} + 1.12 \, 10^{-3} \cdot s^2 \cdot L \cdot C = s \cdot L$$

$$2.52 \, 10^{-3} + 2.52 \, 10^{-3} \cdot s^2 \cdot L \cdot C = 1$$

$$s \cdot L = 0.444$$

$$s^2 \cdot L \cdot C = 395.83$$

$$L_f = 1.415 \, uH$$

$$s \cdot C = 891.51 \qquad C_f = 2.84 \, mF$$

Eqn 4-12

$$C_b = n \cdot C_f = 10 \cdot C_f = 28.4 \cdot mF$$

$$R_o = \sqrt{\frac{L_f}{C_f}} = 0.0223$$

$$\frac{R_f}{R_o} = \sqrt{\frac{(2 + n) \cdot (4 + 3n)}{2 \cdot n^2 \cdot (4 + n)}}$$

$$R_f = 0.215 \cdot R_o = 4.79 \cdot 10^{-3}$$

Choose 10*Rf to be safe $\qquad R_f = 4.79 \, m\Omega$

Eqn 4-13

The performance of the input filter is determined by examining the filter's transfer function and verifying it has sufficient attenuation at the switching frequency and also minimal peaking. The transfer function for the filter is given in Eqn 4-14 [45].

$$TF = \frac{\left(R_f \cdot C_b \cdot s\right) + 1}{\left(L_f \cdot C_f \cdot C_b \cdot R_f \cdot s^3\right) + \left[L_f \cdot \left(C_f + C_c\right) \cdot s^2\right] + \left(R_f \cdot C_b \cdot s\right) + 1}$$

<div align="right">**Eqn 4-14**</div>

Figure 24 shows the Bode plot for the initial input filter and it operates satisfactorily (Appendix F contains the detailed MATLAB code). This overall procedure for designing the converter input filter is utilized later to as the PM generator system is optimized.
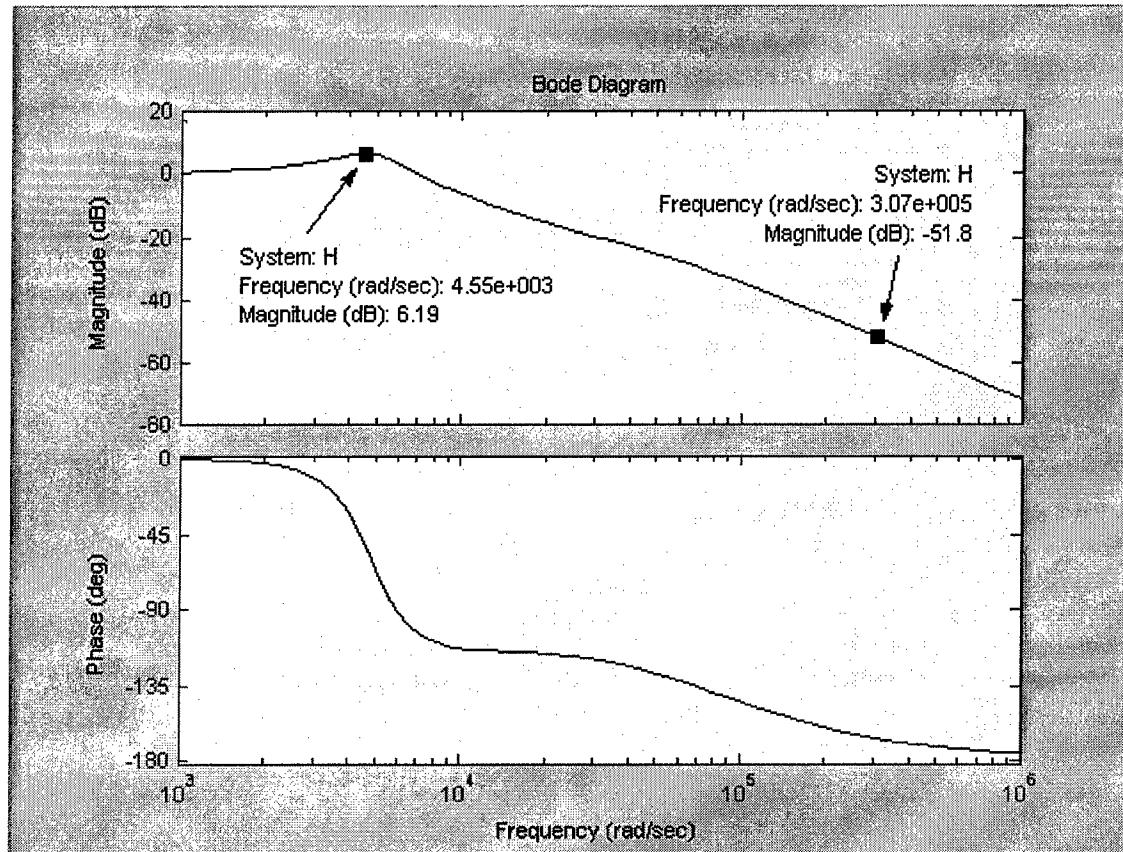
Figure 24: Bode Plot for Converter Input Filter

4.3.4   Converter Control

One control technique that can be used is duty ratio control utilizing a feedback controller. This arrangement is presented as an illustration of one control methodology for the power electronics module but implementation is beyond the scope of this paper.

The control scheme involves negative feedback control using linearized, averaged state-space models. Figure 25 shows a block diagram of this where K represents the controller and H represents the buck converter. It is designed so that the closed-loop system is stable and well

damped for the input voltages and output loads. Voltage-mode control (duty-ratio control) is implemented using a Proportional Integral Derivative (PID) controller.
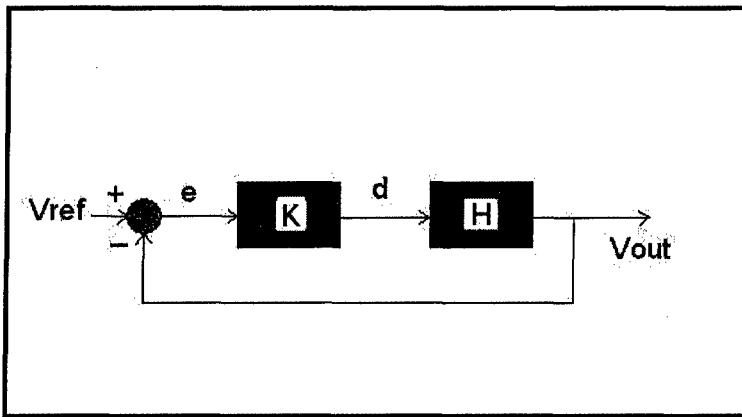
Figure 25: Block Diagram of Control Scheme

The majority of control systems used in industry applications are based on this type of controller. In general, proportional and integral control can be applied independently or together (P, I, or PI), while derivative control can only be applied in combination with one or both of the other two (PD, PID). Testing of a PID controller normally involves plotting the system response to a simple input, such as a step input, and adjusting the gains based on the output.

The first step in developing the control scheme is to obtain a linearized, averaged model for the buck converter and derive the transfer function from perturbation in duty ratio to perturbation in output voltage. The transfer function represents H in Figure 25. Next the PID controlled is developed, consisting of three gains, K_P, K_I, and K_D, and this represents K in Figure 25. The H and K are then combined to form the complete transfer function for the system.

Initially, the state variables are assigned (i_L and v_C) and the state-space equations are determined (neglecting the input filter).

$$L\frac{d}{dt}i_L = \left(v_1 - v_C\right)\cdot q(t) - v_C\cdot(1 - q(t)) \qquad C\frac{d}{dt}v_C = \left(i_L - \frac{v_C}{R}\right)\cdot q(t) - \left(i_L - \frac{v_C}{R}\right)\cdot(1 - q(t))$$

$$\frac{d}{dt}i_L = \frac{1}{L}\cdot\left(v_1\cdot q(t) - v_C\right) \qquad \frac{d}{dt}v_C = \frac{1}{C}\cdot\left(i_L - \frac{v_C}{R}\right)$$

Eqn 4-15

Then, the circuit is averaged and it is assumed that the state variables have slow variation and small ripple, and d = avg(q(t)). All of the variables are now averaged quantities and Eqn 4-15 becomes Eqn 4-16.

70

$$\frac{d}{dt}i_L = \frac{1}{L}\cdot\left(v_1\cdot d - v_C\right) \qquad\qquad \frac{d}{dt}v_C = \frac{1}{C}\cdot\left(i_L - \frac{v_C}{R}\right)$$

The variables are linearized resulting in the equations shown in Eqn 4-17.

$$v_C = V_C + v'_C \qquad\qquad d = D + d'$$

$$i_L = I_L + i'_L \qquad\qquad v_1 = V_1 + v'_1$$

Linearized Equations

$$\frac{d}{dt}i'_L = \frac{D}{L}\cdot v'_1 + \frac{V_1}{L}\cdot d' - \frac{1}{L}\cdot v'_C$$

$$\frac{d}{dt}v'_C = \frac{1}{C}\cdot i'_L - \frac{1}{R\cdot C}\cdot v'_C$$

Since v_C is the output voltage, utilizing the Laplace operator and solving for the transfer function yields Eqn 4-18.

$$\left(s^2 + \frac{1}{R\cdot C}\cdot s + \frac{1}{L\cdot C}\right)\cdot v'_{out} = \frac{D}{L\cdot C}\cdot v'_1 + \frac{V_1}{L\cdot C}\cdot d'$$

$$H = \frac{v'_{out}}{d'} = \frac{\dfrac{V_1}{L\cdot C}}{s^2 + \dfrac{1}{R\cdot C}\cdot s + \dfrac{1}{L\cdot C}}$$

For the controller the transfer function is Eqn 4-19.

$$K = \frac{d'}{e'} = K_P + K_D\cdot s + \frac{K_I}{s} \qquad \text{where e' is } V_{ref} - V_{out}$$

$$K = \frac{K_D\cdot s^2 + K_P\cdot s + K_I}{s}$$

Overall, the total transfer function is then Eqn 4-20.

$$\frac{v'_{out}}{e'} = H \cdot K$$

$$\frac{v'_{out}}{e'} \approx \frac{\frac{V_1}{L \cdot C} \cdot \left(K_D \cdot s^2 + K_P \cdot s + K_I \right)}{s^3 + \frac{1}{R \cdot C} \cdot s^2 + \frac{1}{L \cdot C} \cdot s}$$

<div align="right">**Eqn 4-20**</div>

Using the total system transfer function, the gains on the controller are adjusted to obtain the desired steady-state and transient operation. This type of system can readily be designed and optimized to provide the required overall performance, but this is beyond the scope of this paper.

4.4 Conversion Losses

An integral part of a DC-DC converter's performance is how efficiently it operates during the energy conversion process. Losses that occur include winding losses due to conduction, switching losses, and inductor core losses. A detailed analysis of all of these losses is beyond the scope of this paper and they are only described qualitatively and estimated using analytical equations.

Practical magnetic components, such as inductors, exhibit losses generated by winding conduction, hysteresis, and eddy currents. Resistive components in the converter as well as parasitics (equivalent series resistance) produce I^2R losses. Ideal inductors and capacitors are employed in this paper and parasitic losses are not calculated.

The transistors and diodes have conduction losses based on their on-state resistances. The equations to estimate these losses are shown in Eqn 4-21 and Eqn 4-22. Lastly, the transistors have switching losses associated with the transistors changing states. If the voltage and current waveforms are assumed to rise and fall approximately linearly, the switching losses are determined as shown in Figure 26.

$$P_{cond} = \left(I_L^2 \cdot D \right) \cdot R_{ds}$$

where I_L = average current
              D = duty cycle
              R_{ds} = IGBT on-state resistance

<div align="right">**Eqn 4-21**</div>

$$P_{diode} = (1 - D) \cdot I_L^2 \cdot R_d$$

where I_L = average current
D = duty cycle
R_d = diode on-state resistance

Eqn 4-22

$$P_{diss} = \left[\left(\frac{1}{2} \cdot V_{in} \cdot I_L \cdot t_f \right) + \left(\frac{1}{2} \cdot V_{in} \cdot I_L \cdot t_r \right) \right] \cdot f_{sw}$$
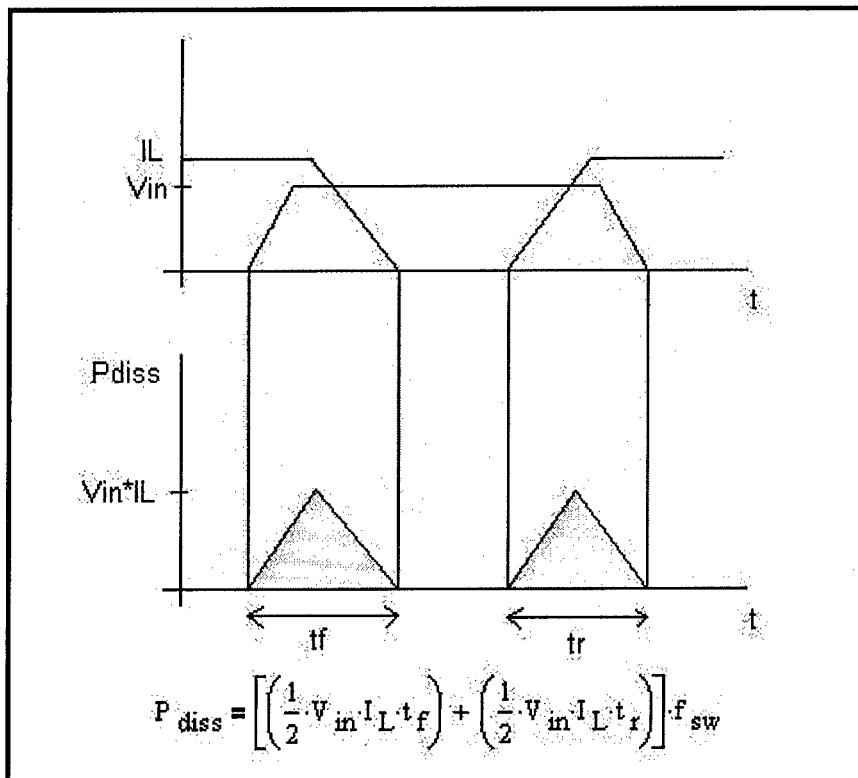
Figure 26: Transistor Switching Losses

4.5   Component Sizes and Weights

The PEM detailed in the previous sections consists of IGBTs, diodes, capacitors, inductors, and resistors. The sizes and weights of the resistors are neglected because they are significantly smaller than the other components. To ascertain reasonable estimates for the other devices, numerous references are utilized [15], [46], [47], [48], [49], [50], [51], [52], [53], [54]. In addition, a 30% service fraction is added to the total component mass and volume calculations to account for heat sinks, cooling, etc.

The power transistor is the main switching device in the converter circuit. In many applications, IGBTs are used because they have the current density and low loss of bipolar

transistors with the high-speed and high input impedance of MOSFETs [54]. Power diodes are needed to complete the buck converter circuit and provide proper operation. Table 13 lists the assumed device parameters for the IGBTs and diodes used. The IGBT and diode values are not from exact devices from particular manufacturers but rather represent data assembled from numerous sources. In order to achieve the high power levels, the semiconductor devices must be connected in parallel. Specifically, since the IGBTs and diodes are rated for 1,200A each, 19 modules (each rated for 845 kW) are connected in parallel to achieve the required 22.5 kA. This can be readily accomplished using IGBTs provided the switching is properly controlled [55].

The inductors and capacitors are needed to perform energy storage and filtering functions. In high-power applications they are usually the dominant components in terms of mass and volume. For estimating their contribution to the converter, component weight and volume energy densities are utilized. Table 13 lists the assumed characteristics for the inductor and capacitor sizing estimations.

Table 13: Power Electronics Module Component Characteristics

IGBT	
Maximum Collector Emitter Voltage	6500 V
Maximum Collector Current	1200 A
Mass (including heat sink)	1200 g
Volume (including heat sink)	0.0106 m^3
Turn On / Rise Time	450 ns
Turn Off / Fall Time	400 ns
On-State Resistance	$0.06 \ \Omega$
Forward Voltage Drop	1.9 V
Maximum Switching Frequency	~100 kHz
Power Diode	
Peak Blocking Voltage	6500 V
Average Forward Current	1200 A
Mass (including heat sink)	450 g
Volume (including heat sink)	0.0136 m^3
On-State Resistance (estimated)	$0.0073 \ \Omega$
Forward Voltage Drop	1.0 V
Capacitors	
Mass Density	0.1 kg/J
Volume Density	8 J/cc
Inductors	
Mass Density	3 kg/J
Volume Density	0.08 J/cc

In addition to using the component values to size the power conversion module, a weight factor (1.0x) and a volume factor (0.20x) are employed to account for portions such as structure, frames, mounts, and maintenance access.

Page Intentionally Left Blank

Chapter 5 Waveforms, Models, and Machine/Module Optimization

5.1 Initial Generator Waveforms

The PM generator produces back EMF waveforms that are dependent on a number of factors as discussed in Chapter 3. The goal is to produce a voltage waveform that closely resembles a sinusoidal waveform with a low total harmonic distortion (THD) because this results in minimal harmonic content which reduces losses in the machine. THD is a measure of the distortion in a waveform caused by undesirable frequency components. It is calculated as shown in Eqn 5-1.

$$THD = \sqrt{\frac{\displaystyle\sum_{(n \neq 1)} I_{nrms}^2}{I_{1rms}^2}}$$

Eqn 5-1

The back EMF waveforms are generated using Eqn 3-18, Eqn 3-19, and Eqn 3-22 which are shown again below.

$$B(\theta) = \sum_{\substack{n=1 \\ n\ odd}}^{\infty} B_n \cdot \sin(np\theta)$$

$$\text{where} \quad B_n = \frac{4}{n\pi} \cdot B_g \cdot k_{gn} \cdot \sin\left(\frac{np\theta_m}{2}\right) \cdot \sin\left(\frac{n\pi}{2}\right)$$

θ_m = magnet physical angle

n = harmonic number

Eqn 5-2

$$\lambda(\theta) = \sum_{\substack{n=1 \\ n\ odd}}^{\infty} \lambda_n \cdot \sin(np\theta)$$

$$\text{where} \quad \lambda_n = \frac{2 \cdot R_s \cdot L_{st} \cdot N_a \cdot B_n \cdot k_{wn} \cdot k_{sn}}{p}$$

Eqn 5-3

$$E_a = \sum_{\substack{n = 1 \\ n \text{ odd}}}^{\infty} V_n \cdot \sin(np\theta)$$

where $V_n = \dfrac{d}{dt}\lambda_n = \omega_0 \cdot \lambda_n$

Eqn 5-4

MATLAB code is developed to create the generator EMF waveforms as well as determine the harmonic content and THD of the generator output waveform. This code is contained in 0. For the initial PM generator designed in section 3.4, the air gap flux density, back EMF waveform, and harmonic content (line-neutral) are shown in Figure 27, Figure 28, and Figure 29. As a frame of reference, MIL-STD-1399 requires Type I 60 Hz AC systems to have a total THD of less than 5 % line-line [56]. This limit does not directly apply to the PM generator AC bus since it is being rectified to DC before supplying loads. However, it is used as a guideline because it provides a reasonable limit to ensure proper rectification and performance on the AC side.
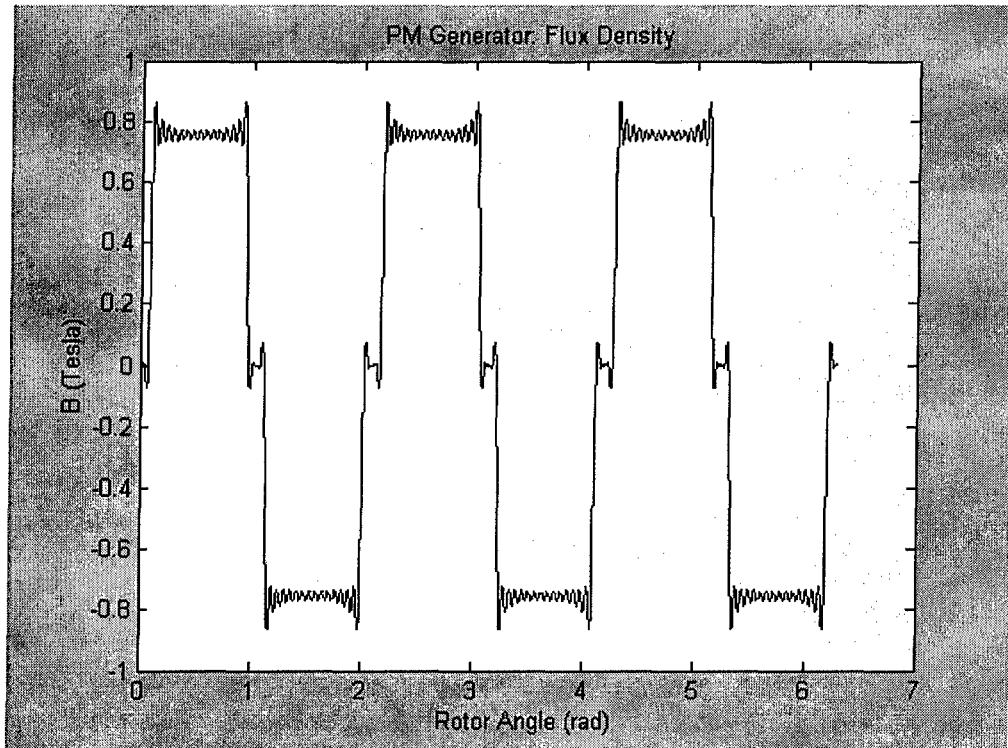
Figure 27: Initial Generator Flux Density Waveform
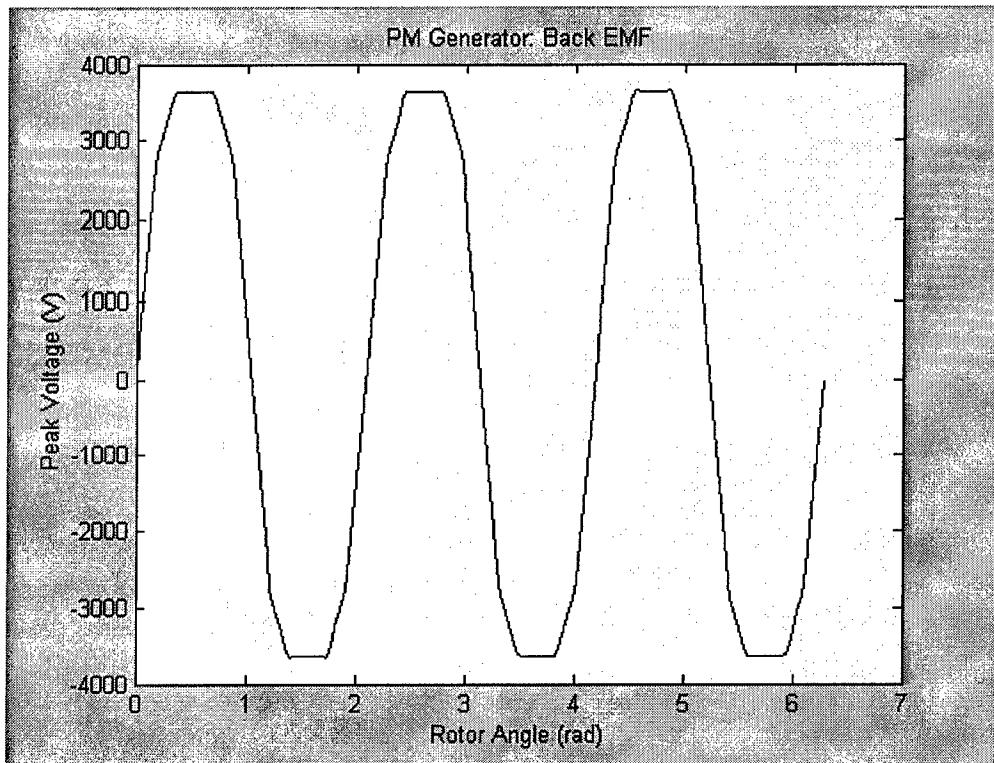
Figure 28: Initial Generator EMF Waveform
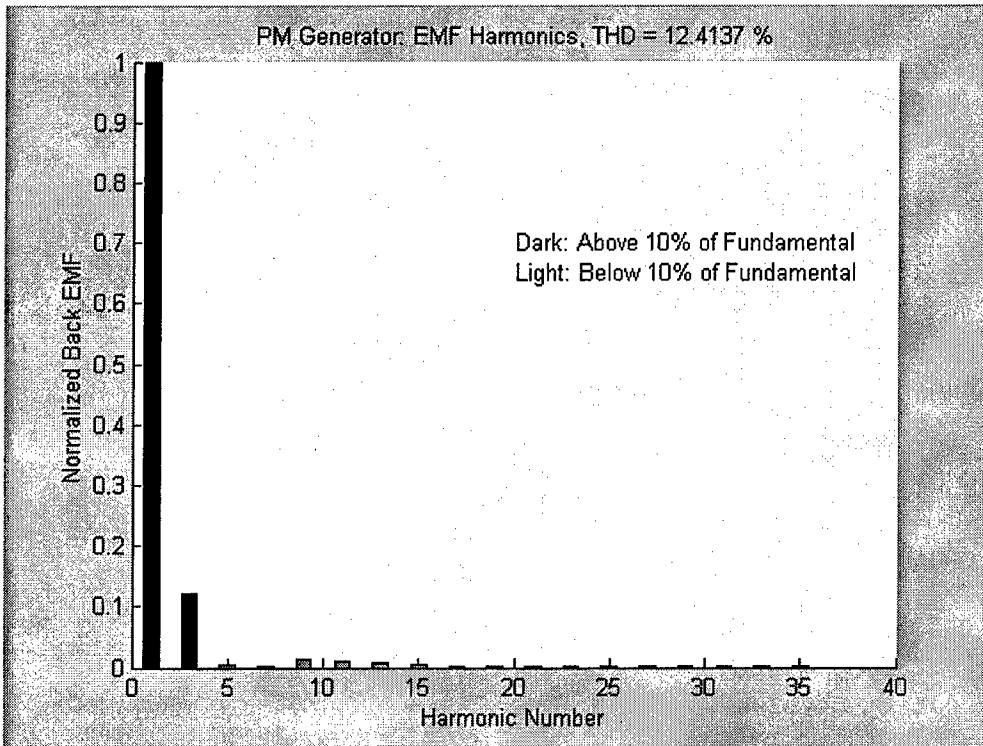
Figure 29: Initial Generator Harmonic Content

79

5.2 Rotational Stress and Retaining Sleeve

Since the PM generator is spinning at high speed, the rotor and permanent magnets are subjected to extremely high centrifugal forces. These forces can cause significant amounts of damage if the magnets and rotor are not properly restrained. The rotational components can be strengthened by enclosing them in a retaining sleeve/can which also increases the air gap length.

The centrifugal force on the magnets due to the rotor spinning is calculated in Eqn 5-5.

$$F_{cen} = \frac{M_m \cdot v_{mag}^2}{R + h_m}$$

where M_m = mass of magnets

v_{mag} = velocity of magnets (m/s)

Eqn 5-5

Using the inner surface area of the retaining sleeve, this force is converted to an outward pressure. Treating the retaining sleeve as a thin-walled vessel, the hoop stress felt by the sleeve is determined as shown in Figure 30 and Eqn 5-6.
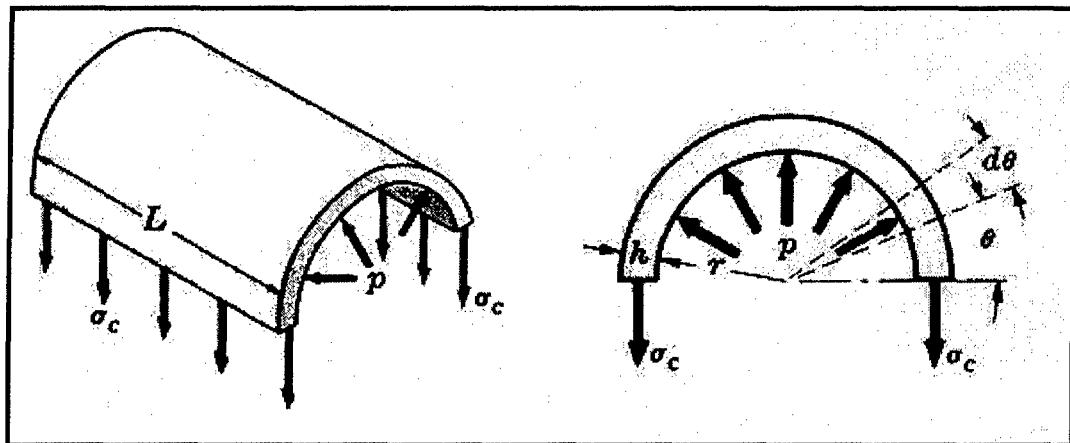
Figure 30: Retaining Sleeve Hoop Stress

$$\sum_{vert} F_v = -2 \cdot \sigma_c \cdot h \cdot L + \int_0^{\pi} P \cdot r \cdot L \cdot \sin(\theta) \cdot L \, d\theta = 0$$

$$\sigma_c = \frac{P \cdot r}{h}$$

Eqn 5-6

To provide a margin for mechanical tolerances and imperfections, a safety factor (SF) of 1.2 is applied to the hoop stress calculated in Eqn 5-6 to get a final SF stress for the retaining sleeve.

The retaining sleeve can be made from many different types of materials including metal alloys and composites. A disadvantage of a metallic sleeve is eddy currents are induced in the sleeve by variations in the flux density caused by the stator slots. The advantages of a metallic sleeve are that it shields the magnets from most of the flux density variations and it has a high thermal conductivity for heat removal.

A composite, such as carbon-fiber, provides reasonable strength while having lower losses since the lower conductivity reduces the eddy currents. However, the composite sleeve has low thermal conductivity and does not shield the magnets from the flux variations. This results in increased losses in the magnets themselves. In general, when the sleeve conductivity is low, the rotor losses are in the permanent magnets, while when the sleeve conductivity is high, the PM losses decrease and the sleeve losses increase. The materials considered for use as in the retaining sleeve are listed in Table 14 [10], [57], [58], [59], [60], [61], [62], [63], [64]. The numbers for the carbon fiber composite are in the middle of a range of typical values (0.5 – 18.0 $\mu\Omega$-m) since wide variations exist depending on how the composite is made.

Table 14: Retaining Sleeve Materials

Material	Yield Stress (ksi)	Resistivity ($\mu\Omega$-m)
Stainless Steel	90	0.72
Aluminum Alloy	75	0.05
Titanium Alloy	110	0.78
Inconel	132	0.98
Carbon Fiber	100	9.25

0 contains detailed MATLAB code to perform the retaining sleeve stress calculations. The initial PM generator from section 3.4.2 is analyzed with the results below.

```
Retaining Sleeve Stress:
Stress Limits:
Stainless Steel =      90.0 ksi      Aluminum Alloy =    75.0 ksi
Titanium Alloy =      110.0 ksi      Carbon Fiber =     100.0 ksi
Inconel =             132.0 ksi
Actual Sleeve Stress:
Sleeve Thickness    Actual Stress      SF Stress
     0.50 mm         1136.9 ksi        1364.2 ksi
     1.00 mm          568.4 ksi         682.1 ksi
     1.50 mm          379.0 ksi         454.7 ksi
```

2.00 mm	284.2 ksi	341.1 ksi
2.50 mm	227.4 ksi	272.8 ksi
3.00 mm	189.5 ksi	227.4 ksi
3.50 mm	162.4 ksi	194.9 ksi
4.00 mm	142.1 ksi	170.5 ksi
4.50 mm	126.3 ksi	151.6 ksi
5.00 mm	113.7 ksi	136.4 ksi
5.50 mm	103.4 ksi	124.0 ksi
6.00 mm	94.7 ksi	113.7 ksi
6.50 mm	87.5 ksi	104.9 ksi
7.00 mm	81.2 ksi	97.4 ksi
7.50 mm	75.8 ksi	90.9 ksi
8.00 mm	71.1 ksi	85.3 ksi

It is evident that the initial 4 mm gap length is not sufficient once the retaining sleeve is considered (since the air gap dimension includes the retaining sleeve thickness). The machine must therefore be revised to allow for the retaining can. In this modification process, the aluminum alloy is removed as a sleeve material possibility since it has lower strength and much higher conductivity than the other materials which together would produce a larger air gap and higher eddy current losses.

The PM generator will be redesigned taking the retaining sleeve and hoop stress limits into consideration. The updated PM generator will be a bigger machine with a much larger air gap, greater magnet height, lower B_g, lower voltage, and higher current density.

5.3 Rotor Losses

5.3.1 Model for Time Harmonics & Winding Space Harmonics

The permanent magnets used in high-speed generators are electrically conductive and therefore support eddy currents. The retaining sleeves are sometimes made from electrically conductive material that also can carry eddy currents. These eddy currents are primarily caused by fluctuations in the magnetic flux density produced by time and space harmonics of the winding currents. The currents produce losses which can potentially cause excessive heating or demagnetization of the permanent magnets. An analytical model is developed using the winding and current harmonics and the surface impedance to estimate the rotor losses.

Figure 31 shows the PM generator geometry "flattened out" into rectilinear coordinates. This is an accurate representation provided the dimensions are on a radial scale that is much smaller than the radius of the machine so that curvature is not important [65].
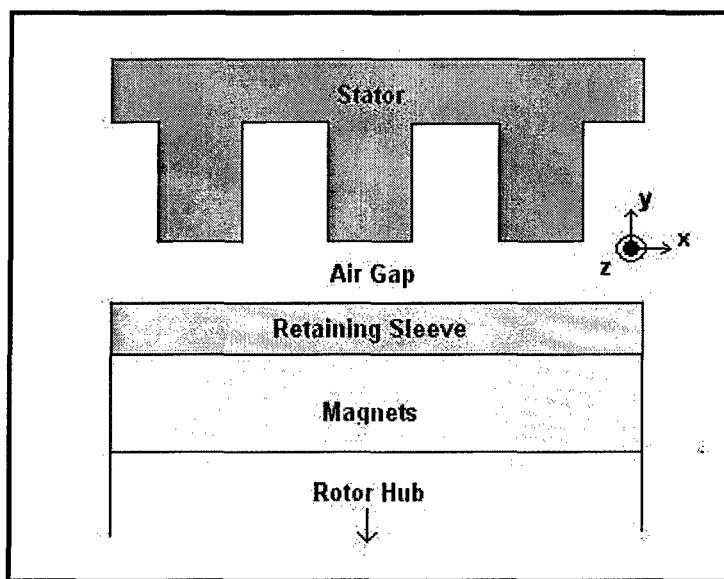
Figure 31: General Magnet Loss Model

The direction of rotation is in the positive x-direction, the radial direction is y, and the armature current flows in the axial dimension, z. In addition to the arrangement of Figure 31, the geometry shown in Figure 32 is also utilized.
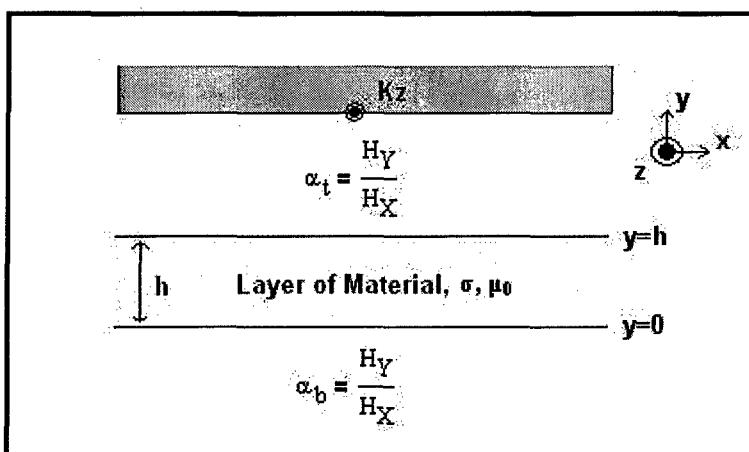
Figure 32: Layer of Material

The following assumptions are made in developing the rotor analytical loss model:

- Layers of material extend to ± infinity in the ± x direction
- Layers effectively extend to negative infinity in the negative y direction

- Motion/rotation is in the + x direction

- The physical constants of the layers are homogeneous, isentropic, and linear

- The ferromagnetic material does not saturate

- The machine is long axially so magnetic variations in the z direction are ignored (H and B only vary in x, y directions)

- All currents flow in the z direction

- The rotor and stator are constructed of laminated steel so their conductivity in the z direction is negligible

- The time and space variations are approximately sinusoidal

- Flux density at y = infinity is zero

- A traveling flux wave harmonic can be represented by an equivalent traveling current sheet (K_z) on the surface of the stator

- The normal component of the flux density is continuous at all interfaces

- The tangential component of the flux density is continuous at all interfaces except at the stator/air gap where it is increased by the current sheet density

- The magnetic flux density crossing the air gap and magnets is perpendicular

- The effect of magnet eddy currents on the magnetic flux density is negligible – this is accurate below 10 kHz [66]

- The magnet flux density is constant over the magnet breadth

One of Maxwell's Law states that there is no magnetic charge and therefore flux lines must close on themselves, represented by Eqn 5-7.

$$\nabla \cdot \vec{B} = 0$$

Eqn 5-7

Knowing this, the flux density B can be represented as the divergence of the magnetic scalar potential A (Eqn 5-8).

$$\vec{B} = \nabla \times \vec{A}$$

Eqn 5-8

Substituting in $\mu_0 H$ for B, taking the gradient of Eqn 5-8, and using Ampere's Law for current density yields Eqn 5-9.

$$\mu_0 \cdot \vec{H} = \nabla \times \vec{A}$$

$$\mu_0 \cdot \nabla \times \vec{H} = \nabla \times \nabla \times \vec{A}$$

$$\mu_0 \cdot \nabla \times \vec{H} = \nabla\left(\nabla \cdot \vec{A}\right) - \nabla^2 \cdot \vec{A}$$

$$\mu_0 \cdot \vec{J} = -\nabla^2 \cdot \vec{A}$$

$$\mu_0 \cdot \sigma \cdot \vec{E} = -\nabla^2 \cdot \vec{A}$$

<div align="right">**Eqn 5-9**</div>

Faraday's Law is then employed to determine a relationship between E and A as shown below.

$$\nabla \times \vec{E} = -\frac{d}{dt}\vec{B} \qquad \text{(Faraday's Law)}$$

$$\nabla \times \vec{E} = -\nabla \times \frac{d}{dt}\vec{A}$$

$$\vec{E} = -\frac{d}{dt}\vec{A}$$

<div align="right">**Eqn 5-10**</div>

Combining Eqn 5-9 and Eqn 5-10 gives Eqn 5-11.

$$\nabla^2 \cdot \vec{A} = \mu_0 \cdot \sigma \cdot \frac{d}{dt}\vec{A}$$

<div align="right">**Eqn 5-11**</div>

Since H and B vary only in the x and y directions, A and E are in the z direction and A can be represented by Eqn 5-12.

$$A_z = \text{Re}\left[\left(A_z(y)\right) \cdot e^{j \cdot (\omega t - kx)}\right]$$

$$\text{where } k = 2\,\pi/\lambda$$

<div align="right">**Eqn 5-12**</div>

Performing the mathematical operations and solving, Eqn 5-12 becomes Eqn 5-13.

$$\nabla^2 \cdot A_z = \mu_0 \cdot \sigma \cdot \frac{d}{dt} A_z$$

Since $\vec{B} = \nabla \times \vec{A}$ and A is in z-dir, then $B_x = \frac{d}{dy} A_z$ and $B_y = -\frac{d}{dx} A_z$

$$\nabla^2 = \left(\frac{d^2}{dx^2}\blacksquare + \frac{d^2}{dy^2}\blacksquare + \frac{d^2}{dz^2}\blacksquare \right) = -k^2 + \frac{d^2}{dy^2}\blacksquare$$

$$-k^2 \cdot A_z(y) + \frac{d^2}{dy^2} A_z(y) = j \cdot \omega \cdot \mu_0 \cdot \sigma \cdot A_z(y)$$

$$\frac{d^2}{dy^2} A_z(y) - \left(k^2 + j \cdot \omega \cdot \mu_0 \cdot \sigma \right) \cdot A_z(y) = 0$$

Let $\gamma = \sqrt{k^2 + j \cdot \omega \cdot \mu_0 \cdot \sigma}$

Solution of the form:

$$A_z(y) = A_p \cdot e^{\gamma y} + A_n \cdot e^{-\gamma y}$$

$$A_z = Re\left[\left(A_p \cdot e^{\gamma y} + A_n \cdot e^{-\gamma y} \right) \cdot e^{j \cdot (\omega t - kx)} \right]$$

Eqn 5-13

Solving for the magnetic flux densities and magnetic fields produces Eqn 5-15.

$$B_x = \frac{d}{dy} A_z = Re\left[\left(\gamma \cdot A_p \cdot e^{\gamma y} - \gamma \cdot A_n \cdot e^{-\gamma y} \right) \cdot e^{j \cdot (\omega t - kx)} \right]$$

$$B_y = -\frac{d}{dx} A_z = Re\left[\left(j \cdot k \cdot A_p \cdot e^{\gamma y} + j \cdot k \cdot A_n \cdot e^{-\gamma y} \right) \cdot e^{j \cdot (\omega t - kx)} \right]$$

$$H_x = Re\left[\left(\frac{\gamma \cdot A_p}{\mu_0} \cdot e^{\gamma y} - \frac{\gamma \cdot A_n}{\mu_0} \cdot e^{-\gamma y} \right) \cdot e^{j \cdot (\omega t - kx)} \right]$$

$$H_y = Re\left[\left(\frac{j \cdot k \cdot A_p}{\mu_0} \cdot e^{\gamma y} + \frac{j \cdot k \cdot A_n}{\mu_0} \cdot e^{-\gamma y} \right) \cdot e^{j \cdot (\omega t - kx)} \right]$$

Eqn 5-14

Let $H_p = \dfrac{\gamma \cdot A_p}{\mu_0}$ and $H_n = \dfrac{-\gamma \cdot A_n}{\mu_0}$

$$H_x = Re\left[\left(H_p \cdot e^{\gamma y} + H_n \cdot e^{-\gamma y}\right) \cdot e^{j \cdot (\omega t - kx)}\right] \qquad\qquad H_x = Re\left[H_X \cdot e^{j \cdot (\omega t - kx)}\right]$$

$$H_y = Re\left[\left(j \cdot \frac{k}{\gamma} \cdot H_p \cdot e^{\gamma y} - j \cdot \frac{k}{\gamma} \cdot H_n \cdot e^{-\gamma y}\right) \cdot e^{j \cdot (\omega t - kx)}\right] \qquad H_y = Re\left[H_Y \cdot e^{j \cdot (\omega t - kx)}\right]$$

Eqn 5-15

The layer from Figure 32 can now be examined utilizing a "surface coefficient." A surface coefficient is defined as the ratio of the y-directed to x-directed magnetic field amplitude ($\alpha = H_Y/H_X$). At the bottom of the layer where $y = 0$, the surface coefficient is given by Eqn 5-16.

$$\alpha_b(y = 0) = \frac{H_Y}{H_X} = j \cdot \frac{k}{\gamma} \cdot \frac{H_p - H_n}{H_p + H_n} \qquad \alpha_b = j \cdot \frac{k}{\gamma} \left(\frac{\dfrac{H_p}{H_n} - 1}{\dfrac{H_p}{H_n} + 1}\right)$$

Eqn 5-16

At the top of the layer ($y = h$), the surface coefficient is shown in Eqn 5-17.

$$\alpha_t(y = h) = j \cdot \frac{k}{\gamma} \cdot \left(\frac{H_p \cdot e^{\gamma h} - H_n \cdot e^{-\gamma h}}{H_p \cdot e^{\gamma h} + H_n \cdot e^{-\gamma h}}\right) \qquad \alpha_t = j \cdot \frac{k}{\gamma} \left(\frac{\dfrac{H_p}{H_n} \cdot e^{\gamma h} - e^{-\gamma h}}{\dfrac{H_p}{H_n} \cdot e^{\gamma h} + e^{-\gamma h}}\right)$$

Eqn 5-17

Using Eqn 5-16 to solve for the ratio H_p/H_n, a final expression for the top surface coefficient is determined (Eqn 5-18), and it is applicable to any uniform region.

$$\alpha_b \cdot \left(\frac{H_p}{H_n} + 1 \right) = j \cdot \frac{k}{\gamma} \cdot \left(\frac{H_p}{H_n} - 1 \right)$$

$$\frac{H_p}{H_n} \cdot \left(j \cdot \frac{k}{\gamma} - \alpha_b \right) = j \cdot \frac{k}{\gamma} + \alpha_b \qquad \frac{H_p}{H_n} = \frac{j \cdot \frac{k}{\gamma} + \alpha_b}{j \cdot \frac{k}{\gamma} - \alpha_b}$$

$$\alpha_t = j \cdot \frac{k}{\gamma} \cdot \left(\frac{\dfrac{\frac{j \cdot k}{\gamma} + \alpha_b}{\frac{j \cdot k}{\gamma} - \alpha_b} e^{\gamma h} - e^{-\gamma h}}{\dfrac{\frac{j \cdot k}{\gamma} + \alpha_b}{\frac{j \cdot k}{\gamma} - \alpha_b} \cdot e^{\gamma h} + e^{-\gamma h}} \right)$$

$$\alpha_t = j \cdot \frac{k}{\gamma} \cdot \left[\frac{\left(\frac{j \cdot k}{\gamma} + \alpha_b \right) e^{\gamma h} - \left(\frac{j \cdot k}{\gamma} - \alpha_b \right) \cdot e^{-\gamma h}}{\left(\frac{j \cdot k}{\gamma} + \alpha_b \right) \cdot e^{\gamma h} + \left(\frac{j \cdot k}{\gamma} - \alpha_b \right) \cdot e^{-\lambda h}} \right]$$

$$\alpha_t = j \cdot \frac{k}{\gamma} \cdot \left(\frac{j \cdot \frac{k}{\gamma} \cdot \sinh(\gamma h) + \alpha_b \cdot \cosh(\gamma h)}{j \cdot \frac{k}{\gamma} \cdot \cosh(\gamma h) + \alpha_b \cdot \sinh(\gamma h)} \right)$$

Eqn 5-18

If the region being examined is positioned on top of a ferromagnetic surface, such as the magnets on the steel rotor shaft, the boundary condition at the bottom of the layer ($\alpha_b \rightarrow$ infinity as $H_x \rightarrow$ 0) produces Eqn 5-19.

$$\alpha_t = j \cdot \frac{k}{\gamma} \cdot \coth(\gamma h)$$

Eqn 5-19

In the case of the air gap where the conductivity is zero, Eqn 5-18 reduces to Eqn 5-20.

$$\alpha_t = j \cdot \left(\frac{j \cdot \sinh(\gamma h) + \alpha_b \cdot \cosh(\gamma h)}{j \cdot \cosh(\gamma h) + \alpha_b \cdot \sinh(\gamma h)} \right)$$

<div align="right">**Eqn 5-20**</div>

The electric field (E) is z-directed and the magnetic flux density and field (B and H) are y-directed so a relationship is determined between them using Faraday's Law. The surface impedance is then determined. Surface impedance (Z_s) is the ratio of the z-directed electric field to the z-directed current. Eqn 5-21 and Eqn 5-22 show the detailed calculations.

$$\nabla \times \vec{E} = -\frac{d}{dt}\vec{B} \qquad \text{(Faraday's Law)}$$

$$\nabla \times \vec{E} = -\mu_0 \cdot \frac{d}{dt}H$$

$$\frac{d}{dz}E_x - \frac{d}{dx}E_z = -\mu_0 \cdot \frac{d}{dt}H_y$$

$$j \cdot k \cdot E_z = -j \cdot \omega \cdot \mu_0 \cdot H_y$$

$$E_z = -\frac{\omega_n}{k_n} \cdot \mu_0 \cdot H_y$$

<div align="right">**Eqn 5-21**</div>

$$Z_s = \frac{E_{surf}}{K_{surf}} = \frac{E_z}{-H_x} = \frac{\dfrac{-\omega_n}{k_n} \cdot \mu_0 \cdot H_y}{-H_x}$$

$$Z_s = \frac{\omega_n}{k_n} \cdot \mu_0 \cdot \alpha$$

<div align="right">**Eqn 5-22**</div>

Since electromagnetic power flow into the rotor is the desired quantity, Poynting's vector is employed (Eqn 5-23).

$$\vec{S} = \vec{E} \times \vec{H}$$

<div align="right">**Eqn 5-23**</div>

Dissipation in the rotor is in the negative y direction producing Eqn 5-24.

<div align="center">89</div>

$$-S_y = -\left(E_z{\cdot}H_x - E_x{\cdot}H_z\right)$$

There is no z-directed magnetic field ($H_z = 0$)

$$-S_y = -E_z{\cdot}H_x$$

In time average form, Eqn 5-24 becomes Eqn 5-25.

$$- <S_y> = -\frac{1}{2}\mathrm{Re}(E_z \cdot \overline{H}_x)$$

$$- <S_y> = -\frac{1}{2}|H_x|^2 \cdot \mathrm{Re}(\frac{E_z}{H_x})$$

$$- <S_y> = \frac{1}{2}|K_z|^2 \cdot \mathrm{Re}(Z_s)$$

Eqn 5-25 yields the power dissipated at the stator surface. This is the correct result for the rotor because there is no mechanism for dissipating power between the stator and rotor. The power estimated by Poynting's theorem flows directly from the stator to the rotor [65].

In order to calculate the rotor losses, the above analytical model is applied to the geometry in Figure 31. For this model, the stator is assumed to be a smooth surface without slots because the slot effects are considered later in section 5.3.2. The first step is calculating the surface coefficient at the bottom of the magnet layer. It is assumed that this is formed by the highly permeable rotor shaft below the magnets. This assumption allows the surface coefficient at the top of the magnet layer to be calculated using Eqn 5-19.

Next, the surface coefficient at the top of the retaining sleeve is determined using the sleeve material's conductivity and Eqn 5-18. Traveling across the air gap to the surface of the stator, the surface coefficient is estimated using Eqn 5-20. The surface impedance is then computed utilizing Eqn 5-22.

Once the surface impedance is known, the rotor losses caused by the stator winding time and space harmonics are calculated using Eqn 5-25. Only the more significant harmonics are considered as shown in Figure 33. The higher order harmonic effects are ignored because the products of higher order time harmonics (small number) and higher order space harmonics

(small number) produce negligible contributions (small number * small number = very small number). Appendix I contains the detailed MATLAB code that performs all of the above calculations.
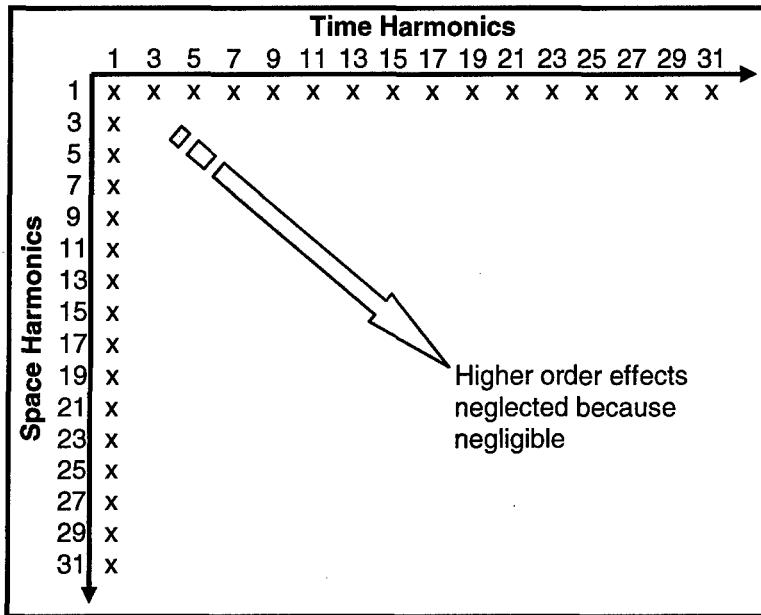
Figure 33: Relevant Harmonics

5.3.2 Model for Stator Slot Effects

The stator slots cause variations in the magnetic field which produce losses in the retaining sleeve and magnets of the rotor. Accurate calculation of the losses in the retaining sleeve is extremely difficult. Several different methods have been developed and in this paper, the technique from reference [18] is employed. Figure 34 shows the geometry of the retaining can and the currents that are induced.
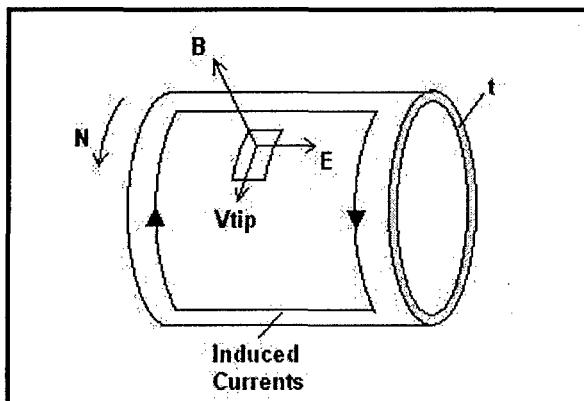
Figure 34: Retaining Sleeve Induced Currents

As the rotor spins past the slot openings of the stator, the air gap flux density undergoes modulation due to the change in reluctance. The dip in B_g (shown in Figure 35) travels along the B-waveform which is otherwise moving synchronously with the rotor.
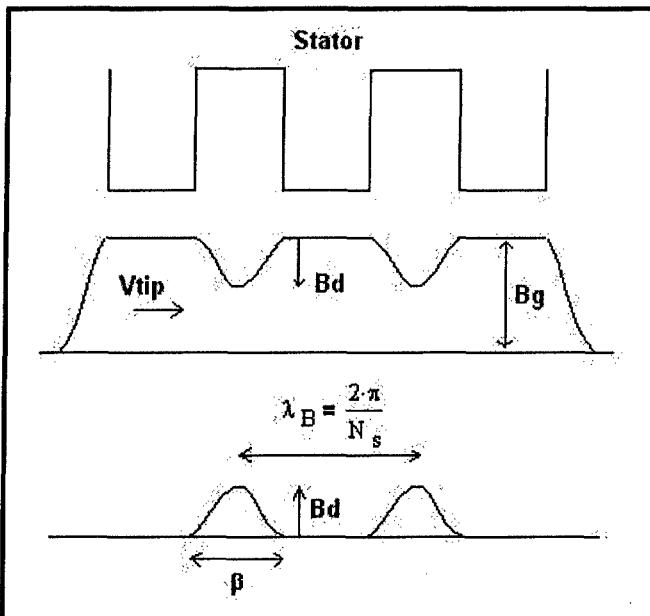
Figure 35: Flux Density Variation

The rotation of the rotor generates an E-field in the sleeve and a subsequent axial current density $J = E/\rho$. When this current density is integrated over the volume of the can, the average loss per unit area is determined (Eqn 5-26) [18].

$$w = \frac{\pi^2}{3600} \cdot \frac{\left[B \cdot N \cdot (R + h_m) \right]^2 \cdot t}{\rho} \quad \text{where} \quad B = \frac{B_d}{\sqrt{2}} \sqrt{\frac{\beta}{\lambda_B}}$$

Eqn 5-26

It is evident from Eqn 5-26 that as the slot width increases, the width of the flux density dip (β) gets larger causing the sleeve losses to increase. The above equation only considers eddy currents flowing in the axial direction but there are also circumferential components. These portions are accounted for using a factor K_s as shown in Eqn 5-27 where the total can losses are determined [18].

$$P_{can} = K_s \cdot w \cdot A$$

where $\quad A = \pi \cdot 2 \cdot \left(R + h_m\right) \cdot L_{st}$

$$K_s = 1 - \frac{\tanh\left[\dfrac{p \cdot L_{st}}{2\left(R + h_m\right)}\right]}{\left[\dfrac{p \cdot L_{st}}{2\left(R + h_m\right)}\right]}$$

Eqn 5-27

One way to reduce the retaining can losses is to split the sleeve cylinder into separate rings. This reduces the effective flow path length for the eddy currents thus lowering the losses. There is a limit to how much this can be done since as the number of rings increases, the construction becomes more difficult. In this paper it is assumed that the maximum feasible number of sleeve sections is ten.

When metal alloys are used as the retaining sleeve material, they effectively shield the magnets from the flux density variations, whereas there is little or no shielding with the carbon fiber composite because of its low conductivity. Therefore, with a metal alloy can, the rotor losses occur largely in the can compared to the carbon fiber sleeve, where the losses mostly occur in the magnets. These magnet losses are calculated using methods similar to Eqn 5-26 and Eqn 5-27 assuming that the eddy currents flow in the top 10% of the magnet volume. Appendix J contains the MATLAB code that performs the detailed rotor loss calculations caused by the stator slot effects.

5.4   Complete System Model & Design Procedure

The complete model for the power generation module consists of the PM generator, the rectifier, the filtering/energy storage components, the buck converter, and the load. The program PSIM (Version 6.0, Powersim, Inc.) is utilized to construct the circuit model, perform detailed time series and waveform analysis, and determine voltage and current values. An example of a 7-phase version of this model system is shown in Figure 36. In each of the models, the converter and rectifier are simulated as one IGBT/diode module for simplicity but for actual implementation/construction, 19 modules are required as described in section 4.5.

93
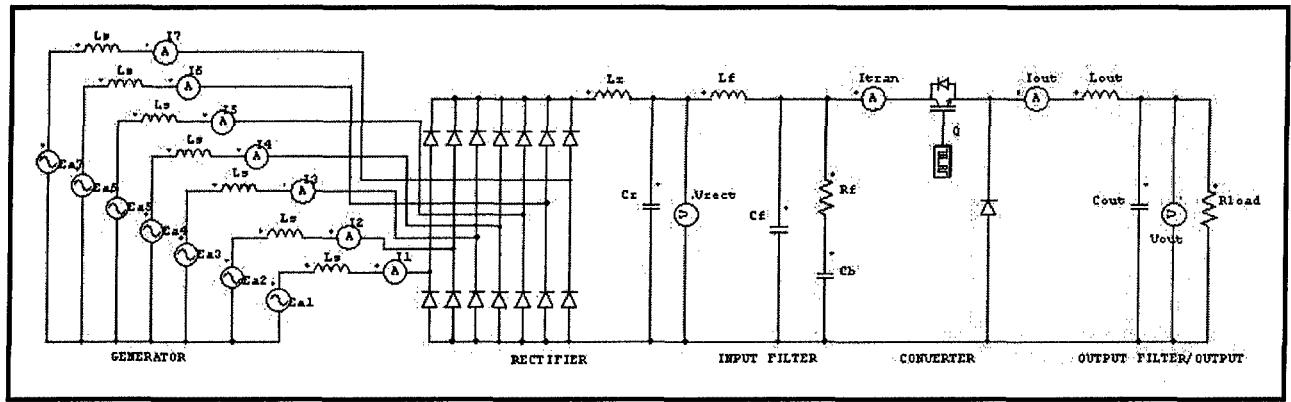
Figure 36: System Model

The procedure for designing and analyzing the power generation module consists of the following:

- Design a PM generator using the methodology from sections 3.4.2 and 5.2, iterating to ensure the sizes, current density, magnetic saturation, and sleeve thickness/stresses are all satisfactory

- Verify the PM generator has proper output waveforms and THD per section 5.1

- Calculate the rotor losses caused by stator slot harmonics as outlined in section 5.3.2

- Determine the rectifier circuit parameters utilizing the procedures from section 4.2

- Design the buck converter and associated input and output filters employing the methods of section 4.3

- Construct the PSIM circuit using the correct generator parameters (number of phases, back voltage (E_a), and synchronous inductance (L_s)), rectifier values, converter parameters, and filtering components

- Simulate and analyze the PSIM model verifying the system meets the required specifications for power and output voltage

- Determine the generator line harmonic current magnitudes from the PSIM model

- Using the harmonic current values, calculate the rotor losses caused by the winding time and space harmonics as detailed in section 5.3.1

- Calculate the switching losses and conduction losses of the power conversion module per section 4.4

- Determine the overall losses and efficiency of the system

- Calculate the masses and volumes of the generator and power conversion module using the methodology of sections 3.4.2 and 4.5

5.5 Optimization

Optimizing the overall power generation module involves designing numerous PM generators and associated power conversion electronics to achieve an ideal result. Using the design procedure from section 5.4, machine parameters are varied producing different generator designs. For each unique generator, a power conversion module is devised so that its values are matched with the output of the generator. This results in a wide range of power generation modules.

The main machine parameters that are varied are the number of poles, number of phases, and the retaining sleeve material as shown in Figure 37. This results in 80 different machines and associated power conversion modules. For each of these generators, the magnet thickness (h_m), air gap (g), magnet angle (θ_m), and stack length (L_{st}) are iterated to ensure the sizes, current density, magnetic saturation, sleeve thickness/stresses, output waveforms, and THD are all satisfactory.

Rotational speed (13,000 RPM) and magnet skew angle (10^0) are held constant. The number of slots (N) is set to 36 for the 3 and 5-phase machines and to 72 for the 7, 9, and 11-phase machines to properly fit the windings and ensure a reasonably sinusoidal back voltage waveform. Other parameters including the number of slots/pole/phase (m), number of armature turns (N_a), back voltage (E_a), synchronous inductance (L_s), electrical frequency (f), breadth factor (k_b), pitch factor (k_p), skew factor (k_s), magnet factor (k_g), and air gap flux density (B_g) all change as a result of the machine variations.
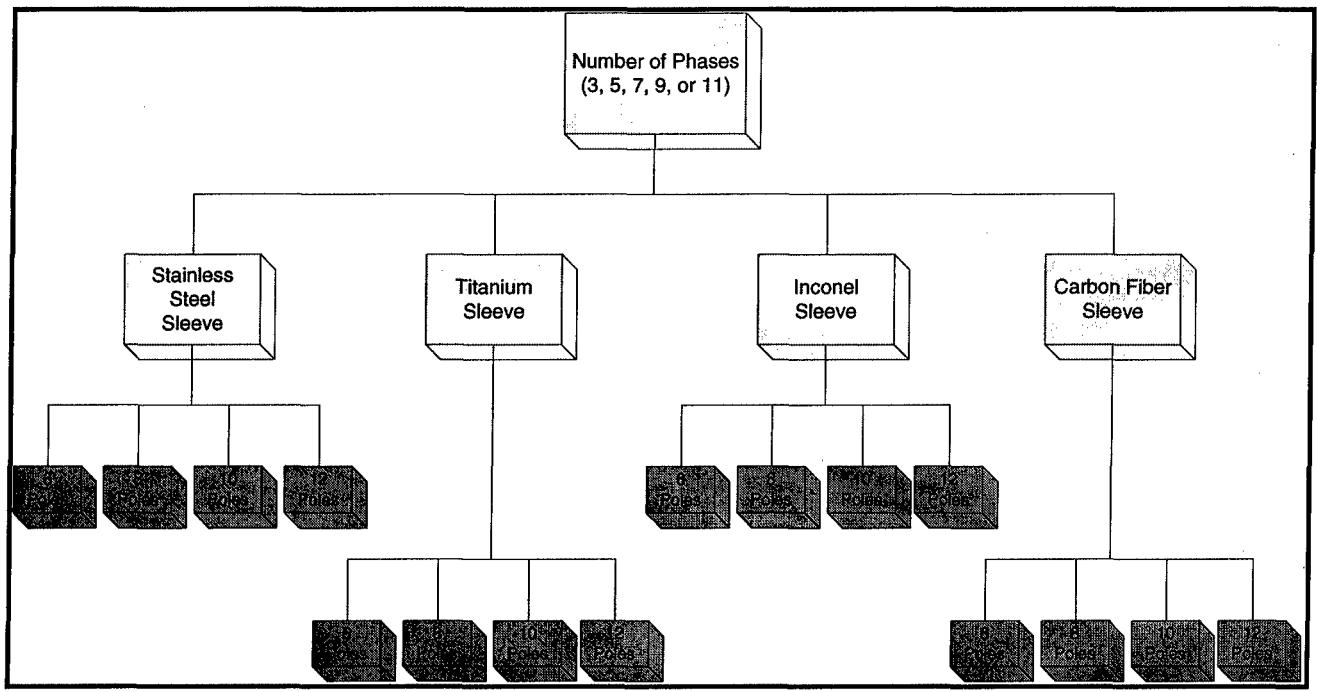
Figure 37: Machine Optimization Parameters

Each machine is optimized to have minimal back voltage, size, and mass while ensuring it remains within the current density and magnetic saturation limits. The power conversion modules are then developed matching component ratings to those of the PM generators. The power electronics are designed to produce maximum power factor and minimal line harmonics as discussed in section 4.3. This yields the lowest possible losses in the PM generator thus maximizing efficiency and minimizing rotor heat generation.

Chapter 6 Results and Analysis

6.1 General

As discussed in section 5.5, the main machine parameters that are varied are the number of poles, number of phases, and the retaining sleeve material and resulting in 80 different machines and associated power conversion modules. These PM machines and power conversions modules are developed with varying results. Appendix K and Appendix L contain the detailed specifications for each of the generators and power conversion modules. Appendix M and Appendix N have the in-depth losses and weights for each design. Appendix O lists the mass and volume results for the rectifiers and Appendix P contains the mass and volume data for the converters. A summary of the range of values for the designs is contained in Table 15 and Table 16.

Table 15: General Module Specifications

	Back Voltage E_a (RMS)	Synch Inductance L_s (mH)	Gen Volt THD	Stack Length L_{st} (m)	Overall Machine Length L (m)	Machine Diameter D (m)	Air Gap Flux Density B_g (T)	PCM Vol (m^3)
Minimum	1,136.0	0.020	3.12%	0.850	1.732	0.834	0.61	6.54
Maximum	3,380.0	0.348	23.05%	1.080	2.057	0.900	0.77	7.96
Average	1,977.0	0.110	11.61%	0.943	1.861	0.866	0.68	7.14

Table 16: General Module Results

	Machine Weight (kg)	PCM Weight (kg)	Total Weight (kg)	Machine Losses (kW)	PCM Losses (kW)	Total Losses (kW)	Line Current THD
Minimum	1,388.6	2,302.7	3,900.1	241.7	1,688.3	2,126.7	6.80%
Maximum	2,302.9	3,954.7	6,101.8	1,259.8	3,293.7	3,535.4	24.19%
Average	1,754.6	3,025.5	4,780.2	463.8	2,124.0	2,587.8	14.56%

In general, the PCM losses are too high due to the IGBT switching losses. This is because high-frequency hard switching is used in the power conversion module as opposed to soft switching or a lower frequency. Soft switching involves using snubber circuits or resonant converters to minimize device switching losses by constraining the switching of the power devices to time intervals when the voltage across the device or the current through it is nearly

zero. Soft switching can reduce switching losses as much as 50-80% [67], [68]. In addition to lowering switching losses, soft switching reduces EMI, permits higher switching frequencies, and achieves higher efficiencies. Analyzing different soft-switching topologies is beyond the scope of this paper but the effects soft switching has on the PCM are studied. Using a lower switching frequency is not examined because this would produce a larger converter since the passive components would have to be bigger.

In order to select a final design, the different variants are examined to ascertain which one is optimal. Parameters such as weights, machine losses, PCM losses, and THD are used to help facilitate the selection process.

6.2 Number of Phases

To facilitate studying the effects the number of phases has on the power generation module, several parameters are held constant. The retaining sleeve material and number of poles are arbitrarily set to inconel and 12. This does not affect the analysis because the trends related to varying the number of phases are consistent across all 80 power modules as indicated in the detailed results contained in the appendices.

As the number of phases varies from 3 to 11, the weights of the PM generator and the power conversion module change, but only slightly. Figure 38 shows this and there is a maximum variation of approximately 242 kg, or 5.7%. The 11-phase machine produces the lowest weight power module but only by a small amount.
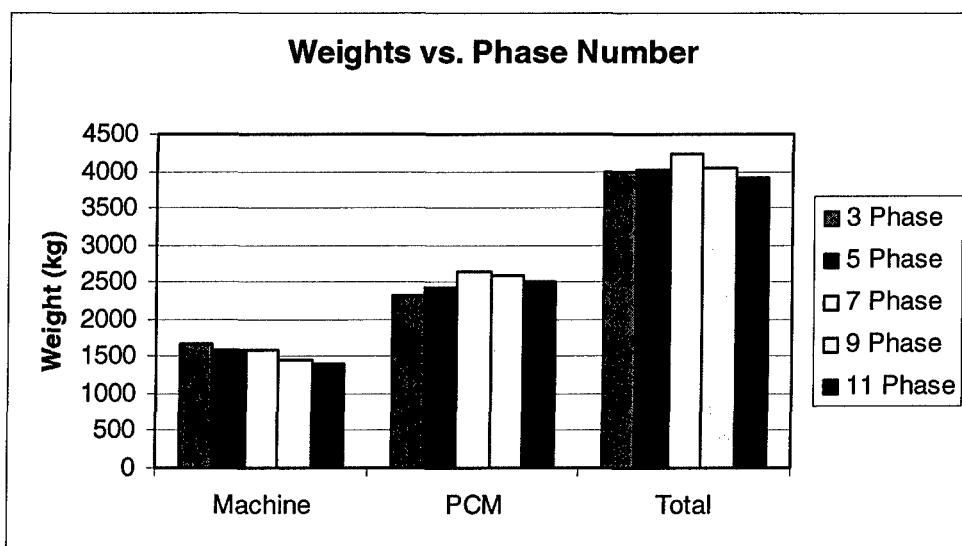
Figure 38: Weights vs. Number of Phases

The machine losses fluctuate significantly as the phase number changes with the 3-phase machine having 48.8% of the losses of the 11 phase machine (see Figure 39). The core, windage, and armature losses are approximately constant for the different phase generators, but the rotor losses vary considerably. This disparity is caused predominately by the AC line current harmonics from the rectifier being much greater in the higher phase machines. Their triple-n harmonics are higher order thus allowing lower order harmonics to have a greater effect, specifically the 3rd harmonic.

The higher rotor losses are also caused by the geometry of the machine. As the phase number increases, the number of slots/pole/phase (m) decreases which causes the winding factors to have less of an effect in reducing higher harmonic effects. The exception is the jump from 5-phases to 7-phases because the number of slots is doubled from 36 to 72 so that m increases initially. Overall, the 3-phase generator has the lowest rotor and total machine losses.
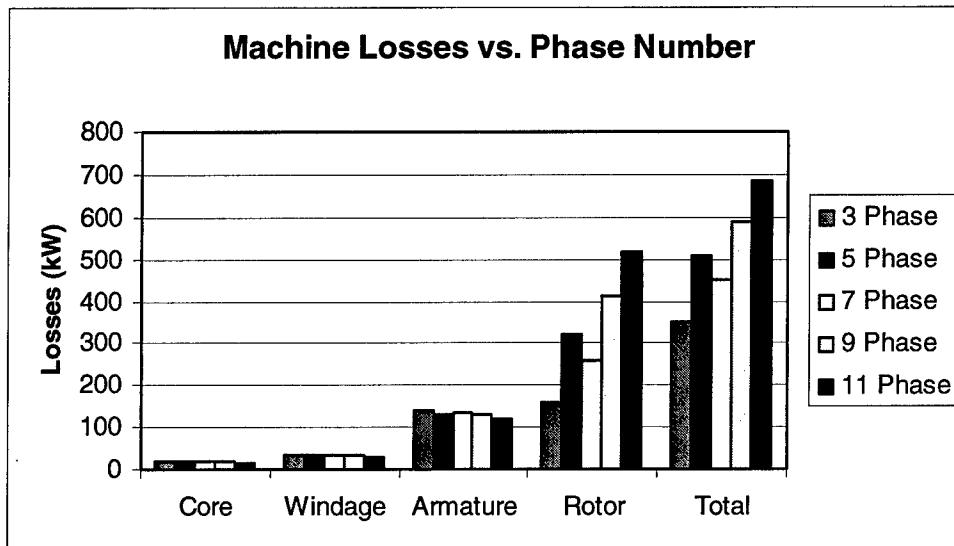
Figure 39: Machine Losses vs. Number of Phases

PCM Losses vs. Phase Number
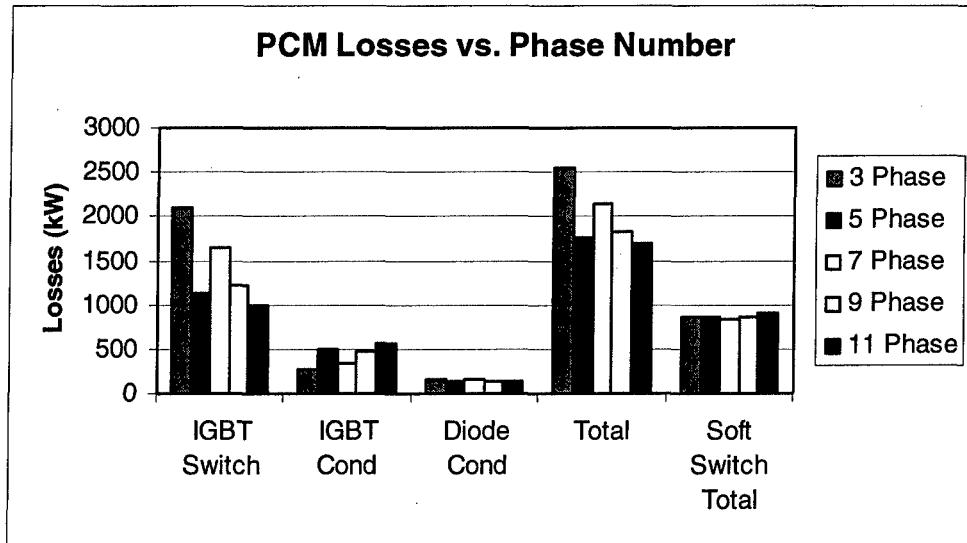
Figure 40: PCM Losses vs. Number of Phases

The PCM losses also differ greatly depending on the number of phases (Figure 40). The 11-phase machine has the lowest total losses due to it having the lowest IGBT switching losses. This is because it has a smaller rectified voltage which reduces the stresses and switching losses in the IGBTs (see section 4.4). However, if soft switching is implemented, the PCM losses are similar for the different phase machines varying by a maximum of 63.5 kW instead of the 843 kW associated with hard switching. Therefore, the lower phase machines become more attractive if soft switching is utilized.

Lastly, as the number of phases increases, Figure 41 shows that in general, the generator voltage and line current THD increase. This is caused by the same effects as with the rotor losses, the slots/pole/phase and the AC line harmonics from the rectifier. As mentioned in section 5.1, the specification from MIL-STD-1399 for voltage THD is normally 5% so using these standards as guidelines, only the 3-phase and the 7-phase power modules are satisfactory. The line current THD should be made as low as possible because this directly affects the amount of losses and heating in the rotor. The typical limit for line current THD is 10% making the 3-phase generator the only one with acceptable THD performance [69].
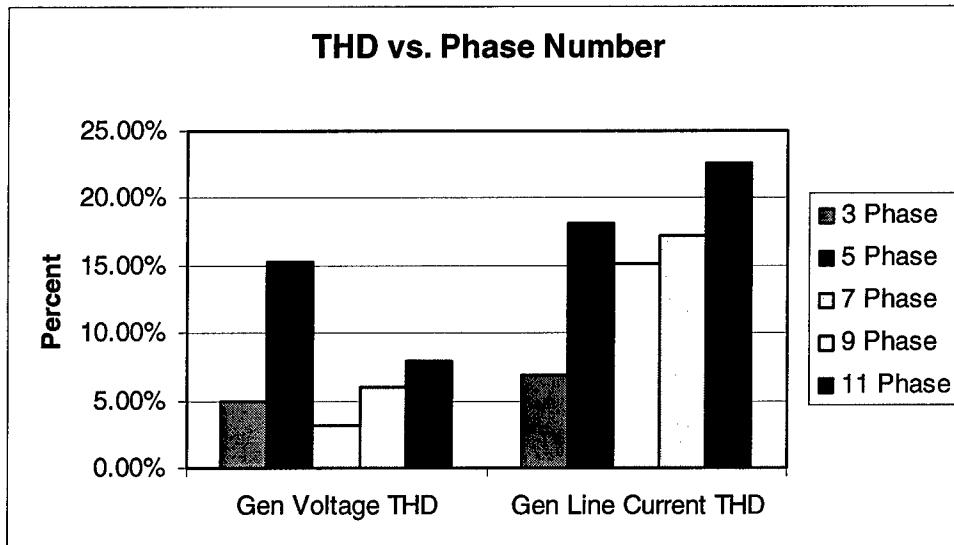
THD vs. Phase Number

Figure 41: THD vs. Number of Phases

6.3 Retaining Material

Similar to the analysis of the number of phases, several parameters are held constant when examining the various retaining sleeve materials. Specifically, the number of phases is arbitrarily set to 3 and the number of poles is fixed at 6. This does not affect the analysis because the trends related to varying the retaining material are consistent across the continuum of power modules as shown in the detailed results contained in the appendices.

With respect to the weights of the PM generator and the PCM, the type of retaining sleeve has little effect. Using a stainless steel retaining can produces the largest power module but it is not appreciably larger than the others. When the retaining sleeve is constructed from titanium, inconel, or carbon fiber, the difference in total weight is less than 0.11%. Figure 42 shows the effects the retaining sleeve material has on the weights of the power generation module.
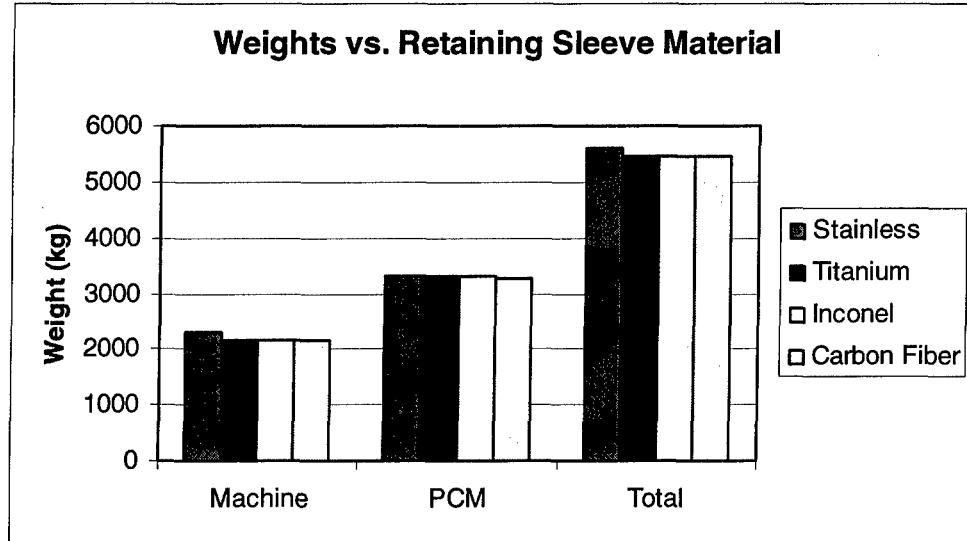
Figure 42: Weights vs. Retaining Sleeve Material
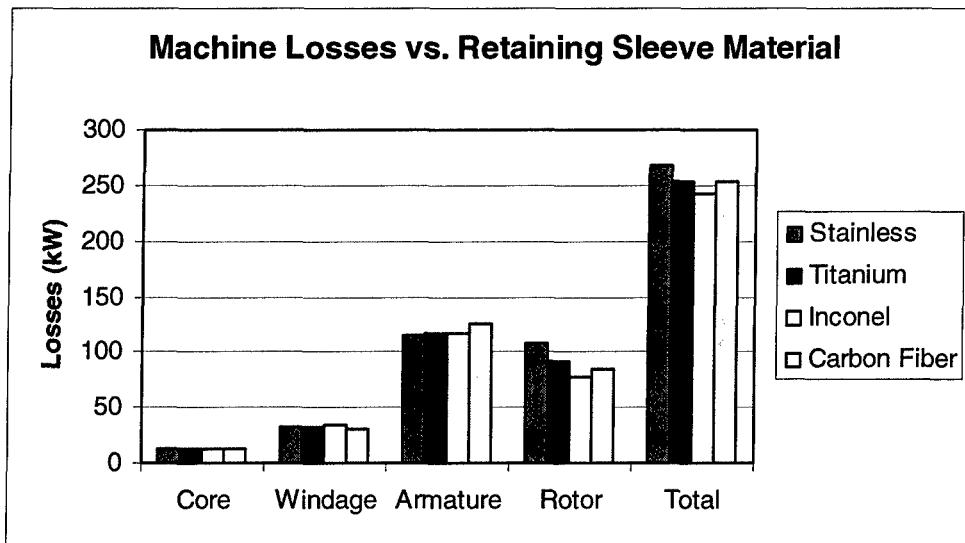
Figure 43: Machine Losses vs. Retaining Sleeve Material

The type of retaining sleeve material does affect the losses in the PM generator. The core, windage, and armature losses vary only slightly but the rotor losses fluctuate a great deal. Inconel has the lowest rotor losses (77.3 kW) while stainless steel has the highest (107.1 kW). The carbon fiber has the smallest losses in the actual can but larger losses in the magnets. This is because the carbon fiber provides no shielding for the magnets from flux variations and winding

current harmonics. Overall, the inconel sleeve produces the lowest rotor and total machine losses as shown in Figure 43.

The PCM losses are not influenced considerably by the kind of retaining can material (Figure 44). Depending on the type, the losses vary by about 157.2 kW, or 4.2%. When soft switching is utilized, the losses fluctuate by only 23.7 kW or 2.5%. Therefore, the PCM losses are not a major factor in selecting the retaining can material.
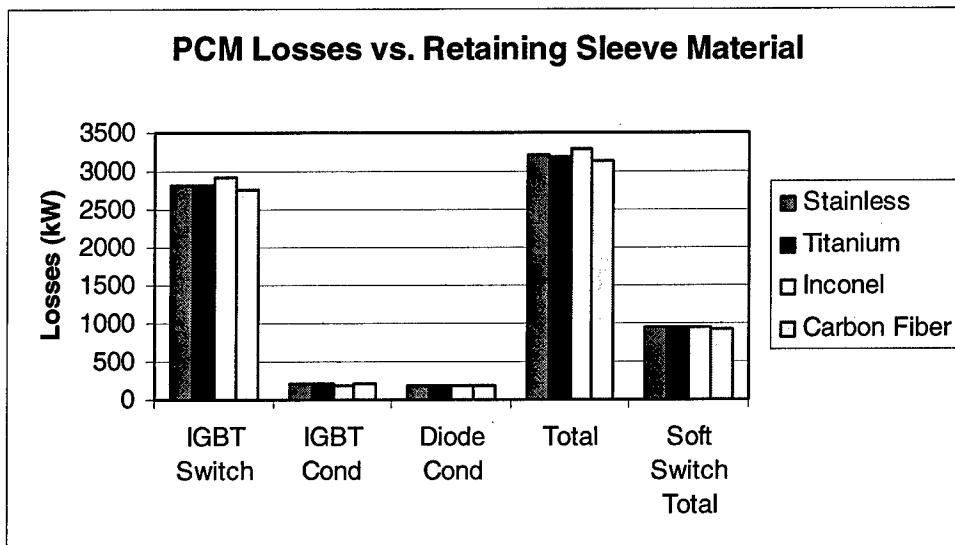
Figure 44: PCM Losses vs. Retaining Sleeve Material

Lastly, the selection of a retaining sleeve material is not a factor in the generator voltage THD or the AC line current THD. The voltage THD varies by only 0.5% and the line current by less than 0.15% depending on the type of material as indicated in Figure 45. It is evident, however, that selected a 3-phase, 6-pole, 36-slot machine would not be wise since the voltage THD is above the 5% limit in all cases.

THD vs. Retaining Sleeve Material

Figure showing bar chart with Percent on y-axis (0.00% to 14.00%) and two groups on x-axis: Gen Voltage THD and Gen Line Current THD. Legend: Stainless, Titanium, Inconel, Carbon Fiber.
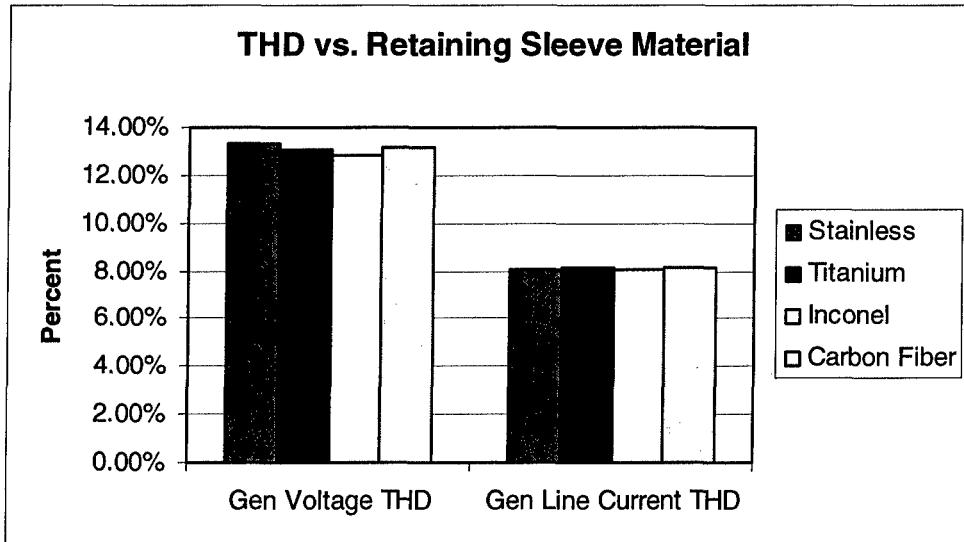
Figure 45: THD vs. Retaining Sleeve Material

6.4   Number of Poles

The number of poles in a machine is an important factor because it affects numerous parameters including the electrical frequency, the magnet pole pitch, and the magnetic air gap flux density. To facilitate studying the effects of the number of poles, several parameters are held constant. The retaining sleeve material and number of phases are arbitrarily set to inconel and 3. This does not affect the analysis because the trends related to varying the number of poles are consistent across the range of machines as indicated in the detailed results in the appendices.

First, the weights of the generator and PCM are examined to ascertain the effects of the number of poles. As Figure 46 indicates, as the number of poles increases the weights of both the machine and the PCM decrease. The generator weight goes down because assuming the same flux density and circumferential arc, a greater number of poles produces the same radial flux but requires less stator core back iron (see Figure 5). The PCM weight decreases because the higher frequencies and lower rectified voltage associated with the increased pole numbers reduce the size and energy requirements of the passive components, especially the capacitors. Therefore, the total power generation module weight decreases as the number of poles increases making the 12-pole machine the most attractive in terms of weight.
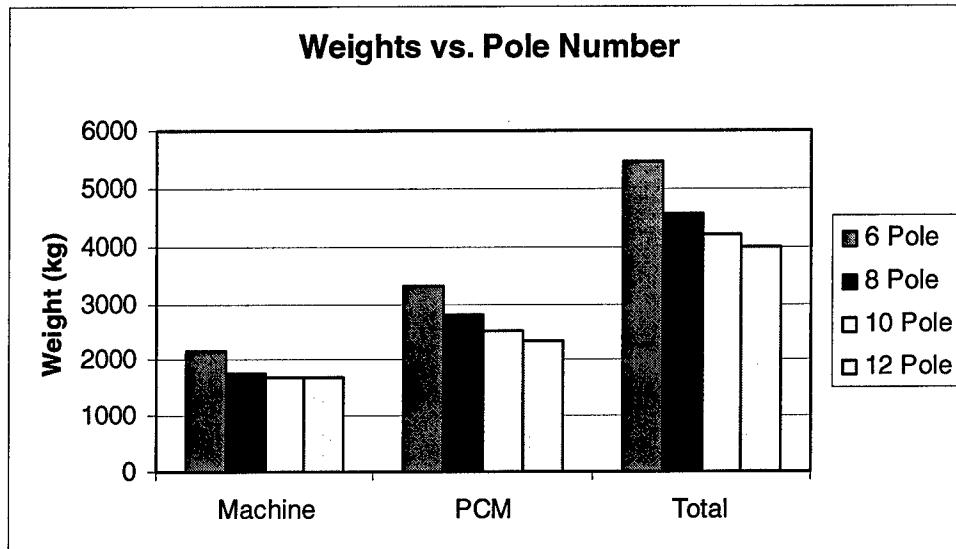
Figure 46: Weights vs. Number of Poles

Next, looking at Figure 47, as the number of poles goes up, the losses in the machine increase, some more than others. The core losses increase because the higher frequencies cause the eddy currents and hysteresis to have a greater effect. However, the range in core losses is only 7 kW so this increase is not a major contributor. The windage losses are not significantly affected by the number of poles differing by only 3 kW across the pole variation.
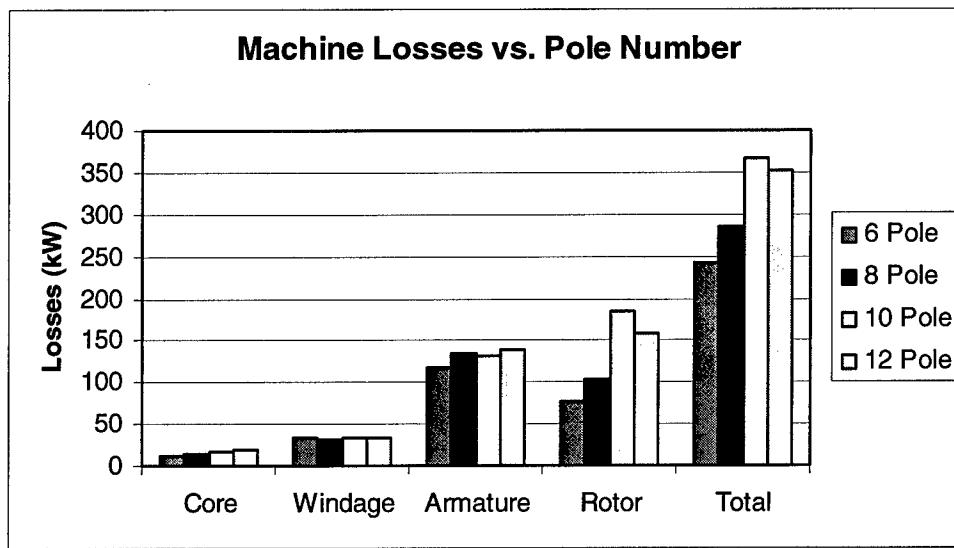
Figure 47: Machine Losses vs. Number of Poles

The armature losses do fluctuate some as the pole number changes with the 6-pole machine having the lowest (117.6 kW) and the 12-pole machine having the highest (137.9 kW).

This is due to the higher pole machines having higher stator current densities as the machine performance is optimized. The rotor losses also increase as the number of poles gets higher mainly because of the winding time and space harmonics. As the pole number increases, the number of slots/pole/phase (m) decreases which causes the winding factors to have less of an influence in reducing higher harmonic effects.

Overall, all of the different pole machines have less than 160 kW of rotor losses with the 6-pole machine having the lowest. However, as mentioned in section 6.3, the generator voltage THD is more significant in this machine causing the higher pole machines to become viable options.

The number of poles also produces sizeable effects on the PCM losses. As the pole number increases, the PCM losses decrease due to much lower IGBT switching losses. This is because the higher pole machines have lower rectified voltages which reduce the stresses and switching losses in the IGBTs (see section 4.4). The difference between having 6-poles and 12-poles is 754.3 kW in PCM losses, a 22.9% reduction. If soft switching is implemented, the PCM losses are still lower for the higher pole machines, but the difference is now 98.1 kW, a 10.3% reduction. Overall, as shown in Figure 48, the 12-pole machine is the best option when considering PCM losses.
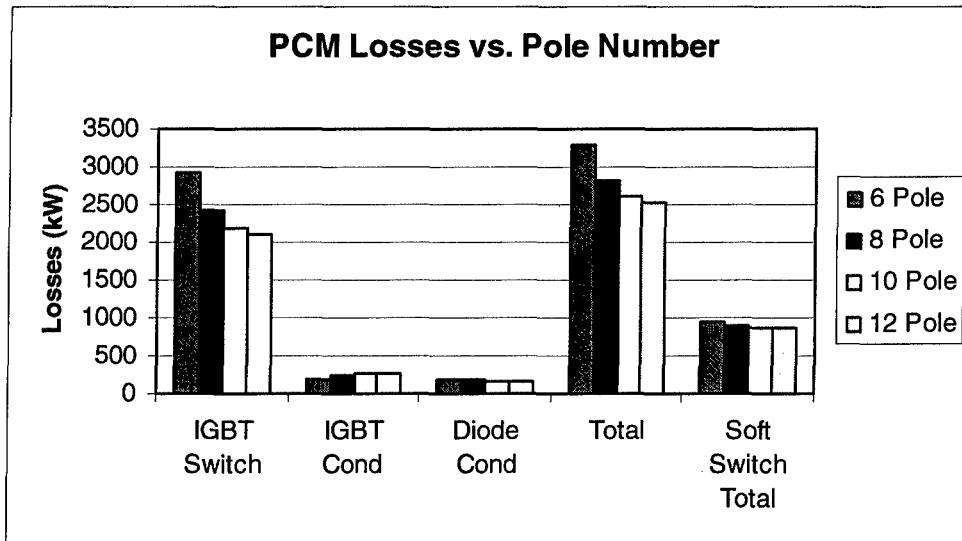
Figure 48: PCM Losses vs. Number of Poles

The generator voltage THD and the AC line current THD are both affected by the number of poles. Examining Figure 49, the 10-pole and 12-pole generators are the only variants

that produce voltage waveforms that have acceptable THD levels, 3.74% and 4.95% respectively. The AC line current THD values are satisfactory for all of the pole numbers with the 12-pole machine having the lowest value (6.82%). If the THD is examined in conjunction with the machine losses, the12-pole machine is the best option. It has the top overall THD performance, has 25.8 kW lower rotor losses compared to the 10-pole generator, and has 14.6 kW lower total machine losses compared to the 10-pole design.
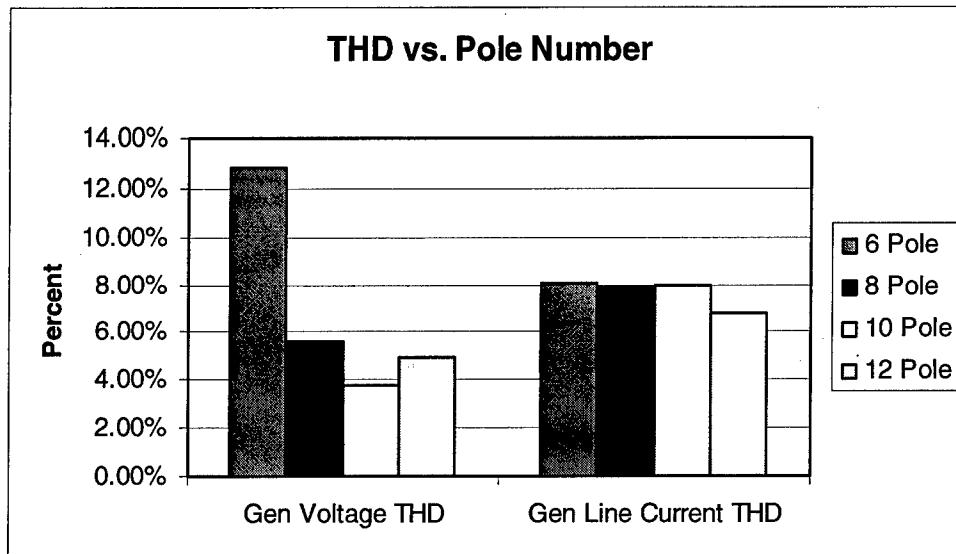
Figure 49: THD vs. Number of Poles

6.5   Final Power Module

6.5.1   PM Generator

Based on the previous analysis and the goal of producing an optimal power generation module, a final design is selected. The sizing codes and analysis from sections 3.4.1, 3.4.2, 3.4.3, and 3.4.4 are also utilized in this process. The final PM generator is a 3-phase, 12-pole machine with an inconel retaining sleeve. The final design is not a fully optimized in terms of all parameters but represents the best selection using the methodology of this paper. Detailed characteristics for the PM generator are listed in Table 17.

Table 17: PM Generator Final Design Parameters

Machine Size			
Total Machine Diameter	0.848 m	Total Machine Length	1.868 m
Rotor Radius	0.147 m	Active Length	1.000 m
Slot Average Width	16.973 mm	Slot Height	25.000 mm
Back Iron Thickness	17.150 mm	Tooth Width	15.882 mm
Machine Ratings			
Power Rating	16,000 kW	Speed	13,000 RPM
V_a (RMS)	1,739 V	Phase Current	3,169.3 A
E_a (RMS)	2,380 V	Armature Resistance	0.00457 Ω
Synchronous Reactance	0.377 Ω	Synchronous Inductance	0.046 mH
Stator Current Density	2,987.6 A/cm²	Tip Speed	200 m/s
Efficiency	0.979	Power Factor	0.960
Phases	3	Frequency	1,300 Hz
Stator Parameters			
Number of Slots	36	Number of Armature Turns	12
Fund Breadth Factor	1.000	Fund Pitch Factor	0.866
Tooth Flux Density	1.30 T	Back Iron Flux Density	0.93 T
Slots/pole/phase (m)	1.00		
Rotor Parameters			
Magnet Height	29.00 mm	Magnet Angle	20 deg
Air Gap	5.00 mm	Pole Paris	6
Magnet Remanence	1.20 T	Air Gap B_g	0.69 T
Magnet Factor	0.961	Skew Factor	0.955
Machine Losses			
Core Loss	19.9 kW	Armature Loss	137.9 kW
Windage Loss	34.4 kW	Rotor Loss	158.9 kW
Machine Weights			
Core	292.49 kg	Shaft	522.73 kg
Magnet	72.59 kg	Armature	82.48 kg
Services	145.54 kg	Structure	557.92 kg
Total	1,673.75 kg		

A diagram of the PM generator is shown in Figure 50 with the stator winding layout given in Table 18. The numbers in the winding layout table refer to the slot number locations of Figure 50.
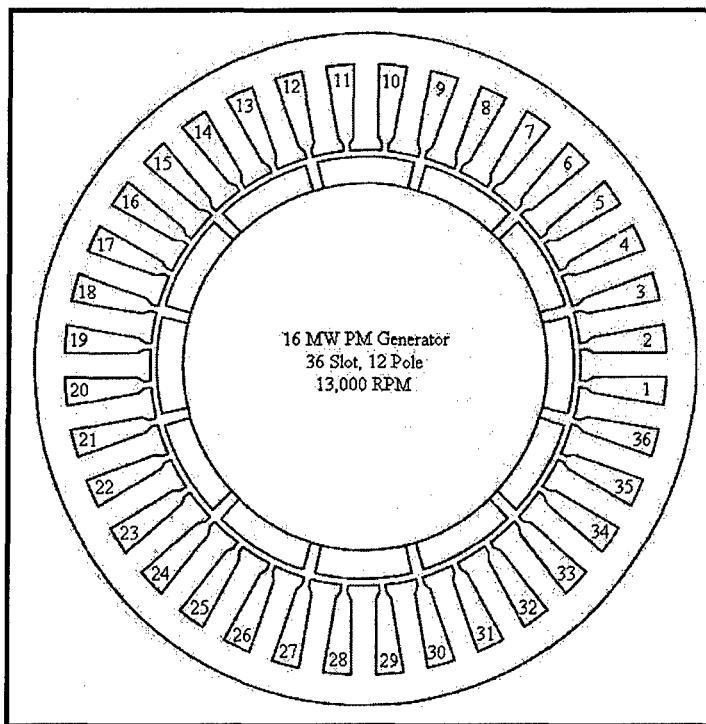
Figure 50: Diagram of PM Generator Final Design

Table 18: Winding Layout

Coil Number	Phase A		Phase B		Phase C	
	Slot In	Slot Out	Slot In	Slot Out	Slot In	Slot Out
1	1	3	3	5	5	7
2	6	4	8	6	10	8
3	7	9	9	11	11	13
4	12	10	14	12	16	14
5	13	15	15	17	17	19
6	18	16	20	18	22	20
7	19	21	21	23	23	25
8	24	22	26	24	28	26
9	25	27	27	29	29	31
10	30	28	32	30	34	32
11	31	33	33	35	35	1
12	36	34	2	36	4	2

6.5.2 Power Electronics Module

In conjunction with selecting the final PM generator design, the associated power electronics module is determined. Figure 51 shows the complete power module, including individual component values.
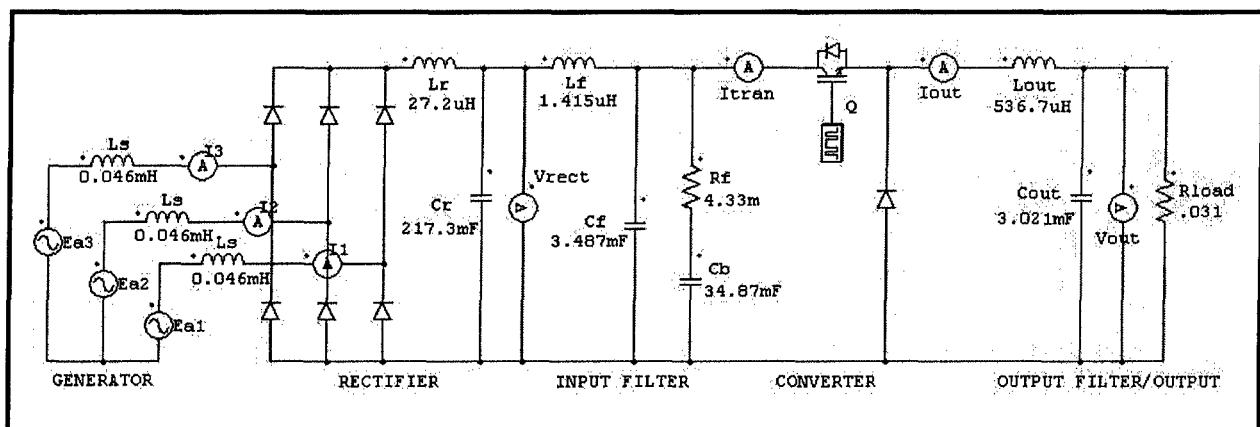
Figure 51: Power Module Final Design Diagram

Along with Figure 51, additional characteristics for the final power module are given in Table 19 with detailed data contained in the appendices.

Table 19: PCM Final Design Parameters

PCM Losses w/ Hard Switching			
IGBT Switching Losses	2,103.6 kW	Diode Conduction Losses	168.2 kW
IGBT Conduction Losses	267.6 kW	Total PCM Losses	2,539.4 kW
Efficiency	0.841		
PCM Losses w/ Soft Switching			
IGBT Switching Losses	420.7 kW	Diode Conduction Losses	168.2 kW
IGBT Conduction Losses	267.6 kW	Total PCM Losses	856.5 kW
Efficiency	0.946		
PCM Weights			
Capacitors	396.2 kg	Inductors	420.9 kg
IGBTs	22.8 kg	Diodes	51.8 kg
Services	267.5 kg	Structure	1,159.2 kg
Total	2,318.4 kg		
PCM Dimensions			
Length	2.0 m	Width	1.66 m
Height	2.0 m	Volume	6.64 m^3
PCM Ratings			
Max Rectified Voltage	5,567 V	Output Voltage	700.0 V
Duty Cycle (@16MW load)	0.1622	Output Voltage Ripple (@16MW load)	0.09 V
Duty Cycle (@100kW load)	0.1277	Output Voltage Ripple (@100 kW load)	1.40 V

6.5.3 Performance/Waveforms

As discussed in section 5.4, all 80 power modules are constructed and simulated using PSIM. In order to conserve space, only the simulation results for the final design are presented here. The module is simulated operating at the maximum load of 16 MW and at the minimum load of 100 kW.

For the 16 MW loading, Figure 52 shows the generator voltage waveforms. Since the THD is low, the curves fairly closely resemble sine waves.
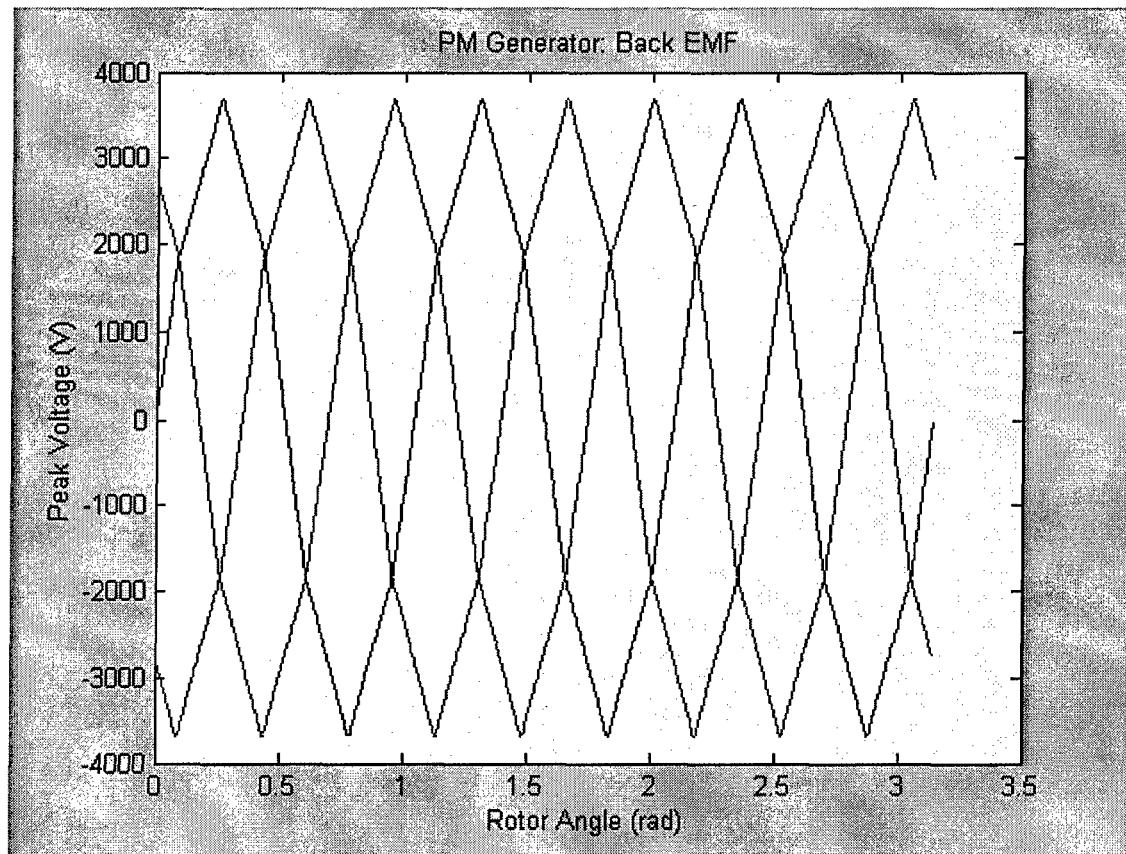
Figure 52: PM Generator Voltage Waveforms

Figure 53 through Figure 55 show plots for various parameters for the complete module loaded at 16 MW. The output voltage fluctuates approximately 0.09 V (0.0013%) which is within specification, the output current varies by less than 22 A (0.0096%), and the AC line currents have low harmonic content.
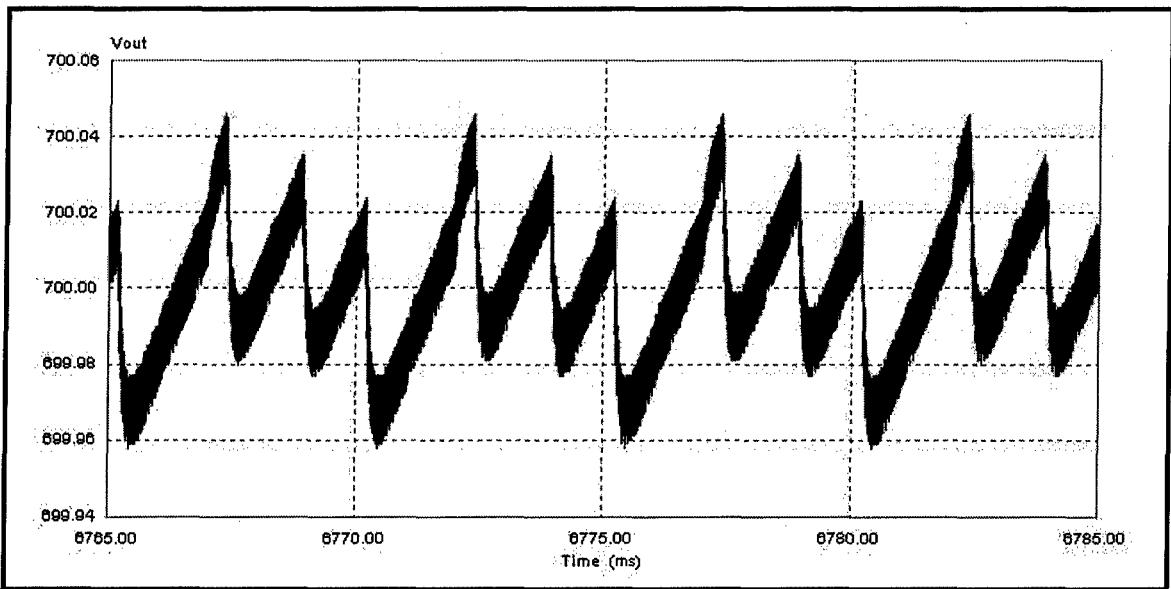
Figure 53: Output Voltage (16 MW)
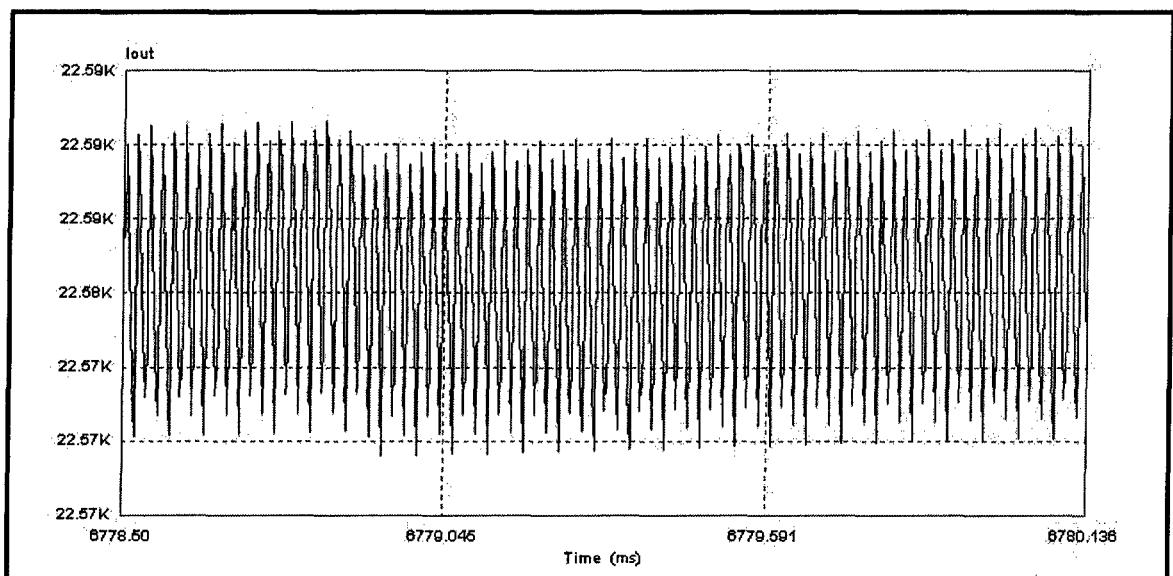
Figure 54: Output Current (16 MW)

112
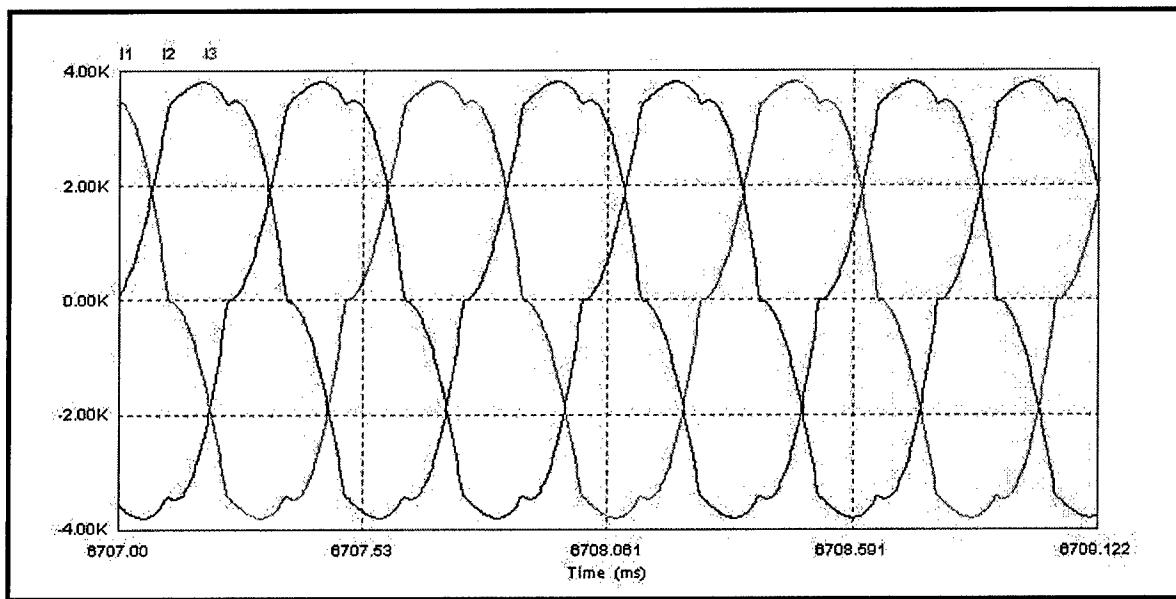
Figure 55: AC Line Current (16 MW)

Figure 56 through Figure 58 display the module performance at the minimum load of 100 kW. The output voltage ripple is 1.4 V, higher than at full load but still not significant. The output current also has some variation (about 25 A) but this is acceptable at the lower power levels. The AC line current has much higher harmonic content because of notches that occur in the waveforms caused by the DC link capacitor charging and discharging at the low load. However, the magnitudes of the harmonics are insignificant since the magnitude of the fundamental is low and therefore the rotor losses and heating are not adversely affected.
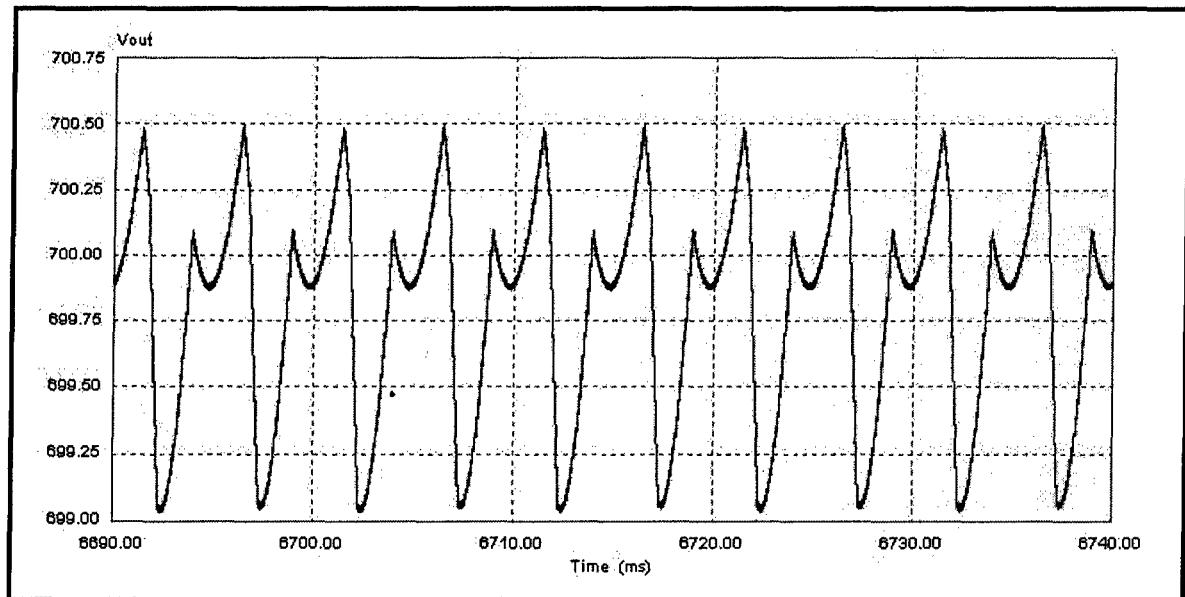
Figure 56: Output Voltage (100 kW)
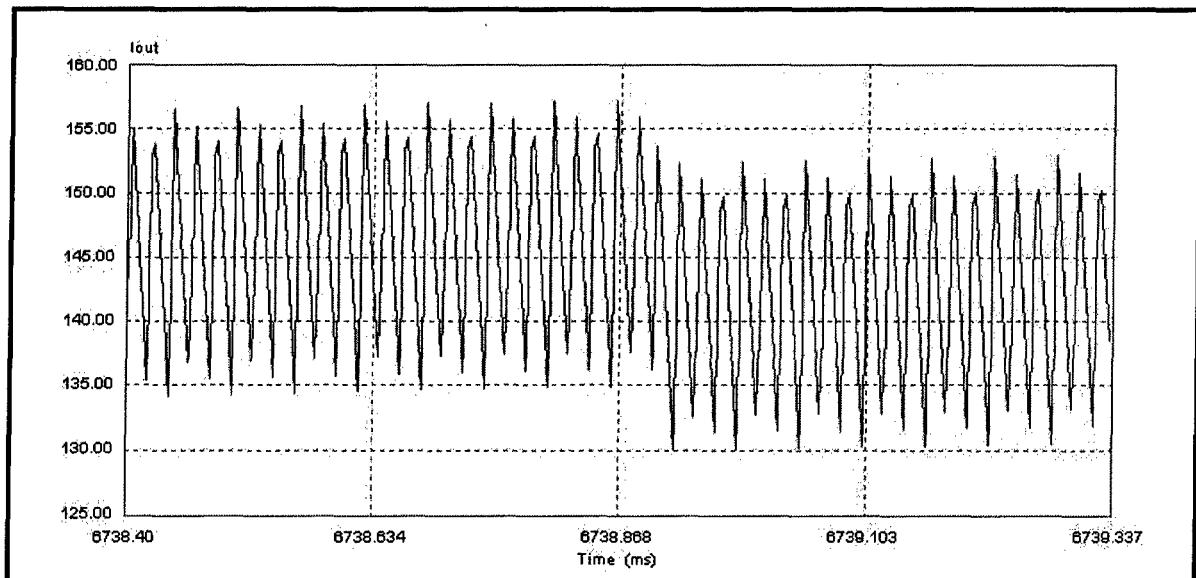
Figure 57: Output Current (100 kW)

114
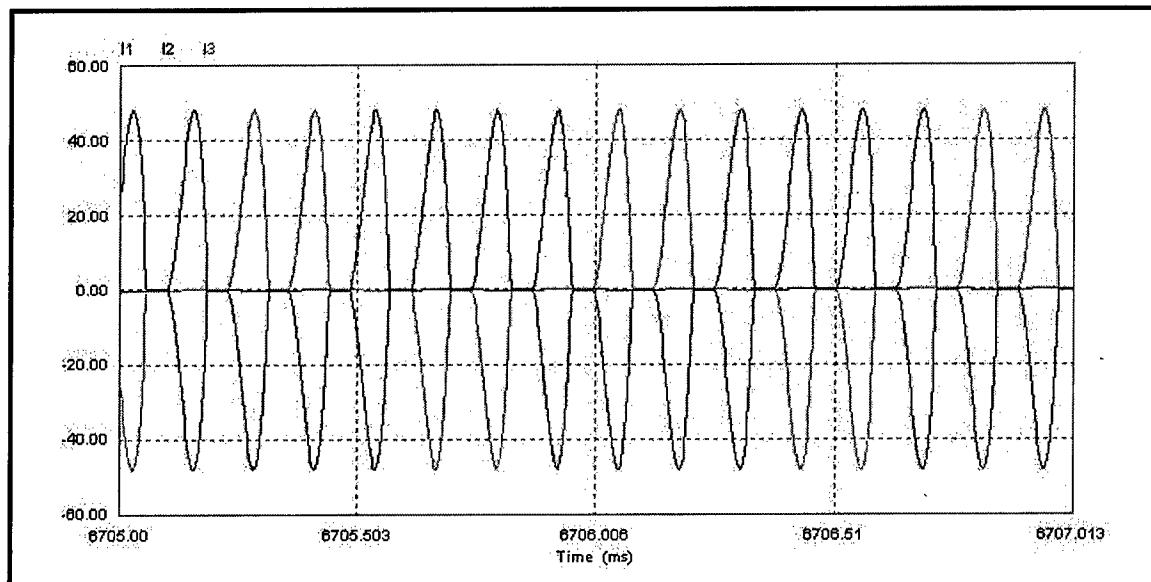
Figure 58: AC Line Current (100 kW)

6.6 Comparison

The premise for designing and employing a high-speed PM generator and power conversion module is to offer a light weight, power dense alternative to existing wound rotor machines. In Table 1 in section 1.3.2, parameters for some typical wound rotor machines are presented. In order to compare them with the new design power module, these machines are scaled to 16 MW using the general relationship of Eqn 6-1.

$$Pwr \propto Vol^{\frac{4}{3}}$$

Eqn 6-1

Table 20 then provides an evaluation of the different machines and power modules.

Table 20: Comparison of Machines/Modules

Machine	Phases	Power (MW)	Speed (RPM)	Length (m)	Width (m)	Height (m)	Volume (m³)	Weight (MT)
1	3	16	3,600	4.4	3.7	3.2	52.0	40.8
2	3	16	3,600	5.0	3.6	3.1	54.3	34.3
3	3	16	3,600	5.5	3.2	4.0	69.0	47.3
4	3	16	3,600	4.6	2.8	3.7	47.6	41.0
PM Gen	3	16	13,000	1.87	0.85	0.85	1.4	1.67
PCM	N/A	16	N/A	2.0	1.66	2.0	6.6	2.32
Total PM	3	16	13,000	3.87	Varies	Varies	8.0	3.99

115

Examining Table 20, the new design offers significant reductions in both weight and volume. Specifically, the new total power module is 11.6 – 16.8% the volume and 8.5 – 11.7% the weight of the other machines. This translates to about a 7x reduction in volume and a 10x reduction in weight. These reductions can provide flexibility to naval architects since power, weight, and volume are integral parts of the design and construction processes.

Chapter 7 Conclusions and Recommendations

7.1 Design Lessons Learned

Numerous lessons are learned from both the generator and power electronics design processes. The entire 16 MW power module is a complex system with many interrelated components that affect the overall performance.

7.1.1 PM Generator

The final generator is the product of examining multiple parameters to determine an optimal design. Various lessons are learned relating to different portions of the machine including the number of slots, the number of poles, the number of phases, the magnetic geometry, the windings and output voltage, and optimization methods.

7.1.1.1 Number of Slots

Initially, it was thought that the number of slots could be held constant over the range of machine designs. However, this is not possible because as the number of phases increases, additional slots are necessary to fit the greater number of windings. One of the most important parameters that can be used to help reduce the harmonics in a rotating machine is the number of slots/pole/phase (m). Therefore, the number of slots can be used to help optimize this parameter and improve the shape of the output voltage waveform and THD.

The number of slots also influences the electrical loading of the machine. The number of slots directly affects the slot size which helps determine the current density in the machine. This is usually one of the limits on the machine's performance because of cooling. Overall, the number of slots is an important parameter that must be carefully selecting when designing a machine.

7.1.1.2 Number of Poles

Traditionally, the number of poles is driven by the system frequency and prime mover speed. With a high-speed generator rectified to a DC distribution system, the number of poles becomes an important design variable. Therefore, throughout the design progression, careful consideration should be given to the number of poles. This proved to be true throughout this

paper since the number of poles affects the electrical, magnetic, and structural performance, including the electrical frequency, the voltage waveforms, the magnetic flux, the magnet volume, the magnet pole pitch, the air gap size, and the stator back iron thickness.

It is recommended that initially the designer select a range of acceptable output electrical frequencies which puts bounds on the allowable number of poles. From there, the number of poles can be varied to help determine the size, waveforms, and performance of the generator. In general, if the rotational speed is held constant as the number of poles increases:

- The number of slots/pole/phase (m) changes affecting the output waveforms and THD
- The weight of the machine decreases
- The electrical frequency increases

7.1.1.3 Number of Phases

An odd number of phases is usually the best option for rotating machines because it produces balanced operation with limited mechanical fluctuations. Initially, it was assumed that a higher number of phases (greater than 3) would produce a more optimal power module. It is discovered that this is not necessarily the case. As the number of phases increases, m decreases which can adversely affect the voltage THD. Also, the AC line current harmonics are more substantial in increased phase machines because the triple-n harmonics are higher order as the phase number increases. However, a big advantage of having a higher number of phases is that it reduces the requirements for the PCM because of lower rectifier voltage ripple and lower phase voltages and currents.

It is concluded that the benefits of 3-phases and a higher number of phases can be simultaneously realized through a modified design. Multiple 3-phase sets of windings can be located equidistant around the stator and then connected to the PCM to achieve the desired results. An example of this would be three 3-phase sets of windings, one set at 0^0, 120^0, and 240^0; one at 45^0, 165^0, and 285^0; and one at 90^0, 210^0, and 330^0.

7.1.1.4 Magnetic Geometry

Designing the magnetic geometry in a PM generator is an intricate process. Careful consideration should be given to the type of retaining material, the magnet material, and the desired voltage. It is determined that the magnet height and air gap length greatly affect the overall machine performance, and if they are not properly selected, the generator does not

118

operated properly. A typical starting point in a design is to have the magnet height be approximately 5 – 10x the length of the air gap [17], [18], [30]. This ensures that the magnetic flux is adequate while not saturating the core material.

7.1.1.5 Windings and Output Voltage

As discussed in section 3.2.7, wye series connected windings are used in this paper. This produces a generator output voltage that is too high compared to the desired PCM output voltage of 700 V. It also unnecessarily stresses the PCM devices and produces a lower than optimal duty cycle. It is concluded that connecting some of the generator windings in parallel or using a lower number of turns to produce a lower output voltage might be viable options to alleviate this problem. However, care must be taken to account for possible circulating currents in the parallel windings in the event of a fault.

7.1.1.6 Optimization Methods

When designing the PM generator, the goal was to produce an optimal design that met the required performance criteria while minimizing the rotor losses, the size, and the weight of the machine. Optimizing the design involves trying to simultaneously maximize both the electrical loading (current density) and magnetic loading (air gap flux density). It is concluded that it is extremely difficult to do both at the same time since there are competing factors such as saturation limits, cooling limits, and rotational stress limits.

In this paper, each of the 80 machines is optimized by trying to maximize the current density (within the limits) while ensuring an adequate air gap flux density. This is done because it seems to produce the smallest, high-performance machines. It is therefore recommended in any PM generator design process that careful consideration be given to both the electrical and magnetic loading.

7.1.2 Power Electronics

The power electronics module (PEM) designed in conjunction with the PM generator uses one of many possible topologies. The combination of the passive rectifier and buck converter is a stable, well-proven design. It is optimized to match the generator by selecting the passive components properly. However, the design does have limitations because it uses hard-switching and large passive components.

7.1.2.1 Rectification

Passive rectification is utilized in the PEM because of its simplicity and potential for lower input harmonics. It is concluded that the rectification scheme is satisfactory and couples well with the PM generator. However, it is recognized that a more detailed analysis of the rectification scheme could produce a better topology.

7.1.2.2 Conversion and Switching

As discussed in Chapter 6, one of the main problems with the power electronics module is that the losses are too high due to the IGBT switching losses. This is because hard switching is used in the power conversion module as opposed to soft switching. Soft switching minimizes device switching losses, reduces EMI, permits higher switching frequencies, and achieves higher efficiencies.

Analyzing different soft-switching topologies is beyond the scope of this paper but the effects soft switching has on the PCM are studied. It is concluded that if soft switching is implemented in the PCM, the efficiency increases by 10 – 20% with the losses reduced by overall 1 MW. Given the power requirements of the power generation module, soft switching should be employed. It is therefore recommended that in any high-power system that utilizes power conversion modules, soft switching should be examined to ascertain its usefulness.

7.1.2.3 Control

One control scheme for providing voltage regulation for the power generation module is discussed in section 4.3.4. This control methodology utilizing duty ratio control with a PID controller is relatively simple to implement. This ease of control is possible because the buck converter is a straightforward topology. It is concluded that if a more complex, soft-switching design is implemented, more extensive control schemes would be required.

Even though it is not discussed in detail, the PM generator provides for easy control because it is a synchronous machine. This is a distinct advantage over an induction generation which requires extremely complicated control algorithms.

7.2 Power Generation Module

Overall, 80 different 16 MW machines and power conversion modules are sized, designed, and analyzed with a final design selected. The permanent magnet generation module,

consisting of the generator and associated power electronics, provides an excellent alternative to traditional wound rotor machines for naval applications. It is concluded that the new design offers significant reductions in both weight and volume. Specifically, it is estimated that the PM generation module has a 7x reduction in volume and a 10x reduction in weight compared to similarly rated wound rotor systems. These reductions can provide flexibility to naval architects since power, weight, and volume are integral parts of the design and construction processes. However, further study is necessary to verify the 16 MW PM generation module's thermal, structural, and mechanical performance.

7.3 Recommendations/Further Study

This paper discussed the electrical and magnetic design and analysis of a permanent magnet generation module including sizing, detailed machine design and analysis, analytical models for different rotor loss mechanisms as well as with other machine losses, power electronics and conversion for connecting the high-speed generator to a DC distribution system, and in depth simulation of the complete system. Numerous design issues are addressed and several issues are raised about the potential improvements a PM generation system can offer. A proposed PM generation module design is presented along with a detailed design methodology.

However, this paper does not full cover all aspects associated with the design and analysis of a PM generation module. In order to fully ascertain whether the proposed design is technically sound, further study is required in both the machine and power electronics areas. Specifically, with the respect to the generator, the following is recommended:

- Using the calculated losses, perform a detailed thermal analysis of the machine including development of the required cooling systems
- Conduct an in-depth structural and mechanical study of the PM generator, including vibration and acoustic analysis

For the power electronics portions, the further examination is recommended, including:

- Examine different rectification schemes to see what effects they would have on the whole system
- Explore soft switching topologies and perform detailed analysis on how to implement them to ensure acceptable switching losses while matching performance with the generator

121

For the complete PM generation system, the following is recommended:

- Using the developed PM generator and power electronics module, implement a control scheme and conduct in-depth analysis with the system connected to an entire distribution system under changing load conditions

Glossary

α	Winding Pitch
α_b	Bottom Surface Coefficient
α_m	Magnet Pitch Coverage Coefficient
α_t	Top Surface Coefficient
β	Flux Density Dip Width
ε_b	Flux Density Exponent
ε_f	Frequency Exponent
γ	Winding Electrical Angle
λ	Flux Linkage or Wavelength (depending)
λ_B	Flux Density Dip Interval
λ_s	Slot Fill Fraction
η	Efficiency
ν_{air}	Kinematic Viscosity of Air at 20^0 C (m^2/s)
ψ	Power Factor Angle
ρ	Resistivity
ρ_{air}	Air Density at 20^0 C (kg/m^3)
ρ_s	Steel Density (kg/m^3)
ρ_m	Magnet Density (kg/m^3)
ρ_c	Conductor Density (kg/m^3)
σ_{st}	Stator Conductivity (S/m)
θ_m	Magnet physical angle
θ_{sk}	Magnet skew angle
τ	Air Gap Shear Stress
τ_s	Stator Tooth Width + Stator Slot Width
μ_0	Free Space Permeability
μ_{rec}	Recoil Permeability
ω	Electrical Frequency (rad/sec)
ω_m	Mechanical Frequency (rad/sec)
A	Magnetic Vector Potential
A_{ac}	Armature Conductor Area
A_g	Air Gap Area
A_m	Magnet Area
A_s	Slot Cross-sectional Area
B_0	Base Flux Density for Core Losses
B_1	Fundamental Flux Density
B_b	Back Iron Flux Density
B_d	Flux Density Dip
B_{flux}	Ideal Radial Flux Density
B_g	Air Gap Flux Density
B_r	Remnant Flux Density
B_t	Tooth Flux Density

c_p	Specific Heat Capacity of Air (J/kg*C)
C_Φ	Flux Concentration Factor
C_f	Friction Coefficient
d	Buck Controller Average Duty Cycle
d_c	Stator Core Back Iron Thickness
D	Duty Ratio
D_{mach}	Overall Machine Diameter
e	Buck Controller Error Signal
E_a	Back Voltage (EMF)
f	Electrical Frequency (Hz)
F_0	Base Frequency for Core Losses
g	Air Gap
g_e	Effective Air Gap
h_d	Slot Depression Depth
h_m	Magnet Height/Thickness
h_s	Slot Depth
I_a	Phase Current
I_L	Average Converter Output Current
J_a	Current Density
k	Wave Number
k_{bn}	Winding Breadth/Distribution Factor
k_e	Electrical Power Waveform Factor
k_{gn}	Magnet Factor
k_i	Current Waveform Factor
k_{pn}	Winding Pitch Factor
k_{sn}	Winding Skew Factor
k_{wn}	Winding Factor
K_c	Carter Coefficient
K_l	Leakage Factor
K_r	Reluctance Factor
K_s	Retaining Can Loss Factor
K_z	Surface Current Density
L	Overall Machine Length
L_{ac}	Armature Conductor Length
L_{ag}	Air Gap Inductance
L_{as}	Self Slot Leakage Inductance

L_{am}	Mutual Slot Leakage Inductance
L_e	End Turn Inductance
L_{mach}	Overall Machine Length
L_{slot}	Slot Leakage Inductance
L_s	Synchronous Inductance
L_{st}	Rotor Stack Length
m	Slots per Pole per Phase
M_{ac}	Mass of Armature Conductor
M_c	Mass of Core
M_{cb}	Mass of Core Back Iron
M_{ct}	Mass of Core Teeth
M_m	Mass of Magnets
M_s	Mass of Shaft
M_{tot}	Total Mass
N	Rotational Speed (RPM)
N_a	Number of Armature Turns
N_c	Turns per Coil
N_s	Number of Stator Slots
N_{sct}	Actual Coil Throw (in slots)
N_{sfp}	Full-pitch Coil Throw (in slots)
N_{sp}	Number of Stator Slots Short Pitched
p	Pole Pairs
pf	Power Factor
P_0	Base Power for Core Losses
P_c	Total Core Loss
P_{cb}	Core Iron Loss
P_{can}	Retaining Can Loss
P_{ct}	Tooth Loss
P_{in}	Input Power
P_{wind}	Friction & Windage Losses
PC	Permeance Coefficient
PCM	Power Conversion Module
PEM	Power Electronics Module
Perm	Permeance
Pwr	Machine Power
q	Number of phases
R	Rotor Radius
R_1	Inner Bound of Magnet
R_2	Outer Bound of Magnet
R_a	Armature Resistance
R_{ci}	Core Inside Radius

R_{co}	Core Outside Radius
R_d	Diode On-State Resistance
R_{ds}	IGBT On-State Resistance
R_i	Inner Magnetic Boundary
R_s	Outer Magnetic Boundary
Rey	Reynold's Coefficient
syrat	Stator Back Iron Ratio (Yoke Thickness/Rotor Radius)
t	Retaining Sleeve Thickness
tfrac	Peripheral Tooth Fraction
THD	Total Harmonic Distortion
v_{mag}	Magnet Speed (m/s)
v_{tip}	Rotor Tip Speed (m/s)
V_a	Terminal Voltage
w	Retaining Can Loss per Unit Area
w_d	Slot Depression Width
w_s	Slot Average Width
w_{sb}	Slot Bottom Width
w_{st}	Slot Top Width (closest to rotor)
w_t	Tooth Width
X_s	Synchronous Reactance
Z_s	Surface impedance

Acknowledgements

Page Intentionally Left Blank

List of References

[1]   T. F. Chan, L. L. Lai, & Lie-Tong Yan, "Performance of a Three-Phase AC Generator with Inset NdFeB Permanent Magnet Rotor," IEEE Transactions on Energy Conversion, Vol. 19, No. 1, March 2004.

[2]   Surong Huang, Jian Luo, Franco Leonardi, & Thomas A. Lipo, "A General Approach to Sizing and Power Density Equations for Comparison of Electric Machines," IEEE Transactions on Industry Applications, Vol. 14, No. 1, Jan/Feb 1998.

[3]   Anteon Corporation, "Future Shipboard Power System Architecture Analysis Interim Report: Shipboard Electrical Distribution System Characteristics," December 2001.

[4]   LCDR Timothy McCoy, Matthew Stauffer, & Edward Harvey, "Full Scale Land Based Testing of the U.S. Navy's Integrated Power System (IPS)," Naval Sea System Command, March 2000.

[5]   GMS, Inc. & Draper Laboratory, Electric Power Applications to Naval Ships, A Technology Review, May 1997.

[6]   Timothy J. Doyle, Howard O. Stevens, & Henry Robey, "An Historical Overview of Navy Electric Drive."

[7]   Ronald O'Rourke, Electric Drive Propulsion for U.S. Navy Ships: Background and Issues for Congress, Congressional Research Service, The Library of Congress, July 2000.

[8]   Jason Pepi & Dr. Peter Mongeau, "High Power Density Permanent Magnet Generators," DRS Electric Power Technologies, Inc., 2004.

[9]   Wang Fengxiang, Zheng Wenpeng, Zong Ming, & Wang Baoguo, "Design Considerations of High-Speed PM Generators for Micro Turbines," IEEE Transactions, 2002.

[10]   Thomas C. Gillmer & Bruce Johnson, Introduction to Naval Architecture, Naval Institute Press, Dec 1982.

[11]   Dr. Timothy McCoy, "Contemporary Naval Electric Power Systems," Course 13.412 Lecture, Massachusetts Institute of Technology, Fall 2003.

[12]   Richard J. Newman, "For the Navy, an Engine of Change," U. S. News & World Report, December 1999.

[13]   LCDR Andy Gish, LCDR Bill Hardman, LCDR Steve Ramsey, Concept Design of a Reduced Displacement Fast Attack Submarine, MIT 13A, May 2004.

[14]   Dr. Makhlouf Benatmane, LCDR Timothy McCoy, & Ms. Tracey L. Cooper, "Electric Propulsion Full-Scale Development in U.S. Navy Surface Ships," October 1998.

[15]   Science Applications International Corporation, Superconducting Generator Study Final Report, Dec 2002.

[16]   James L. Kirtley, "Course 6.685: Electric Machines, Class Notes 1," Massachusetts Institute of Technology, 2003.

[17]   Dr. Duane Hanselman, Brushless Permanent Magnet Motor Design, The Writer's Collective, 2003.

[18]   J. R. Hendershot, Jr. & T. J. E. Miller, Design of Brushless Permanent Magnet Motors, Magna Physics Publishing and Clarendon Press, 1994.

[19]   James L. Kirtley, "Course 6.685: Electric Machines, Class Notes 7," Massachusetts Institute of Technology, 2003.

[20]   E. Spooner & A. C. Williamson, "Direct Coupled, Permanent Magnet Generators for Wind Turbine Applications," IEEE Proceedings, Electrical Power Applications, Vol. 143, No. 1, Jan 1996.

[21]   Johannes J. H. Paulides, Geraint W. Jewell, & David Howe, "An Evaluation of Alternative Stator Lamination Materials for a High-Speed, 1.5 MW, Permanent Magnet Generator," IEEE Transactions on Magnetics, Vol. 40, No. 4, July 2004.

[22]   Mark Rippy, An Overview Guide for the Selection of Lamination Materials, Proto Laminations, Inc., 2004.

[23]   D. Pavlik, V. K. Garg, J. R. Repp, & J. Weiss, "A Finite Element Technique for Calculating the Magnet Sizes and Inductances of Permanent Magnet Machines," IEEE Transactions of Energy Conversion, Vol. 3, No. 1, March 1988.

[24]   Do Hyun Kang, Paul Curiac, Yeon Ho Jung, & Soo Jin Jung, "Prospects for Magnetization of Large PM Rotors: Conclusions from a Development Case Study," IEEE Transactions on Energy Conversion, Vol. 18, No. 3, Sept 2003.

[25]   Website for Magnetic Component Engineering, Inc., 2004.

[26]   James L. Kirtley, "Course 6.685: Electric Machines, Class Notes 5," Massachusetts Institute of Technology, 2003.

[27]   N. Bianchi & A. Lorenzoni, "Permanent Magnet Generators for Wind Power Industry: An Overall Comparison with Traditional Generators," Opportunities and Advances in International Power Generation, Conference Publication No. 419, 1996.

[28]   Co Huynh, Larry Hawkins, Ali Farahani, & Patrick McMullen, "Design and Development of a Two-Megawatt, High-Speed Permanent Magnet Alternator fro Shipboard Application," Calnetix, Inc., 2004.

[29]   Website www.consult-g2.com/course/chapter7/chapter.html.

[30]   M. A. Rahman & G. R. Slemon, "Promising Applications of Neodymium Iron Boron Iron Magnets in Electrical Machines," IEEE Transactions on Magnetics, Vol. No. 5, Sept 1985.

[31]   Dr. Peter Mongeau, "High Torque Density Propulsion Motors," DRS Electric Power Technologies, Inc., 2004.

[32]   O. Aglen & A. Andersson, "Thermal Analysis of a High-Speed Generator," IEEE Transactions, 2003.

[33]   S. M. Abu Sharkh, M. R. Harris, & N. Taghizadeh Irenji, "Calculation of Rotor Eddy-Current Loss in High-Speed PM Alternators," IEE Conference Publication No. 444, 1997.

[34]   D. K. Yue, "Course 13.021: Marine Hydrodynamics, Lecture Notes 17," Massachusetts Institute of Technology, 2002.

[35]   H. Polinder & M. J. Hoeijmakers, "Eddy-Current Losses in the Segmented Surface-Mounted Magnets of a PM Machine," IEE Proceedings, Electrical Power Applications, Vol. 146, No. 3, May 1999.

[36]   James L. Kirtley, "Course 6.685: Electric Machines, Class Notes 3," Massachusetts Institute of Technology, 2003.

[37]   Mihai Comanescu, Ali Keyhani, & Min Dai, "Design and Analysis of 42V Permanent Magnet Generator for Automotive Applications," IEEE Transactions on Energy Conversion, Vol. 18, No. 1, 2003.

[38]   A. Munoz-Garcia & D. W. Novotny, "Utilization of Third Harmonic-Induced-Voltages in PM Generators," IEEE, 1996.

[39]   R. W. Erickson, Fundamentals of Power Electronics, Prentice-Hall, 1997.

[40]   Arthur Kelley & William F. Yadusky, "Rectifier Design for Minimum Line-Current Harmonics and Maximum Power Factor," IEEE Transactions on Power Electronics, Vol. 7, No. 2, 1992.

[41]   John G. Kassakian, Martin F. Schlecht, & George C. Verghese, Principles of Power Electronics, Addison-Wesley Publishing Company, Inc., 1991.

[42]   Ned Mohan, Tore M. Undeland, & William P. Robbins, Power Electronics: Converters, Applications, and Design, John Wiley & Sons, Inc., 1995.

[43]   Dr. David Perreault, Course 6.334: Power Electronics Notes, Massachusetts Institute of Technology, 2004.

[44]   Website http://henry.fbe.fh-darmstadt.de/smps_e/

[45]   T. K. Phelps & W. S. Tate, "Optimizing Passive Input Filter Design," Proceedings of the 6th National Solid State Power Conversion Conference, 1979.

[46]   Website www.electronicstalk.com, March 2002.

[47]   Website www.pwrx.com.

[48]   Website www.pi.hitachi.co/jp/pse/index.html.

[49]   Website www.ThinGap.com.

[50]   Website www.pulseeng.com.

[51]   Ming-Jen Pan, Barry Bender, Roy Rayne, & Michael Lanagan, Development of Advanced Dialectrics for High Energy Density Capacitors, 2004.

[52]   Troy W. Barbee, Gary W. Johnson, High Energy Density Capacitors for Power Electronic Applications using Nano-Structure Multilayer Technology, Lawrence Livermore National Laboratory, 1995.

[53]   Technology for the United States Navy and Marine Corps, 2000-2035: Becoming a 21st Century Force, Vol. 2: Technology, 2004.

[54]   E. R. Brown, Megawatt Solid-State Electronics, DARPA Microsystems Technology Office, 1998.

[55]   Yahya Shakweh, "MV Inverter Stack Toplogies," Power Engineering Journal, June 2001.

[56]   MIL-STD-1399, Interface Standard for Shipboard Systems, Section 300A: Electric Power, Alternating Current, 1987.

[57]   Irving H. Shames & James M. Pitarresi, Introduction to Solid Mechanics, 3rd Ed., Prentice Hall, 2000.

[58]   Website www.specialmetals.com.

[59]   Website home.san.rr.com/nessengr/techdata/metalresis.html.

[60]   Website www.eddy-current.com/condres.htm.

[61]   Elsevier, <u>Carbon Fiber Composites</u>, 1994.

[62]   Website www.grc.nasa.gov/www/epbranch/other/interlabs.htm.

[63]   Michael F. Ashby & David R. H. Jones, <u>Engineering Materials</u>, Pergamon Press, 1991.

[64]   Wole Soboyejo, <u>Mechanical Properties of Engineering Materials</u>, 2003.

[65]   James L. Kirtley & Edward C. Lovelace, "Drag Loss in Retaining Rings of Permanent Magnet Motors," SatCon Technology Corporation, March, 2003.

[66]   H. Polinder & M. J. Hoeijmakers, "Eddy-Current Losses in the Permanent Magnets of a PM Machine," EMD97, Conference Publication No. 444, 1997.

[67]   Website www.powerdesigners.com/InfoWeb/design_center/articles/SSI/ssi.shtm.

[68]   Kunrong Wang, Fred C. Lee, Guichao Jua, and Dusan Borojevic, "A Comparative Study of Switching Losses of IGBTs Under Hard-Switching, Zero-Voltage-Switching, and Zero-Current-Switching," <u>IEEE Transactions</u>, 1994.

[69]   IEEE Standards Board, <u>IEEE Recommended Practice for Monitoring Electric Power Quality</u>, 1995.

Page Intentionally Left Blank

Appendix A.   Detailed Power Requirements

In order to properly size the PM generator being designed, a typical load list is developed for an IPS naval ship. For the propulsion portion, it is assumed that the ship contains a single shaft requiring 30,000 SHP. Shaft horsepower (SHP) is the power measured in the shafting within the ship by a torsion meter as close as possible to the propeller or stern tube [10]. This SHP then translates to 32,552.1 BHP (24,275 kW) assuming a 96% efficient electric propulsion motor and a 96% efficient power control module for the motor. Brake horsepower (BHP) is the power required at the engines/generators. It is also assumed that the ship contains two equal-sized generators. Overall, Table 21 lists the systems and their associated connected (maximum) electrical power requirements.

Table 21: Ship Connected Loads

System	Connected Load (kW)	System	Connected Load (kW)
Engineering Systems			
Hydraulics	150	Engine Room Fresh Water	50
Main Sea Water	300	Electronics Fresh Water	25
Aux Sea Water	80	Reactor Cooling	2,000
Air Conditioning	300	Reactor Fresh Water	50
Chill Water	50	Reactor Heating	350
Distilling	20	Steam Feed System	300
Lube Oil	50	Steam Condensing System	80
Miscellaneous	25		
Auxiliary Systems			
Atmosphere Control	150	Drain System	100
Refrigeration	10	Ventilation	250
High Pressure Air	100	Damage Control	20
Low Pressure Air	25	Sanitary System	10
Trim System	100		
Combat Systems			
Sonar	250	Radio/ESM	40
Combat Control	250	Navigation	20
Hotel Loads			
Lighting	60	Water Heating	50
Laundry	20	Galley	70
Total Non-Propulsion			5,355
Propulsion			
Main Motor	24,275		
Auxiliary Propulsion	300		
Total Electrical Loads			29,930

Classic U.S. Navy design practices (DDS 310-1) determine generator sizes by first estimating the expected load during the preliminary design phases. Propulsion load is a function of the hull form, maximum speed, and drive technology. Ship service loads are a function of the ship's mission, crew size, and ship's size. Once this is complete, the estimates are adjusted for anticipated construction and life cycle growth. Propulsion load is not expected to change but ship service loads are given a 20% margin for construction growth and a 20% margin for life cycle growth [11]. The generators are then sized using Eqn A- 1, where P_{gen} is the power provided by one generator.

$$P_{gen} = \frac{(1.2 \cdot 1.2 \cdot MaxLoad)}{[0.9 \cdot (n - 1)]}$$

where n = number of generators

Eqn A- 1

Applying this method to the total electrical load from Table 21 produces two generators that are each capable of 47.9 MW.

Since IPS ships require electrical power for ship loads and propulsion, efficient power management should be implemented. This means that power is shared among all systems so that at top speed, more power is diverted to the propulsion motor, and at lower speeds power is available for other uses. It is assumed that rated ship service power and full propulsion power are possible at the same time only if both PM generators are available. If one generator is lost, the rated ship service load is still provided with the remaining power sent to the propulsion motor. In addition, full power for both the main motor and auxiliary propulsion is not required simultaneously. Similar to the classical method, a 20% margin for construction growth and a 20% margin for life cycle growth are allotted. Based on these ideas, Eqn A- 2 is developed to size the generators, where P_{total} is the total generation capacity (both generators).

$$P_{total} = \frac{(1.2 \cdot 1.2 \cdot MaxNonPropulsionLoad) + MainMotorLoad}{n - 1}$$

where n = number of generators

Eqn A- 2

Utilizing this process produces a total generation capacity of 31.99 MW or two generators that are each capable of 16 MW.

136

A standard U.S. Navy ship spends 95% of its time at less than full speed [12]. Because of this, the classical method unnecessarily over-estimates the power requirements for the ship and results in generator sets that are too large. If the average demand for each system is also considered, then the disparity becomes even worse. Table 22 lists each system along with a demand factor which represents the average amount of power required for normal operation of the systems. Based on the 9.8 MW total average loads, the classical method generators would each be loaded to only 10.2 % capacity which is extremely inefficient.

The improved generator sizing method does a better job of ensuring efficient operation while not excessively limiting the ship if one generator is damaged or down for maintenance. If only one of the 16 MW generators is available, the connected ship service load (5.4 MW) can be supplied while still having 10.6 MW for propulsion, giving 44 % propulsion capability which is acceptable when operating in reduced status.

Table 22: Ship Average Loads

System	Connected Load (kW)	Demand Factor	Average Load (kW)
Engineering Systems			
Hydraulics	150	1.00	150
Main Sea Water	300	0.20	60
Aux Sea Water	80	0.20	16
Air Conditioning	300	0.75	225
Chill Water	50	1.00	50
Distilling	20	0.50	10
Lube Oil	50	1.00	50
Engine Room Fresh Water	50	1.00	50
Electronics Fresh Water	25	1.00	25
Reactor Cooling	2,000	0.25	500
Reactor Fresh Water	50	1.00	50
Reactor Heating	350	0.25	88
Steam Feed System	300	0.75	225
Steam Condensing System	80	1.00	80
Miscellaneous	25	1.00	25
Auxiliary Systems			
Atmosphere Control	150	0.50	75
Refrigeration	10	1.00	10
High Pressure Air	100	0.50	50
Low Pressure Air	25	0.25	6
Trim System	100	0.50	50
Drain System	100	0.25	25
Ventilation	250	0.75	188
Damage Control	20	0.10	2
Sanitary System	10	0.50	5
Combat Systems			
Sonar	250	0.50	125
Combat Control	250	0.50	125
Radio/ESM	40	0.80	32
Navigation	20	1.00	20
Hotel Loads			
Lighting	60	0.75	45
Laundry	20	0.50	10
Water Heating	50	1.00	50
Galley	70	0.75	53
Total Non-Propulsion	**5,355**		**2,474**
Propulsion			
Main Motor	24,275	0.30	7,283
Auxiliary Propulsion	300	0.05	15
Total Electrical Loads	**29,930**		**9,771**

Appendix B.   MATLAB Code: Basic Sizing Method

Jonathan Rucker, MIT Thesis

```
% May 2005
% Program: pm1basic
% Program performs basic sizing and parameter calculations
% for generators.

%%%%%%%%%%%%%%%%%%%%%%%%%%%%%%%%%%%%%%%%%%%%%%%%%%%
% Definition of variables
% Name                   Variable
% General variables
% Pwr                    Required power
% rpm                    Speed (RPM)
% psi                    Power factor angle
% f                      Electrical frequency (Hz)
% omega                  Electrical frequency (rad/sec)
% vtip                   Tip speed (m/s)
% LovD                   L/D ratio
% stress                 Gap shear stress (psi)
% Rotor variables
% R                      Rotor radius (m)
% D                      Rotor diameter (m)
% Lst                    Rotor stack length (m)
% p                      Number of pole pairs
% Bg                     Expected air gap flux density (T)
% Stator variables
% Kz                     Surface current density (A/m)
% Jz                     Current density (A/m2)
% hs                     Slot height (m)
%%%%%%%%%%%%%%%%%%%%%%%%%%%%%%%%%%%%%%%%%%%%%%%%%%%

clear;
% Constants & conversion factors
hs = .015;             % Assume slot depth of 15 mm
lams = 0.5;            % Assume slot fill fraction
conv1 = 9.81;          % 9.81 W per Nm/s
conv2 = 703.0696;      % 703.0696 N/m2 per psi

%%%%%%%%%%%%%%%%%%%%%%%%%%%%%%%%%%%%%%%%%%%%%%%%%%%
% INPUTS
%%%%%%%%%%%%%%%%%%%%%%%%%%%%%%%%%%%%%%%%%%%%%%%%%%%
Pwr = 16e6;            % Required power
vtip = 200;            % Max tip speed (m/s)
LovD = 2.851;          % Wound rotor usually 0.5-1.0, PM 1.0-3.0
% Shear stress usually 1-10 psi small machines, 10-20 large liquid
% liquid cooled machines
stress = 15;
p = 3;                 % Pole pairs
Bg = 0.8;              % Tesla

%%%%%%%%%%%%%%%%%%%%%%%%%%%%%%%%%%%%%%%%%%%%%%%%%%%
% Calculations
% Size
```

```
% Initially use Pwr = 2*pi*R*Lst*stress*vtip
% Lst = 2*LovD*R
hscm = hs*100;
R = sqrt(Pwr/(2*pi*(LovD*2)*vtip*stress*conv1*conv2));
D = 2*R;
Lst = LovD*D;
% Speed
omega = (p*vtip)/R;
f = omega/(2*pi);
rpm = (60*f)/p;
% Current densities
Kz = (stress*conv2)/(Bg*100);
Ja = 10*Kz/(hscm*lams);

% Output
fprintf('Basic Machine Design\n');
fprintf('Input Parameters:\n');
fprintf('Power     = %10.1f kW   Shear Stress = %10.1f psi\n',Pwr/1e3,stress);
fprintf('L/D Ratio = %10.2f     Tip Speed    = %10.1f m/s\n',LovD,vtip);
fprintf('Pole Pairs = %10.1f    Air Gap Bg   = %10.1f T\n',p,Bg);
fprintf('Output:\n');
fprintf('Rotor Radius = %10.3f m     Stack Length = %10.3f m\n',R,Lst);
fprintf('Speed      = %10.0f RPM  Frequency    = %10.1f Hz\n',rpm,f);
fprintf('Ja         = %10.2f A/cm2\n',Ja);
```

Appendix C.   PM Machine Database

Parameter	Specific Machines (Motor or Generator - specify w/ M or G)											
	1	2	3	4	5	6	7	8	9	10	11	12
Type (M-Motor, G-Generator)	G	G	M	M	M	M	M	G	G	G	G	G
Power (kW)	36500	2030	20000	5.6	36500	5000	20000	2.562	1500	100	2.5	400
Power factor								0.854				
Rotational Speed (rpm)	3600	19000	150		127	150	180	1800	20000	159.1	1500	36
Rotor radius (cm)		11	42.5	6.2				4.5	15	3.56	4.37	105
Air gap (mm)								1	2		1.6	
Magnet thickness (mm)								3.3	22		4.5	25.4
Active length (m)								0.124	0.225		0.1	1.05
Pole pairs		2	6	2				2	4	8	2	83
Number of phases		3	15	3				3	3	3	3	3
Number of Slots				36				24	12		36	180
Slots per pole per phase				3				2	0.5		3	
Slots short pitched				2				1			2	
Slot depth (mm)								22.5	40			21
Slot depression depth (mm)								0	0			0
Slot depression width (mm)								5.99	0			17
Peripheral Tooth Fraction								0.5	0.5			0.5
Back iron thickness (mm)								14.2	28			
Turns per coil				30				2	2		6	9
Coils per phase								16	4			
Slot fill fraction								0.4				
Magnet remant flux density (T)				1.21				1.16	1.18	1.1	1.128	0.925
Magnet electrical angle (deg e)								143.1	80		144	
Base frequency (Hz)	60			60				60	50	133.3	50	50
Mass (MT)	14		112.5		118.8	71	39		5	0.2205		
Volume (cubic m)	4.75	2.08	48		155.05	81.65	21.93	0.02				
Width (m)	1.2	1.4	3.25	0.229	5.5	5.4	2.8		0.44	0.463	0.155	
Length (m)	2.64	1.35	4.87	0.102	5.3	2.8	2.9			0.222		
Height (m)	1.5	1.1	3.35	0.229	5.3	5.4	2.8		0.44	0.463	0.155	
Flux Layout	Radial	Radial	Radial	Radial	Radial	Radial	Radial	Radial	Radial	Radial	Radial	Radial
Voltage		800 VDC		460 VAC			5000 VAC	42 VDC	800 VDC		110 VAC	2200 VAC

Parameter	Specific Machines (Motor or Generator - specify w/ M or G)											
	13	14	15	16	17	18	19	20	21	22	23	24
Type (M-Motor, G-Generator)	M	G	G	G	G	M	M	M	G	G	G	G
Power (kW)	10	200	200	250	250	3800	5000	4300		1400	25	110
Power factor												
Rotational Speed (rpm)	1265	3600	3600	1050	10500	120	120	150	90000	18000	60000	70000
Rotor radius (cm)									5		2.16	3.3
Air gap (mm)	1.1	3	3.5	3	9						0.51	
Magnet thickness (mm)	5	3.5	6						3.5		5.84	
Active length (m)	0.12								0.125		0.097	0.16
Pole pairs	3	12	12	14	3			100	2	2	3	2
Number of phases	3	3	3	5	3				3	3	3	3
Number of Slots	36			40	36			192	12	36	9	24
Slots per pole per phase	2			0.286	2				2	3		4
Slots short pitched	1								0	0		
Slot depth (mm)												
Slot depression depth (mm)												
Slot depression width (mm)												
Peripheral Tooth Fraction												
Back iron thickness (mm)									12.5			
Turns per coil									2			
Coils per phase												
Slot fill fraction												
Magnet remant flux density (T)		1.17	1.08									
Magnet electrical angle (deg e)	84	180	120									
Base frequency (Hz)	60	720	720	245	525				3000	600		
Mass (MT)				0.2833	0.0871	52	67	65				
Volume (cubic m)												
Width (m)						2.325	2.67	3.7	0.107			0.135
Length (m)						3.47	3.41	3.8				
Height (m)						2.325	2.67	3.7	0.107			
Flux Layout	Radial	Radial	Radial	Radial	Radial	Radial	Radial	Radial	Radial	Radial	Radial	Radial
Voltage	18 VAC			730 VAC		600 VDC	600 VDC	705 VDC				500 VDC

Page Intentionally Left Blank

Appendix D. MATLAB Code: Sizing Method 1

```
% Jonathan Rucker, MIT Thesis
% May 2005
% Program: pm1input
% Program used as input file for pm1calc
% All necessary input parameters entered here.

clear;
%%%%%%%%%%%%%%%%%%%%%%%%%%%%%%%%%%%%%%%%%%%%%%%%%%%%%%%%
% Definition & Entry of variables
% General variables
Pwr = 16e6;              % Required power (W)
rpm = 13000;             % Speed (RPM)
psi = 0;                 % Power factor angle
% Rotor variables
R = 0.147;               % Rotor radius (m)
hm = 0.025;              % Magnet thickness (m)
Lst = 0.838;             % Rotor stack length (m)
p = 3;                   % Number of pole pairs
Br = 1.2;                % Magnet remnant flux density (T)
thm = 50;                % Magnet physical angle (deg)
thsk = 10;               % Magnet skew angle (actual deg)
% Stator variables
q = 3;                   % Number of phases
Ns = 36;                 % Number of slots
Nsp = 1;                 % Number of slots short pitched
g = .004;                % Air gap (m)
tfrac = 0.5;             % Peripheral tooth fraction
hs = .025;               % Slot depth (m)
hd = .0005;              % Slot depression depth (m)
wd = 1e-6;               % Slot depression width (m)
syrat = 0.7;             % Stator back iron ratio (yoke thick/rotor radius)
Nc = 1;                  % Turns per coil
lams = 0.5;              % Slot fill fraction
sigst = 6.0e+7;          % Stator winding conductivity
% Densities
rhos = 7700;             % Steel density (kg/m3)
rhom = 7400;             % Magnet density (kg/m3)
rhoc = 8900;             % Conductor density (kg/m3)



% Jonathan Rucker, MIT Thesis
% May 2005
% Program: pm1calc
% Program performs sizing and parameter calculations
% for permanent magnet machines with surface magnets and
% slotted stators.
% Program developed from J.L. Kirtley script with permission

% MUST RUN pm1input PRIOR TO RUNNING pm1calc
```

```
%%%%%%%%%%%%%%%%%%%%%%%%%%%%%%%%%%%%%%%%%%%%%%%%%%%
% Definition of variables
% Name                 Variable
% General variables
% Pwr                  Required power (W)
% rpm                  Speed (RPM)
% psi                  Power factor angle
% f                    Electrical frequency (Hz)
% omega                Electrical frequency (rad/sec)
% vtip                 Tip speed (m/s)
% lambda               Flux linkage
% Ea                   RMS Internal voltage (V)
% Rotor variables
% R                    Rotor radius (m)
% hm                   Magnet thickness (m)
% Lst                  Rotor stack length (m)
% p                    Number of pole pairs
% Br                   Magnet remnant flux density (T)
% thm                  Magnet physical angle (deg)
% thsk                 Magnet skew angle (actual deg)
% Stator variables
% q                    Number of phases
% m                    Slots per pole per phase
% Ns                   Number of slots
% Nsp                  Number of slots short pitched
% g                    Air gap (m)
% ge                   Effective air gap (m)
% tfrac                Peripheral tooth fraction
% hs                   Slot depth (m)
% hd                   Slot depression depth (m)
% wd                   Slot depression width (m)
% syrat                Stator back iron ratio (yoke thick/rotor radius)
% Nc                   Turns per coil
% lams                 Slot fill fraction
% sigst                Stator conductivity
% Kc                   Carter coefficient
% Loss Models
% P0                   Base power for core losses
% F0                   Base frequency for core loss
% B0                   Base flux density
% epsb                 Flux density exponent
% epsf                 Frequency exponent
% rhos                 Steel density
% rhom                 Magnet density
% rhoc                 Conductor density
%%%%%%%%%%%%%%%%%%%%%%%%%%%%%%%%%%%%%%%%%%%%%%%%%%%

% Constants to be used
mu0 = 4*pi*1e-7;       % Free space permeability
tol = 1e-2;            % Tolerance factor
cpair = 1005.7;        % Specific heat capacity of air (J/kg*C)
rhoair = 1.205 ;       % Density of air at 20 C (kg/m3)
nuair = 1.5e-5;        % Kinematic viscosity of air at 20 C (m2/s)
P0 = 36.79;            % Base Power Losss, W/lb
F0 = 1000;             % Base freuency, 60 Hz
B0 = 1.0;              % Base flux density, 1.0 T
```

144

```
epsb = 2.12;
epsf = 1.68;

% Generate geometry of machine

% Number of slots/pole/phase
m = Ns/(2*p*q);
% Number of armature turns (each slot has 2 half coils)
Na = 2*p*m*Nc;
% Tooth width
wt = 2*pi*(R+g+hm+hd)*tfrac/Ns;
% Slot top width (at air gap)
wst = 2*pi*(R+g+hm+hd)*(1-tfrac)/Ns;
% Slot bottom width
wsb = wst*(R+g+hd+hs)/(R+g+hm+hd);
% Stator core back iron depth (as p increases, dc decreases)
dc = syrat*R/p;
% Full-pitch coil throw
Nsfp = floor(Ns/(2*p));
% Actual coil throw
Nsct = Nsfp - Nsp;
% Estimate end turn length
% End turn travel (one end)
laz = pi*(R+g+hm+hd+0.5*hs)*Nsct/Ns;
% End length (half coil)
le2 = pi*laz;
% End length (axial direction)
le1 = 2*le2/(2*pi);

% Calculate electrical frequency & surface speed
f = p*rpm/60;
omega = 2*pi*f;
vtip = R*omega/p;

% Winding & skew factors
gama = 2*pi*p/Ns;
alfa = pi*Nsct/Nsfp;
kp = sin(pi/2)*sin(alfa/2);
kb = sin(m*gama/2)/(m*sin(gama/2));
kw = kp*kb;
ths = ((p*thsk)+1e-6)*(pi/180);      % skew angle (elec rad)
ks = sin(ths/2)/(ths/2);

% Calculate magnetic gap factor
Rs = R+hm+g;
Ri = R;
R1 = R;
R2 = R+hm;
kg = ((Ri^(p-1))/(Rs^(2*p)-Ri^(2*p)))*((p/(p+1))*(R2^(p+1)-R1^(p+1))...
   +(p*Rs^(2*p)/(p-1))*(R1^(1-p)-R2^(1-p)));

% Calculate air gap magnetic flux density

% Account for slots, reluctance, and leakage
ws = (wst+wsb)/2;           % Average slot width
taus = ws + wt;             % Width of slot and tooth
```

```matlab
Kc = 1/(1-(1/((taus/ws)*((5*g/ws)+1))));
ge = Kc*g;
Cphi = (p*thm)/180;        % Flux concentration factor
Kl = 0.95;                 % Leakage factor
Kr = 1.05;                 % Reluctance factor
murec = 1.05;              % Recoil permeability
PC = hm/(ge*Cphi);         % Permeance coefficient
Bg = ((Kl*Cphi)/(1+(Kr*murec/PC)))*Br;

% Calculate magnetic flux and internal voltage
thmrad = thm*(pi/180);
B1 = (4/pi)*Bg*kg*sin(p*thmrad/2);
lambda = 2*Rs*Lst*Na*kw*ks*B1/p;
Ea = omega*lambda/sqrt(2);  % RMS back voltage

% Calculation of inductances/reactances

% Air-gap inductance
Lag = (q/2)*(4/pi)*(mu0*Na^2*kw^2*Lst*Rs)/(p^2*(g+hm));
% Slot leakage inductance
perm = mu0*((1/3)*(hs/wst) + hd/wst);
Las = 2*p*Lst*perm*(4*Nc^2*(m-Nsp)+2*Nsp*Nc^2);
Lam = 2*p*Lst*Nsp*Nc^2*perm;
if q == 3
    Lslot = Las + 2*Lam*cos(2*pi/q);        % 3 phase equation
else
    Lslot = Las - 2*Lam*cos(2*pi/q);        % multiple phases
end
% End-turn inductance (Hanselman)
As = ws*hs;            % Slot area
Le = ((Nc*mu0*(taus)*Na^2)/2)*log(wt*sqrt(pi)/sqrt(2*As));
% Total inductance and reactance
Ls = Lag+Lslot+Le;
Xs = omega*Ls;

% Lengths, Volumes, and Weights

% Armature conductor length
Lac = 2*Na*(Lst+2*le2);
% Armature conductor area (assumes form wound)
Aac = As*lams/(2*Nc);
% Mass of armature conductor
Mac = q*Lac*Aac*rhoc;
% Overall machine length
Lmach = Lst+2*le1;
% Core inside radius
Rci = R+hm+g+hd+hs;
% Core outside radius
Rco = Rci+dc;
% Overall diameter
Dmach = 2*Rco;
% Core mass
Mcb = rhos*pi*(Rco^2-Rci^2)*Lst;                    % Back iron
Mct = rhos*Lst*(Ns*wt*hs+2*pi*R*hd-Ns*hd*wd);       % Teeth
Mc = Mcb + Mct;
% Magnet mass
```

```
Mm = 0.5*(p*thmrad)*((R+hm)^2-R^2)*Lst*rhom;
% Shaft mass
Ms = pi*R^2*Lst*rhos;
% 15% service fraction
Mser = 0.15*(Mc+Ms+Mm+Mac);
% Total mass
Mtot = Mser+Mc+Ms+Mm+Mac;

% Stator resistance
Ra = Lac/(sigst*Aac);

% Core Loss Calculations

% Tooth Flux Density
Bt = Bg/tfrac;
% Back iron flux density (Hanselman)
Bb = Bg*R/(p*dc);
% Core back iron loss
Pcb = Mcb*P0*abs(Bb/B0)^epsb*abs(f/F0)^epsf;
% Teeth Loss
Pct = Mct*P0*abs(Bt/B0)^epsb*abs(f/F0)^epsf;
% Total core loss
Pc = Pcb + Pct;

% Start loop to determine terminal voltage and current
notdone = 1;
i = 0;
Ia = Pwr/(q*Ea);
while notdone ==1
    i = i + 1;
    xa = Xs*Ia/Ea;
    % Conductor losses
    Pa = q*Ia^2*Ra;

    % Gap friction losses
    % Reynold's number in air gap
    omegam = omega/p;
    Rey = omegam*R*g/nuair;
    % Friction coefficient
    Cf = .0725/Rey^.2;
    % Windage losses
    Pwind = Cf*pi*rhoair*omegam^3*R^4*Lst;

    % Get terminal voltage
    Va = sqrt(Ea^2-((Xs+Ra)*Ia*cos(psi))^2)-(Xs+Ra)*Ia*sin(psi);

    Ptemp = q*Va*Ia*cos(psi)-Pwind;
    error = Pwr/Ptemp;
    err(i) = error;
    if abs(error-1) < tol
        notdone = 0;
    else
        Ia = Ia*error;
    end
end
```

```
% Remaining performance parameters

% Current density
Ja = Ia/Aac;
% Power and efficiency
Pin = Pwr+Pc+Pa+Pwind;
eff = Pwr/Pin;
pf = cos(psi);

fprintf('pm1calc complete: Ready.\n');




% Jonathan Rucker, MIT Thesis
% May 2005
% Program: pm1output
% Program outputs values from pm1calc.
% Program developed from J.L. Kirtley script with permission

% MUST RUN pm1input and pm1calc PRIOR TO RUNNING pm1output

% Variables for output display
Pout = Pwr/1e3;
Jao = Ja/1e4;
Pco = Pc/1e3;
Pwindo = Pwind/1e3;
Pao = Pa/1e3;
wso = ws*1000;
hso = hs*1000;
wto = wt*1000;
dco = dc*1000;
Lso = Ls*1000;
hmo = hm*1000;
go = g*1000;


% Output Section:
fprintf('\nPM Machine Design, Version 1: Surface Magnet, Slotted Stator\n');

fprintf('Machine Size:\n');
fprintf('Machine Diameter =  %8.3f m      Machine Length = %8.3f m\n',Dmach,Lmach);
fprintf('Rotor radius =      %8.3f m      Active length =  %8.3f m\n',R,Lst);
fprintf('Slot Avg Width =    %8.3f mm     Slot Height =    %8.3f mm\n',wso,hso);
fprintf('Back Iron Thick =   %8.3f mm     Tooth Width =    %8.3f mm\n',dco,wto);

fprintf('Machine Ratings:\n');
fprintf('Power Rating =      %8.1f kW     Speed  =       %8.0f RPM\n', Pout,rpm);
fprintf('Va (RMS) =          %8.0f V      Current  =     %8.1f A\n', Va,Ia);
fprintf('Ea (RMS) =          %8.0f V      Arm Resistance = %8.5f ohm\n',Ea,Ra);
fprintf('Synch Reactance =   %8.3f ohm    Synch Induct =  %8.3f mH\n',Xs,Lso);
fprintf('Stator Cur Den  =   %8.1f A/cm2   Tip Speed  =   %8.0f m/s\n', Jao,vtip);
fprintf('Efficiency  =       %8.3f        Power Factor = %8.3f\n', eff,pf);
fprintf('Phases =            %8.0f        Frequency  =   %8.1f Hz\n',q,f);

fprintf('Stator Parameters:\n');
fprintf('Number of Slots =   %8.0f        Num Arm Turns = %8.0f \n',Ns,Na);
```

148

```
fprintf('Breadth Factor =    %8.3f        Pitch Factor =   %8.3f \n', kb,kp);
fprintf('Tooth Flux Den =   %8.2f T       Back Iron   =   %8.2f T\n', Bt,Bb);
fprintf('Slots/pole/phase =  %8.2f\n',m);

fprintf('Rotor Parameters:\n');
fprintf('Magnet Height =     %8.2f mm     Magnet Angle  =  %8.1f degm\n',hmo,thm);
fprintf('Air gap =          %8.2f mm      Pole Pairs =    %8.0f \n',go,p);
fprintf('Magnet Remanence = %8.2f T       Aig Gap Bg =    %8.2f T\n',Br,Bg);
fprintf('Magnet Factor =     %8.3f        Skew Factor =    %8.3f \n',kg,ks);

fprintf('Machine Losses:\n');
fprintf('Core Loss =        %8.1f kW      Armature Loss  = %8.1f kW\n', Pco,Pao);
fprintf('Windage Loss =     %8.1f kW      Rotor Loss =       TBD kW\n', Pwindo);

fprintf('Machine Weights:\n');
fprintf('Core  =          %8.2f kg        Shaft =       %8.2f kg\n',Mc,Ms);
fprintf('Magnet =          %8.2f kg       Armature =     %8.2f kg\n',Mm,Mac);
fprintf('Services =        %8.2f kg       Total =       %8.2f kg\n',Mser,Mtot);
```

Page Intentionally Left Blank

Appendix E.   MATLAB Code: Sizing Method 2

```
% Jonathan Rucker, MIT Thesis
% May 2005
% Program: pm2input
% Program used as input file for pm2calc
% All necessary input parameters entered here.

clear;
%%%%%%%%%%%%%%%%%%%%%%%%%%%%%%%%%%%%%%%%%%%%%%%%%%%%%%%%%%%
% Definition & Entry of variables
% General variables
Pwr = 16e6;             % Required power (W)
rpm = 13000;            % Speed (RPM)
psi = 0;                % Power factor angle
Bsat = 1.65;            % Stator saturation flux density
% Rotor variables
vtip = 200;             % Tip speed limit (m/s)
p = 3;                  % Number of pole pairs
Br = 1.2;               % Magnet remnant flux density (T)
thsk = 10;              % Magnet skew angle (elec deg)
PC = 5.74;              % Permeance coefficient for magnets
% Stator variables
Ja = 2200;              % Initial current density (A/cm2)
q = 3;                  % Number of phases
m = 2;                  % Slots/pole/phase
Nsp = 1;                % Number of slots short pitched
g = .004;               % Air gap (m)
hs = .025;              % Slot depth (m)
hd = .0005;             % Slot depression depth (m)
wd = 1e-6;              % Slot depression width (m)
ws = .016;              % Avg slot width (m)
Nc = 1;                 % Turns per coil
lams = 0.5;             % Slot fill fraction
sigst = 6.0e+7;         % Stator winding conductivity
% Densities
rhos = 7700;            % Steel density (kg/m3)
rhom = 7400;            % Magnet density (kg/m3)
rhoc = 8900;            % Conductor density (kg/m3)


% Jonathan Rucker, MIT Thesis
% May 2005
% Program: pm2calc
% Program performs sizing and parameter calculations
% for permanent magnet machines with surface magnets and
% slotted stators.

% MUST RUN pm2input PRIOR TO RUNNING pm2calc

%%%%%%%%%%%%%%%%%%%%%%%%%%%%%%%%%%%%%%%%%%%%%%%%%%%%%%%%%%%
% Definition of variables
% Name                  Variable
```

```
% General variables
% Pwr                Required power (W)
% rpm                Speed (RPM)
% psi                Power factor angle
% f                  Electrical frequency (Hz)
% omega              Electrical frequency (rad/sec)
% vtip               Tip speed (m/s)
% lambda             Flux linkage
% Ea                 RMS Internal voltage (V)
% Rotor variables
% R                  Rotor radius (m)
% hm                 Magnet thickness (m)
% Lst                Rotor stack length (m)
% p                  Number of pole pairs
% Br                 Magnet remnant flux density (T)
% thm                Magnet physical angle (deg)
% thsk               Magnet skew angle (actual deg)
% Stator variables
% q                  Number of phases
% m                  Slots per pole per phase
% Ns                 Number of slots
% Nsp                Number of slots short pitched
% g                  Air gap (m)
% ge                 Effective air gap (m)
% tfrac              Peripheral tooth fraction
% hs                 Slot depth (m)
% hd                 Slot depression depth (m)
% wd                 Slot depression width (m)
% syrat              Stator back iron ratio (yoke thick/rotor radius)
% Nc                 Turns per coil
% lams               Slot fill fraction
% sigst              Stator conductivity
% Kc                 Carter coefficient
% Loss Models
% P0                 Base power for core losses
% F0                 Base frequency for core loss
% B0                 Base flux density
% epsb               Flux density exponent
% epsf               Frequency exponent
% rhos               Steel density
% rhom               Magnet density
% rhoc               Conductor density
%%%%%%%%%%%%%%%%%%%%%%%%%%%%%%%%%%%%%%%%%%%%%%%%%%%%%%%%%%%%%%%

% Constants to be used
mu0 = 4*pi*1e-7;      % Free space permeability
tol = 1e-2;           % Tolerance factor
cpair = 1005.7;       % Specific heat capacity of air (J/kg*C)
rhoair = 1.205 ;      % Density of air at 20 C (kg/m3)
nuair = 1.5e-5;       % Kinematic viscosity of air at 20 C (m2/s)
P0 = 36.79;           % Base Power Losss, W/lb
F0 = 1000;            % Base freuency, 60 Hz
B0 = 1.0;             % Base flux density, 1.0 T
epsb = 2.12;
epsf = 1.68;
```

```
% Calculate electrical frequency & rotor radius
f = p*rpm/60;
omega = 2*pi*f;
R = p*vtip/omega;

% Winding & skew factors
Ns = floor(2*q*p*m);        % Number of slots
gama = 2*pi*p/Ns;
Nsfp = floor(Ns/(2*p));
Nsct = Nsfp - Nsp;
alfa = pi*Nsct/Nsfp;
kp = sin(pi/2)*sin(alfa/2);
kb = sin(m*gama/2)/(m*sin(gama/2));
kw = kp*kb;
ths = ((p*thsk)+1e-6)*(pi/180);    . % skew angle (elec rad)
ks = sin(ths/2)/(ths/2);

% Calculate magnet dimensions, tooth width, & air gap flux density
thme = 1;                   % Initial Magnet angle (deg e)
notdone = 1;
ge = g;                     % Initial effective air gap
while notdone == 1
  alpham = thme/180;                % Pitch coverage coefficient
  Cphi = (2*alpham)/(1+alpham);     % Flux concentration factor
  hm = ge*Cphi*PC;                  % Magnet height
  Ds = 2*(R+hm+g);                  % Inner stator/air gap diameter
  Kl = 0.95;                        % Leakage factor
  Kr = 1.05;                        % Reluctance factor
  murec = 1.05;                     % Recoil permeability
  Bg = ((Kl*Cphi)/(1+(Kr*murec/PC)))*Br;
  wt = ((pi*Ds)/Ns)*(Bg/Bsat);      % Tooth width
  taus = ws + wt;                   % Width of slot and tooth
  Kc = 1/(1-(1/((taus/ws)*((5*g/ws)+1))));  % Carter's coefficient
  ge = Kc*g;
  eratio = ws/wt;
  if abs(eratio - 1) < tol
    notdone = 0;
  else
    thme = thme + 1;
  end
end

% Set final values
thm = thme/p;               % Magnet physical angle
thmrad = thm*(pi/180);
hm = ge*Cphi*PC;            % Magnet height
Ds = 2*(R+hm+g);           % Inner stator/air gap diameter

% Generate geometry of machine

% Peripheral tooth fraction
tfrac = wt/(wt+ws);
% Slot top width (at air gap)
wst = 2*pi*(R+g+hm+hd)*tfrac/Ns;
% Slot bottom width
wsb = wst*(R+g+hm+hd+hs)/(R+g+hm+hd);
```

```
% Stator core back iron depth
dc = (pi*Ds*thmrad/(4*p))*(Bg/Bsat);
% Core inside radius
Rci = R+hm+g+hd+hs;
% Core outside radius
Rco = Rci+dc;
% Slot area
As = ws*hs;
% Estimate end turn length
% End turn travel (one end)
laz = pi*(R+g+hm+hd+0.5*hs)*Nsct/Ns;
% End length (half coil)
le2 = pi*laz;
% End length (axial direction)
le1 = 2*le2/(2*pi);


% Calculate magnetic gap factor
Rs = R+hm+g;
Ri = R;
R1 = R;
R2 = R+hm;
kg = ((Ri^(p-1))/(Rs^(2*p)-Ri^(2*p)))*((p/(p+1))*(R2^(p+1)-R1^(p+1))...
    +(p*Rs^(2*p)/(p-1))*(R1^(1-p)-R2^(1-p)));


% Core loss calculations (per length)


% Core mass per length
McbperL = rhos*pi*(Rco^2-Rci^2);                    % Back iron
MctperL = rhos*(Ns*wt*hs+2*pi*R*hd-Ns*hd*wd);        % Teeth
McperL = McbperL + MctperL;
% Tooth Flux Density
Bt = Bg/tfrac;
% Back iron flux density (Hanselman)
Bb = Bg*R/(p*dc);
% Core back iron loss per length
PcbperL = McbperL*P0*abs(Bb/B0)^epsb*abs(f/F0)^epsf;
% Teeth Loss per length
PctperL = MctperL*P0*abs(Bt/B0)^epsb*abs(f/F0)^epsf;
% Total core loss per length
PcperL = PcbperL + PctperL;


% Current and surface current density
% Armature turns (each slot has 2 half coils)
Na = 2*p*m*Nc;
% Arm cond area (assumes form wound)
Aac = (As*lams)/(2*Nc);


% Power & Current waveform factors (Lipo)
ke = 0.52;
ki = sqrt(2);


% Initial terminal current
Ia = Ns*lams*As*Ja*1e4/(2*q*Na);
notfin = 1;
Lst = 0.1;                  % Initial stack length
i = 1;
```

```
% Start loop to determine Lst, Ea, Va, and Ia
notdone = 1;
k = 0;
while notdone == 1
 k = k + 1;
 % Surface current density
 A = 2*q*Na*Ia/(pi*Ds);

 % Calculate stack length of machine
 % Loop to get stack length
 while notfin == 1
  % Gap power
  Pgap = 4*pi*ke*ki*kw*ks*kg*sin(thmrad)*(f/p)*A*Bg*(Ds^2)*Lst;
  % Length of conductor
  Lac = 2*Na*(Lst+2*le2);
  % Stator resistance
  Ra = Lac/(sigst*Aac);
  % Copper Loss
  Pa = q*Ia^2*Ra;
  % Core losses
  Pc = PcperL*Lst;

  % Iterate to get length
  Ptemp1 = Pgap-Pa-Pc;
  error = Pwr/Ptemp1;
  err(i) = error;
  if abs(error-1) < tol
    notfin = 0;
  else
    Lst = Lst*error;
    i = i + 1;
  end
 end
% Calculate magnetic flux and internal voltage
thmrad = thm*(pi/180);
B1 = (4/pi)*Bg*kg*sin(p*thmrad/2);
lambda = 2*Rs*Lst*Na*kw*ks*B1/p;
Ea = omega*lambda/sqrt(2);  % RMS back voltage

% Calculation of inductances/reactances

% Air-gap inductance
Lag = (q/2)*(4/pi)*(mu0*Na^2*kw^2*Lst*Rs)/(p^2*(g+hm));
% Slot leakage inductance
perm = mu0*((1/3)*(hs/wst) + hd/wst);
Las = 2*p*Lst*perm*(4*Nc^2*(m-Nsp)+2*Nsp*Nc^2);
Lam = 2*p*Lst*Nsp*Nc^2*perm;
if q == 3
  Lslot = Las + 2*Lam*cos(2*pi/q);        % 3 phase equation
else
  Lslot = Las - 2*Lam*cos(2*pi/q);        % multiple phases
end
% End-turn inductance (Hanselman)
taus = ws + wt;         % Width of slot and tooth
Le = ((Nc*mu0*(taus)*Na^2)/2)*log(wt*sqrt(pi)/sqrt(2*As));
```

```
% Total inductance and reactance
Ls = Lag+Lslot+Le;
Xs = omega*Ls;

% Lengths, Volumes, and Weights

% Armature conductor length
Lac = 2*Na*(Lst+2*le2);
% Mass of armature conductor
Mac = q*Lac*Aac*rhoc;
% Overall machine length
Lmach = Lst+2*le1;
% Overall diameter
Dmach = 2*Rco;
% Core mass
Mc = McperL*Lst;
% Magnet mass
Mm = 0.5*(p*thmrad)*((R+hm)^2-R^2)*Lst*rhom;
% Shaft mass
Ms = pi*R^2*Lst*rhos;
% 15% service fraction
Mser = 0.15*(Mc+Ms+Mm+Mac);
% Total mass
Mtot = Mser+Mc+Ms+Mm+Mac;

% Gap friction losses
% Reynold's number in air gap
omegam = omega/p;
Rey = omegam*R*g/nuair;
% Friction coefficient
Cf = .0725/Rey^.2;
% Windage losses
Pwind = Cf*pi*rhoair*omegam^3*R^4*Lst;

% Get terminal voltage
xa = Xs*Ia/Ea;
Va = sqrt(Ea^2-((Xs+Ra)*Ia*cos(psi))^2)-(Xs+Ra)*Ia*sin(psi);

Ptemp = q*Va*Ia*cos(psi)-Pwind;
Perror = Pwr/Ptemp;
Perr(k) = Perror;
if abs(Perror-1) < tol
   notdone = 0;
else
   Ia = Ia*Perror;
end
end

% Remaining performance parameters

% Current density
Ja = Ia/Aac;
% Power and efficiency
Pin = Pwr+Pc+Pa+Pwind;
eff = Pwr/Pin;
pf = cos(psi);
```

```
fprintf('pm2calc complete: Ready.\n');




% Jonathan Rucker, MIT Thesis
% May 2005
% Program: pm2output
% Program outputs values from pm2calc.
% Program developed from J.L. Kirtley script with permission

% MUST RUN pm2input and pm2calc PRIOR TO RUNNING pm2output

% Variables for output display
Pout = Pwr/1e3;
Jao = Ja/1e4;
Pco = Pc/1e3;
Pwindo = Pwind/1e3;
Pao = Pa/1e3;
wso = ws*1000;
hso = hs*1000;
wto = wt*1000;
dco = dc*1000;
Lso = Ls*1000;
hmo = hm*1000;
go = g*1000;


% Output Section:
fprintf('\nPM Machine Design, Version 2: Surface Magnet, Slotted Stator\n');

fprintf('Machine Size:\n');
fprintf('Machine Diameter = %8.3f m        Machine Length = %8.3f m\n',Dmach,Lmach);
fprintf('Rotor radius =      %8.3f m        Active length = %8.3f m\n',R,Lst);
fprintf('Slot Avg Width =    %8.3f mm       Slot Height =    %8.3f mm\n',wso,hso);
fprintf('Back Iron Thick =   %8.3f mm       Tooth Width =    %8.3f mm\n',dco,wto);

fprintf('Machine Ratings:\n');
fprintf('Power Rating =      %8.1f kW       Speed =         %8.0f RPM\n', Pout,rpm);
fprintf('Va (RMS) =          %8.0f V        Current =       %8.1f A\n', Va,Ia);
fprintf('Ea (RMS) =          %8.0f V        Arm Resistance = %8.5f ohm\n',Ea,Ra);
fprintf('Synch Reactance =   %8.3f ohm      Synch Induct =   %8.3f mH\n',Xs,Lso);
fprintf('Stator Cur Den =    %8.1f A/cm2    Tip Speed =      %8.0f m/s\n', Jao,vtip);
fprintf('Efficiency =        %8.3f          Power Factor =  %8.3f\n', eff,pf);
fprintf('Phases =            %8.0f          Frequency =      %8.1f Hz\n',q,f);

fprintf('Stator Parameters:\n');
fprintf('Number of Slots =   %8.0f          Num Arm Turns =  %8.0f \n',Ns,Na);
fprintf('Breadth Factor =    %8.3f          Pitch Factor =   %8.3f \n', kb,kp);
fprintf('Tooth Flux Den =    %8.2f T        Back Iron   =    %8.2f T\n', Bt,Bb);
fprintf('Slots/pole/phase =  %8.2f\n',m);

fprintf('Rotor Parameters:\n');
fprintf('Magnet Height =     %8.2f mm       Magnet Angle  = %8.1f degm\n',hmo,thm);
fprintf('Air gap =           %8.2f mm       Pole Pairs =     %8.0f \n',go,p);
fprintf('Magnet Remanence =  %8.2f T        Aig Gap Bg =     %8.2f T\n',Br,Bg);
```

```
fprintf('Magnet Factor =    %8.3f          Skew Factor =    %8.3f \n',kg,ks);

fprintf('Machine Losses:\n');
fprintf('Core Loss =        %8.1f kW        Armature Loss  = %8.1f kW\n', Pco,Pao);
fprintf('Windage Loss =     %8.1f kW        Rotor Loss =        TBD kW\n', Pwindo);

fprintf('Machine Weights:\n');
fprintf('Core   =           %8.2f kg        Shaft =        %8.2f kg\n',Mc,Ms);
fprintf('Magnet =           %8.2f kg        Armature =      %8.2f kg\n',Mm,Mac);
fprintf('Services =         %8.2f kg        Total =        %8.2f kg\n',Mser,Mtot);
```

Appendix F.   MATLAB Code: Bode Plot

```
% Jonathan Rucker, MIT Thesis
% May 2005
% Program: Buckfilter
% Program calculates transfer function and outputs
% Bode plot for buck converter input filter

clear;

% Input parameters
R = 4.79e-3;
Cf = 2.84e-3;
Cb = 28.4e-3;
Lf = 1.415e-6;

% Set up transfer function
num = [R*Cb  1];
den = [Lf*R*Cf*Cb  Lf*(Cf+Cb)  R*Cb  1];
H = tf(num,den);
bode(H)
```

Page Intentionally Left Blank

Appendix G.   MATLAB Code: PM Generator Waveforms

```
% Jonathan Rucker, MIT Thesis
% May 2005
% Program: pmwave
% Program calculates and outputs different waveforms,
% calculates THD, and computes the harmonic content
% for permanent magnet machines with surface magnets and
% slotted stators.


% MUST RUN pm1input and pm1calc PRIOR TO RUNNING pmwave


%%%%%%%%%%%%%%%%%%%%%%%%%%%%%%%%%%%%%%%%%%%%%%%%%%%%%%%%%%
% Definition of variables
% Name                 Variable
% General variables
% Pwr                  Required power (W)
% rpm                  Speed (RPM)
% psi                  Power factor angle
% f                    Electrical frequency (Hz)
% omega                Electrical frequency (rad/sec)
% vtip                 Tip speed (m/s)
% lambda               Flux linkage
% Ea                   RMS Internal voltage (V)
% Rotor variables
% R                    Rotor radius (m)
% hm                   Magnet thickness (m)
% Lst                  Rotor stack length (m)
% p                    Number of pole pairs
% Br                   Magnet remnant flux density (T)
% thm                  Magnet physical angle (deg)
% thsk                 Magnet skew angle (actual deg)
% Stator variables
% q                    Number of phases
% m                    Slots per pole per phase
% Ns                   Number of slots
% Nsp                  Number of slots short pitched
% g                    Air gap (m)
% ge                   Effective air gap (m)
% tfrac                Peripheral tooth fraction
% hs                   Slot depth (m)
% hd                   Slot depression depth (m)
% wd                   Slot depression width (m)
% syrat                Stator back iron ratio (yoke thick/rotor radius)
% Nc                   Turns per coil
% lams                 Slot fill fraction
% sigst                Stator conductivity
% Kc                   Carter coefficient
%%%%%%%%%%%%%%%%%%%%%%%%%%%%%%%%%%%%%%%%%%%%%%%%%%%%%%%%%%


% Constants to be used
mu0 = 4*pi*1e-7;       % Free space permeability
tol = 1e-2;            % Tolerance factor
```

```
% Harmonics to be evaluated
n = 1:2:35;
np = p .* n;                % Use in kgn equation
w = n .* omega;             % Harmonic angular frequencies
freq = w ./ (2*pi);         % Harmonic frequencies

% Harmonic winding and skew factors
gama = 2*pi*p/Ns;
alfa = pi*Nsct/Nsfp;
kpn = sin(n .* pi/2) .* sin(n .* alfa/2);
kbn = sin(n .* m*gama/2) ./ (m*sin(n .* gama/2));
kwn = kpn .* kbn;
ths = ((p*thsk)+1e-6)*(pi/180);       % skew angle (elec rad)
ksn = sin(n .* ths/2) ./ (n .* ths/2);

% Calculate magnetic gap factor
Rs = R+hm+g;
Ri = R;
R1 = R;
R2 = R+hm;
kgn = ((Ri.^(np-1))./(Rs.^(2.*np)-Ri.^(2.*np))).*((np./(np+1))...
    .*(R2.^(np+1)-R1.^(np+1))+(np.*Rs.^(2.*np)./(np-1))...
    .*(R1.^(1-np)-R2.^(1-np)));

% Calculate magnetic flux and internal voltage
thmrad = thm*(pi/180);
thmerad = p*thmrad;
Bn = Bg.*((4/pi)./n).*kgn.*sin(n.*thmerad/2).*sin(n.*pi/2);
lambdan = ((2*Rs*Lst*Na).*kwn.*ksn.*Bn)./p;
Ean = (omega.*lambdan);       % Peak back voltage

% Normalized values for plotting
Eanorm = abs(Ean) ./ Ean(1);

% Voltage THD
Eah = 0;
for r = 2:length(n)
    Eah = Eah + Ean(r)^2;
end
THD = 100*sqrt(Eah/(Ean(1)^2));

% Generate waveforms
% Rotor physical angle goes from 0 to 2*pi - electrical to 2*p*pi
ang = 0:pi/100:2*pi;
angp = p*ang;
Bout = zeros(size(angp));
Eaout = zeros(size(angp));
for i = 1:length(n)
    Bout = Bout + Bn(i).*sin(n(i).*angp);
    Eaout = Eaout + Ean(i).*sin(n(i).*angp);
end

% Plot waveforms
figure(1)
plot(ang,Bout);
title('PM Generator: Flux Density');
```

```
ylabel('B (Tesla)');
xlabel('Rotor Angle (rad)');

figure(2)
plot(ang,Eaout);
title('PM Generator: Back EMF');
ylabel('Peak Voltage (V)');
xlabel('Rotor Angle (rad)');

figure(3)
hold on
title(['PM Generator: EMF Harmonics, THD = ',num2str(THD),' %']);
ylabel('Normalized Back EMF');
xlabel('Harmonic Number');
text(20,0.7,'Dark: Above 10% of Fundamental','FontSize',10);
text(20,0.65,'Light: Below 10% of Fundamental','FontSize',10);
for z = 1:length(Eanorm)
    if Eanorm(z) < 0.10
        bar(n(z),Eanorm(z),'c');
    else
        bar(n(z),Eanorm(z),'b');
    end
end
hold off
```

Page Intentionally Left Blank

Appendix H. MATLAB Code: Retaining Sleeve Stress Calculations

```
% Jonathan Rucker, MIT Thesis
% May 2005
% Program: pmcanstress
% Program calculates and outputs retaining can stress
% for permanent magnet machines with surface magnets and
% slotted stators.

% MUST RUN pm1input, pm1calc, and pmwave PRIOR TO RUNNING pmcanstress

%%%%%%%%%%%%%%%%%%%%%%%%%%%%%%%%%%%%%%%%%%%%%%%%%%%%%%%%%%%%%
% Calculate retaining sleeve stresses
%%%%%%%%%%%%%%%%%%%%%%%%%%%%%%%%%%%%%%%%%%%%%%%%%%%%%%%%%%%%%
% Conversion
Patopsi = 1.45038e-4;      % psi per Pa
% Material yield stresses (ksi)
Stain_str = 90;
Alum_str = 75;
Titan_str = 110;
CarFib_str = 100;
Inconel_str = 132;
% Safety factor
SF = 1.2;

% Force on magnets/sleeves is centrifugal force
% Magnet tangential velocity
vmag = ((R+hm)*omega)/p;
% Centrifugal force
Fm = (Mm*vmag^2)/(R+hm);
% Outward pressure
Phoop = Fm/(2*pi*(R+hm)*Lst);
% Hoop Stress (in general, str = P*R/t)
stop = 22;
for i = 1:stop
    t(i) = i*.0005;         % sleeve thickness t
    slev(i) = t(i)*1000;
    Sthoop(i) = (Phoop*(R+hm)/t(i))*Patopsi/1000;
    SFHoop(i) = Sthoop(i)*SF;
end

% Output results
fprintf('Retaining Sleeve Stress:\n');
fprintf('Stress Limits:\n');
fprintf('Stainless Steel = %6.1f ksi  Aluminum Alloy = %6.1f ksi\n',Stain_str,Alum_str);
fprintf('Titanium Alloy = %6.1f ksi  Carbon Fiber =  %6.1f ksi\n',Titan_str,CarFib_str);
fprintf('Inconel =       %6.1f ksi\n',Inconel_str);
fprintf('Actual Sleeve Stress:\n');
fprintf('Sleeve Thickness    Actual Stress      SF Stress\n');
for i = 1:stop
    fprintf('  %5.2f mm          %6.1f ksi        %6.1f ksi\n',...
        slev(i),Sthoop(i),SFHoop(i));
end
```

Page Intentionally Left Blank

Appendix I. MATLAB Code: Rotor Losses from Winding Time and Space Harmonics

```
% Jonathan Rucker, MIT Thesis
% May 2005
% Program: pmharmloss
% Program performs rotor loss calculations caused by
% winding time and space harmonics for permanent magnet
% machines with surface magnets and slotted stators.

% MUST RUN pm1input, pm1calc, pm1output, and get harmonic
% current data from PSIM prior to running pmharmloss

% Constants to be used
mu0 = 4*pi*1e-7;          % Free space permeability
tol = 1e-2;               % Tolerance factor

% Retaining sleeve/magnet material resistivity (ohm-m)
Stain_res = 0.72e-6;
Titan_res = 0.78e-6;
CarFib_res = 9.25e-6;
Inconel_res = 0.98e-6;
Magnet_res = 1.43e-6;

% Retaining sleeve thickness set at 0.5mm less than air gap
h_sl = g - 0.0005;        % Sleeve thickness
g_act = g - h_sl;         % Actual air gap

% Retaining sleeve conductivities (S/m)
cond_s = 1/Stain_res;
cond_t = 1/Titan_res;
cond_c = 1/CarFib_res;
cond_i = 1/Inconel_res;

% Magnet & actual sleeve cond (S/m)
cond_m = 1/Magnet_res;
cond_sl = cond_s;

% Input time harmonic peak currents from PSIM
I1 = 2895;
I3 = 0;
I5 = 209;
I7 = 89.2;
I9 = 0;
I11 = 39.2;
I13 = 27.6;
I15 = 0;
I17 = 17.0;
I19 = 12.8;
I21 = 0;
I23 = 7.3;
I25 = 6.3;
I27 = 0;
```

```
I29 = 4.8;
I31 = 3.9;

% Put currents in array
Iharm = [I1 I3 I5 I7 I9 I11 I13 I15 I17 I19 I21 I23 I25...
    I27 I29 I31];

% Calculate current THD
Iah = 0;
for r = 2:length(Iharm)
    Iah = Iah + Iharm(r)^2;
end
THDi = 100*sqrt(Iah/(Iharm(1)^2));

% Calculate current densities
Iz = (1/sqrt(2)).*Iharm;
Kz = ((q/2)*(Na/(2*pi*Rs))).*Iz;
Iz_1 = (1/sqrt(2)).*I1;              % Fundamental RMS current
Kz_1 = ((q/2)*(Na/(2*pi*Rs))).*Iz_1;  % Fundamental current density

% Harmonics to be evaluated
n = 1:2:31;
w = n .* omega;                      % Harmonic angular frequencies
freq = w ./ (2*pi);                  % Harmonic frequencies
lam = (2*(2*pi/(2*p)))./n;
k = (2*pi)./lam;                     % Wavenumbers

% Eta values
eta_m = sqrt((j*mu0*cond_m).*w + (k.^2));
eta_s = sqrt((j*mu0*cond_sl).*w + (k.^2));

% Surface coefficient at top of magnet layer
alpha_m = j.*(k./eta_m).*coth(eta_m.*hm);

% Surface coefficient at top of retaining sleeve
top1 = (j.*(k./eta_s).*sinh(eta_s.*h_sl)) + (alpha_m.*cosh(eta_s.*h_sl));
bot1 = (j.*(k./eta_s).*cosh(eta_s.*h_sl)) + (alpha_m.*sinh(eta_s.*h_sl));
alpha_s = j.*(k./eta_s).*(top1./bot1);

% Surface coefficient at surface of stator
top2 = (j.*sinh(k.*g_act)) + (alpha_s.*cosh(k.*g_act));
bot2 = (j.*cosh(k.*g_act)) + (alpha_s.*sinh(k.*g_act));
alpha_f = j.*(top2./bot2);

% Surface impedance
Zs = (mu0.*w./k).*alpha_f;

% Calculate losses due to time harmonics
% Use only fundamental space harmonic factors
Kz_t = kw.*Kz;
Syt = 0;
for i = 1:length(n)
    Sy_t(i) = 0.5*(abs(Kz_t(i))^2)*real(Zs(1));
    Syt = Syt + Sy_t(i);
end
```

```
% Calculate losses due to space harmonics
% Use only fundamental time harmonic current
kpn = sin(n .* pi/2) .* sin(n .* alfa/2);
kbn = sin(n .* m*gama/2) ./ (m.*sin(n .* gama/2));
kwn = kpn .* kbn;
Kz_s = kwn .* Kz_1 ./ n;
Sys = 0;
for i = 1:length(n)
    Sy_s(i) = 0.5*(abs(Kz_s(i))^2)*real(Zs(i));
    Sys = Sys + Sy_s(i);
end

fprintf('\nRotor Losses Caused by Harmonics:\n');
fprintf('Time Harmonic Losses =  %6.1f kW\n',Syt/1000);
fprintf('Space Harmonic Losses = %6.1f kW\n',Sys/1000);
fprintf('Total Losses =      %6.1f kW\n',(Syt+Sys)/1000);
fprintf('Current THD =       %6.2f %%\n',THDi);
```

Page Intentionally Left Blank

Appendix J.   MATLAB Code: Rotor Losses from Slot Effects

```
% Jonathan Rucker, MIT Thesis
% May 2005
% Program: pmcanloss
% Program calculates and outputs rotor losses caused by
% stator slot effects for permanent magnet machines
% with surface magnets and slotted stators.

% MUST RUN pm1input, pm1calc, pmwave, and pmcanstress
% PRIOR TO RUNNING pmcanloss

%%%%%%%%%%%%%%%%%%%%%%%%%%%%%%%%%%%%%%%%%%%%%%%%%%%%%%%%%%%
% Calculate retaining sleeve losses
%%%%%%%%%%%%%%%%%%%%%%%%%%%%%%%%%%%%%%%%%%%%%%%%%%%%%%%%%%%

% Retaining sleeve/magnet material resistivity (ohm-m)
Stain_res = 0.72e-6;
Titan_res = 0.78e-6;
CarFib_res = 9.25e-6;
Inconel_res = 0.98e-6;
Magnet_res = 1.43e-6;

% Calculate Bd as function of wst and wt (max 10% of Bg)
Bd = (wst/wt)*0.1*Bg;
% Calculate flux variation parameters
beta = (wst/(2*pi*Rs))*2*pi;
lamB = 2*pi/Ns;
B = (Bd/sqrt(2))*sqrt(beta/lamB);
% Calculate geometry and can loss factor for different rings
% k is number of rings
for k = 1:10
    A(k) = pi*2*(R+hm)*Lst/k;
    Ks(k) = 1 - ((tanh(p*Lst/(k*2*(R+hm))))/(p*Lst/(k*2*(R+hm))));
end

% Input Stainless Steel sleeve thickness based on stress results
for i = 1:stop
    if SFHoop(i) <= Stain_str
        t_Stain = t(i);
        break
    elseif t(stop) > Stain_str
        fprintf('Hoop Stress too high for Stainless Steel.\n');
    else
        dummy = t(i);
    end
end

% Input Titanium sleeve thickness based on stress results
for i = 1:stop
    if SFHoop(i) <= Titan_str
        t_Titan = t(i);
        break
    elseif t(stop) > Titan_str
```

```
            fprintf('Hoop Stress too high for Titanium.\n');
        else
            dummy = t(i);
        end
    end

    % Input Carbon Fiber sleeve thickness based on stress results
    for i = 1:stop
        if SFHoop(i) <= CarFib_str
            t_CarFib = t(i);
            break
        elseif t(stop) > CarFib_str
            fprintf('Hoop Stress too high for Carbon Fiber.\n');
        else
            dummy = t(i);
        end
    end

    % Input Inconel sleeve thickness based on stress results
    for i = 1:stop
        if SFHoop(i) <= Inconel_str
            t_Inconel = t(i);
            break
        elseif t(stop) > Inconel_str
            fprintf('Hoop Stress too high for Inconel.\n');
        else
            dummy = t(i);
        end
    end

    % Calculate can losses
    w_Stain = (pi^2/3600)*((B*rpm*(R+hm))^2*t_Stain)/Stain_res;
    w_Titan = (pi^2/3600)*((B*rpm*(R+hm))^2*t_Titan)/Titan_res;
    w_CarFib = (pi^2/3600)*((B*rpm*(R+hm))^2*t_CarFib)/CarFib_res;
    w_Inconel = (pi^2/3600)*((B*rpm*(R+hm))^2*t_Inconel)/Inconel_res;

    for k = 1:10
        P_Stain(k) = k*w_Stain*Ks(k)*A(k)/1000;
        P_Titan(k) = k*w_Titan*Ks(k)*A(k)/1000;
        P_CarFib(k) = k*w_CarFib*Ks(k)*A(k)/1000;
        P_Inconel(k) = k*w_Inconel*Ks(k)*A(k)/1000;
    end

    % Calculate magnet losses (only with carbon steel)
    % Calculate geometry and can loss factor
    Am = pi*2*R*Lst;
    Ksm = 1 - ((tanh(p*Lst/(2*R)))/(p*Lst/(2*R)));
    % Calculate magnet losses
    % Assumes only 10% of magnet thickness sees effects
    w_Magnet = (pi^2/3600)*((B*rpm*R)^2*0.1*hm)/Magnet_res;
    P_Magnet = w_Magnet*Ksm*Am/1000;

    % Output Results
    z = [1 5 10];
    fprintf('Retaining Can Losses:\n');
    for i=1:3
```

```
    k = z(i);
    fprintf('%1.0f Rings:\n',k)
    fprintf('Material        Thickness       Can Loss\n');
    fprintf('Stainless Steel  %5.2f mm      %6.1f kW\n',t_Stain*1000,P_Stain(k));
    fprintf('Titanium         %5.2f mm      %6.1f kW\n',t_Titan*1000,P_Titan(k));
    fprintf('Carbon Fiber     %5.2f mm       %6.1f kW\n',t_CarFib*1000,P_CarFib(k));
    fprintf('    Associated Magnet Loss     %6.1f kW\n',P_Magnet);
    fprintf('Inconel          %5.2f mm     %6.1f kW\n\n',t_Inconel*1000,P_Inconel(k));
end
```

Page Intentionally Left Blank

Appendix K.   Results for PM Machine Variants

Phases	Retaining Can	Poles	N_s	m	N_a	E_a (RMS)	L_s (mH)	f (Hz)	θ_M (deg)	θ_S (deg)	Gen THD	k_s	h_M (mm)	g (mm)	L_{st} (m)	L (m)	D (m)	k_b	k_p	k_d	B_g (T)
3 Phase	Stainless Steel	6	36	2.00	12	3,255	0.181	650.0	50.0	10.0	13.31%	0.989	32.0	11.0	1.080	2.057	0.900	0.966	0.966	0.867	0.70
		8	36	1.50	12	2,733	0.094	866.7	35.0	10.0	5.88%	0.980	32.0	10.5	0.995	1.901	0.881	0.975	0.924	0.887	0.67
		10	36	1.20	12	2,367	0.056	1,083.3	26.0	10.0	3.88%	0.960	32.0	9.5	0.965	1.835	0.869	0.986	0.866	0.914	0.65
		12	36	1.00	12	2,263	0.041	1,300.0	20.0	10.0	5.11%	0.955	32.0	9.0	1.000	1.870	0.861	1.000	0.866	0.933	0.61
	Titanium	6	36	2.00	12	3,256	0.182	650.0	50.0	10.0	13.04%	0.989	31.0	9.0	1.030	2.005	0.894	0.966	0.966	0.891	0.72
		8	36	1.50	12	2,760	0.098	866.7	35.0	10.0	5.73%	0.980	30.0	8.0	0.965	1.869	0.872	0.975	0.924	0.909	0.70
		10	36	1.20	12	2,458	0.061	1,083.3	26.0	10.0	3.82%	0.960	30.0	7.5	0.980	1.849	0.861	0.986	0.866	0.927	0.67
		12	36	1.00	12	2,352	0.045	1,300.0	20.0	10.0	5.05%	0.955	30.0	7.0	1.020	1.889	0.853	1.000	0.866	0.944	0.63
	Inconel	6	36	2.00	12	3,380	0.197	650.0	50.0	10.0	12.79%	0.989	29.0	7.0	1.032	2.003	0.886	0.966	0.966	0.911	0.75
		8	36	1.50	12	2,790	0.100	866.7	35.0	10.0	5.62%	0.980	29.0	6.5	0.940	1.842	0.867	0.975	0.924	0.928	0.72
		10	36	1.20	12	2,492	0.062	1,083.3	26.0	10.0	3.74%	0.960	29.0	6.0	0.960	1.828	0.856	0.986	0.866	0.945	0.68
		12	36	1.00	12	2,380	0.046	1,300.0	20.0	10.0	4.95%	0.955	29.0	5.5	1.000	1.868	0.848	1.000	0.866	0.961	0.65
	Carbon	6	36	2.00	12	3,182	0.174	650.0	50.0	10.0	13.16%	0.989	32.0	10.0	1.020	1.996	0.898	0.966	0.966	0.883	0.71
		8	36	1.50	12	2,708	0.094	866.7	35.0	10.0	5.79%	0.980	31.0	9.0	0.960	1.865	0.876	0.975	0.924	0.901	0.69
		10	36	1.20	12	2,405	0.058	1,083.3	26.0	10.0	3.85%	0.960	31.0	8.5	0.971	1.841	0.865	0.986	0.866	0.920	0.66
		12	36	1.00	12	2,304	0.043	1,300.0	20.0	10.0	5.08%	0.955	31.0	8.0	1.010	1.879	0.857	1.000	0.866	0.938	0.62

Phases	Retaining Can	Poles	N_s	m	N_a	E_a (RMS)	L_s (mH)	f (Hz)	θ_M (deg)	θ_S (deg)	Gen THD	k_s	h_M (mm)	g (mm)	L_{st} (m)	L (m)	D (m)	k_b	k_p	k_d	B_g (T)
5 Phase	Stainless Steel	6	36	1.20	7	1,928	0.106	650.0	50.0	10.0	17.43%	0.989	32.0	11.0	1.035	2.012	0.900	0.995	0.966	0.867	0.70
		8	36	0.90	7	1,564	0.052	866.7	35.0	10.0	8.98%	0.980	31.0	10.0	0.928	1.833	0.878	1.004	0.924	0.885	0.67
		10	36	0.72	7	1,378	0.030	1,083.3	26.0	10.0	11.62%	0.960	30.0	9.0	0.935	1.804	0.864	1.016	0.866	0.903	0.64
		12	36	0.60	7	1,298	0.020	1,300.0	20.0	10.0	15.82%	0.955	29.0	8.0	0.960	1.829	0.853	1.030	0.921	0.921	0.61
	Titanium	6	36	1.20	7	1,934	0.107	650.0	50.0	10.0	17.07%	0.989	31.0	9.0	0.990	1.965	0.894	0.995	0.966	0.891	0.72
		8	36	0.90	7	1,625	0.057	866.7	35.0	10.0	8.74%	0.980	29.0	7.5	0.922	1.825	0.869	1.004	0.924	0.909	0.70
		10	36	0.72	7	1,429	0.033	1,083.3	26.0	10.0	11.42%	0.960	28.0	7.0	0.945	1.813	0.856	1.016	0.866	0.918	0.66
		12	36	0.60	7	1,336	0.022	1,300.0	20.0	10.0	15.54%	0.955	27.0	6.0	0.962	1.829	0.845	1.030	0.921	0.936	0.63
	Inconel	6	36	1.20	7	2,024	0.117	650.0	50.0	10.0	16.74%	0.989	29.0	7.0	1.000	1.971	0.886	0.995	0.966	0.911	0.75
		8	36	0.90	7	1,661	0.059	866.7	35.0	10.0	8.63%	0.980	28.0	6.5	0.925	1.827	0.865	1.004	0.924	0.919	0.71
		10	36	0.72	7	1,452	0.034	1,083.3	26.0	10.0	11.16%	0.960	27.0	5.5	0.923	1.790	0.851	1.016	0.866	0.938	0.69
		12	36	0.60	7	1,361	0.023	1,300.0	20.0	10.0	15.34%	0.955	26.0	5.0	0.961	1.828	0.841	1.030	0.921	0.947	0.65
	Carbon	6	36	1.20	7	1,956	0.110	650.0	50.0	10.0	17.17%	0.989	31.0	9.5	1.020	1.995	0.895	0.995	0.966	0.882	0.72
		8	36	0.90	7	1,588	0.054	866.7	35.0	10.0	8.83%	0.980	30.0	8.5	0.915	1.819	0.873	1.004	0.924	0.900	0.69
		10	36	0.72	7	1,433	0.034	1,083.3	26.0	10.0	11.52%	0.960	28.0	7.5	0.966	1.834	0.857	1.016	0.866	0.909	0.66
		12	36	0.60	7	1,337	0.023	1,300.0	20.0	10.0	15.83%	0.955	27.0	7.0	0.999	1.867	0.847	1.030	0.921	0.918	0.62

Phases	Retaining Can	Poles	N_s	m	N_a	E_a (RMS)	L_s (mH)	f (Hz)	θ_M (deg)	θ_S (deg)	Gen THD	k_s	h_M (mm)	g (mm)	L_{st} (m)	L (m)	D (m)	k_b	k_p	k_d	B_g (T)
7 Phase	Stainless Steel	6	72	1.71	10	2,800	0.314	650.0	50.0	10.0	22.14%	0.989	32.0	11.0	1.010	2.005	0.900	0.994	0.991	0.867	0.71
		8	72	1.29	10	2,367	0.168	866.7	35.0	10.0	14.54%	0.980	31.0	10.0	0.915	1.855	0.878	0.997	0.985	0.885	0.68
		10	72	1.03	10	2,130	0.107	1,083.3	26.0	10.0	7.02%	0.960	30.0	9.0	0.900	1.804	0.864	1.000	0.975	0.903	0.65
		12	72	0.86	10	1,999	0.075	1,300.0	20.0	10.0	3.21%	0.955	29.0	8.0	0.940	1.826	0.853	1.003	0.966	0.921	0.62
	Titanium	6	72	1.71	10	2,822	0.318	650.0	50.0	10.0	21.69%	0.989	31.0	9.0	0.970	1.962	0.894	0.994	0.991	0.891	0.74
		8	72	1.29	10	2,462	0.182	866.7	35.0	10.0	14.15%	0.980	29.0	7.5	0.910	1.847	0.869	0.997	0.985	0.909	0.71
		10	72	1.03	10	2,227	0.118	1,083.3	26.0	10.0	6.88%	0.960	28.0	7.0	0.917	1.819	0.856	1.000	0.975	0.918	0.67
		12	72	0.86	10	2,086	0.083	1,300.0	20.0	10.0	3.15%	0.955	27.0	6.0	0.955	1.839	0.845	1.003	0.966	0.936	0.64
	Inconel	6	72	1.71	10	2,955	0.348	650.0	50.0	10.0	21.27%	0.989	29.0	7.0	0.980	1.968	0.886	0.994	0.991	0.911	0.76
		8	72	1.29	10	2,522	0.191	866.7	35.0	10.0	13.99%	0.980	28.0	6.5	0.915	1.851	0.865	0.997	0.985	0.919	0.73
		10	72	1.03	10	2,260	0.122	1,083.3	26.0	10.0	6.74%	0.960	27.0	5.5	0.895	1.796	0.851	1.000	0.975	0.938	0.70
		12	72	0.86	10	2,127	0.087	1,300.0	20.0	10.0	3.12%	0.955	26.0	5.0	0.955	1.838	0.841	1.003	0.966	0.947	0.65
	Carbon	6	72	1.71	10	2,841	0.324	650.0	50.0	10.0	21.82%	0.989	31.0	9.5	0.995	1.987	0.895	0.994	0.991	0.882	0.73
		8	72	1.29	10	2,397	0.173	866.7	35.0	10.0	14.30%	0.980	30.0	8.5	0.900	1.839	0.873	0.997	0.985	0.900	0.70
		10	72	1.03	10	2,179	0.112	1,083.3	26.0	10.0	6.96%	0.960	29.0	8.0	0.910	1.813	0.860	1.000	0.975	0.910	0.66
		12	72	0.86	10	2,044	0.079	1,300.0	20.0	10.0	3.18%	0.955	28.0	7.0	0.950	1.835	0.849	1.003	0.966	0.927	0.63

Phases	Retaining Can	Poles	N_s	m	N_a	E_a (RMS)	L_s (mH)	f (Hz)	θ_M (deg)	θ_S (deg)	Gen THD	k_s	h_M (mm)	g (mm)	L_{st} (m)	L (m)	D (m)	k_b	k_p	k_d	B_g (T)
9 Phase	Stainless Steel	6	72	1.33	8	2,192	0.247	650.0	50.0	10.0	22.75%	0.989	31.0	10.5	1.020	2.013	0.897	0.998	0.991	0.866	0.71
		8	72	1.00	8	1,841	0.131	866.7	35.0	10.0	14.89%	0.980	29.0	9.5	0.940	1.879	0.873	1.000	0.985	0.874	0.68
		10	72	0.80	8	1,588	0.074	1,083.3	26.0	10.0	7.97%	0.960	28.0	8.5	0.885	1.788	0.859	1.003	0.975	0.892	0.65
		12	72	0.67	8	1,437	0.043	1,300.0	20.0	10.0	6.16%	0.955	27.0	7.5	0.890	1.775	0.848	1.006	0.966	0.910	0.62
	Titanium	6	72	1.33	8	2,194	0.248	650.0	50.0	10.0	22.27%	0.989	30.0	8.5	0.970	1.961	0.891	0.998	0.991	0.891	0.74
		8	72	1.00	8	1,868	0.134	866.7	35.0	10.0	14.52%	0.980	28.0	7.5	0.905	1.841	0.867	1.000	0.985	0.900	0.71
		10	72	0.80	8	1,664	0.083	1,083.3	26.0	10.0	7.80%	0.960	26.0	6.5	0.900	1.801	0.851	1.003	0.975	0.909	0.67
		12	72	0.67	8	1,501	0.050	1,300.0	20.0	10.0	6.04%	0.955	25.0	5.5	0.900	1.783	0.840	1.006	0.966	0.928	0.64
	Inconel	6	72	1.33	8	2,223	0.255	650.0	50.0	10.0	21.92%	0.989	29.0	7.0	0.945	1.933	0.886	0.998	0.991	0.911	0.76
		8	72	1.00	8	1,893	0.138	866.7	35.0	10.0	14.24%	0.980	27.0	6.0	0.880	1.815	0.862	1.000	0.985	0.921	0.73
		10	72	0.80	8	1,698	0.087	1,083.3	26.0	10.0	7.62%	0.960	25.0	5.0	0.878	1.777	0.846	1.003	0.975	0.932	0.70
		12	72	0.67	8	1,527	0.053	1,300.0	20.0	10.0	5.96%	0.955	24.0	4.5	0.895	1.777	0.836	1.006	0.966	0.941	0.66
	Carbon	6	72	1.33	8	2,150	0.238	650.0	50.0	10.0	22.49%	0.989	31.0	9.5	0.965	1.957	0.895	0.998	0.991	0.882	0.73
		8	72	1.00	8	1,819	0.127	866.7	35.0	10.0	14.68%	0.980	29.0	8.5	0.895	1.833	0.871	1.000	0.985	0.891	0.70
		10	72	0.80	8	1,627	0.079	1,083.3	26.0	10.0	7.83%	0.960	27.0	7.5	0.895	1.797	0.855	1.003	0.975	0.900	0.66
		12	72	0.67	8	1,474	0.047	1,300.0	20.0	10.0	6.11%	0.955	26.0	6.5	0.900	1.784	0.844	1.006	0.966	0.918	0.63

Phases	Retaining Can	Poles	N_s	m	N_a	E_a (RMS)	L_s (mH)	f (Hz)	θ_M (deg)	θ_S (deg)	Gen THD	k_s	h_M (mm)	g (mm)	L_{st} (m)	L (m)	D (m)	k_b	k_p	k_d	B_g (T)
11 Phase	Stainless Steel	6	72	1.09	7	1,735	0.189	650.0	50.0	10.0	23.05%	0.989	31.0	10.5	0.985	1.978	0.897	0.999	0.991	0.866	0.71
		8	72	0.82	7	1,456	0.100	866.7	35.0	10.0	15.25%	0.980	28.0	9.0	0.913	1.851	0.870	1.002	0.985	0.873	0.68
		10	72	0.65	7	1,258	0.054	1,083.3	26.0	10.0	9.11%	0.960	26.0	7.5	0.865	1.766	0.853	1.005	0.975	0.890	0.66
		12	72	0.55	7	1,136	0.028	1,300.0	20.0	10.0	8.20%	0.955	24.0	6.5	0.887	1.770	0.840	1.008	0.966	0.898	0.62
	Titanium	6	72	1.09	7	1,803	0.205	650.0	50.0	10.0	22.48%	0.989	29.0	8.0	0.975	1.964	0.888	0.999	0.991	0.891	0.74
		8	72	0.82	7	1,477	0.103	866.7	35.0	10.0	14.86%	0.980	27.0	7.0	0.875	1.810	0.864	1.002	0.985	0.900	0.71
		10	72	0.65	7	1,287	0.058	1,083.3	26.0	10.0	8.91%	0.960	25.0	6.0	0.850	1.750	0.848	1.005	0.975	0.910	0.68
		12	72	0.55	7	1,163	0.031	1,300.0	20.0	10.0	8.01%	0.955	23.0	5.0	0.870	1.752	0.835	1.008	0.966	0.920	0.64
	Inconel	6	72	1.09	7	1,823	0.210	650.0	50.0	10.0	22.12%	0.989	28.0	6.5	0.945	1.932	0.883	0.999	0.991	0.903	0.77
		8	72	0.82	7	1,518	0.109	866.7	35.0	10.0	14.67%	0.980	26.0	6.0	0.880	1.814	0.860	1.002	0.985	0.912	0.72
		10	72	0.65	7	1,318	0.061	1,083.3	26.0	10.0	8.78%	0.960	24.0	5.0	0.850	1.749	0.844	1.005	0.975	0.923	0.69
		12	72	0.55	7	1,164	0.031	1,300.0	20.0	10.0	7.90%	0.955	23.0	4.5	0.850	1.732	0.834	1.008	0.966	0.932	0.65
	Carbon	6	72	1.09	7	1,775	0.199	650.0	50.0	10.0	22.83%	0.989	30.0	9.5	0.995	1.987	0.893	0.999	0.991	0.873	0.72
		8	72	0.82	7	1,497	0.106	866.7	35.0	10.0	15.08%	0.980	27.0	8.0	0.925	1.861	0.866	1.002	0.985	0.881	0.69
		10	72	0.65	7	1,288	0.058	1,083.3	26.0	10.0	9.00%	0.960	25.0	6.5	0.870	1.770	0.849	1.005	0.975	0.899	0.67
		12	72	0.55	7	1,162	0.031	1,300.0	20.0	10.0	8.11%	0.955	23.0	5.5	0.890	1.772	0.836	1.008	0.966	0.909	0.63

Page Intentionally Left Blank

Appendix L. Results for Power Conversion Module Variants

Inputs			Rectifier				Converter Input Filter								Converter Output Filter		
Phases	Retaining Can	Poles	Ea (RMS)	Max Rectified Voltage	L_r (uH)	C_r (mF)	Fund I_{conv}	G_f	Z_f	s^2LC	L_f (uH)	C_f (mF)	C_b (mF)	R_f (mΩ)	LC	L_{out} (uH)	C_{out} (mF)
3 Phase	Stainless Steel	6	3,255	7,613.7	101.9	232.3	2,675.7	2.80E-03	1.25E-03	3.56E+02	1.415	2.548	25.48	5.07	1.62E-06	557.5	2.908
		8	2,733	6,392.7	53.9	247.2	3,186.7	2.35E-03	1.05E-03	4.24E+02	1.415	3.036	30.36	4.64	1.62E-06	546.7	2.965
		10	2,367	5,536.6	32.3	263.6	3,679.5	2.04E-03	9.06E-04	4.90E+02	1.415	3.506	35.06	4.32	1.62E-06	536.3	3.023
		12	2,263	5,293.4	24.6	240.3	3,848.6	1.95E-03	8.66E-04	5.12E+02	1.415	3.668	36.68	4.22	1.62E-06	532.7	3.043
	Titanium	6	3,256	7,616.1	101.9	232.2	2,674.8	2.80E-03	1.25E-03	3.56E+02	1.415	2.547	25.47	5.07	1.62E-06	557.5	2.908
		8	2,760	6,455.9	54.9	242.3	3,155.5	2.38E-03	1.06E-03	4.20E+02	1.415	3.006	30.06	4.66	1.62E-06	547.3	2.962
		10	2,458	5,749.5	34.9	244.5	3,543.2	2.12E-03	9.41E-04	4.71E+02	1.415	3.376	33.76	4.40	1.62E-06	539.1	3.007
		12	2,352	5,501.5	26.6	222.5	3,702.9	2.03E-03	9.00E-04	4.93E+02	1.415	3.529	35.29	4.30	1.62E-06	535.8	3.026
	Inconel	6	3,380	7,906.1	109.9	215.5	2,576.7	2.91E-03	1.29E-03	3.43E+02	1.415	2.453	24.53	5.16	1.62E-06	559.6	2.897
		8	2,790	6,526.1	56.1	237.2	3,121.6	2.40E-03	1.07E-03	4.15E+02	1.415	2.974	29.74	4.69	1.62E-06	548.1	2.958
		10	2,492	5,829.0	35.8	237.8	3,494.9	2.15E-03	9.54E-04	4.65E+02	1.415	3.330	33.30	4.43	1.62E-06	540.2	3.001
		12	2,380	5,567.0	27.2	217.3	3,659.4	2.05E-03	9.11E-04	4.87E+02	1.415	3.487	34.87	4.33	1.62E-06	536.7	3.021
	Carbon	6	3,182	7,443.0	97.4	243.1	2,737.1	2.74E-03	1.22E-03	3.64E+02	1.415	2.607	26.07	5.01	1.62E-06	556.2	2.915
		8	2,708	6,334.3	52.9	251.7	3,216.1	2.33E-03	1.04E-03	4.28E+02	1.415	3.064	30.64	4.62	1.62E-06	546.1	2.969
		10	2,405	5,625.5	33.4	255.4	3,621.3	2.07E-03	9.20E-04	4.82E+02	1.415	3.451	34.51	4.35	1.62E-06	537.5	3.016
		12	2,304	5,389.3	25.5	231.9	3,780.1	1.98E-03	8.82E-04	5.03E+02	1.415	3.603	36.03	4.26	1.62E-06	534.1	3.035
5 Phase	Stainless Steel	6	1,928	5,101.4	35.7	662.2	3,993.4	1.88E-03	8.35E-04	5.31E+02	1.415	3.806	38.06	4.15	1.62E-06	529.6	3.061
		8	1,564	4,139.3	17.6	754.7	4,922.8	1.52E-03	6.77E-04	6.55E+02	1.415	4.694	46.94	3.73	1.62E-06	510.0	3.179
		10	1,378	3,646.1	11.0	777.8	5,587.2	1.34E-03	5.97E-04	7.44E+02	1.415	5.328	53.28	3.50	1.62E-06	495.9	3.269
		12	1,298	3,434.5	8.1	730.5	5,931.6	1.26E-03	5.62E-04	7.90E+02	1.415	5.657	56.57	3.40	1.62E-06	488.7	3.318
	Titanium	6	1,934	5,117.3	36.0	658.1	3,981.0	1.88E-03	8.37E-04	5.30E+02	1.415	3.794	37.94	4.15	1.62E-06	529.9	3.059
		8	1,625	4,299.7	19.0	699.1	4,738.0	1.58E-03	7.04E-04	6.31E+02	1.415	4.517	45.17	3.80	1.62E-06	513.9	3.155
		10	1,429	3,781.1	11.8	723.3	5,387.8	1.39E-03	6.19E-04	7.17E+02	1.415	5.138	51.38	3.57	1.62E-06	500.1	3.241
		12	1,336	3,535.0	8.6	689.5	5,762.9	1.30E-03	5.78E-04	7.67E+02	1.415	5.496	54.96	3.45	1.62E-06	492.2	3.294
	Inconel	6	2,024	5,355.4	39.4	600.9	3,804.0	1.97E-03	8.76E-04	5.06E+02	1.415	3.625	36.25	4.25	1.62E-06	533.6	3.038
		8	1,661	4,394.9	19.9	669.1	4,635.3	1.62E-03	7.19E-04	6.17E+02	1.415	4.419	44.19	3.85	1.62E-06	516.1	3.141
		10	1,452	3,841.9	12.2	700.5	5,302.5	1.41E-03	6.29E-04	7.06E+02	1.415	5.056	50.56	3.60	1.62E-06	502.0	3.230
		12	1,361	3,601.2	8.9	664.4	5,657.0	1.33E-03	5.89E-04	7.53E+02	1.415	5.395	53.95	3.48	1.62E-06	494.5	3.279
	Carbon	6	1,956	5,175.5	36.8	643.4	3,936.2	1.91E-03	8.47E-04	5.24E+02	1.415	3.752	37.52	4.18	1.62E-06	530.8	3.054
		8	1,588	4,201.8	18.2	732.1	4,848.4	1.55E-03	6.88E-04	6.45E+02	1.415	4.623	46.23	3.76	1.62E-06	511.6	3.169
		10	1,433	3,791.7	11.8	719.2	5,372.8	1.40E-03	6.20E-04	7.15E+02	1.415	5.123	51.23	3.57	1.62E-06	500.5	3.239
		12	1,337	3,537.7	8.6	688.5	5,758.6	1.30E-03	5.79E-04	7.67E+02	1.415	5.492	54.92	3.45	1.62E-06	492.3	3.293
7 Phase	Stainless Steel	6	2,800	7,656.4	75.4	314.0	2,660.8	2.82E-03	1.25E-03	3.54E+02	1.415	2.534	25.34	5.08	1.62E-06	557.8	2.906
		8	2,367	6,472.4	40.4	329.5	3,147.5	2.38E-03	1.06E-03	4.19E+02	1.415	2.998	29.98	4.67	1.62E-06	547.5	2.961
		10	2,130	5,824.3	26.2	325.5	3,497.7	2.14E-03	9.53E-04	4.65E+02	1.415	3.333	33.33	4.43	1.62E-06	540.1	3.002
		12	1,999	5,466.1	19.2	308.0	3,726.9	2.01E-03	8.94E-04	4.96E+02	1.415	3.552	35.52	4.29	1.62E-06	535.3	3.029
	Titanium	6	2,822	7,716.6	76.6	309.1	2,640.0	2.84E-03	1.26E-03	3.51E+02	1.415	2.514	25.14	5.10	1.62E-06	558.2	2.904
		8	2,462	6,732.2	43.7	304.6	3,026.0	2.48E-03	1.10E-03	4.02E+02	1.415	2.882	28.82	4.76	1.62E-06	550.1	2.947
		10	2,227	6,089.6	28.6	297.8	3,345.4	2.24E-03	9.96E-04	4.45E+02	1.415	3.187	31.87	4.53	1.62E-06	543.3	2.984
		12	2,086	5,704.0	20.9	282.8	3,571.5	2.10E-03	9.33E-04	4.75E+02	1.415	3.403	34.03	4.38	1.62E-06	538.5	3.010
	Inconel	6	2,955	8,080.2	84.0	281.9	2,521.2	2.97E-03	1.32E-03	3.35E+02	1.415	2.400	24.00	5.22	1.62E-06	560.8	2.891
		8	2,522	6,896.2	45.9	290.2	2,954.1	2.54E-03	1.13E-03	3.93E+02	1.415	2.814	28.14	4.82	1.62E-06	551.6	2.939
		10	2,260	6,179.8	29.5	289.2	3,296.5	2.28E-03	1.01E-03	4.39E+02	1.415	3.141	31.41	4.56	1.62E-06	544.4	2.978
		12	2,127	5,816.1	21.8	272.0	3,502.6	2.14E-03	9.52E-04	4.66E+02	1.415	3.338	33.38	4.43	1.62E-06	540.0	3.002
	Carbon	6	2,841	7,768.5	77.6	305.0	2,622.4	2.86E-03	1.27E-03	3.49E+02	1.415	2.497	24.97	5.12	1.62E-06	558.6	2.902
		8	2,397	6,554.4	41.4	321.3	3,108.1	2.41E-03	1.07E-03	4.13E+02	1.415	2.961	29.61	4.70	1.62E-06	548.3	2.956
		10	2,179	5,958.3	27.4	311.1	3,419.1	2.19E-03	9.75E-04	4.45E+02	1.415	3.258	32.58	4.48	1.62E-06	541.8	2.992
		12	2,044	5,589.2	20.1	294.6	3,644.9	2.06E-03	9.15E-04	4.85E+02	1.415	3.473	34.73	4.34	1.62E-06	537.0	3.019
9 Phase	Stainless Steel	6	2,192	6,074.8	46.2	512.3	3,353.5	2.24E-03	9.94E-04	4.46E+02	1.415	3.195	31.95	4.52	1.62E-06	543.2	2.985
		8	1,841	5,102.0	24.4	544.7	3,992.9	1.88E-03	8.35E-04	5.31E+02	1.415	3.806	38.06	4.15	1.62E-06	529.6	3.061
		10	1,588	4,400.9	14.5	585.7	4,629.0	1.62E-03	7.20E-04	6.16E+02	1.415	4.413	44.13	3.85	1.62E-06	516.2	3.141
		12	1,437	3,982.4	9.9	596.0	5,115.5	1.47E-03	6.52E-04	6.81E+02	1.415	4.878	48.78	3.66	1.62E-06	505.9	3.204
	Titanium	6	2,194	6,080.3	46.3	511.4	3,350.5	2.24E-03	9.95E-04	4.46E+02	1.415	3.192	31.92	4.53	1.62E-06	543.2	2.984
		8	1,868	5,176.9	25.2	529.1	3,935.2	1.91E-03	8.47E-04	5.24E+02	1.415	3.751	37.51	4.18	1.62E-06	530.9	3.054
		10	1,664	4,611.5	16.0	533.4	4,417.6	1.70E-03	7.55E-04	5.88E+02	1.415	4.211	42.11	3.94	1.62E-06	520.7	3.114
		12	1,501	4,159.8	10.8	546.3	4,897.3	1.53E-03	6.81E-04	6.52E+02	1.415	4.669	46.69	3.74	1.62E-06	510.5	3.175
	Inconel	6	2,223	6,160.7	47.5	498.1	3,306.7	2.27E-03	1.01E-03	4.40E+02	1.415	3.151	31.51	4.56	1.62E-06	544.1	2.979
		8	1,893	5,246.1	25.8	515.2	3,883.2	1.93E-03	8.58E-04	5.17E+02	1.415	3.701	37.01	4.20	1.62E-06	532.0	3.048
		10	1,698	4,705.7	16.6	512.3	4,329.2	1.73E-03	7.70E-04	5.76E+02	1.415	4.127	41.27	3.98	1.62E-06	522.5	3.103
		12	1,527	4,231.8	11.2	527.8	4,814.0	1.56E-03	6.92E-04	6.41E+02	1.415	4.590	45.90	3.77	1.62E-06	512.3	3.165
	Carbon	6	2,150	5,958.4	44.4	532.5	3,419.0	2.19E-03	9.75E-04	4.55E+02	1.415	3.258	32.58	4.48	1.62E-06	541.8	2.992
		8	1,819	5,041.1	23.9	557.9	4,041.2	1.86E-03	8.25E-04	5.38E+02	1.415	3.852	38.52	4.12	1.62E-06	528.6	3.067
		10	1,627	4,509.0	15.3	558.0	4,518.1	1.66E-03	7.38E-04	6.01E+02	1.415	4.307	43.07	3.90	1.62E-06	518.5	3.126
		12	1,474	4,085.0	10.4	566.5	4,987.0	1.50E-03	6.68E-04	6.64E+02	1.415	4.755	47.55	3.71	1.62E-06	508.6	3.187
11 Phase	Stainless Steel	6	1,735	4,840.9	28.9	817.7	4,208.3	1.78E-03	7.92E-04	5.60E+02	1.415	4.011	40.11	4.04	1.62E-06	525.1	3.087
		8	1,456	4,062.4	15.3	870.8	5,014.7	1.50E-03	6.65E-04	6.68E+02	1.415	4.782	47.82	3.70	1.62E-06	508.0	3.191
		10	1,258	3,510.0	9.1	933.3	5,804.0	1.29E-03	5.74E-04	7.73E+02	1.415	5.535	55.35	3.44	1.62E-06	491.4	3.299
		12	1,136	3,169.6	6.2	953.7	6,427.3	1.17E-03	5.19E-04	8.56E+02	1.415	6.130	61.30	3.27	1.62E-06	478.2	3.390
	Titanium	6	1,803	5,030.6	31.3	757.2	4,049.6	1.85E-03	8.23E-04	5.39E+02	1.415	3.860	38.60	4.12	1.62E-06	528.4	3.068
		8	1,477	4,121.0	15.7	846.2	4,943.4	1.52E-03	6.74E-04	6.58E+02	1.415	4.713	47.13	3.72	1.62E-06	509.5	3.182
		10	1,287	3,590.9	9.6	891.7	5,673.2	1.32E-03	5.88E-04	7.55E+02	1.415	5.410	54.10	3.48	1.62E-06	494.1	3.281
		12	1,163	3,244.9	6.5	909.9	6,278.1	1.19E-03	5.31E-04	8.36E+02	1.415	5.988	59.88	3.30	1.62E-06	481.3	3.368
	Inconel	6	1,823	5,086.4	32.0	740.7	4,005.1	1.87E-03	8.32E-04	5.33E+02	1.415	3.817	38.17	4.14	1.62E-06	529.4	3.062
		8	1,518	4,235.4	16.6	801.1	4,809.9	1.56E-03	6.93E-04	6.40E+02	1.415	4.586	45.86	3.78	1.62E-06	512.4	3.164
		10	1,318	3,677.4	10.0	850.2	5,539.7	1.35E-03	6.02E-04	7.38E+02	1.415	5.283	52.83	3.52	1.62E-06	496.9	3.262
		12	1,164	3,247.7	6.5	908.4	6,272.7	1.20E-03	5.31E-04	8.35E+02	1.415	5.983	59.83	3.31	1.62E-06	481.4	3.367
	Carbon	6	1,775	4,952.5	30.3	781.3	4,113.5	1.82E-03	8.10E-04	5.47E+02	1.415	3.921	39.21	4.08	1.62E-06	527.1	3.076
		8	1,497	4,176.8	16.2	823.8	4,877.3	1.54E-03	6.83E-04	6.49E+02	1.415	4.650	46.50	3.75	1.62E-06	510.9	3.173
		10	1,288	3,593.7	9.6	890.3	5,668.8	1.32E-03	5.88E-04	7.55E+02	1.415	5.406	54.06	3.48	1.62E-06	494.2	3.280
		12	1,162	3,242.1	6.5	911.5	6,283.5	1.19E-03	5.30E-04	8.37E+02	1.415	5.993	59.93	3.30	1.62E-06	481.2	3.369

Page Intentionally Left Blank

Appendix M.   Results for Power Module Losses

Phases	Retaining Can	Poles	Core Losses	Windage Losses	Armature Losses	Slot Space Harm	Winding Time Harm	Winding Space Harm	Machine Total Losses	IGBT Switching Losses	IGBT Cond Losses	Diode Cond Losses	PCM Total Losses	Total Losses	Line Current THD
						Rotor Losses									
3 Phase	Stainless Steel	6	12.0	32.3	115.5	66.1	19.3	21.7	266.9	2,825.3	199.3	176.5	3,201.0	3,467.9	9.02%
		8	13.8	30.1	118.5	71.7	29.3	31.0	294.4	2,388.3	235.6	172.1	2,796.0	3,090.4	8.05%
		10	15.9	29.8	139.6	74.1	39.9	92.2	391.5	2,073.0	271.7	167.7	2,512.4	2,903.9	7.65%
		12	18.2	31.2	144.4	82.1	47.7	57.9	381.5	2,008.3	280.5	166.6	2,455.4	2,836.9	6.96%
	Titanium	6	12.2	32.1	117.1	46.8	21.0	23.7	252.9	2,821.3	199.5	176.5	3,197.2	3,450.1	8.09%
		8	14.3	30.8	139.2	49.2	32.5	34.4	300.4	2,392.3	235.1	172.1	2,799.5	3,099.9	7.90%
		10	16.8	31.7	136.4	57.1	41.3	94.0	377.3	2,146.6	262.2	168.8	2,577.6	2,954.9	7.80%
		12	19.4	33.4	141.0	62.3	49.9	60.4	366.4	2,077.4	271.1	167.8	2,516.3	2,882.7	6.80%
	Inconel	6	13.0	33.8	117.6	30.2	22.1	25.0	241.7	2,923.9	192.5	177.3	3,293.7	3,535.4	8.08%
		8	14.6	31.3	134.6	30.9	35.2	37.4	284.0	2,418.9	232.6	172.4	2,824.0	3,108.0	7.91%
		10	17.3	32.5	131.2	35.8	44.4	104.5	365.7	2,184.0	257.9	169.4	2,611.2	2,976.9	7.93%
		12	19.9	34.4	137.9	38.4	54.3	66.2	351.1	2,103.6	267.6	168.2	2,539.4	2,890.5	6.62%
	Carbon	6	11.8	31.1	124.9	28.5	25.9	30.7	252.9	2,757.0	203.6	176.0	3,136.5	3,389.4	8.14%
		8	13.8	29.9	137.5	25.5	39.0	42.5	288.2	2,350.9	239.2	171.6	2,761.8	3,050.0	7.95%
		10	16.3	30.6	139.8	25.0	49.9	143.5	405.1	2,105.3	267.3	168.2	2,540.8	2,945.9	7.89%
		12	18.8	32.2	143.5	24.4	60.8	78.8	358.5	2,038.0	276.3	167.1	2,481.4	2,839.9	6.85%
5 Phase	Stainless Steel	6	11.5	31.0	120.4	59.4	27.3	37.5	287.1	1,505.3	373.5	155.3	2,034.1	2,321.2	15.66%
		8	12.8	28.3	144.3	57.6	45.8	57.9	346.7	1,224.5	459.6	144.8	1,828.9	2,175.6	16.66%
		10	15.1	29.1	132.0	63.6	58.6	528.9	827.3	1,116.0	504.2	139.4	1,759.6	2,586.9	17.56%
		12	17.2	30.6	132.6	64.8	72.9	178.6	496.7	1,092.0	515.1	138.1	1,745.1	2,241.8	19.47%
	Titanium	6	11.8	30.9	120.9	42.3	29.7	40.7	276.3	1,507.0	373.0	155.3	2,035.4	2,311.7	15.55%
		8	13.7	29.8	140.7	41.2	48.0	60.5	333.9	1,261.3	446.4	146.4	1,854.1	2,188.0	16.19%
		10	16.0	31.0	130.6	47.9	61.0	545.0	831.5	1,146.9	490.3	141.1	1,778.3	2,609.8	16.92%
		12	18.1	32.5	133.0	45.9	77.8	190.3	497.6	1,109.5	507.3	139.0	1,755.8	2,253.4	18.34%
	Inconel	6	12.6	32.8	108.5	27.9	30.7	42.5	255.0	1,578.3	356.5	157.4	2,092.2	2,347.2	15.59%
		8	14.1	30.8	140.1	29.1	49.7	63.4	327.2	1,296.8	434.1	147.9	1,878.8	2,206.0	15.50%
		10	16.5	31.8	126.0	29.3	65.1	620.6	889.3	1,166.3	493.6	140.7	1,800.6	2,689.9	16.96%
		12	18.6	33.7	131.5	30.6	81.8	209.4	505.6	1,118.2	499.6	139.9	1,757.7	2,263.3	18.11%
	Carbon	6	11.9	31.5	116.5	27.7	35.0	54.9	277.5	1,521.3	370.2	155.7	2,047.2	2,324.7	15.38%
		8	13.2	28.9	141.4	22.8	57.4	80.1	343.8	1,238.1	454.7	145.4	1,838.2	2,182.0	15.44%
		10	16.0	31.2	135.9	22.2	71.2	874.5	1151.0	1,137.2	495.0	140.5	1,772.6	2,923.6	16.18%
		12	18.0	32.7	138.1	20.2	89.5	269.4	567.9	1,092.5	515.1	138.1	1,745.6	2,313.5	17.17%
7 Phase	Stainless Steel	6	11.6	30.2	121.4	57.5	29.8	41.3	291.8	2,117.2	265.8	168.4	2,551.4	2,843.2	15.22%
		8	13.1	27.9	139.1	57.3	49.1	70.5	357.0	1,791.8	314.0	162.5	2,268.3	2,625.3	15.13%
		10	15.0	28.1	140.4	60.2	67.6	89.8	401.1	1,630.1	345.1	158.7	2,133.9	2,535.0	15.43%
		12	17.4	30.0	136.7	63.9	82.6	125.3	455.9	1,564.7	359.8	157.0	2,081.5	2,537.4	15.71%
	Titanium	6	11.9	30.2	113.2	41.4	31.9	44.1	272.7	2,138.8	263.0	168.7	2,570.5	2,843.2	15.34%
		8	13.9	29.4	130.5	41.2	50.9	72.9	338.8	1,860.7	302.4	163.9	2,327.1	2,665.9	15.05%
		10	16.0	30.1	139.6	46.2	69.2	91.7	392.8	1,695.1	331.8	160.4	2,187.3	2,580.1	15.14%
		12	18.5	32.3	137.0	46.5	85.6	129.0	448.9	1,620.0	347.5	158.5	2,125.9	2,574.8	15.26%
	Inconel	6	12.7	32.1	101.3	27.3	32.9	46.1	252.4	2,241.9	250.9	170.2	2,663.0	2,915.4	15.39%
		8	14.4	30.4	124.6	29.3	52.7	76.7	328.1	1,908.0	294.7	164.9	2,367.5	2,695.6	15.09%
		10	16.5	30.8	135.7	28.2	74.6	100.2	386.0	1,715.1	328.2	160.8	2,204.1	2,590.1	15.00%
		12	19.1	33.5	136.4	31.1	89.7	138.2	448.0	1,645.8	341.8	159.1	2,146.8	2,594.8	15.06%
	Carbon	6	12.0	30.7	114.9	27.7	37.9	59.3	262.5	2,146.2	262.2	168.8	2,577.2	2,859.7	15.18%
		8	13.4	28.4	144.1	23.5	61.6	101.1	372.1	1,810.1	302.4	163.9	2,276.5	2,648.6	15.01%
		10	15.5	29.0	138.7	21.9	82.5	119.3	406.9	1,666.1	337.7	159.6	2,163.5	2,570.4	15.38%
		12	17.9	31.1	135.2	20.8	99.5	168.9	473.4	1,594.8	352.9	157.8	2,105.5	2,578.9	15.53%
9 Phase	Stainless Steel	6	11.7	30.8	113.6	56.1	31.0	49.3	292.5	1,639.3	343.3	159.0	2,141.6	2,434.1	15.03%
		8	13.2	29.0	152.3	56.4	52.2	63.5	366.6	1,374.0	469.3	143.6	1,986.9	2,353.5	14.78%
		10	14.5	27.9	138.8	53.1	76.7	434.4	745.4	1,222.1	460.1	144.7	1,827.0	2,572.4	16.20%
		12	16.2	28.8	130.6	52.0	96.6	245.8	570.0	1,184.8	474.8	143.0	1,802.6	2,372.6	19.68%
	Titanium	6	12.0	30.6	118.3	39.0	33.8	53.6	287.3	1,638.9	343.3	159.0	2,141.2	2,428.5	14.99%
		8	13.6	29.3	135.8	39.7	55.3	67.2	340.9	1,400.3	401.9	151.8	1,954.0	2,294.9	14.99%
		10	15.5	29.9	136.3	40.0	78.6	437.4	737.7	1,265.6	445.0	146.6	1,857.1	2,594.8	15.64%
		12	17.2	31.0	128.3	36.7	100.7	254.8	568.7	1,207.3	465.6	144.1	1,817.0	2,385.7	17.85%
	Inconel	6	12.3	31.0	111.1	24.9	36.5	58.9	274.7	1,658.7	339.2	159.5	2,157.4	2,432.1	14.92%
		8	14.0	29.7	132.9	24.5	59.4	73.2	333.7	1,417.3	397.0	152.4	1,966.7	2,300.4	14.93%
		10	16.0	30.8	131.3	23.9	83.3	477.5	762.8	1,287.3	437.2	147.5	1,872.1	2,634.9	15.36%
		12	17.7	32.0	128.1	23.8	106.5	282.0	590.1	1,215.8	462.4	144.5	1,822.7	2,412.9	17.15%
	Carbon	6	11.6	29.8	117.6	26.6	41.5	78.5	305.6	1,605.7	350.6	158.1	2,114.3	2,419.9	14.96%
		8	13.1	28.2	141.5	22.3	67.1	86.7	358.9	1,364.8	412.3	150.6	1,927.6	2,286.5	15.04%
		10	15.0	28.9	137.1	19.5	92.8	655.3	948.6	1,241.8	453.2	145.6	1,840.6	2,789.2	15.73%
		12	16.8	29.9	128.5	17.9	114.8	356.4	664.3	1,198.2	469.2	143.6	1,811.0	2,475.3	18.60%
11 Phase	Stainless Steel	6	11.3	29.8	122.8	51.3	33.6	43.8	292.6	1,290.3	436.1	147.7	1,874.0	2,166.6	14.91%
		8	12.8	28.5	150.3	49.6	57.7	92.4	391.3	1,081.7	520.2	137.4	1,739.4	2,130.7	14.70%
		10	14.2	28.0	133.5	44.0	84.6	652.1	956.4	986.5	570.5	131.3	1,688.3	2,644.7	17.48%
		12	15.9	29.5	125.9	43.0	100.7	319.5	634.5	1,004.4	559.6	132.6	1,696.7	2,331.2	24.19%
	Titanium	6	12.1	31.1	118.3	37.1	34.9	45.5	279.0	1,336.7	420.9	149.5	1,907.1	2,186.1	14.78%
		8	13.2	28.7	142.8	34.1	61.7	98.4	378.9	1,096.0	513.6	138.2	1,747.8	2,126.7	14.65%
		10	14.7	28.7	129.9	32.4	88.5	672.0	966.2	997.5	563.7	132.1	1,693.4	2,659.6	16.74%
		12	16.5	30.5	122.5	30.2	107.9	344.0	651.6	1,002.4	560.9	132.5	1,695.8	2,347.4	22.69%
	Inconel	6	12.4	31.4	118.1	23.1	37.9	50.1	273.0	1,350.1	416.6	150.0	1,916.7	2,189.7	14.71%
		8	13.7	29.7	138.0	24.0	63.8	103.9	373.1	1,125.3	500.1	139.9	1,765.2	2,138.3	14.60%
		10	15.2	29.8	128.2	21.7	92.1	728.9	1015.9	1,019.7	551.5	133.6	1,704.8	2,720.7	16.64%
		12	16.5	30.4	120.3	20.9	114.4	383.8	686.3	1,003.5	560.5	132.5	1,696.5	2,382.8	22.64%
	Carbon	6	11.7	30.7	123.2	26.5	42.3	60.0	294.4	1,313.6	428.5	148.6	1,890.6	2,185.0	14.68%
		8	13.3	29.5	150.7	21.3	70.2	130.3	415.3	1,109.6	506.8	139.1	1,755.8	2,171.1	14.61%
		10	14.7	28.9	132.7	17.8	101.2	964.5	1259.8	999.2	562.8	132.3	1,694.2	2,954.0	16.79%
		12	16.4	30.6	124.6	15.5	122.1	475.4	784.6	1,000.1	562.3	132.3	1,694.7	2,479.3	22.54%

Page Intentionally Left Blank

Appendix N.   Results for Power Module Weights

Phases	Retaining Can	Poles	Core	Magnet	Shaft	Armature	Services	Structure	Machine Total	Capacitors	Inductors	IGBTs	Diodes	Services	Structure	PCM Total	Total
3 Phase	Stainless Steel	6	545.2	109.1	564.6	116.1	200.3	767.6	2,302.9	754.7	437.6	22.8	51.8	380.0	1646.9	3,293.7	5,596.6
		8	400.0	93.8	520.1	94.0	166.2	637.1	1,911.3	573.3	428.9	22.8	51.8	323.0	1399.9	2,799.8	4,711.0
		10	329.2	84.5	504.4	83.5	150.3	576.0	1,727.9	463.2	420.7	22.8	51.8	287.5	1246.0	2,492.0	4,219.9
		12	301.8	80.8	522.7	85.7	148.7	569.9	1,709.7	393.3	417.8	22.8	51.8	265.7	1151.4	2,302.7	4,012.4
	Titanium	6	513.0	100.5	538.4	100.3	189.3	720.8	2,162.4	754.7	437.6	22.8	51.8	380.1	1646.9	3,293.8	5,456.2
		8	380.0	84.8	504.4	89.3	158.8	608.6	1,825.9	574.0	429.5	22.8	51.8	323.4	1401.4	2,802.8	4,628.8
		10	328.1	80.0	512.3	82.6	150.4	576.7	1,730.0	465.5	422.9	22.8	51.8	288.9	1251.9	2,503.8	4,233.8
		12	302.0	76.8	533.2	85.1	149.6	573.3	1,720.0	395.5	420.2	22.8	51.8	267.1	1157.4	2,314.7	4,034.8
	Inconel	6	504.6	93.6	539.5	107.5	186.8	716.0	2,148.0	757.8	439.2	22.8	51.8	381.5	1653.0	3,306.1	5,454.1
		8	365.8	79.6	491.4	86.2	153.4	588.2	1,764.5	574.8	430.0	22.8	51.8	323.8	1403.1	2,806.2	4,570.8
		10	317.5	75.5	501.8	80.0	146.2	560.5	1,681.6	466.4	423.7	22.8	51.8	289.4	1254.0	2,508.1	4,189.7
		12	292.5	72.6	522.7	82.5	145.5	557.9	1,673.7	396.2	420.9	22.8	51.8	267.5	1159.2	2,318.4	3,992.2
	Carbon	6	512.6	103.1	533.2	111.1	189.0	724.5	2,173.5	752.9	436.6	22.8	51.8	379.2	1643.2	3,286.4	5,459.8
		8	381.5	87.4	501.8	90.1	159.1	610.0	1,830.0	572.7	428.5	22.8	51.8	322.7	1398.4	2,796.9	4,626.9
		10	328.2	82.1	507.6	83.0	150.1	575.5	1,726.4	464.2	421.6	22.8	51.8	288.1	1248.5	2,497.0	4,223.4
		12	301.9	78.9	528.0	85.4	149.1	571.6	1,714.9	394.3	418.9	22.8	51.8	266.3	1154.2	2,308.3	4,023.2
5 Phase	Stainless Steel	6	522.5	104.6	541.0	112.9	192.2	736.6	2,209.8	916.2	415.6	22.8	51.8	421.9	1828.3	3,656.6	5,866.4
		8	370.5	84.5	485.1	88.4	154.3	591.4	1,774.3	690.5	400.1	22.8	51.8	349.5	1514.7	3,029.4	4,803.7
		10	315.3	76.3	488.8	80.2	144.1	552.3	1,656.9	556.1	389.0	22.8	51.8	305.9	1325.5	2,651.0	4,307.9
		12	284.2	69.7	501.8	81.0	140.5	538.6	1,615.8	467.6	383.3	22.8	51.8	277.6	1203.1	2,406.1	4,021.9
	Titanium	6	493.1	96.6	517.5	107.5	182.2	698.5	2,095.4	916.4	415.8	22.8	51.8	422.0	1828.8	3,657.6	5,753.0
		8	360.5	78.1	482.0	85.5	150.9	578.5	1,735.4	692.2	403.1	22.8	51.8	351.0	1520.9	3,041.8	4,777.2
		10	312.6	71.5	494.0	79.0	143.6	550.3	1,650.9	557.5	392.3	22.8	51.8	307.3	1331.7	2,663.3	4,314.3
		12	279.3	64.6	502.9	79.2	138.9	532.4	1,597.3	468.7	386.0	22.8	51.8	278.8	1208.1	2,416.2	4,013.4
	Inconel	6	489.0	90.7	522.7	105.3	181.2	694.5	2,083.4	918.9	418.7	22.8	51.8	423.7	1835.9	3,671.8	5,755.2
		8	358.2	75.4	483.5	84.6	150.3	576.0	1,728.0	693.3	404.8	22.8	51.8	351.8	1524.4	3,048.9	4,776.9
		10	301.6	67.2	482.5	76.3	139.1	533.3	1,600.0	558.1	393.7	22.8	51.8	307.9	1334.3	2,668.7	4,268.7
		12	276.3	62.0	502.3	78.1	137.8	528.2	1,584.7	469.4	387.8	22.8	51.8	279.5	1211.3	2,422.5	4,007.3
	Carbon	6	509.2	99.5	533.2	110.0	187.8	719.8	2,159.5	917.0	416.5	22.8	51.8	422.4	1830.6	3,661.1	5,820.6
		8	361.1	80.4	478.3	86.1	150.9	578.4	1,735.3	691.2	401.3	22.8	51.8	350.1	1517.2	3,034.4	4,769.6
		10	320.3	73.1	505.0	80.7	146.9	562.9	1,688.8	557.6	392.6	22.8	51.8	307.4	1332.1	2,664.3	4,353.1
		12	291.5	67.1	522.2	82.2	144.4	553.7	1,661.1	468.7	386.1	22.8	51.8	278.8	1208.2	2,416.4	4,077.5
7 Phase	Stainless Steel	6	509.9	102.1	528.0	115.1	188.3	721.6	2,164.8	1,002.0	437.6	22.8	51.8	454.3	1968.5	3,936.9	6,101.8
		8	365.3	83.3	478.3	95.3	153.3	587.8	1,763.3	759.3	429.5	22.8	51.8	379.0	1642.3	3,284.7	5,048.0
		10	303.5	73.4	470.5	85.4	139.9	536.3	1,608.9	614.4	423.6	22.8	51.8	333.8	1446.3	2,892.7	4,501.6
		12	278.3	68.2	491.4	83.3	138.2	529.7	1,589.1	518.6	419.7	22.8	51.8	303.9	1316.7	2,633.4	4,222.5
	Titanium	6	483.1	94.7	507.1	110.0	179.2	687.0	2,061.0	1,002.7	438.0	22.8	51.8	454.6	1969.7	3,939.5	6,000.5
		8	355.8	77.1	475.7	92.1	150.1	575.3	1,726.0	761.1	431.5	22.8	51.8	380.4	1648.5	3,297.1	5,023.1
		10	303.3	69.4	479.3	84.4	140.5	538.4	1,615.3	617.3	426.1	22.8	51.8	335.4	1453.3	2,906.6	4,521.9
		12	277.3	64.1	499.2	82.3	138.4	530.7	1,592.0	521.1	422.3	22.8	51.8	305.4	1323.4	2,646.7	4,238.7
	Inconel	6	479.2	88.9	512.3	107.6	178.2	683.1	2,049.3	1,006.5	440.0	22.8	51.8	456.3	1977.3	3,954.7	6,004.0
		8	354.3	74.6	478.3	91.2	149.8	574.1	1,722.3	763.8	432.7	22.8	51.8	381.3	1652.4	3,304.7	5,027.0
		10	292.5	65.1	467.8	81.5	136.0	521.5	1,564.5	618.2	426.9	22.8	51.8	335.9	1455.6	2,911.2	4,475.6
		12	274.5	61.6	499.2	81.2	137.5	527.0	1,581.0	522.3	423.4	22.8	51.8	306.1	1326.4	2,652.8	4,233.8
	Carbon	6	496.7	97.1	520.1	112.1	183.9	704.9	2,114.8	1,003.2	438.3	22.8	51.8	454.8	1970.8	3,941.7	6,056.5
		8	355.2	79.1	470.5	92.6	149.6	573.5	1,720.5	760.2	430.1	22.8	51.8	379.5	1644.3	3,288.6	5,009.1
		10	303.9	71.6	475.7	85.0	140.4	538.3	1,614.8	615.9	424.9	22.8	51.8	334.6	1449.9	2,899.7	4,514.6
		12	278.6	66.4	496.6	83.0	138.7	531.6	1,594.7	519.9	421.1	22.8	51.8	304.7	1320.2	2,640.4	4,235.1
9 Phase	Stainless Steel	6	511.5	99.5	533.2	114.6	188.8	723.8	2,171.5	1,010.2	426.2	22.8	51.8	453.3	1964.2	3,928.3	6,099.8
		8	371.0	79.6	491.4	95.4	155.6	596.5	1,789.4	763.5	415.4	22.8	51.8	376.0	1629.5	3,259.0	5,048.5
		10	294.9	67.0	462.6	83.0	136.1	521.8	1,565.3	614.3	404.8	22.8	51.8	328.1	1421.8	2,843.5	4,408.8
		12	260.3	59.8	465.2	78.6	129.6	496.8	1,490.3	515.3	396.7	22.8	51.8	296.0	1282.5	2,565.0	4,055.3
	Titanium	6	479.8	91.3	507.1	108.8	178.1	682.5	2,047.6	1,010.3	426.2	22.8	51.8	453.3	1964.3	3,928.6	5,976.2
		8	352.1	73.8	473.1	91.1	148.5	569.3	1,707.9	764.3	416.4	22.8	51.8	376.6	1631.8	3,263.6	4,971.5
		10	294.1	62.9	470.5	81.9	136.4	522.8	1,568.5	616.5	408.3	22.8	51.8	329.8	1429.2	2,858.4	4,426.9
		12	258.1	55.6	470.5	77.3	129.2	495.3	1,486.0	517.2	400.3	22.8	51.8	297.6	1289.7	2,579.3	4,065.4
	Inconel	6	462.1	85.7	494.0	105.2	172.1	659.6	1,978.7	1,011.1	426.9	22.8	51.8	453.8	1966.4	3,932.7	5,911.4
		8	338.4	69.0	460.0	87.9	143.3	549.2	1,647.7	765.0	417.3	22.8	51.8	377.0	1633.9	3,267.8	4,915.5
		10	283.4	58.8	459.0	79.1	132.0	506.1	1,518.3	617.5	409.8	22.8	51.8	330.6	1432.4	2,864.9	4,383.2
		12	254.1	52.9	467.8	76.0	127.6	489.2	1,467.7	517.9	401.7	22.8	51.8	298.3	1292.5	2,584.9	4,052.6
	Carbon	6	481.7	94.2	504.4	110.0	178.6	684.4	2,053.3	1,009.0	425.1	22.8	51.8	452.6	1961.1	3,922.3	5,975.5
		8	351.6	75.8	467.8	91.7	148.0	567.5	1,702.4	762.8	414.6	22.8	51.8	375.6	1627.6	3,255.3	4,957.5
		10	295.3	65.1	467.8	82.6	136.6	523.8	1,571.3	615.4	406.7	22.8	51.8	329.0	1425.6	2,851.3	4,422.5
		12	260.7	58.0	470.5	78.3	130.1	498.8	1,496.3	516.4	398.9	22.8	51.8	296.9	1286.7	2,573.4	4,069.7
11 Phase	Stainless Steel	6	493.9	96.1	514.9	112.2	182.6	699.8	2,099.5	1,009.9	412.0	22.8	51.8	448.9	1945.4	3,890.8	5,990.3
		8	357.8	74.4	477.3	92.6	150.3	576.2	1,728.6	762.1	398.5	22.8	51.8	370.5	1605.7	3,211.3	4,939.9
		10	284.0	60.4	452.2	80.0	131.5	504.1	1,512.2	612.5	385.4	22.8	51.8	321.7	1394.2	2,788.3	4,300.5
		12	254.4	52.5	463.7	76.4	127.0	487.0	1,460.9	513.0	375.0	22.8	51.8	288.8	1251.4	2,502.8	3,963.7
	Titanium	6	479.0	88.5	509.7	108.0	177.8	681.5	2,044.4	1,011.9	414.6	22.8	51.8	450.3	1951.4	3,902.9	5,947.2
		8	338.0	68.6	457.4	88.2	142.8	547.5	1,642.5	762.7	399.7	22.8	51.8	371.1	1608.0	3,216.0	4,858.5
		10	275.7	56.9	444.3	77.7	128.2	491.4	1,474.3	613.3	387.6	22.8	51.8	322.6	1398.1	2,796.2	4,270.4
		12	246.4	49.2	454.8	74.1	123.7	474.0	1,422.0	513.8	377.5	22.8	51.8	289.8	1255.6	2,511.3	3,933.3
	Inconel	6	458.9	82.5	494.0	104.1	170.9	655.2	1,965.6	1,012.5	415.4	22.8	51.8	450.7	1953.2	3,906.3	5,872.0
		8	336.7	66.2	460.0	87.3	142.5	546.4	1,639.1	765.9	401.9	22.8	51.8	372.1	1612.5	3,224.9	4,864.1
		10	273.0	54.5	444.3	76.7	127.3	487.9	1,463.6	614.3	389.8	22.8	51.8	323.6	1402.2	2,804.3	4,267.9
		12	240.1	48.0	444.3	72.5	120.8	462.9	1,388.6	513.9	377.6	22.8	51.8	289.8	1255.8	2,511.6	3,900.1
	Carbon	6	494.4	93.7	520.1	111.3	182.9	701.2	2,103.7	1,011.1	413.6	22.8	51.8	449.8	1949.0	3,898.0	6,001.7
		8	359.1	72.5	483.5	92.2	151.1	579.2	1,737.5	763.3	400.8	22.8	51.8	371.6	1610.2	3,220.4	4,957.9
		10	282.9	58.3	454.8	79.3	131.3	503.3	1,509.8	613.4	387.6	22.8	51.8	322.7	1398.2	2,796.4	4,306.2
		12	252.7	50.3	465.2	75.7	126.6	485.2	1,455.6	513.8	377.4	22.8	51.8	289.7	1255.5	2,511.0	3,966.6

Page Intentionally Left Blank

Appendix O. Rectifier/Input Filter Mass and Volume Calculations

Rectifier & Input Filter Mass Calculations

Phases	Retaining Can	Poles	Max Rectified Voltage	Actual Duty Cycle	Actual Rectified Voltage	Total Capacitance (mF)	Total Capacitor Energy (J)	Total Capacitor Mass (kg)	Average Current	Total Inductance (uH)	Total Inductor Energy (J)	Total Inductor Mass (kg)	Module Diode Mass (kg)	Number of Modules	Total Inductor Mass (kg)	Total Capacitor Mass (kg)	Total Diode Mass (kg)	Total Mass (kg)
3 Phase	Stainless Steel	6	7,613.7	0.1208	5,816.7	260.4	7,546.3	754.6	2,101.5	103.3	0.23	0.684	2.7	19	0.684	754.6	51.3	806.6
		8	6,392.7	0.1428	4,917.1	280.6	5,732.7	573.3	2,502.8	55.3	0.17	0.519	2.7	19	0.519	573.3	51.3	625.1
		10	5,536.6	0.1647	4,268.0	302.2	4,631.7	463.2	2,889.8	33.7	0.14	0.423	2.7	19	0.423	463.2	51.3	514.9
		12	5,293.4	0.1700	4,134.8	280.7	3,932.2	393.2	3,022.7	26.0	0.12	0.357	2.7	19	0.357	393.2	51.3	444.9
	Titanium	6	7,616.1	0.1209	5,808.5	260.2	7,546.6	754.7	2,100.8	103.4	0.23	0.684	2.7	19	0.684	754.7	51.3	806.6
		8	6,455.9	0.1425	4,925.3	275.4	5,739.4	573.9	2,478.4	56.3	0.17	0.519	2.7	19	0.519	573.9	51.3	625.8
		10	5,749.5	0.1589	4,419.4	281.6	4,654.4	465.4	2,782.9	36.3	0.14	0.421	2.7	19	0.421	465.4	51.3	517.2
		12	5,501.5	0.1643	4,277.1	261.3	3,954.4	395.4	2,908.3	28.0	0.12	0.355	2.7	19	0.355	395.4	51.3	447.1
	Inconel	6	7,906.1	0.1167	6,019.7	242.5	7,577.4	757.7	2,023.7	111.3	0.23	0.684	2.7	19	0.684	757.7	51.3	809.7
		8	6,526.1	0.1410	4,980.1	269.9	5,746.9	574.7	2,451.7	57.5	0.17	0.519	2.7	19	0.519	574.7	51.3	626.5
		10	5,829.0	0.1563	4,496.4	274.5	4,662.8	466.3	2,744.9	37.2	0.14	0.421	2.7	19	0.421	466.3	51.3	518.0
		12	5,567.0	0.1622	4,331.0	255.6	3,961.4	396.1	2,874.1	28.6	0.12	0.355	2.7	19	0.355	396.1	51.3	447.8
	Carbon	6	7,443.0	0.1234	5,676.1	271.8	7,528.1	752.8	2,149.7	98.8	0.23	0.685	2.7	19	0.685	752.8	51.3	804.8
		8	6,334.3	0.1450	4,840.1	285.4	5,726.4	572.6	2,525.9	54.3	0.17	0.520	2.7	19	0.520	572.6	51.3	624.5
		10	5,625.5	0.1620	4,334.4	293.3	4,641.2	464.1	2,844.2	34.8	0.14	0.422	2.7	19	0.422	464.1	51.3	515.8
		12	5,389.3	0.1675	4,195.8	271.5	3,942.5	394.2	2,968.9	26.9	0.12	0.356	2.7	19	0.356	394.2	51.3	445.9
5 Phase	Stainless Steel	6	5,101.4	0.2264	3,099.1	704.1	9,161.6	916.2	3,136.4	37.2	0.18	0.548	2.7	19	0.548	916.2	51.3	968.0
		8	4,138.3	0.2786	2,521.0	806.3	6,904.4	690.4	3,866.3	19.1	0.14	0.427	2.7	19	0.427	690.4	51.3	742.2
		10	3,646.1	0.3056	2,297.6	836.4	5,559.8	556.0	4,388.2	12.4	0.12	0.357	2.7	19	0.357	556.0	51.3	607.6
		12	3,434.5	0.3122	2,248.2	792.7	4,675.4	467.5	4,658.7	9.5	0.10	0.310	2.7	19	0.310	467.5	51.3	519.1
	Titanium	6	5,117.3	0.2261	3,102.7	699.8	9,163.3	916.3	3,126.7	37.4	0.18	0.548	2.7	19	0.548	916.3	51.3	968.2
		8	4,299.7	0.2706	2,596.7	748.8	6,921.6	692.2	3,721.2	20.5	0.14	0.425	2.7	19	0.425	692.2	51.3	743.9
		10	3,781.1	0.2972	2,361.2	779.8	5,574.2	557.4	4,231.6	13.2	0.12	0.354	2.7	19	0.354	557.4	51.3	609.1
		12	3,535.0	0.3075	2,284.2	750.0	4,686.1	468.6	4,526.2	10.0	0.10	0.307	2.7	19	0.307	468.6	51.3	520.2
	Inconel	6	5,355.4	0.2161	3,249.4	640.8	9,188.6	918.9	2,987.6	40.8	0.18	0.546	2.7	19	0.546	918.9	51.3	970.7
		8	4,394.9	0.2631	2,669.9	717.7	6,931.8	693.2	3,640.5	21.3	0.14	0.424	2.7	19	0.424	693.2	51.3	744.9
		10	3,841.9	0.2992	2,401.2	756.2	5,580.7	558.1	4,164.6	13.6	0.12	0.353	2.7	19	0.353	558.1	51.3	609.7
		12	3,601.2	0.3028	2,302.2	723.8	4,693.2	469.3	4,443.0	10.3	0.10	0.306	2.7	19	0.306	469.3	51.3	520.9
	Carbon	6	5,175.5	0.2244	3,132.1	684.7	9,169.5	916.9	3,091.5	38.2	0.18	0.548	2.7	19	0.548	916.9	51.3	968.8
		8	4,201.8	0.2756	2,549.1	782.9	6,911.2	691.1	3,807.9	19.6	0.14	0.426	2.7	19	0.426	691.1	51.3	742.8
		10	3,791.7	0.3000	2,341.2	775.6	5,575.3	557.5	4,219.8	13.3	0.12	0.354	2.7	19	0.354	557.5	51.3	609.2
		12	3,537.7	0.3122	2,249.2	748.9	4,686.4	468.6	4,522.8	10.0	0.10	0.307	2.7	19	0.307	468.6	51.3	520.2
7 Phase	Stainless Steel	6	7,656.4	0.1611	4,359.0	341.8	10,019.5	1,001.9	2,089.8	76.8	0.17	0.503	2.7	19	0.503	1,001.9	51.3	1,053.8
		8	6,472.4	0.1903	3,689.1	362.5	7,592.5	759.3	2,472.0	41.8	0.13	0.383	2.7	19	0.383	759.3	51.3	810.9
		10	5,824.3	0.2092	3,356.0	362.2	6,143.6	614.4	2,747.1	27.6	0.10	0.312	2.7	19	0.312	614.4	51.3	666.0
		12	5,466.1	0.2181	3,221.4	347.1	5,185.0	518.5	2,927.1	20.6	0.09	0.265	2.7	19	0.265	518.5	51.3	570.1
	Titanium	6	7,716.6	0.1594	4,403.4	336.7	10,025.9	1,002.6	2,073.5	78.0	0.17	0.503	2.7	19	0.503	1,002.6	51.3	1,054.4
		8	6,732.2	0.1833	3,830.9	336.3	7,620.2	762.0	2,376.7	45.1	0.13	0.382	2.7	19	0.382	762.0	51.3	813.7
		10	6,089.6	0.2011	3,490.0	332.9	6,171.8	617.2	2,627.4	30.0	0.10	0.311	2.7	19	0.311	617.2	51.3	668.8
		12	5,704.0	0.2106	3,335.3	320.3	5,210.3	521.0	2,805.0	22.3	0.09	0.264	2.7	19	0.264	521.0	51.3	572.6
	Inconel	6	8,080.2	0.1521	4,615.6	308.3	10,064.6	1,006.5	1,980.1	85.4	0.17	0.502	2.7	19	0.502	1,006.5	51.3	1,058.3
		8	6,896.2	0.1786	3,928.2	321.2	7,637.7	763.8	2,320.1	47.3	0.13	0.382	2.7	19	0.382	763.8	51.3	815.4
		10	6,179.8	0.1989	3,531.1	323.7	6,181.4	618.1	2,589.1	30.9	0.10	0.311	2.7	19	0.311	618.1	51.3	669.8
		12	5,816.1	0.2072	3,388.5	308.8	5,223.3	522.2	2,751.0	23.2	0.09	0.263	2.7	19	0.263	522.2	51.3	573.8
	Carbon	6	7,768.5	0.1589	4,418.7	332.4	10,031.4	1,003.1	2,059.6	79.0	0.17	0.503	2.7	19	0.503	1,003.1	51.3	1,054.9
		8	6,554.4	0.1833	3,726.7	353.9	7,601.3	760.1	2,441.1	42.8	0.13	0.383	2.7	19	0.383	760.1	51.3	811.8
		10	5,958.3	0.2047	3,430.2	346.9	6,157.8	615.8	2,685.3	28.8	0.10	0.312	2.7	19	0.312	615.8	51.3	667.4
		12	5,589.2	0.2139	3,283.4	332.8	5,198.1	519.8	2,862.7	21.5	0.09	0.264	2.7	19	0.264	519.8	51.3	571.4
9 Phase	Stainless Steel	6	6,074.8	0.2081	3,375.0	547.4	10,101.2	1,010.1	2,633.8	47.6	0.17	0.495	2.7	19	0.495	1,010.1	51.3	1,061.9
		8	5,102.0	0.2844	2,828.8	586.5	7,634.1	763.4	3,136.0	25.9	0.13	0.381	2.7	19	0.381	763.4	51.3	815.1
		10	4,400.9	0.2789	2,516.1	634.2	6,141.9	614.2	3,635.6	16.0	0.11	0.317	2.7	19	0.317	614.2	51.3	665.8
		12	3,982.4	0.2878	2,439.3	649.7	5,151.8	515.2	4,017.7	11.3	0.09	0.275	2.7	19	0.275	515.2	51.3	566.8
	Titanium	6	6,080.3	0.2081	3,374.2	546.5	10,101.8	1,010.2	2,631.4	47.7	0.17	0.495	2.7	19	0.495	1,010.2	51.3	1,062.0
		8	5,176.9	0.2436	2,883.0	570.3	7,642.1	764.2	3,090.7	26.6	0.13	0.381	2.7	19	0.381	764.2	51.3	815.9
		10	4,611.5	0.2697	2,605.6	579.7	6,164.4	616.4	3,469.6	17.4	0.10	0.314	2.7	19	0.314	616.4	51.3	668.0
		12	4,159.8	0.2822	2,485.7	597.6	5,170.7	517.1	3,846.4	12.2	0.09	0.272	2.7	19	0.272	517.1	51.3	568.6
	Inconel	6	6,160.7	0.2056	3,415.0	532.8	10,110.4	1,011.0	2,597.1	48.9	0.17	0.495	2.7	19	0.495	1,011.0	51.3	1,062.8
		8	5,246.1	0.2406	2,918.0	555.9	7,649.5	764.9	3,049.9	27.3	0.13	0.380	2.7	19	0.380	764.9	51.3	816.6
		10	4,705.7	0.2650	2,650.4	557.7	6,174.4	617.4	3,400.1	18.0	0.10	0.313	2.7	19	0.313	617.4	51.3	669.1
		12	4,231.8	0.2803	2,503.1	578.3	5,178.4	517.8	3,780.9	12.6	0.09	0.271	2.7	19	0.271	517.8	51.3	569.4
	Carbon	6	5,958.4	0.2125	3,305.8	568.3	10,088.8	1,008.9	2,685.3	45.9	0.17	0.496	2.7	19	0.496	1,008.9	51.3	1,060.7
		8	5,041.1	0.2499	2,809.8	600.3	7,627.6	762.8	3,173.9	25.3	0.13	0.382	2.7	19	0.382	762.8	51.3	814.4
		10	4,509.0	0.2747	2,556.6	605.3	6,153.4	615.3	3,548.5	16.7	0.11	0.315	2.7	19	0.315	615.3	51.3	667.0
		12	4,085.0	0.2844	2,466.8	618.8	5,162.8	516.3	3,916.8	11.9	0.09	0.273	2.7	19	0.273	516.3	51.3	567.8
11 Phase	Stainless Steel	6	4,840.9	0.2643	2,656.4	861.9	10,098.4	1,009.8	3,305.2	30.4	0.17	0.497	2.7	19	0.497	1,009.8	51.3	1,061.6
		8	4,062.4	0.3153	2,227.1	923.4	7,619.7	762.0	3,938.5	16.7	0.13	0.389	2.7	19	0.389	762.0	51.3	813.7
		10	3,510.0	0.3458	2,031.0	994.2	6,124.0	612.4	4,558.4	10.5	0.11	0.329	2.7	19	0.329	612.4	51.3	664.0
		12	3,169.6	0.3392	2,067.9	1021.2	5,129.4	512.9	5,048.0	7.6	0.10	0.291	2.7	19	0.291	512.9	51.3	564.5
	Titanium	6	5,030.6	0.2551	2,752.0	799.7	10,118.6	1,011.9	3,180.5	32.7	0.17	0.496	2.7	19	0.496	1,011.9	51.3	1,063.7
		8	4,121.0	0.3113	2,256.4	898.1	7,626.0	762.6	3,882.5	17.1	0.13	0.388	2.7	19	0.388	762.6	51.3	814.3
		10	3,590.9	0.3417	2,053.7	951.2	6,132.7	613.3	4,455.7	11.0	0.11	0.327	2.7	19	0.327	613.3	51.3	664.9
		12	3,244.9	0.3400	2,063.7	975.8	5,137.4	513.7	4,930.8	7.9	0.10	0.289	2.7	19	0.289	513.7	51.3	565.3
	Inconel	6	5,086.4	0.2525	2,779.6	782.7	10,124.5	1,012.5	3,145.6	33.4	0.17	0.495	2.7	19	0.495	1,012.5	51.3	1,064.2
		8	4,235.4	0.3031	2,316.7	851.6	7,638.2	763.8	3,777.7	18.0	0.13	0.386	2.7	19	0.386	763.8	51.3	815.5
		10	3,677.4	0.3343	2,099.3	908.3	6,141.9	614.2	4,350.9	11.4	0.11	0.325	2.7	19	0.325	614.2	51.3	665.8
		12	3,247.7	0.3397	2,066.1	974.2	5,137.7	513.8	4,926.5	7.9	0.10	0.289	2.7	19	0.289	513.8	51.3	565.4
	Carbon	6	4,952.5	0.2597	2,704.4	824.4	10,110.3	1,011.0	3,230.7	31.7	0.17	0.496	2.7	19	0.496	1,011.0	51.3	1,062.8
		8	4,176.8	0.3072	2,285.1	874.9	7,631.9	763.2	3,830.7	17.6	0.13	0.387	2.7	19	0.387	763.2	51.3	814.9
		10	3,593.7	0.3411	2,057.1	949.8	6,133.0	613.3	4,452.2	11.0	0.11	0.327	2.7	19	0.327	613.3	51.3	664.9
		12	3,242.1	0.3408	2,059.0	977.4	5,137.1	513.7	4,935.0	7.9	0.10	0.289	2.7	19	0.289	513.7	51.3	565.3

Rectifier & Input Filter Volume Calculations

Phases	Retaining Can	Poles	Max Rectified Voltage	Actual Duty Cycle	Actual Rectified Voltage	Total Capacitance (mF)	Total Capacitor Energy (J)	Total Capacitor Volume (m³)	Average Current	Total Inductance (uH)	Total Inductor Energy (J)	Total Inductor Volume (m³)	Module Diode Volume (m³)	Number of Modules	Total Inductor Volume (m³)	Total Capacitor Volume (m³)	Total Diode Volume (m³)	Service Volume (m³)	Total Volume (m³)
3 Phase	Stainless Steel	6	7,613.7	0.1208	5,816.7	260.4	7,546.3	0.94	2,101.5	103.3	0.228	0.003	0.0816	19	0.003	0.94	1.55	0.75	3.25
		8	6,392.7	0.1428	4,917.1	280.6	5,732.7	0.72	2,502.8	55.3	0.173	0.002	0.0816	19	0.002	0.72	1.55	0.68	2.95
		10	5,536.6	0.1647	4,268.0	302.2	4,631.7	0.58	2,889.8	33.7	0.141	0.002	0.0816	19	0.002	0.58	1.55	0.64	2.77
		12	5,293.4	0.1700	4,134.8	280.7	3,932.2	0.49	3,022.7	26.0	0.119	0.001	0.0816	19	0.001	0.49	1.55	0.61	2.66
	Titanium	6	7,616.1	0.1209	5,808.5	260.2	7,546.6	0.94	2,100.8	103.4	0.228	0.003	0.0816	19	0.003	0.94	1.55	0.75	3.25
		8	6,455.9	0.1425	4,925.3	275.4	5,739.4	0.72	2,478.4	56.3	0.173	0.002	0.0816	19	0.002	0.72	1.55	0.68	2.95
		10	5,749.5	0.1589	4,419.4	281.6	4,654.4	0.58	2,782.9	36.3	0.140	0.002	0.0816	19	0.002	0.58	1.55	0.64	2.77
		12	5,501.5	0.1643	4,277.1	261.3	3,954.4	0.49	2,908.3	28.0	0.118	0.001	0.0816	19	0.001	0.49	1.55	0.61	2.66
	Inconel	6	7,906.1	0.1167	6,019.7	242.5	7,577.4	0.95	2,023.7	111.3	0.228	0.003	0.0816	19	0.003	0.95	1.55	0.75	3.25
		8	6,526.1	0.1410	4,980.1	269.9	5,746.9	0.72	2,451.7	57.5	0.173	0.002	0.0816	19	0.002	0.72	1.55	0.68	2.95
		10	5,829.0	0.1563	4,496.4	274.5	4,662.8	0.58	2,744.9	37.2	0.140	0.002	0.0816	19	0.002	0.58	1.55	0.64	2.78
		12	5,567.0	0.1622	4,331.0	255.6	3,961.4	0.50	2,874.1	28.6	0.118	0.001	0.0816	19	0.001	0.50	1.55	0.61	2.66
	Carbon	6	7,443.0	0.1234	5,676.1	271.8	7,528.1	0.94	2,149.7	98.8	0.228	0.003	0.0816	19	0.003	0.94	1.55	0.75	3.24
		8	6,334.3	0.1450	4,840.1	285.4	5,726.4	0.72	2,525.9	54.3	0.173	0.002	0.0816	19	0.002	0.72	1.55	0.68	2.95
		10	5,625.5	0.1620	4,334.4	293.3	4,641.2	0.58	2,844.2	34.8	0.141	0.002	0.0816	19	0.002	0.58	1.55	0.64	2.77
		12	5,389.3	0.1675	4,195.8	271.5	3,942.5	0.49	2,968.9	26.9	0.119	0.001	0.0816	19	0.001	0.49	1.55	0.66	2.66
5 Phase	Stainless Steel	6	5,101.4	0.2264	3,099.1	704.1	9,161.6	1.15	3,136.4	37.2	0.183	0.002	0.0816	19	0.002	1.15	1.55	0.81	3.51
		8	4,138.3	0.2786	2,521.0	806.3	6,904.4	0.86	3,866.3	19.1	0.142	0.002	0.0816	19	0.002	0.86	1.55	0.72	3.14
		10	3,646.1	0.3056	2,297.6	836.4	5,559.8	0.69	4,388.2	12.4	0.119	0.001	0.0816	19	0.001	0.69	1.55	0.67	2.92
		12	3,434.5	0.3122	2,248.2	792.7	4,675.4	0.58	4,658.7	9.5	0.103	0.001	0.0816	19	0.001	0.58	1.55	0.64	2.78
	Titanium	6	5,117.3	0.2261	3,102.7	699.8	9,163.3	1.15	3,126.7	37.4	0.183	0.002	0.0816	19	0.002	1.15	1.55	0.81	3.51
		8	4,299.7	0.2706	2,596.7	748.8	6,921.6	0.87	3,721.2	20.5	0.142	0.002	0.0816	19	0.002	0.87	1.55	0.73	3.14
		10	3,781.1	0.2972	2,361.2	779.8	5,574.2	0.70	4,231.6	13.2	0.118	0.001	0.0816	19	0.001	0.70	1.55	0.67	2.92
		12	3,535.0	0.3075	2,284.2	750.0	4,686.1	0.59	4,526.2	10.0	0.102	0.001	0.0816	19	0.001	0.59	1.55	0.64	2.78
	Inconel	6	5,355.4	0.2161	3,249.4	640.8	9,188.6	1.15	2,987.6	40.8	0.182	0.002	0.0816	19	0.002	1.15	1.55	0.81	3.51
		8	4,394.9	0.2631	2,669.9	717.7	6,931.8	0.87	3,640.5	21.3	0.141	0.002	0.0816	19	0.001	0.87	1.55	0.73	3.14
		10	3,841.9	0.2992	2,401.2	756.2	5,580.7	0.70	4,164.6	13.6	0.118	0.001	0.0816	19	0.001	0.70	1.55	0.67	2.92
		12	3,601.2	0.3028	2,302.2	723.8	4,693.2	0.59	4,443.0	10.3	0.102	0.001	0.0816	19	0.001	0.59	1.55	0.64	2.78
	Carbon	6	5,175.5	0.2244	3,132.1	684.7	9,169.5	1.15	3,091.5	38.2	0.183	0.002	0.0816	19	0.002	1.15	1.55	0.81	3.51
		8	4,201.8	0.2756	2,549.1	782.9	6,911.2	0.86	3,807.9	19.6	0.142	0.002	0.0816	19	0.002	0.86	1.55	0.72	3.14
		10	3,791.7	0.3000	2,341.2	775.6	5,575.3	0.70	4,219.8	13.3	0.118	0.001	0.0816	19	0.001	0.70	1.55	0.67	2.92
		12	3,537.7	0.3122	2,249.2	748.9	4,686.4	0.59	4,522.8	10.0	0.102	0.001	0.0816	19	0.001	0.59	1.55	0.64	2.78
7 Phase	Stainless Steel	6	7,656.4	0.1611	4,359.0	341.8	10,019.5	1.25	2,089.8	76.8	0.168	0.002	0.0816	19	0.002	1.25	1.55	0.84	3.65
		8	6,472.4	0.1903	3,689.1	362.5	7,592.5	0.95	2,472.0	41.8	0.128	0.002	0.0816	19	0.002	0.95	1.55	0.75	3.25
		10	5,824.3	0.2092	3,356.0	362.2	6,143.6	0.77	2,747.1	27.6	0.104	0.001	0.0816	19	0.001	0.77	1.55	0.70	3.02
		12	5,466.1	0.2181	3,221.4	347.1	5,185.0	0.65	2,927.1	20.6	0.088	0.001	0.0816	19	0.001	0.65	1.55	0.66	2.86
	Titanium	6	7,716.6	0.1594	4,403.4	336.7	10,025.9	1.25	2,073.5	78.0	0.168	0.002	0.0816	19	0.002	1.25	1.55	0.84	3.65
		8	6,732.2	0.1833	3,830.9	336.3	7,620.2	0.95	2,376.7	45.1	0.127	0.002	0.0816	19	0.002	0.95	1.55	0.75	3.26
		10	6,089.6	0.2011	3,490.0	332.9	6,171.8	0.77	2,627.4	30.0	0.104	0.001	0.0816	19	0.001	0.77	1.55	0.70	3.02
		12	5,704.0	0.2106	3,335.3	320.3	5,210.3	0.65	2,805.0	22.3	0.088	0.001	0.0816	19	0.001	0.65	1.55	0.66	2.86
	Inconel	6	8,080.2	0.1521	4,615.6	308.3	10,064.6	1.26	1,980.1	85.4	0.167	0.002	0.0816	19	0.002	1.26	1.55	0.84	3.65
		8	6,896.2	0.1786	3,928.2	321.2	7,637.7	0.95	2,320.1	47.3	0.127	0.002	0.0816	19	0.002	0.95	1.55	0.75	3.26
		10	6,179.8	0.1989	3,531.1	323.7	6,181.4	0.77	2,589.1	30.9	0.104	0.001	0.0816	19	0.001	0.77	1.55	0.70	3.02
		12	5,816.1	0.2072	3,388.5	308.8	5,222.3	0.65	2,751.0	23.2	0.088	0.001	0.0816	19	0.001	0.65	1.55	0.66	2.87
	Carbon	6	7,768.5	0.1589	4,418.7	332.4	10,031.4	1.25	2,059.6	79.0	0.168	0.002	0.0816	19	0.002	1.25	1.55	0.84	3.65
		8	6,554.4	0.1833	3,726.7	353.9	7,601.3	0.95	2,441.1	42.8	0.128	0.002	0.0816	19	0.002	0.95	1.55	0.75	3.25
		10	5,958.3	0.2047	3,430.2	346.9	6,157.8	0.77	2,685.3	28.8	0.104	0.001	0.0816	19	0.001	0.77	1.55	0.70	3.02
		12	5,589.2	0.2139	3,283.4	332.8	5,198.1	0.65	2,862.7	21.5	0.088	0.001	0.0816	19	0.001	0.65	1.55	0.66	2.86
9 Phase	Stainless Steel	6	6,074.8	0.2081	3,375.0	547.4	10,101.2	1.26	2,633.8	47.6	0.165	0.002	0.0816	19	0.002	1.26	1.55	0.84	3.66
		8	5,102.0	0.2844	2,828.8	586.5	7,634.1	0.95	3,136.0	25.9	0.127	0.002	0.0816	19	0.002	0.95	1.55	0.75	3.26
		10	4,400.9	0.2789	2,516.1	634.2	6,141.9	0.77	3,635.6	16.0	0.106	0.001	0.0816	19	0.001	0.77	1.55	0.70	3.02
		12	3,982.4	0.2878	2,439.3	649.7	5,151.8	0.64	4,017.7	11.3	0.092	0.001	0.0816	19	0.001	0.64	1.55	0.66	2.85
	Titanium	6	6,080.3	0.2081	3,374.2	546.5	10,101.8	1.26	2,631.4	47.7	0.165	0.002	0.0816	19	0.002	1.26	1.55	0.84	3.66
		8	5,176.9	0.2436	2,883.0	570.3	7,642.1	0.96	3,090.7	26.6	0.127	0.002	0.0816	19	0.002	0.96	1.55	0.75	3.26
		10	4,611.5	0.2697	2,605.6	579.7	6,164.4	0.77	3,469.6	17.4	0.105	0.001	0.0816	19	0.001	0.77	1.55	0.70	3.02
		12	4,159.8	0.2822	2,485.7	597.6	5,170.7	0.65	3,846.4	12.2	0.091	0.001	0.0816	19	0.001	0.65	1.55	0.66	2.86
	Inconel	6	6,160.7	0.2056	3,415.0	532.8	10,110.4	1.26	2,597.1	48.9	0.165	0.002	0.0816	19	0.002	1.26	1.55	0.84	3.66
		8	5,246.1	0.2406	2,918.0	555.9	7,649.5	0.96	3,049.9	27.3	0.127	0.002	0.0816	19	0.002	0.96	1.55	0.75	3.26
		10	4,705.7	0.2650	2,650.4	557.7	6,174.4	0.77	3,400.1	18.0	0.104	0.001	0.0816	19	0.001	0.77	1.55	0.70	3.02
		12	4,231.8	0.2803	2,503.1	578.3	5,178.4	0.65	3,780.9	12.6	0.090	0.001	0.0816	19	0.001	0.65	1.55	0.66	2.86
	Carbon	6	5,958.4	0.2125	3,305.8	568.3	10,088.8	1.26	2,685.3	45.9	0.165	0.002	0.0816	19	0.002	1.26	1.55	0.84	3.66
		8	5,041.1	0.2499	2,809.8	600.3	7,627.6	0.95	3,173.9	25.3	0.127	0.002	0.0816	19	0.002	0.95	1.55	0.75	3.26
		10	4,509.0	0.2747	2,556.6	605.3	6,153.4	0.77	3,548.5	16.7	0.105	0.001	0.0816	19	0.001	0.77	1.55	0.70	3.02
		12	4,085.0	0.2844	2,466.8	618.8	5,162.8	0.65	3,916.8	11.9	0.091	0.001	0.0816	19	0.001	0.65	1.55	0.66	2.86
11 Phase	Stainless Steel	6	4,840.9	0.2643	2,656.4	861.9	10,098.4	1.26	3,305.2	30.4	0.166	0.002	0.0816	19	0.002	1.26	1.55	0.84	3.66
		8	4,062.4	0.3153	2,227.1	923.4	7,619.7	0.95	3,938.5	16.7	0.130	0.002	0.0816	19	0.002	0.95	1.55	0.75	3.26
		10	3,510.0	0.3458	2,031.0	994.2	6,124.0	0.77	4,558.4	10.5	0.110	0.001	0.0816	19	0.001	0.77	1.55	0.70	3.01
		12	3,169.6	0.3392	2,067.9	1021.2	5,129.4	0.64	5,048.0	7.6	0.097	0.001	0.0816	19	0.001	0.64	1.55	0.66	2.85
	Titanium	6	5,030.6	0.2551	2,752.0	799.7	10,118.6	1.26	3,180.5	32.7	0.165	0.002	0.0816	19	0.002	1.26	1.55	0.85	3.66
		8	4,121.0	0.3113	2,256.4	898.1	7,626.0	0.95	3,882.5	17.1	0.129	0.002	0.0816	19	0.002	0.95	1.55	0.75	3.26
		10	3,590.9	0.3417	2,053.7	951.2	6,132.7	0.77	4,455.7	11.0	0.109	0.001	0.0816	19	0.001	0.77	1.55	0.70	3.01
		12	3,244.9	0.3400	2,063.7	975.8	5,137.4	0.64	4,930.8	7.9	0.096	0.001	0.0816	19	0.001	0.64	1.55	0.66	2.85
	Inconel	6	5,086.4	0.2525	2,779.6	782.7	10,124.5	1.27	3,145.6	33.4	0.165	0.002	0.0816	19	0.002	1.27	1.55	0.85	3.66
		8	4,235.4	0.3031	2,316.7	851.6	7,638.2	0.95	3,777.7	18.0	0.129	0.002	0.0816	19	0.002	0.95	1.55	0.75	3.26
		10	3,677.4	0.3343	2,099.3	908.3	6,141.9	0.77	4,350.9	11.4	0.108	0.001	0.0816	19	0.001	0.77	1.55	0.70	3.02
		12	3,247.7	0.3397	2,066.1	974.2	5,137.7	0.64	4,926.5	7.9	0.096	0.001	0.0816	19	0.001	0.64	1.55	0.66	2.85
	Carbon	6	4,952.5	0.2597	2,704.4	824.4	10,110.3	1.26	3,230.7	31.7	0.165	0.002	0.0816	19	0.002	1.26	1.55	0.84	3.66
		8	4,176.8	0.3072	2,285.1	874.9	7,631.9	0.95	3,830.7	17.6	0.129	0.002	0.0816	19	0.002	0.95	1.55	0.75	3.26
		10	3,593.7	0.3411	2,057.1	949.8	6,133.0	0.77	4,452.2	11.0	0.109	0.001	0.0816	19	0.001	0.77	1.55	0.70	3.01
		12	3,242.1	0.3408	2,059.0	977.4	5,137.1	0.64	4,935.0	7.9	0.096	0.001	0.0816	19	0.001	0.64	1.55	0.66	2.85

Converter & Output Filter Mass Calculations

Phases	Retaining Can	Poles	Output Voltage	Total Capacitance (mF)	Total Capacitor Energy (J)	Total Capacitor Mass (kg)	Average Output Current	Total Inductance (uH)	Total Inductor Energy (J)	Total Inductor Mass (kg)	Module IGBT Mass (kg)	Module Diode Mass (kg)	Number of Modules	Total Inductor Mass (kg)	Total Capacitor Mass (kg)	Total IGBT Mass (kg)	Total Diode Mass (kg)	Total Mass (kg)
3 Phase	Stainless Steel	6	700.0	2.908	0.71	0.071	22,857	557.5	145.6	436.9	1.2	0.45	19	436.9	0.071	22.8	0.45	460.2
		8	700.0	2.965	0.73	0.073	22,857	546.7	142.8	428.4	1.2	0.45	19	428.4	0.073	22.8	0.45	451.7
		10	700.0	3.023	0.74	0.074	22,857	536.3	140.1	420.3	1.2	0.45	19	420.3	0.074	22.8	0.45	443.6
		12	700.0	3.043	0.75	0.075	22,857	532.7	139.2	417.5	1.2	0.45	19	417.5	0.075	22.8	0.45	440.8
	Titanium	6	700.0	2.908	0.71	0.071	22,857	557.5	145.6	436.9	1.2	0.45	19	436.9	0.071	22.8	0.45	460.2
		8	700.0	2.962	0.73	0.073	22,857	547.3	143.0	428.9	1.2	0.45	19	428.9	0.073	22.8	0.45	452.3
		10	700.0	3.007	0.74	0.074	22,857	539.1	140.8	422.5	1.2	0.45	19	422.5	0.074	22.8	0.45	445.8
		12	700.0	3.026	0.74	0.074	22,857	535.8	140.0	419.9	1.2	0.45	19	419.9	0.074	22.8	0.45	443.2
	Inconel	6	700.0	2.897	0.71	0.071	22,857	559.6	146.2	438.5	1.2	0.45	19	438.5	0.071	22.8	0.45	461.8
		8	700.0	2.958	0.72	0.072	22,857	548.1	143.2	429.5	1.2	0.45	19	429.5	0.072	22.8	0.45	452.8
		10	700.0	3.001	0.74	0.074	22,857	540.2	141.1	423.3	1.2	0.45	19	423.3	0.074	22.8	0.45	446.6
		12	700.0	3.021	0.74	0.074	22,857	536.7	140.2	420.6	1.2	0.45	19	420.6	0.074	22.8	0.45	443.9
	Carbon	6	700.0	2.915	0.71	0.071	22,857	556.2	145.3	435.9	1.2	0.45	19	435.9	0.071	22.8	0.45	459.2
		8	700.0	2.969	0.73	0.073	22,857	546.1	142.6	427.9	1.2	0.45	19	427.9	0.073	22.8	0.45	451.3
		10	700.0	3.016	0.74	0.074	22,857	537.5	140.4	421.2	1.2	0.45	19	421.2	0.074	22.8	0.45	444.5
		12	700.0	3.035	0.74	0.074	22,857	534.1	139.5	418.6	1.2	0.45	19	418.6	0.074	22.8	0.45	441.9
5 Phase	Stainless Steel	6	700.0	3.061	0.75	0.075	22,857	529.6	138.4	415.1	1.2	0.45	19	415.1	0.075	22.8	0.45	438.4
		8	700.0	3.179	0.78	0.078	22,857	510.0	133.2	399.7	1.2	0.45	19	399.7	0.078	22.8	0.45	423.0
		10	700.0	3.269	0.80	0.080	22,857	495.9	129.5	388.6	1.2	0.45	19	388.6	0.080	22.8	0.45	412.0
		12	700.0	3.318	0.81	0.081	22,857	488.7	127.6	382.9	1.2	0.45	19	382.9	0.081	22.8	0.45	406.3
	Titanium	6	700.0	3.059	0.75	0.075	22,857	529.9	138.4	415.3	1.2	0.45	19	415.3	0.075	22.8	0.45	438.6
		8	700.0	3.155	0.77	0.077	22,857	513.9	134.2	402.7	1.2	0.45	19	402.7	0.077	22.8	0.45	426.0
		10	700.0	3.241	0.79	0.079	22,857	500.1	130.7	392.0	1.2	0.45	19	392.0	0.079	22.8	0.45	415.3
		12	700.0	3.294	0.81	0.081	22,857	492.2	128.6	385.7	1.2	0.45	19	385.7	0.081	22.8	0.45	409.1
	Inconel	6	700.0	3.038	0.74	0.074	22,857	533.6	139.4	418.2	1.2	0.45	19	418.2	0.074	22.8	0.45	441.5
		8	700.0	3.141	0.77	0.077	22,857	516.1	134.8	404.4	1.2	0.45	19	404.4	0.077	22.8	0.45	427.7
		10	700.0	3.230	0.79	0.079	22,857	502.0	131.1	393.4	1.2	0.45	19	393.4	0.079	22.8	0.45	416.7
		12	700.0	3.279	0.80	0.080	22,857	494.5	129.2	387.5	1.2	0.45	19	387.5	0.080	22.8	0.45	410.8
	Carbon	6	700.0	3.054	0.75	0.075	22,857	530.8	138.7	416.0	1.2	0.45	19	416.0	0.075	22.8	0.45	439.3
		8	700.0	3.169	0.78	0.078	22,857	511.6	133.6	400.9	1.2	0.45	19	400.9	0.078	22.8	0.45	424.2
		10	700.0	3.239	0.79	0.079	22,857	500.5	130.7	392.2	1.2	0.45	19	392.2	0.079	22.8	0.45	415.5
		12	700.0	3.293	0.81	0.081	22,857	492.3	128.6	385.8	1.2	0.45	19	385.8	0.081	22.8	0.45	409.1
7 Phase	Stainless Steel	6	700.0	2.906	0.71	0.071	22,857	557.8	145.7	437.1	1.2	0.45	19	437.1	0.071	22.8	0.45	460.5
		8	700.0	2.961	0.73	0.073	22,857	547.5	143.0	429.1	1.2	0.45	19	429.1	0.073	22.8	0.45	452.4
		10	700.0	3.002	0.74	0.074	22,857	540.1	141.1	423.3	1.2	0.45	19	423.3	0.074	22.8	0.45	446.6
		12	700.0	3.029	0.74	0.074	22,857	535.3	139.8	419.5	1.2	0.45	19	419.5	0.074	22.8	0.45	442.8
	Titanium	6	700.0	2.904	0.71	0.071	22,857	558.2	145.8	437.5	1.2	0.45	19	437.5	0.071	22.8	0.45	460.8
		8	700.0	2.947	0.72	0.072	22,857	550.1	143.7	431.1	1.2	0.45	19	431.1	0.072	22.8	0.45	454.4
		10	700.0	2.984	0.73	0.073	22,857	543.3	141.9	425.8	1.2	0.45	19	425.8	0.073	22.8	0.45	449.1
		12	700.0	3.010	0.74	0.074	22,857	538.5	140.7	422.0	1.2	0.45	19	422.0	0.074	22.8	0.45	445.4
	Inconel	6	700.0	2.891	0.71	0.071	22,857	560.8	146.5	439.4	1.2	0.45	19	439.4	0.071	22.8	0.45	462.8
		8	700.0	2.939	0.72	0.072	22,857	551.6	144.1	432.3	1.2	0.45	19	432.3	0.072	22.8	0.45	455.6
		10	700.0	2.978	0.73	0.073	22,857	544.4	142.2	426.6	1.2	0.45	19	426.6	0.073	22.8	0.45	449.9
		12	700.0	3.002	0.74	0.074	22,857	540.0	141.1	423.2	1.2	0.45	19	423.2	0.074	22.8	0.45	446.5
	Carbon	6	700.0	2.902	0.71	0.071	22,857	558.6	145.9	437.8	1.2	0.45	19	437.8	0.071	22.8	0.45	461.1
		8	700.0	2.956	0.72	0.072	22,857	548.3	143.2	429.7	1.2	0.45	19	429.7	0.072	22.8	0.45	453.0
		10	700.0	2.992	0.73	0.073	22,857	541.8	141.5	424.6	1.2	0.45	19	424.6	0.073	22.8	0.45	447.9
		12	700.0	3.019	0.74	0.074	22,857	537.0	140.3	420.8	1.2	0.45	19	420.8	0.074	22.8	0.45	444.2
9 Phase	Stainless Steel	6	700.0	2.985	0.73	0.073	22,857	543.2	141.9	425.7	1.2	0.45	19	425.7	0.073	22.8	0.45	449.0
		8	700.0	3.061	0.75	0.075	22,857	529.6	138.4	415.1	1.2	0.45	19	415.1	0.075	22.8	0.45	438.4
		10	700.0	3.141	0.77	0.077	22,857	516.2	134.8	404.5	1.2	0.45	19	404.5	0.077	22.8	0.45	427.8
		12	700.0	3.204	0.79	0.079	22,857	505.9	132.2	396.5	1.2	0.45	19	396.5	0.079	22.8	0.45	419.8
	Titanium	6	700.0	2.984	0.73	0.073	22,857	543.2	141.9	425.7	1.2	0.45	19	425.7	0.073	22.8	0.45	449.0
		8	700.0	3.054	0.75	0.075	22,857	530.9	138.7	416.0	1.2	0.45	19	416.0	0.075	22.8	0.45	439.3
		10	700.0	3.114	0.76	0.076	22,857	520.7	136.0	408.0	1.2	0.45	19	408.0	0.076	22.8	0.45	431.4
		12	700.0	3.175	0.78	0.078	22,857	510.5	133.4	400.1	1.2	0.45	19	400.1	0.078	22.8	0.45	423.4
	Inconel	6	700.0	2.979	0.73	0.073	22,857	544.1	142.1	426.4	1.2	0.45	19	426.4	0.073	22.8	0.45	449.8
		8	700.0	3.048	0.75	0.075	22,857	532.0	139.0	416.9	1.2	0.45	19	416.9	0.075	22.8	0.45	440.2
		10	700.0	3.103	0.76	0.076	22,857	522.5	136.5	409.5	1.2	0.45	19	409.5	0.076	22.8	0.45	432.8
		12	700.0	3.165	0.78	0.078	22,857	512.3	133.8	401.5	1.2	0.45	19	401.5	0.078	22.8	0.45	424.8
	Carbon	6	700.0	2.992	0.73	0.073	22,857	541.8	141.5	424.6	1.2	0.45	19	424.6	0.073	22.8	0.45	447.9
		8	700.0	3.067	0.75	0.075	22,857	528.6	138.1	414.3	1.2	0.45	19	414.3	0.075	22.8	0.45	437.6
		10	700.0	3.126	0.77	0.077	22,857	518.5	135.5	406.4	1.2	0.45	19	406.4	0.077	22.8	0.45	429.7
		12	700.0	3.187	0.78	0.078	22,857	508.6	132.9	398.6	1.2	0.45	19	398.6	0.078	22.8	0.45	421.9
11 Phase	Stainless Steel	6	700.0	3.087	0.76	0.076	22,857	525.1	137.2	411.5	1.2	0.45	19	411.5	0.076	22.8	0.45	434.8
		8	700.0	3.191	0.78	0.078	22,857	508.0	132.7	398.1	1.2	0.45	19	398.1	0.078	22.8	0.45	421.5
		10	700.0	3.299	0.81	0.081	22,857	491.4	128.4	385.1	1.2	0.45	19	385.1	0.081	22.8	0.45	408.4
		12	700.0	3.390	0.83	0.083	22,857	478.2	124.9	374.7	1.2	0.45	19	374.7	0.083	22.8	0.45	398.1
	Titanium	6	700.0	3.068	0.75	0.075	22,857	528.4	138.0	414.1	1.2	0.45	19	414.1	0.075	22.8	0.45	437.4
		8	700.0	3.182	0.78	0.078	22,857	509.5	133.1	399.3	1.2	0.45	19	399.3	0.078	22.8	0.45	422.6
		10	700.0	3.281	0.80	0.080	22,857	494.1	129.1	387.2	1.2	0.45	19	387.2	0.080	22.8	0.45	410.6
		12	700.0	3.368	0.83	0.083	22,857	481.3	125.7	377.2	1.2	0.45	19	377.2	0.083	22.8	0.45	400.5
	Inconel	6	700.0	3.062	0.75	0.075	22,857	529.4	138.3	414.9	1.2	0.45	19	414.9	0.075	22.8	0.45	438.2
		8	700.0	3.164	0.78	0.078	22,857	512.4	133.8	401.5	1.2	0.45	19	401.5	0.078	22.8	0.45	424.9
		10	700.0	3.262	0.80	0.080	22,857	496.9	129.8	389.4	1.2	0.45	19	389.4	0.080	22.8	0.45	412.8
		12	700.0	3.367	0.82	0.082	22,857	481.4	125.8	377.3	1.2	0.45	19	377.3	0.082	22.8	0.45	400.6
	Carbon	6	700.0	3.076	0.75	0.075	22,857	527.1	137.7	413.1	1.2	0.45	19	413.1	0.075	22.8	0.45	436.4
		8	700.0	3.173	0.78	0.078	22,857	510.9	133.5	400.4	1.2	0.45	19	400.4	0.078	22.8	0.45	423.7
		10	700.0	3.280	0.80	0.080	22,857	494.2	129.1	387.3	1.2	0.45	19	387.3	0.080	22.8	0.45	410.6
		12	700.0	3.369	0.83	0.083	22,857	481.2	125.7	377.1	1.2	0.45	19	377.1	0.083	22.8	0.45	400.5

Converter & Output Filter Volume Calculations

Phases	Retaining Can	Poles	Output Voltage	Total Capacitance (mF)	Total Capacitor Energy (J)	Total Capacitor Volume (m³)	Average Output Current	Total Inductance (uH)	Total Inductor Energy (J)	Total Inductor Volume (m³)	Module IGBT Volume (m³)	Module Diode Volume (m³)	Number of Modules	Total Inductor Volume (m³)	Total Capacitor Volume (m³)	Total IGBT Volume (m³)	Total Diode Volume (m³)	Service Volume (m³)	Total Volume (m³)
3 Phase	Stainless Steel	6	700.0	2.908	0.71	0.0001	22,857	557.5	145.6	1.82	0.0106	0.0136	19	1.82	0.0001	0.20	0.26	0.68	2.96
		8	700.0	2.965	0.73	0.0001	22,857	546.7	142.8	1.79	0.0106	0.0136	19	1.79	0.0001	0.20	0.26	0.67	2.92
		10	700.0	3.023	0.74	0.0001	22,857	536.3	140.1	1.75	0.0106	0.0136	19	1.75	0.0001	0.20	0.26	0.66	2.87
		12	700.0	3.043	0.75	0.0001	22,857	532.7	139.2	1.74	0.0106	0.0136	19	1.74	0.0001	0.20	0.26	0.66	2.86
	Titanium	6	700.0	2.908	0.71	0.0001	22,857	557.5	145.6	1.82	0.0106	0.0136	19	1.82	0.0001	0.20	0.26	0.68	2.96
		8	700.0	2.962	0.73	0.0001	22,857	547.3	143.0	1.79	0.0106	0.0136	19	1.79	0.0001	0.20	0.26	0.67	2.92
		10	700.0	3.007	0.74	0.0001	22,857	539.1	140.8	1.76	0.0106	0.0136	19	1.76	0.0001	0.20	0.26	0.67	2.89
		12	700.0	3.026	0.74	0.0001	22,857	535.8	140.0	1.75	0.0106	0.0136	19	1.75	0.0001	0.20	0.26	0.66	2.87
	Inconel	6	700.0	2.897	0.71	0.0001	22,857	559.6	146.2	1.83	0.0106	0.0136	19	1.83	0.0001	0.20	0.26	0.69	2.97
		8	700.0	2.958	0.72	0.0001	22,857	548.1	143.2	1.79	0.0106	0.0136	19	1.79	0.0001	0.20	0.26	0.67	2.92
		10	700.0	3.001	0.74	0.0001	22,857	540.2	141.1	1.76	0.0106	0.0136	19	1.76	0.0001	0.20	0.26	0.67	2.89
		12	700.0	3.021	0.74	0.0001	22,857	536.7	140.2	1.75	0.0106	0.0136	19	1.75	0.0001	0.20	0.26	0.66	2.88
	Carbon	6	700.0	2.915	0.71	0.0001	22,857	556.2	145.3	1.82	0.0106	0.0136	19	1.82	0.0001	0.20	0.26	0.68	2.96
		8	700.0	2.969	0.73	0.0001	22,857	546.1	142.6	1.78	0.0106	0.0136	19	1.78	0.0001	0.20	0.26	0.67	2.92
		10	700.0	3.016	0.74	0.0001	22,857	537.5	140.4	1.76	0.0106	0.0136	19	1.76	0.0001	0.20	0.26	0.66	2.88
		12	700.0	3.035	0.74	0.0001	22,857	534.1	139.5	1.74	0.0106	0.0136	19	1.74	0.0001	0.20	0.26	0.66	2.87
5 Phase	Stainless Steel	6	700.0	3.061	0.75	0.0001	22,857	529.6	138.4	1.73	0.0106	0.0136	19	1.73	0.0001	0.20	0.26	0.66	2.85
		8	700.0	3.179	0.78	0.0001	22,857	510.0	133.2	1.67	0.0106	0.0136	19	1.67	0.0001	0.20	0.26	0.64	2.76
		10	700.0	3.269	0.80	0.0001	22,857	495.9	129.5	1.62	0.0106	0.0136	19	1.62	0.0001	0.20	0.26	0.62	2.70
		12	700.0	3.318	0.81	0.0001	22,857	488.7	127.6	1.60	0.0106	0.0136	19	1.60	0.0001	0.20	0.26	0.62	2.67
	Titanium	6	700.0	3.059	0.75	0.0001	22,857	529.9	138.4	1.73	0.0106	0.0136	19	1.73	0.0001	0.20	0.26	0.66	2.85
		8	700.0	3.155	0.77	0.0001	22,857	513.9	134.2	1.68	0.0106	0.0136	19	1.68	0.0001	0.20	0.26	0.64	2.78
		10	700.0	3.241	0.79	0.0001	22,857	500.1	130.7	1.63	0.0106	0.0136	19	1.63	0.0001	0.20	0.26	0.63	2.72
		12	700.0	3.294	0.81	0.0001	22,857	492.2	128.6	1.61	0.0106	0.0136	19	1.61	0.0001	0.20	0.26	0.62	2.69
	Inconel	6	700.0	3.038	0.74	0.0001	22,857	533.6	139.4	1.74	0.0106	0.0136	19	1.74	0.0001	0.20	0.26	0.66	2.86
		8	700.0	3.141	0.77	0.0001	22,857	516.1	134.8	1.69	0.0106	0.0136	19	1.69	0.0001	0.20	0.26	0.64	2.79
		10	700.0	3.230	0.79	0.0001	22,857	502.0	131.1	1.64	0.0106	0.0136	19	1.64	0.0001	0.20	0.26	0.63	2.73
		12	700.0	3.279	0.80	0.0001	22,857	494.5	129.2	1.61	0.0106	0.0136	19	1.61	0.0001	0.20	0.26	0.62	2.70
	Carbon	6	700.0	3.054	0.75	0.0001	22,857	530.8	138.7	1.73	0.0106	0.0136	19	1.73	0.0001	0.20	0.26	0.66	2.85
		8	700.0	3.169	0.78	0.0001	22,857	511.6	133.6	1.67	0.0106	0.0136	19	1.67	0.0001	0.20	0.26	0.64	2.77
		10	700.0	3.239	0.79	0.0001	22,857	500.5	130.7	1.63	0.0106	0.0136	19	1.63	0.0001	0.20	0.26	0.63	2.72
		12	700.0	3.293	0.81	0.0001	22,857	492.3	128.6	1.61	0.0106	0.0136	19	1.61	0.0001	0.20	0.26	0.62	2.69
7 Phase	Stainless Steel	6	700.0	2.906	0.71	0.0001	22,857	557.8	145.7	1.82	0.0106	0.0136	19	1.82	0.0001	0.20	0.26	0.68	2.97
		8	700.0	2.961	0.73	0.0001	22,857	547.5	143.0	1.79	0.0106	0.0136	19	1.79	0.0001	0.20	0.26	0.67	2.92
		10	700.0	3.002	0.74	0.0001	22,857	540.1	141.1	1.76	0.0106	0.0136	19	1.76	0.0001	0.20	0.26	0.67	2.89
		12	700.0	3.029	0.74	0.0001	22,857	535.3	139.8	1.75	0.0106	0.0136	19	1.75	0.0001	0.20	0.26	0.66	2.87
	Titanium	6	700.0	2.904	0.71	0.0001	22,857	558.2	145.8	1.82	0.0106	0.0136	19	1.82	0.0001	0.20	0.26	0.68	2.97
		8	700.0	2.947	0.72	0.0001	22,857	550.1	143.7	1.80	0.0106	0.0136	19	1.80	0.0001	0.20	0.26	0.68	2.93
		10	700.0	2.984	0.73	0.0001	22,857	543.3	141.9	1.77	0.0106	0.0136	19	1.77	0.0001	0.20	0.26	0.67	2.90
		12	700.0	3.010	0.74	0.0001	22,857	538.5	140.7	1.76	0.0106	0.0136	19	1.76	0.0001	0.20	0.26	0.67	2.88
	Inconel	6	700.0	2.891	0.71	0.0001	22,857	560.8	146.5	1.83	0.0106	0.0136	19	1.83	0.0001	0.20	0.26	0.69	2.98
		8	700.0	2.939	0.72	0.0001	22,857	551.6	144.1	1.80	0.0106	0.0136	19	1.80	0.0001	0.20	0.26	0.68	2.94
		10	700.0	2.978	0.73	0.0001	22,857	544.4	142.2	1.78	0.0106	0.0136	19	1.78	0.0001	0.20	0.26	0.67	2.91
		12	700.0	3.002	0.74	0.0001	22,857	540.0	141.1	1.76	0.0106	0.0136	19	1.76	0.0001	0.20	0.26	0.67	2.89
	Carbon	6	700.0	2.902	0.71	0.0001	22,857	558.6	145.9	1.82	0.0106	0.0136	19	1.82	0.0001	0.20	0.26	0.69	2.97
		8	700.0	2.956	0.72	0.0001	22,857	548.3	143.2	1.79	0.0106	0.0136	19	1.79	0.0001	0.20	0.26	0.68	2.93
		10	700.0	2.992	0.73	0.0001	22,857	541.8	141.5	1.77	0.0106	0.0136	19	1.77	0.0001	0.20	0.26	0.67	2.90
		12	700.0	3.019	0.74	0.0001	22,857	537.0	140.3	1.75	0.0106	0.0136	19	1.75	0.0001	0.20	0.26	0.66	2.88
9 Phase	Stainless Steel	6	700.0	2.985	0.73	0.0001	22,857	543.2	141.9	1.77	0.0106	0.0136	19	1.77	0.0001	0.20	0.26	0.67	2.90
		8	700.0	3.061	0.75	0.0001	22,857	529.6	138.4	1.73	0.0106	0.0136	19	1.73	0.0001	0.20	0.26	0.66	2.85
		10	700.0	3.141	0.77	0.0001	22,857	516.2	134.8	1.69	0.0106	0.0136	19	1.69	0.0001	0.20	0.26	0.64	2.79
		12	700.0	3.204	0.79	0.0001	22,857	505.9	132.2	1.65	0.0106	0.0136	19	1.65	0.0001	0.20	0.26	0.63	2.75
	Titanium	6	700.0	2.984	0.73	0.0001	22,857	543.2	141.9	1.77	0.0106	0.0136	19	1.77	0.0001	0.20	0.26	0.67	2.90
		8	700.0	3.054	0.75	0.0001	22,857	530.9	138.7	1.73	0.0106	0.0136	19	1.73	0.0001	0.20	0.26	0.66	2.85
		10	700.0	3.114	0.76	0.0001	22,857	520.7	136.0	1.70	0.0106	0.0136	19	1.70	0.0001	0.20	0.26	0.65	2.81
		12	700.0	3.175	0.78	0.0001	22,857	510.5	133.4	1.67	0.0106	0.0136	19	1.67	0.0001	0.20	0.26	0.64	2.76
	Inconel	6	700.0	2.979	0.73	0.0001	22,857	544.1	142.1	1.78	0.0106	0.0136	19	1.78	0.0001	0.20	0.26	0.67	2.91
		8	700.0	3.048	0.75	0.0001	22,857	532.0	139.0	1.74	0.0106	0.0136	19	1.74	0.0001	0.20	0.26	0.66	2.86
		10	700.0	3.103	0.76	0.0001	22,857	522.5	136.5	1.71	0.0106	0.0136	19	1.71	0.0001	0.20	0.26	0.65	2.82
		12	700.0	3.165	0.78	0.0001	22,857	512.3	133.8	1.67	0.0106	0.0136	19	1.67	0.0001	0.20	0.26	0.64	2.77
	Carbon	6	700.0	2.992	0.73	0.0001	22,857	541.8	141.5	1.77	0.0106	0.0136	19	1.77	0.0001	0.20	0.26	0.67	2.90
		8	700.0	3.067	0.75	0.0001	22,857	528.6	138.1	1.73	0.0106	0.0136	19	1.73	0.0001	0.20	0.26	0.66	2.84
		10	700.0	3.126	0.77	0.0001	22,857	518.5	135.5	1.69	0.0106	0.0136	19	1.69	0.0001	0.20	0.26	0.65	2.80
		12	700.0	3.187	0.78	0.0001	22,857	508.6	132.9	1.66	0.0106	0.0136	19	1.66	0.0001	0.20	0.26	0.64	2.76
11 Phase	Stainless Steel	6	700.0	3.087	0.76	0.0001	22,857	525.1	137.2	1.71	0.0106	0.0136	19	1.71	0.0001	0.20	0.26	0.65	2.83
		8	700.0	3.191	0.78	0.0001	22,857	508.0	132.7	1.66	0.0106	0.0136	19	1.66	0.0001	0.20	0.26	0.64	2.75
		10	700.0	3.299	0.81	0.0001	22,857	491.4	128.4	1.60	0.0106	0.0136	19	1.60	0.0001	0.20	0.26	0.62	2.68
		12	700.0	3.390	0.83	0.0001	22,857	478.2	124.9	1.56	0.0106	0.0136	19	1.56	0.0001	0.20	0.26	0.61	2.63
	Titanium	6	700.0	3.068	0.75	0.0001	22,857	528.4	138.0	1.73	0.0106	0.0136	19	1.73	0.0001	0.20	0.26	0.66	2.84
		8	700.0	3.182	0.78	0.0001	22,857	509.5	133.1	1.66	0.0106	0.0136	19	1.66	0.0001	0.20	0.26	0.64	2.76
		10	700.0	3.281	0.80	0.0001	22,857	494.1	129.1	1.61	0.0106	0.0136	19	1.61	0.0001	0.20	0.26	0.62	2.70
		12	700.0	3.368	0.83	0.0001	22,857	481.3	125.7	1.57	0.0106	0.0136	19	1.57	0.0001	0.20	0.26	0.61	2.64
	Inconel	6	700.0	3.062	0.75	0.0001	22,857	529.4	138.3	1.73	0.0106	0.0136	19	1.73	0.0001	0.20	0.26	0.66	2.85
		8	700.0	3.164	0.78	0.0001	22,857	512.4	133.8	1.67	0.0106	0.0136	19	1.67	0.0001	0.20	0.26	0.64	2.77
		10	700.0	3.262	0.80	0.0001	22,857	496.9	129.8	1.62	0.0106	0.0136	19	1.62	0.0001	0.20	0.26	0.62	2.71
		12	700.0	3.367	0.82	0.0001	22,857	481.4	125.8	1.57	0.0106	0.0136	19	1.57	0.0001	0.20	0.26	0.61	2.64
	Carbon	6	700.0	3.076	0.75	0.0001	22,857	527.1	137.7	1.72	0.0106	0.0136	19	1.72	0.0001	0.20	0.26	0.65	2.84
		8	700.0	3.173	0.78	0.0001	22,857	510.9	133.5	1.67	0.0106	0.0136	19	1.67	0.0001	0.20	0.26	0.64	2.77
		10	700.0	3.280	0.80	0.0001	22,857	494.2	129.1	1.61	0.0106	0.0136	19	1.61	0.0001	0.20	0.26	0.62	2.70
		12	700.0	3.369	0.83	0.0001	22,857	481.2	125.7	1.57	0.0106	0.0136	19	1.57	0.0001	0.20	0.26	0.61	2.64